THE UNIVERSITY of ADELAIDE

AXIAL COMPRESSIVE BEHAVIOR OF FRP-CONCRETE-STEEL DOUBLE-SKIN TUBULAR COLUMNS

Butje Alfonsius Louk Fanggi

BEng and MEng (Structural Engineering)

Thesis submitted to The University of Adelaide

School of Civil, Environmental, and Mining Engineering

In fulfilment of the requirements

For the degree of Doctor of Philosophy

2015

To my wife, Melinda Louk Fanggi-Moata

And my kids, Kayleen and Keanu Louk Fanggi

CONTENTS

ABSTRACT

A new type of composite structural system has been proposed in terms of FRP-concrete-steel double-skin tubular columns (DSTCs). This composite system consists of a steel tube inside, an FRP tube outside with concrete in between, and it combines the advantages of all three materials to achieve a high-performance structural member. This thesis is aimed at developing an improved understanding of the axial compressive behavior of DSTCs.

To this end, six experimental studies were undertaken at the University of Adelaide. In each of these studies, the key parameters that influence the axial compressive behavior of DSTCs were identified and investigated. The results of these experimental studies indicate that concrete in a DSTC system is confined effectively by FRP and steel tubes. Both the normal-and high-strength concrete DSTCs exhibited a highly ductile compressive behavior under monotonic and cyclic axial compression. However, it is found that, for a given nominal confinement ratio, an increase in the concrete strength results in a decrease in the ultimate axial strain of DSTCs. The results also indicate that increasing the inner steel tube diameter leads to an increase in the ultimate axial stress and strain of concrete in DSTCs. It is observed that the concrete-filling of the inner steel tubes of DSTCs results in an increase in the compressive strength and a slight decrease in the ultimate axial strain of concrete in DSTCs, compared to the values observed in companion specimens with hollow inner steel tubes. It is also observed that cyclically loaded normal-strength concrete (NSC) DSTCs developed similar strength and strain enhancement ratios to those of monotonically loaded NSC DSTCs. The results also show that concrete in hollow DSTCs manufactured with square inner steel tubes develops significantly lower ultimate axial stresses and strains than those of concrete in

companion hollow DSTCs with circular inner steel tubes. It is found, however, that the performance of these specimens improves dramatically when the square inner steel tube is filled with concrete.

Apart from these experimental studies, this thesis also presents analytical models that were developed to predict the compressive strength and ultimate axial strain of concrete in DSTCs. The first of these models was developed to predict the compressive strength and ultimate axial strain of concrete in hollow circular DSTCs. After undertaking additional studies to expand the test database of square and concrete-filled DSTCs a second model that is applicale both circular and square and hollow and concrete-filled DSTCs was proposed. Comparison with experimental test results show that of the proposed models are in close agreement with the test results, and the models provide improved accuracy compared to the existing models.

STATEMENT OF ORIGINALITY

I certify that this work contains no material which has been accepted for the award of any other degree or diploma in my name, in any university or other tertiary institution and, to the best of my knowledge and belief, contains no material previously published or written by another person, except where due reference has been made in the text. In addition, I certify that no part of this work will, in the future, be used in a submission in my name, for any other degree or diploma in any university or other tertiary institution without the prior approval of the University of Adelaide and where applicable, any partner institution responsible for the joint-award of this degree.

I give consent to this copy of my thesis when deposited in the University Library, being made available for loan and photocopying, subject to the provisions of the Copyright Act 1968.

The author acknowledges that copyright of published works contained within this thesis resides with the copyright holder(s) of those works.

I also give permission for the digital version of my thesis to be made available on the web, via the University's digital research repository, the Library Search and also through web search engines, unless permission has been granted by the University to restrict access for a period of time.

Signed:_____ Date:_____

ACKNOWLEDGEMENTS

Firstly, I would like to express my deepest gratitude to my supervisors, Dr. Togay Ozbakkaloglu and Assoc. Prof. Yung Ngothai, for their supervision, support and encouragement over the course of my PhD candidature. I would particularly like to thank Dr. Togay Ozbakkaloglu for his continual enthusiasm, vision, and determination for my research to succeed. I am also grateful to Assoc. Prof. Yung Ngothai for her help and motivation during the time of my candidature.

I acknowledge the financial support from the Government of the Republic of Indonesia through their Directorate General of Higher Education (DIKTI) Scholarships that sponsored my study at the University of Adelaide.

I would also like to thank all academics and technical staff who have helped me with this thesis in their fields of expertise. In particular, I thank Mr. Gary Bowman and Jon Ayoub who provided technical assistance throughout the experimental program and Barbara Brougham who provided technical reviews of most of the publications presented in this thesis.

I am very grateful to my fellow PhD students Mr. Thomas Vincent, Jian Lim, Mohammad Albitar, Tianyu Xie, Lei Gu, Junai Zhang, and Ms. Yunita Idris for their friendship, encouragement, and help. I would particularly like to thank Jian Lim who was always willing to help and give suggestions during development of my model papers. Many thanks also to other PhD students in the School of Civil, Environmental and Mining Engineering who have helped me throughout the course.

I would also like to thank my fellow brothers and sisters in Christ, for their continued support during the last year of my study.

Finally, and most importantly, I thank God, who put and helped me in this journey.

LIST OF NOTATIONS

B	=	Internal width of square outer FRP tube (mm)
c_1	=	Parameter in the compressive strength expression
c_2	=	Parameter in the ultimate strain expression
D	=	Internal diameter of FRP tube (mm)
D_s	=	External diameter of steel tube (mm)
E_f	=	Elastic modulus of fibers (MPa)
E_{frp}	=	Elastic modulus of FRP material (MPa)
f'_{cc}	=	Peak axial compressive stress of concrete in DSTC (MPa)
f'_{cu}	=	Ultimate axial compressive stress of concrete in DSTC (MPa)
f'_{co}	=	Peak axial compressive stress of unconfined-concrete (MPa)
f_y	=	Yield strength of steel tube (MPa)
f_u	=	Ultimate tensile strength of steel tube (MPa)
f'_{c1}	=	Axial compressive stress of concrete in DSTC at first peak (MPa)
f'_{c2}	=	Axial compressive stress of concrete in DSTC at second transition (MPa)
f_{l1}	=	Confining pressure at f'_{c1} (MPa)
f_{l2}	=	Confining pressure at f'_{c2} (MPa)
f_{lu}	=	Nominal lateral confining pressure at ultimate (MPa)
$f_{lu,a}$	=	Actual lateral confining pressure at ultimate (MPa)
f_{lo}	=	Threshold confining pressure at ultimate (MPa)
f_f	=	Ultimate tensile strength of fibers (MPa)
f_{frp}	=	Ultimate tensile strength of FRP material (MPa)
H	=	DSTC specimen height (mm)
k_1	=	Axial strength enhancement coefficient

k_2 = Axial strain enhancement coefficient

K_l = Lateral confinement stiffness (MPa)

K_{lo} = Threshold confinement stiffness (MPa)

$K_{\varepsilon,f}$ = Hoop strain reduction factor of fibers

P_T = Axial load capacity of DSTC (kN)

P_s = Axial load capacity of steel tube (kN)

P_{co} = Axial load capacity of unconfined concrete (kN)

r = Corner radius (mm)

t_f = Total nominal thickness of fibers (mm)

t_{frp} = Total nominal thickness of FRP material (mm)

t_s = Thickness of steel tube (mm)

ε_{co} = Axial strain of unconfined concrete at f'_{co}

ε_{cu} = Ultimate axial strain of concrete in DSTC

$\varepsilon_{h,rup}$ = Hoop rupture strain of FRP shell

ε_{l1} = Hoop rupture strain of DSTC at f'_{c1}

ε_{l2} = Hoop rupture strain of DSTC at f'_{c2}

ε_f = Ultimate tensile strain of fibers

ε_{frp} = Ultimate tensile strain of FRP material

ε_s = Ultimate tensile strain of steel tube

$\emptyset_F$ = Solidity factor of inner steel tube

INTRODUCTION

An important application of fiber reinforced polymer (FRP) composites is as a confining material for concrete, in both the seismic retrofit of existing reinforced concrete columns and in the construction of new compaosite columns. Following from research on concrete-filled FRP tubes (CFFTs), a new type of composite system was recently proposed in the form of FRP-concrete-steel double-skin tubular columns (DSTCs). This composite system consists of a steel tube inside, an FRP tube outside with concrete in between, and it combines the advantages of all three materials to achieve a high-performance structural member. Reliable design of these structural members necessitates clear understanding and accurate modeling of the stress-strain relationship of confined concrete.

Research objectives

The objective of this research is to improve the understanding of axial compressive behavior of DSTCs. To this end, a large number of axial compression tests on DSTCs have been performed to address the identified research gaps. The comprehensive experimental program undertaken at the University of Adelaide has enabled the development of confinement models to predict the behaviour of concrete in DSTCs.

Thesis overview

This thesis is organized into nine chapters. Chapters 1 and 9 are the introduction and conclusions, whereas each of Chapters 2 to 8 is a manuscript that had been submitted for publication as a journal article throughout the course of this study [1-7]. The parameters investigated in each of the experimatal studies are summarized in Table 1. Information regarding the proposed models is presented in Table 2.

As can be seen in Table 1, ten parameters were identified and investigated in this research program, which include the types and thickness of FRP, concrete strength, diameter, thickness, cross sectional shape, strength, and end condition of inner steel tube, presence (or absence) of concrete filling inner tube, and loading patterns. The results of the experimental studies were then used together with the test results that are available in literature to develop the confinement models presented in Refs. [2,7].

The first of these models was developed to predict the compressive strength and ultimate axial strain of concrete in hollow circular DSTCs. After undertaking additional studies to expand the test database of square and concrete-filled DSTCs a second model that is applicale both circular and square and hollow and concrete-filled DSTCs was proposed.Comparison with experimental test results show that of the proposed models are in close agreement with the test results, and the models provide improved accuracy compared to the existing models.

Table 1 Summary of experimental studies

Publications	Research area focused	Key parameters investigated									
		Type of FRP	Thickness of FRP	Diameter of steel tube	Thickness of steel tube	Strength of steel tube	Cross sectional shape of steel tube	End condition of inner steel tube	Concrete strength	Presence (absence) of concrete filling inner steel tube	Loading patterns
Ozbakkaloglu and Louk Fanggi [1]	Influence of key parameters on axial compressive behavior of DSTCs made of carbon FRP.	-	Yes	Yes	Yes	Yes	-	-	Yes	Yes	-
Louk Fanggi and Ozbakkaloglu [2]	Influence of key parameters on axial compressive behavior of DSTCs made of aramid FRP and model development	-	Yes	Yes	Yes	-	Yes	-	Yes	-	-
Ozbakkaloglu and Louk Fanggi [3]	Influence of key parameters on axial compressive behavior of DSTCs made of aramid FRP	-	-	Yes	Yes	-	-	Yes	Yes	Yes	Yes
Louk Fanggi and Ozbakkaloglu [4]	Influence of key parameters on axial compressive behavior of DSTCs made of glass FRP	-	-	Yes	-	-	-	-	-	Yes	Yes
Albitar et al. [5]	Influence of key parameters on cyclic axial compressive behavior of DSTCs made of aramid and glass FRP	Yes	Yes	Yes	-	-	-	-	Yes	Yes	-
Louk Fanggi and Ozbakkaloglu [6]	Influence of key parameters on axial compressive behavior of square DSTCs made of aramid FRP	-	-	Yes	-	-	Yes	-	Yes	Yes	-

Table 2 Summary of models proposed

Publications	Type of proposed model	Databased used						Application range of modeled proposed						Stress-strain modeled	
		Normal-strength concrete (NSC)	High-strength concrete (NSC)	Circular hollow DSTCs	Circular Concrete-filled DSTCs	Square hollow DSTCs	Square Concrete-filled DSTCs	Normal-strength concrete (NSC)	High-strength concrete (NSC)	Circular hollow DSTCs	Circular Concrete-filled DSTCs	Square hollow DSTCs	Square Concrete-filled DSTCs	Shape of curve	Ultimate conditions of concrete
Louk Fanggi and Ozbakkaloglu [2]	Design-oriented model	Yes	Yes	Yes	-	-	-	Yes	Yes	Yes	-	-	-	Ascending	Yes
Louk Fanggi and Ozbakkaloglu [7]	Design-oriented model	Yes	Yes	Yes	Yes	Yes	Yes	Yes	Yes	Yes	Yes	Yes	Yes	Ascending	Yes

REFFERENCES

[1] Ozbakkaloglu, T., and Louk Fanggi, B.A. (2013). "Axial compressive behavior of FRP-concrete-steel double-skin tubular columns made of normal- and high-strength concrete." *Journal of Composites for Construction*, 18(1): 04013027-1-040113027-13.

[2] Louk Fanggi, B.A., and Ozbakkaloglu, T. (2013). "Compressive behavior of aramid FRP-HSC-steel double-skin tubular columns." *Construction and Building Materials*. 48: 554-565.

[3] Ozbakkaloglu, T., and Louk Fanggi, B.A. (2015). "Behavior of FRP-HSC-steel composite tubular columns under monotonic and cyclic axial compression." *Materials and Structures*. 48: 1075-1093.

[4] Louk Fanggi, B.A., and Ozbakkaloglu, T. (2015). "Behavior of Hollow and Concrete-Filled FRP-HSC and FRP-HSC-Steel Composite Columns Subjected to Concentric Compression." *Advanced in Structural Engineering*. 18(5): 715-738.

[5] Albitar, M., Ozbakkaloglu, T., and Louk Fanggi, B.A. (2015). "Behavior of FRP-HSC-Steel double-skin tubular columns under cyclic axial compression." *Journal of Composites for Construction*. 19(2): 04014041.

[6] Louk Fanggi, B.A., and Ozbakkaloglu, T. (2015). "Square FRP-HSC-steel composite columns: Behavior under Axial Compression." *Engineering Structures*. 92: 156-171.

[7] Louk Fanggi, B.A., and Ozbakkaloglu, T. (2015). "Confinement model for concrete in circular and square FRP-concrete-steel double-skin tubular columns." (To be submitted).

PUBLICATIONS

Paper 1 Axial Compressive Behavior of FRP-Concrete-Steel Double-Skin Tubular Columns Made of Normal-and High-Strength Concrete

Togay Ozbakkaloglu and Butje Alfonsius Louk Fanggi

School of Civil, Environmental, and Mining Engineering, University of Adelaide, 5000

Journal of Composites for Construction, ASCE (Published)

Statement of Authorship

Title of Paper	Axial Compressive Behavior of FRP-Concrete-Steel Double-Skin Tubular Columns Made of Normal-and High-Strength Concrete
Publication Status	● Published ○ Accepted for publication ○ Submitted for publication ○ Publication style
Publication Details	Ozbakkaloglu, T., and Louk Fanggi, B.A. (2013). "Axial compressive behavior of FRP-concrete-steel double-skin tubular columns made of normal- and high-strength concrete." Journal of Composites for Construction, 18(1): 04013027-1-040113027-13.

Author Contributions

By signing the Statement of Authorship, each author certifies that their stated contribution to the publication is accurate and that permission is granted for the publication to be included in the candidate's thesis.

Name of Principal Author	Dr. Togay Ozbakkaloglu		
Contribution to the Paper	Research supervision and review of manuscript		
Signature		Date	28/07/2015

Name of Co-Author (Candidate)	Butje Alfonsius Louk Fanggi		
Contribution to the Paper	Review of literature, analysis data, and preparation of manuscript		
Signature		Date	28/07/2015

AXIAL COMPRESSIVE BEHAVIOR OF FRP-CONCRETE-STEEL DOUBLE-SKIN TUBULAR COLUMNS MADE OF NORMAL-AND HIGH-STRENGTH CONCRETE

Togay OZBAKKALOGLU[1] and Butje LOUK FANGGI[2]

ABSTRACT

This paper presents the results of an experimental study that was undertaken to investigate the effects of key parameters on the compressive behavior of fiber-reinforced polymer (FRP)-concrete-steel double-skin tubular columns (DSTCs). A total of 24 normal-strength and high-strength concrete-filled DSTCs were manufactured and tested under axial compression. The key parameters examined included the concrete strength; thickness of FRP tube; diameter, strength, and thickness of inner steel tube; and presence (absence) of concrete filling inside it. The results indicate that both normal- and high-strength concretes in a DSTC system is confined effectively by FRP and steel tubes, resulting in a highly ductile compressive behavior. The results also indicate that increasing the inner steel tube diameter leads to an increase in the ultimate axial stress and strain of concrete in DSTCs. It is observed that the concrete filling of the inner steel tubes results in a slight decrease in the ultimate axial strain and a slight increase in ultimate stress of DSTCs. No clear influence of the strength of inner steel tube is observed on the ultimate condition of concrete in DSTCs. It is found that, for a given nominal confinement ratio, an increase in the concrete strength results in a decrease in the ultimate axial strain of DSTCs.

[1] (Corresponding author) Senior Lecturer, School of Civil, Environmental and Mining Engineering, University of Adelaide, Australia. Tel : + 618 8303 6477; Fax : +618 8303 4359; Email: togay.ozbakkaloglu@adelaide.edu.au

[2] PhD Student, School of Civil, Environmental and Mining Engineering University of Adelaide, Australia.

KEYWORDS: Fiber reinforced polymers (FRP); Concrete, High-strength concrete (HSC), Confinement; Columns; FRP tubes; Steel tubes; Double-skin tubular columns (DSTCs).

1. INTRODUCTION

As an important application of fiber-reinforced polymer (FRP) composites, confinement of concrete with externally bonded FRP has received a great deal of attention over the last two decades. Numerous experimental studies have been conducted to examine the performance of FRP composites in retrofitting existing concrete columns (e.g., Rochette and Labossiere 2000; Chaallal et al. 2003; Lam and Teng 2004; Hadi 2006; Ilki et al. 2008; Ozcan et al. 2010; Wu and Wei 2010; Ozbakkaloglu and Akin 2012; Wang et al. 2012) and in the construction of new high-performance composites columns in the form of concrete-filled FRP tubes (CFFTs) (Seible et al. 1996; Mirmiran et al. 1998; Fam and Rizkalla 2001; Fam et al. 2005; Shao and Mirmiran 2005; Ozbakkaloglu and Saatcioglu 2006, 2007; Ozbakkaloglu and Oehlers 2008a, b; Mohamed and Masmoudi 2010; Ozbakkaloglu 2013a, b, c; Idris and Ozbakkaloglu 2013).

More recently a new type of composite system was proposed by Teng et al. (2004) in the form of FRP-concrete-steel double-skin tubular columns (DSTCs). This composite system consists of a steel tube inside, an FRP tube outside with concrete in between, and it combines the advantages of all three materials to achieve a high-performance structural member. A series of axial compression and flexure tests have been conducted by the research group led by Teng (Teng et al. 2005, 2007, 2010; Yu et al. 2006; Wong et. al 2008; Yu and Teng 2010; Yu et al. 2010; Xie et al. 2011) to investigate the performance of FRP-concrete-steel DST stub columns and beams. Following these, Han et al. (2010) reported on a study in which a few DST beam-column specimens were

tested under cyclic loading. The results of these early tests have demonstrated that the DST beam and column systems provide very effective confinement to concrete, which in turn leads to a highly ductile member behavior. These studies have also demonstrated that the behavior of DSTCs is different from previously studied column forms, including CFFTs, concrete-filled steel tubes (CFSTs), and concrete-filled steel double-skin tubes (CFSDS).

Very much like that of FRP, the popularity of high-strength concrete (HSC) in the construction industry has been on a steady incline during the last two decades because of the superior performance and economy offered by HSC over normal-strength concrete (NSC) in a large number of structural engineering applications. The use of high-strength concrete in the construction of new composite columns such as CFFTs and DSTCs is particularly attractive because the effective combination of these high-strength materials (i.e., HSC, steel and FRP) results in high-performance structural members. However, apart from the six axial compression test specimens reported in Teng et al. (2010), all of the existing studies on DSTCs have been concerned with NSC, and additional studies are required to better understand the compressive behavior of HSC DSTCs.

To contribute towards this end, this paper presents the results of an experimental program that focused on the axial compressive behavior of FRP-HSC-steel DSTCs. The study was aimed at investigating the influence of critical columns parameters on the performance of DSTCs constructed of carbon FRP external tubes. The results of the experimental program are first presented and followed by a discussion on the influence of the key parameters on the behavior of DSTCs.

2. EXPERIMENTAL PROGRAM

2.1. Test Specimens and Materials

A total of 24 DSTCs with circular outer and inner tubes were manufactured and tested under axial compression. Fourteen of the specimens were made of HSC and the remaining 10 with NSC. Each specimen had a diameter of 150 mm, measured at the concrete core, and a height of 300 mm. Details of the specimens are shown in Table 1. The test parameters included the concrete strength, the diameter, thickness, and strength of the inner steel tube, and the provision (or absence) of concrete filling inside the steel tube. Two nominally identical specimens were tested for each unique specimen configuration.

DSTCs 1-8 were manufactured using NSC and their outer tubes were made of two layers of carbon FRP (CFRP). The diameter of the inner steel tube was either 76.1 or 101.6 mm. Inner voids of the steel tubes of four of these specimens were filled with concrete (referred to as filled DSTCs), whereas in the remaining four specimens, this void was left unfilled (referred to as hollow DSTCs). Two additional specimens (DSTCs 9 and 10) were manufactured using NSC and six-layer CFRP tubes to investigate the influence of that amount of confinement. HSC DSTCs 11-18 were analogous to NSC DSTCs 1-8 and they were designed to investigate the same parameters as the NSC specimens. Considering the increased confinement demand of HSC, the amount of confinement was increased proportionally with concrete strength (f'_{co}) and the HSC specimens were designed with FRP tubes made of 6 layers of CFRP. DSTCs 19 to 24 were designed to investigate the influence of the steel tube thickness and strength. Steel tubes with a thickness of 3.2 mm were used in DSTCs 19 and 20, whereas DSTCs 21 to 24 were provided with 1.6-mm-thick steel tubes. DSTCs 19-22 were constructed using normal-strength steel (NSS) tubes, and DSTCs 23 to 24 had high-strength steel (HSS) inner steel tubes.

Table 1. Details of test specimens

Specimen	Number of FRP layers	Concrete strength, f'_c (MPa)	Strain at peak stress, ε_{co} (%)	Steel tube diameter, D_s (mm)	Steel tube thickness, t_s (mm)	Steel tube strength	Inner void*
DSTC-1	2	37.0	0.21	101.6	3.2	NSS	Hollow
DSTC-2							Hollow
DSTC-3		36.7	0.21				Filled
DSTC-4							Filled
DSTC-5	2	36.9	0.21	76.1	3.2	NSS	Hollow
DSTC-6							Hollow
DSTC-7		36.4	0.21				Filled
DSTC-8							Filled
DSTC-9	6	37.0	0.21	101.6	3.2	NSS	Hollow
DSTC-10							Hollow
DSTC-11		106	0.35				Hollow
DSTC-12							Hollow
DSTC-13		106	0.35				Filled
DSTC-14							Filled
DSTC-15	6	106	0.35	76.1	3.2	NSS	Hollow
DSTC-16							Hollow
DSTC-17		107	0.35				Filled
DSTC-18							Filled
DSTC-19	6	106	0.35	38.1	1.6	NSS	Hollow
DSTC-20							Hollow
DSTC-21		106	0.35				Hollow
DSTC-22							Hollow
DSTC-23		108	0.35		1.6	HSS	Hollow
DSTC-24							Hollow

*The same concrete was used to fill the void as the concrete used between the FRP and steel tubes, NSS = Normal-strength steel, HSS = High-strength steel.

The specimens were prepared using NSC and HSC mixes, with average unconfined concrete compressive strengths of 36.8 and 106.4 MPa attained during the period of testing. Both mixes consisted of crushed bluestone as the coarse aggregate, with a nominal maximum size of 10 mm. Silica fume was added to the HSC mix at 8% of the binder content by weight. The testing of the specimens started after the attainment of the 35-day strength and continued for approximately 3 weeks. Concrete cylinder tests have been conducted throughout the testing program to accurately record the variations in the strength of unconfined concrete during testing. The unconfined concrete strengths (f'_{co})

of the specimens at the day of testing are reported together with the corresponding axial strains ε_{co} in Table 1. The ε_{co} values were not measured directly for the control cylinders, and were calculated using the expression given by Tasdemir et al. (1998).

In designing the FRP tubes, due consideration was given to the well-understood influence of the strength of concrete on its confinement demand (Ozbakkaloglu & Saatcioglu 2007; Ozbakkaloglu & Akin 2012). This was done through the use of nominal confinement ratio (f_l /f'_c), calculated from Eq.1 assuming a uniform confinement distribution, as the performance criterion in establishing relative confinement levels of DSTCs with different concrete strengths.

$$\frac{f_l}{f'_c} = \frac{2E_f t_f \varepsilon_f}{D_f f'_c} \tag{1}$$

where, f_l is the confining pressure, E_f is the modulus of elasticity, t_f is the total nominal thickness and ε_f is the ultimate tensile strain of the fibers, and D_f is the internal diameter of the FRP tube.

To establish the material properties of the steel tubes used in the DSTCs, axial compression tests were conducted on hollow steel tubes. For each steel tube type three hollow tubes having the same height as those in the DSTC specimens were tested. For the steel tubes with 38.1 and 76.1 mm diameters, additional three hollow tubes with a height-to-diameter ratio of 3:1 were also tested. The results of the hollow steel tube compression tests are shown in Table 2. All the reduced height specimens failed due to localized elephant foot buckling either at the top or the bottom of the specimen. The full height specimens of 38.1 mm and 76.1 mm tubes, on the other hand, failed due to global buckling. Steel tube load-strain relationships used in establishing the axial load

capacities, ultimate conditions and stress-strain curves of DSTCs with inner steel tube diameters of 38.1 mm and 76.1 mm was obtained from the tests of hollow steel tubes with a height-to-diameter ratio of 3:1.

Table 2. Measured properties of steel tubes

D_s (mm)	t_s (mm)	Grade (MPa)	Height (mm)	Peak axial load (kN)	Yield strength (MPa)	Peak strength (MPa)	Axial strain at peak (%)	Failure mode*
101.6	3.2	350 (NSS)	300	357	302	360	1.71	EF
76.1	3.2	350 (NSS)	228	312	358	426	2.34	EF
			300	321	351	438	2.56	G
38.1	3.2	350 (NSS)	114	213	520	607	7.34	EF
			300	181	473	515	1.11	G
38.1	1.6	350 (NSS)	114	90	411	493	3.22	EF
			300	83	434	452	1.08	G
38.1	1.6	1300 (HSS)	114	280	1360	1520	1.85	EF
			300	274	1410	1500	1.23	G

* EF = Elephant foot buckling, G = Global buckling

2.2. Specimen Preparation

The FRP tubes were prepared using a manual wet lay-up process by wrapping epoxy resin impregnated carbon fiber sheets around precision-cut high-density styrofoam templates in the hoop direction. A thin polyester film was placed on the surface of the Styrofoam template to prevent bonding between the FRP tube and the template to allow easy removal of the template after the resin had dried. The FRP sheets were provided with a 100 mm overlap to prevent premature debonding failure. The FRP tubes with two layers of FRP were wrapped with a single FRP sheet continuously, whereas the tubes with six layers of FRP were wrapped by two FRP sheets, and therefore had two overlap regions. In these tubes the two overlaps were provided along the same region around the circumference of the tube. Properties of the fibers used in the manufacture of the FRP

tubes are shown in Table 3. Both the manufacturer supplied properties and the ones obtained from the flat coupon test are provided in the table.

Table 3. Properties carbon fibers sheets used in DSTCs

Type	Nominal thickness	Provided by manufacturers			Obtained from flat FRP coupon tests		
	t_f (mm/ply)	Tensile strength f_f (MPa)	Ultimate tensile strain, ε_f (%)	Elastic modulus E_f (GPa)	Tensile strength f_{frp} (MPa)	Ultimate tensile strain, ε_{frp} (%)	Elastic modulus E_{frp} (GPa)
Carbon	0.117	3800	1.55	240	3620	1.44	251

To ensure that the FRP and steel tubes remained concentric during concrete pouring, a formwork system was developed and used to support the tubes during the process. At the base, wooden spacers were used to hold the bottom of the FRP tube in place and nails were used to maintain the position of the steel tube relative to the FRP tube. At the top, a cap with three steel arms was used to maintain the position of the two tubes concentrically. Alignment was maintained by anchoring the top cap to the wooden base. Fig. 1 illustrates the formwork.

a) b)

Figure 1. Formwork used in manufacture of DSTC specimens: a) before pouring of concrete, b) after concrete pouring

2.3. Instrumentation and testing

Axial deformations of the specimens were measured with four linear variable displacement transducers (LVDTs), which were mounted at the corners between the loading and supporting steel plates of the compression test machine, as shown in Fig. 2. The recorded deformations were used in the calculation of the average axial strains along the height of the specimens. In addition, FRP tubes of the specimens were instrumented at the mid-height with two unidirectional strain gauges with a gauge length of 20 mm to measure axial strains, which were used to validate LVDT measurements at the early stages of loading. FRP tube lateral strains were measured by three unidirectional strain gauges with 20-mm gauge lengths that were spaced equally around the perimeter at the mid-height of the specimen outside the overlap region. Axial and lateral strains of inner steel tubes were measured at the mid-height by two axially and two laterally oriented strain gauges with 5-mm gauge lengths.

Figure 2. Test setup and instrumentation

The specimens were tested under axial compression using a 5,000 kN capacity universal testing machine. During the initial elastic stage of the behavior, the loading was applied with load control at 3 kN per second, whereas displacement control was used at

approximately 0.003 mm per second beyond the initial softening until specimen failure. Before testing, all specimens were capped at both ends to ensure uniform distribution of the applied pressure, and the load was applied directly to the concrete core through precision-cut high-strength loading discs placed at each end of the specimens.

(a) (b) (c)

Figure 3. Failure modes of DSTCs: a) bond failure, b) localized hoop rupture, c) global rupture

3. TEST RESULTS AND DISCUSSION

3.1. Failure modes

All of the specimens failed by the rupture of their FRP tubes in the hoop direction, apart from the two specimens (i.e. DSTC-7 and DSTC-8) that experienced FRP tube debonding failure, which is believed to be caused by the problems with the epoxy resin used in the manufacture of these tubes. The rupture of the FRP tubes was often localized and corresponded to the location of significant steel tube deformation inside the specimen. It was observed that the rupture was more extensive in specimens with smaller diameter inner steel tubes. The failure modes of the specimens and locations of FRP rupture corresponding to regions of significant steel tube deformation are shown in Figs. 3 and 4, respectively. DSTCs 11 and 12 experienced an early failure caused by elephant foot buckling of their inner steel tubes, which occurred at a lower axial

deformation in the case of DSTC-11 resulting in lower ultimate axial stress and strain of the specimen. Furthermore, DSTC-13 experienced a premature failure caused by manufacturing imperfections. These specimens are excluded from the discussions presented in the following sections.

a)

b)

Figure 4. Interaction between damage regions of FRP and steel tubes: a) DSTC-17, b) DSTC-18

3.2. Axial load capacities

Experimentally recorded axial load capacities of the DSTCs (P_T) are presented in Table 4 together with axial capacities of the steel tubes (P_S), and unconfined concrete (P_{CO}). The axial load capacities of the steel tubes (P_S) were determined from hollow steel tube

tests, whereas the axial load capacities of unconfined concrete (P_{CO}) were obtained by multiplying unconfined concrete strength by the area of the concrete cross-section. As evident from the $P_T/(P_S+P_{CO})$ ratios shown in Table 4, the DSTC specimens develop significantly higher axial load capacities than the combined axial load capacity of the unconfined concrete and steel tube.

Table 4. Axial load capacities of DSTCs

Specimen	Ultimate load of DSTC, P_T (kN)	Average P_T (kN)	Ultimate load of steel tube, P_S (kN)	Ultimate load of unconfined concrete section, P_{co} (kN)	Average P_{co} (kN)	$P_S + P_{co}$ (kN)	$P_T/(P_S + P_{co})$
DSTC-1	914	934	357	354	354	711	1.31
DSTC-2	955			354			
DSTC-3	1,145	1,234	357	612	612	969	1.27
DSTC-4	1,322			612			
DSTC-5	911	922	312	484	484	796	1.16
DSTC-6	932			484			
DSTC-7	1,009	1,028	312	617	617	929	1.11
DSTC-8	1,048			617			
DSTC-9	1,448	1,472	357	354	354	711	2.07
DSTC-10	1,497			354			
DSTC-11	1,513	1,431	357	1,000	1,000	1357	1.05
DSTC-12	1,349			1,000			
DSTC-13*	2,534	3,185	357	1,775	1,775	2132	1.34
DSTC-14	3,185			1,775			
DSTC-15	2,066	1,989	312	1,388	1,388	1700	1.17
DSTC-16	1,912			1,388			
DSTC-17	2,627	2,574	312	1,809	1,809	2121	1.21
DSTC-18	2,521			1,809			
DSTC-19	2,203	2,173	213	1,756	1,756	1969	1.10
DSTC-20	2,142			1,756			
DSTC-21	2,294	2,339	90	1,756	1,756	1846	1.27
DSTC-22	2,384			1,756			
DSTC-23	2,175	2,354	250	1,780	1,780	2030	1.16
DSTC-24	2,533			1,780			

*The specimen was excluded from calculations of P_T average

3.3. Behavior of inner steel tube in DSTCs

3.3.1. Failure modes of inner steel tubes

The compressive behavior of the steel tubes inside the DSTCs was observed to be different from the behavior of hollow steel tubes on their own. Tables 2 and 5 provide the failure modes of hollow steel tubes and steel tubes in DSTCs, respectively. As indicated in these tables, the solitary steel tubes with diameters of 38.1 mm and 76.1 mm experienced global buckling, which was prevented by concrete in the DSTC specimens. Rather than global buckling, in DSTCs the internal steel tubes experienced rippling, bulging or local elephant foot type of buckling as illustrated in Fig. 5.

Table 5. Failure modes of steel tubes in DSTCs

Specimen	D_s (mm)	Concrete Strength	Inner void	Failure mode*
DSTC-1	101.6	NSC	Hollow	Rippling
DSTC-2			Hollow	Rippling
DSTC-3			Filled	N/A
DSTC-4			Filled	N/A
DSTC-5	76.1	NSC	Hollow	Rippling
DSTC-6			Hollow	N/A
DSTC-7			Filled	Bulging at mid-height
DSTC-8			Filled	Bulging at mid-height
DSTC-9	101.6	NSC	Hollow	Rippling
DSTC-10			Hollow	Bulging at top
DSTC-11		HSC	Hollow	EF
DSTC-12			Hollow	EF
DSTC-13			Filled	N/A
DSTC-14			Filled	Bulging at mid-height
DSTC-15	76.1	HSC	Hollow	Bulging at top
DSTC-16			Hollow	Rippling
DSTC-17			Filled	Bulging at mid-height
DSTC-18			Filled	Bulging at top
DSTC-19	38.1 (t_s=3.2)	HSC	Hollow	N/A
DSTC-20			Hollow	N/A
DSTC-21	38.1 (t_s=1.6-NSS)		Hollow	Bulging at mid-height
DSTC-22			Hollow	Rippling
DSTC-23	38.1 (t_s=1.6-HSS)		Hollow	N/A
DSTC-24			Hollow	N/A

* EF = Elephant foot buckling, N/A = No sign of damage

a) b) c)

Figure 5. Steel tube deformation modes inside DSTCs: a) elephant foot buckling (DSTC-11), b) rippling (DSTC-5), c) bulging (DSTC-14)

Rippling was not experienced by any of the specimens with concrete-filled inner steel tubes, although the steel tubes of the filled DSTCs experienced bulging under large axial deformations. Elephant foot buckling occurred only in two of the specimens, which were made of HSC and had 101.6 mm diameter internal steel tubes that were left unfilled. The 38.1-mm diameter NSS tube with 3.2 mm thickness experienced no significant deformation. On the other hand, significant deformations were observed on both the NSS and HSS tubes with a 38.1 mm diameter and 1.6 mm thickness.

3.3.2. Interaction between steel and FRP tubes

As noted previously, the FRP tube rupture locations corresponded to the regions of significant deformation on the steel tube. Fig. 4 shows two nominally identical specimens (i.e., DSTC-17 and DSTC-18) at the end of testing, and Fig. 6 illustrates the variation of lateral strains measured on the FRP tubes of these specimens with axial deformation. As Fig. 6 shows, the lateral strain recorded at the mid-height of DSTC-17 was greater than that of DSTC-18. This is because, in DSTC-17, the strain concentration regions on the steel tube, which lead to the eventual rupture of the FRP tube, corresponded to the location around which hoop strain gauges were placed on the

FRP tube. On the other hand, as shown in Fig. 4, the failure of DSTC-18 took place near one of the ends of the specimen and hence was outside the mid-height region in which the specimen was instrumented. The different FRP tube rupture locations of these nominally identical specimens is believed to be caused by the sensitivity of the FRP tubes to slight imperfections and disturbances caused by the movement of the surrounding concrete. Similar observations were previously reported by Wong et al. (2008) for NSC DSTCs.

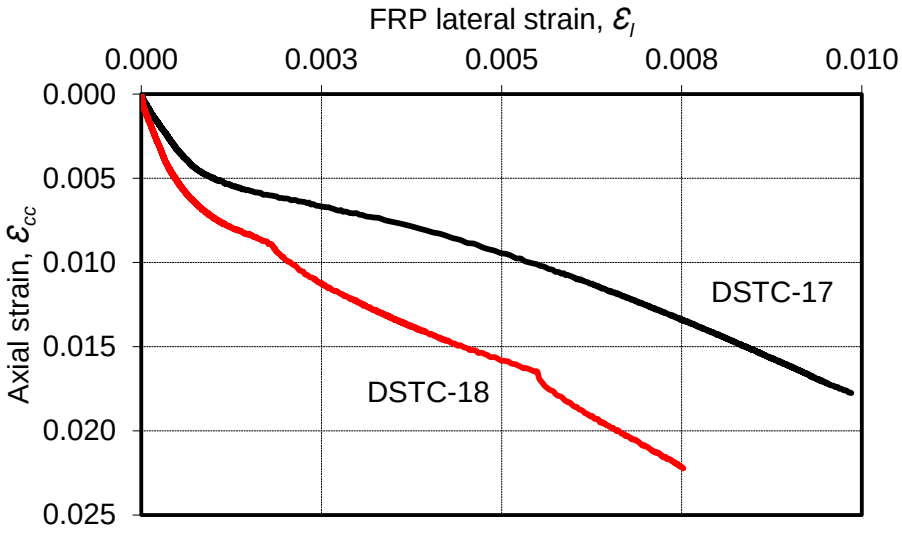

Figure 6. Development of lateral strains on FRP tubes of DSTCs

3.4. Behavior of confined concrete in DSTCs

3.4.1. FRP tube rupture strain

Three horizontally oriented strain gauges were placed equidistantly at mid-height of the specimens outside the overlap region on the FRP tube to record the hoop strains. The average recorded hoop rupture strains ($\varepsilon_{h,rup}$) are given in Table 6 for all the specimens. A closer inspection of the $\varepsilon_{h,rup}$ values reported in the table allows a number of observation to be made on the influence of the important parameters on $\varepsilon_{h,rup}$. These observations are summarized in this section.

The influence of the concrete strength (f'_{co}) on $\varepsilon_{h,rup}$ of hollow DSTCs can be investigated by comparing the hoop rupture strain of the companion NSC DSTCs (DSTC-5 & DSTC-6) and HSC DSTCs (DSTC-15 & DSTC-16). Table 6 shows that the average hoop rupture strains recorded on the NSC and HSC DSTCs were very close (i.e., 0.90 and 0.86%, respectively). A similar comparison can also be made between the filled NSC (DSTC-3 & DSTC-4) and HSC (DSTC-14) DSTCs. As evident from Table 6, once again NSC and HSC DSTCs developed reasonably close hoop rupture strains (i.e., 1.11 and 1.20%, respectively). From these comparisons no clear influence of the concrete strength is evident on $\varepsilon_{h,rup}$.

The effect of concrete-filling on the inner steel tube on the hoop rupture strain of NSC DSTCs can be investigated through the comparison of the companion hollow (DSTC-1 & DSTC-2) and filled NSC DSTCs (DSTC-3 & DSTC-4). As Table 6 shows, almost identical average hoop rupture strains were recorded for hollow and filled DSTCs (i.e., 1.12 and 1.11%, respectively). A similar comparison can be made between the companion hollow (DSTC-15 & DSTC-16) and filled (DSTC-17 & DSTC-18) HSC DSTCs. As evident from Table 6, no significant difference exists between the average hoop rupture strains of these specimens, with hollow and filled DSTCs developing $\varepsilon_{h,rup}$ of 0.86 and 0.90%, respectively. These observations suggest that $\varepsilon_{h,rup}$ is not influenced significantly by the presence (or absence) of concrete-filling inside the inner steel tube.

Table 6. Ultimate condition of concrete in DSTCs

Specimen	f_l / f'_c	f'_{cu} (Mpa)	Ave. f'_{cu} (Mpa)	Ave. f'_{cu} / f'_c	ε_{cu} (%)	Ave. ε_{cu} (%)	Ave. $\varepsilon_{cu} / \varepsilon_{co}$	$\varepsilon_{h,rup}$ (%)
DSTC-1	0.320	58.3	60.4	1.63	2.77	2.63	12.72	1.07
DSTC-2	0.320	62.5			2.49			1.16
DSTC-3	0.323	47.5	52.7	1.44	2.13	2.38	11.55	0.84
DSTC-4	0.323	57.9			2.63			1.37
DSTC-5	0.321	46.8	47.3	1.28	1.86	1.87	9.03	0.82
DSTC-6	0.321	47.7			1.87			0.98
DSTC-7*	0.326	41.8	42.9	1.18	1.58	1.56	7.58	0.92
DSTC-8*	0.326	44.0			1.53			0.85
DSTC-9	0.961	114.0	116.6	3.15	5.40	5.09	24.62	0.95
DSTC-10	0.961	119.2			4.78			0.90
DSTC-11**	0.337	120.9	113.1	1.07	1.63	1.30	3.74	0.54
DSTC-12**	0.337	105.2			0.96			0.11
DSTC-13***	0.334	133.4	169.5	1.59	0.90	2.06	5.93	0.52
DSTC-14	0.334	169.5			2.06			1.20
DSTC-15	0.336	135.5	128.8	1.22	1.74	1.64	4.72	0.86
DSTC-16	0.336	122.1			1.53			0.86
DSTC-17	0.333	137.2	134.0	1.25	1.58	1.54	4.42	0.95
DSTC-18	0.333	130.7			1.50			0.85
DSTC-19	0.335	121.7	117.6	1.11	1.50	1.52	4.38	1.00
DSTC-20	0.335	113.5			1.54			0.72
DSTC-21	0.335	133.7	136.4	1.28	1.66	1.67	4.79	0.58
DSTC-22	0.335	139.1			1.67			0.92
DSTC-23	0.330	114.5	125.4	1.16	1.53	1.60	4.56	0.79
DSTC-24	0.330	136.3			1.66			1.10

*debonding failure, **elephant foot buckling, ***premature failure

The influence of the steel tube diameter (D_s) on the hoop rupture strain of hollow NSC DSTCs can be examined by comparing the hoop rupture strain of the companion DSTCs with 76.1 mm (DSTC-5 & DSTC-6) and 101.6 mm (DSTC-1 & DSTC-2) inner steel tube diameters. Table.6 shows that the larger diameter DSTCs failed at a higher average $\varepsilon_{h,rup}$ of 1.12% compared with 0.90% of the smaller diameter DSTCs. The same influence can be also studied for hollow HSC DSTCs through the comparison of DSTC-15 & DSTC-16 with 76.1-mm diameter inner steel tubes and DSTC-19 & DSTC-20

with 38.1-mm diameter steel tubes. Table 6 illustrates that these two companion pairs failed at the same average $\varepsilon_{h,rup}$ of 0.86%. Finally, the same influence can be investigated for filled HSC DSTCs by comparing the companion 76.1-mm diameter (DSTC-17 and DSTC-18) and 101.6-mm diameter (DSTC-14) DSTCs. Table 6 shows that the filled HSC DSTC with larger inner steel tube diameter developed a higher $\varepsilon_{h,rup}$ (i.e., 1.20%) than the average $\varepsilon_{h,rup}$ developed by the DSTCs with a smaller inner steel tube diameter (i.e., 0.90%). These observations suggest that the diameter of the internal steel tube may have some influence on the hoop rupture strains developed on FRP tubes of DSTCs. Further research is required to better understand this influence. It is worth noting that all the specimens that are referred to in the discussion on the influence of D_s had the same inner steel tube thickness.

3.4.2. Axial stress-strain behavior

The axial stress on the concrete inside the DSTCs was calculated by dividing the axial load resisted by the concrete (P_C) with the cross sectional area of the concrete section. The load applied to the concrete was determined by subtracting the axial load resisted by the steel tube (P_S) for a given axial strain from the total load resisted by the DSTC (P_T) at the same axial strain. The load acting on the steel tube was calculated by assuming that the load-strain behavior of the steel tubes inside a DSTC is similar to the load strain behavior of the corresponding unconfined hollow steel tube obtained from a compression test. The ultimate axial stress (f'_{cu}) and strain (ε_{cu}) of the concrete inside the DSTCs reported in Table 6 were calculated using the approach summarized in this section. It might be worth noting that because of composite actions, it would be reasonable to expect that the compressive behavior of steel tubes inside DSTCs could differ slightly from that of hollow steel tubes.

Figure 7 presents the concrete stress-strain relationships for the DSTCs of the present study. As evident from Fig. 7, all the specimens exhibited almost monotonically ascending stress-strain curves, indicating that the concrete inside the DSTCs was effectively confined. It can also be observed in Fig. 7 that some of the HSC specimens experienced a sudden drop in strength after the transition point between the initial ascending branch and the second branch that follows it. This phenomenon can be attributed to the brittle nature of the high-strength concrete. As expected, the stress-strain behavior of the specimens along the second branch of the curve is influenced by the key parameters of the DSTCs, including the concrete strength; thickness of FRP tube; diameter, strength, and thickness of inner steel tube; and presence (absence) of concrete filling inside it. The influence of these parameters on the stress-strain behavior of DSTCs is discussed in the following sections.

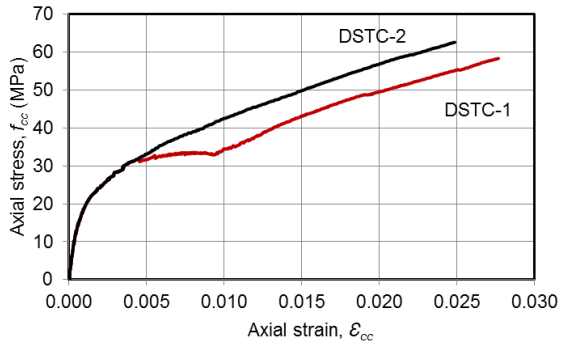

a)

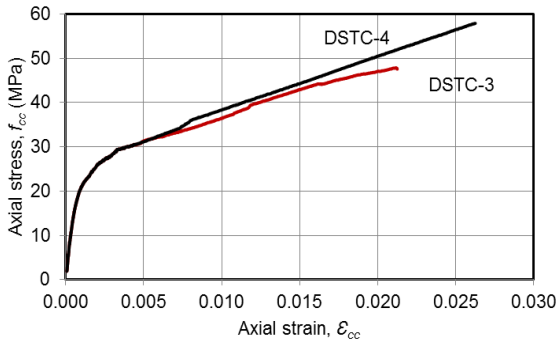

b)

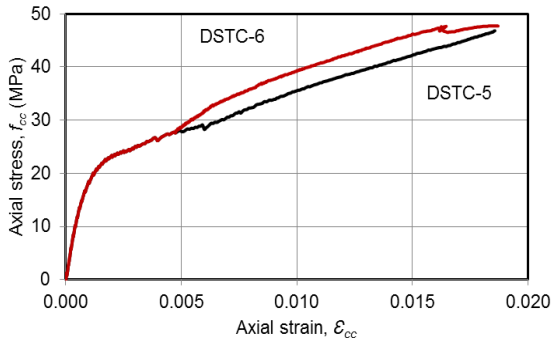

c)

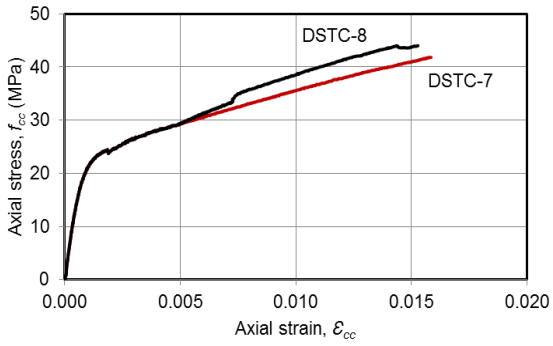

d)

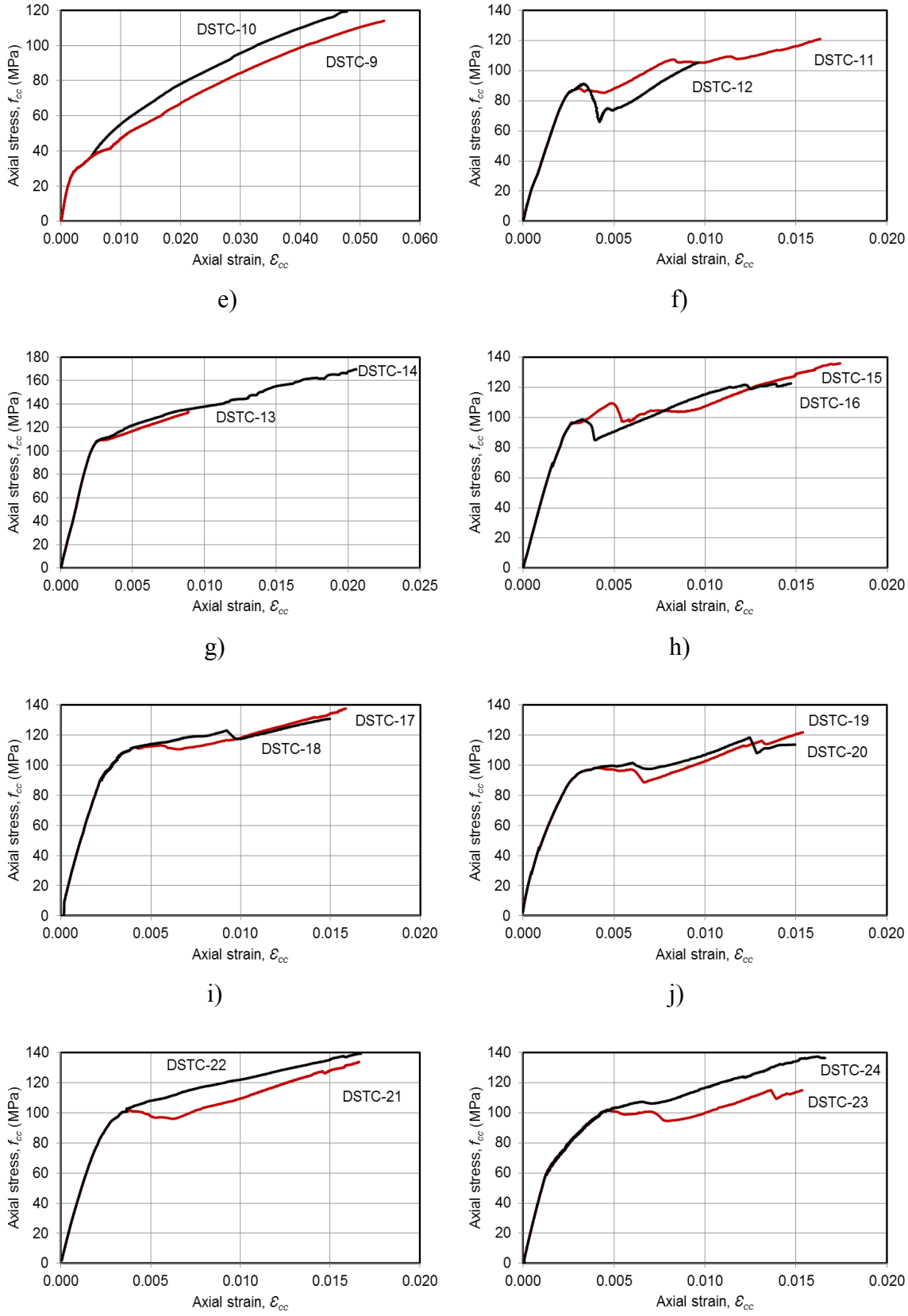

e) f)

g) h)

i) j)

k) l)

Figure 7. Axial stress-strain behavior of concrete in DSTCs: a) 1&2, b) 3&4, c) 5&6, d) 7&8, e) 9 &10, f) 11&12, g) 13&14, h) 15&16, i) 17&18, j)19&20, k) 21&22, l) 23&24

3.5. Effect of FRP tube thickness

It is well understood that the amount of confinement significantly influences the compressive behavior of confined concrete. Hence, the present study made no effort to comprehensively examine the effect of changing the thickness of the FRP tube for a given concrete strength. Only a single additional specimen pair (i.e., DSTC-9 and DSTC-10), which were analogous to DSTC-1 and DSTC-2 with two layers of FRP, were manufactured with 6-layers of FRP to study this influence. These specimens were also identical to DSTC-11 and DSTC-12 except for their concrete strength, hence their presence allowed a direct comparison to be made between NSC and HSC DSTCs confined by the same number of FRP layers. Fig. 8 shows the effect of the FRP tube thickness on the stress-strain behavior of the DSTCs. It is evident from the stress-strain curves shown in Fig. 8 and the ultimate conditions reported in Table 6 that the FRP tube thickness, as expected, has a major influence on the stress-strain behavior and the ultimate axial stress (f'_{cu}) and strain (ε_{cu}) of DSTCs.

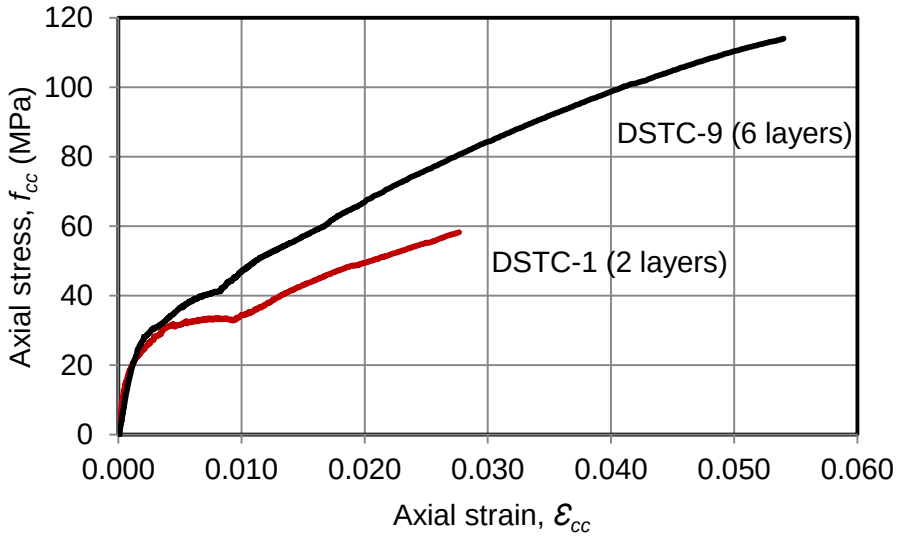

Figure 8. Effect of FRP tube thicknesses on stress-strain behavior of concrete in DSTCs

3.6. Effect of concrete strength

As is shown in Table 6, the companion NSC and HSC DSTCs were designed to have similar levels of confinement, which was established through the use of the nominal confinement ratio [Eq. (1)]. This enabled the investigation of the influence of concrete strength on the compressive behavior of DSTCs. In calculating f_l it was assumed that the confining pressure was uniform and the section was treated as a solid section, ignoring the influence of the inner void when applicable.

Figure 9 illustrates the stress-strain curves of the specimens with inner steel tube diameters of 76.1 and 101.6 mm. Fig. 9(a) shows that the companion hollow NSC and HSC DSTCs with 76.1-mm diameter inner steel tubes exhibited similar stress-strain behaviors, with the NSC DSTC developing a slightly higher ultimate strain (ε_{cu}) and strength enhancement ratio (f'_{cu}/f'_{co}). This observation is also supported by the average values of ε_{cu} and fcu0 =fc0 reported in Table 6 for NSC specimens DSTC-5 & DSTC-6 and HSC specimens DSTC-15 & DSTC-16. The comparison of the stress-strain curves of the filled NSC and HSC DSTCs with 101.6-mm diameter inner steel tubes in Fig. 9(b) indicate that the companion NSC and HSC DSTCs developed an almost identical strength enhancement ratio (f'_{cu}/f'_{co}), whereas the NSC DSTC exhibited a higher ultimate strain (ε_{cu}). The comparison of the average values of ε_{cu} reported in Table 6 for the NSC specimens DSTC-3 & DSTC-4 and the HSC specimen DSTC-14 supports the observation in regards to the influence of the concrete strength on the ultimate axial strain (ε_{cu}) of DSTCs. In contrast, as evident from Table 6, the average value of f'_{cu}/f'_{co} for the NSC DSTCs is lower than the f'_{cu}/f'_{co} of the HSC specimen DSTC-14. DSTC-3 performed significantly worse that its companion, DSTC-4, which is believed to have been caused by minor manufacture related imperfections of the specimen. When the

results from DSTC-3 are excluded, observations from the aforementioned filled and hollow DSTCs on the influence of concrete strength show a better agreement.

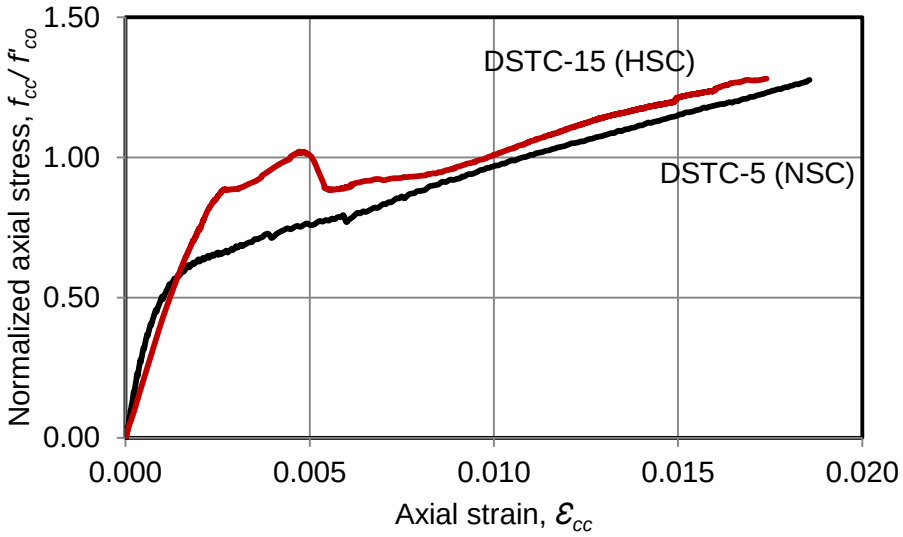

a)

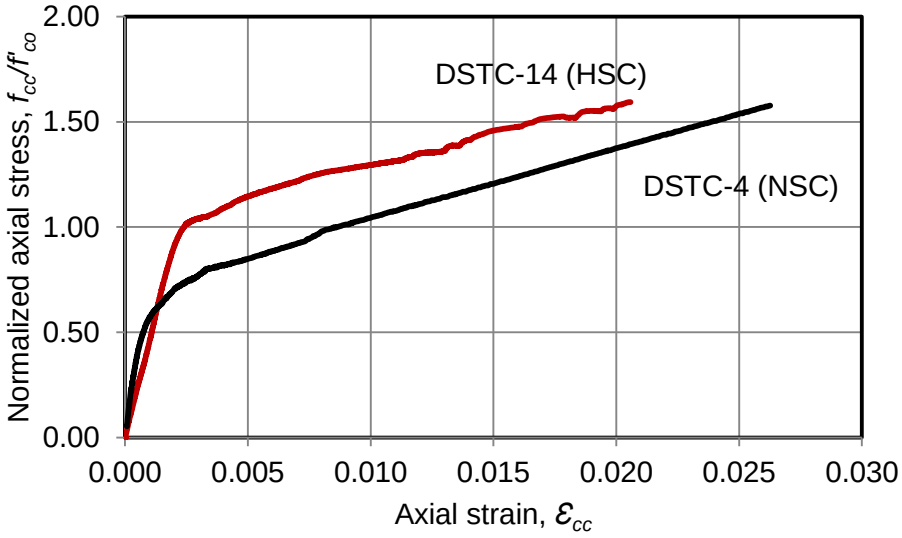

b)

Figure.9. Effect of concrete strength on stress-strain behavior of concrete in DSTCs: a) hollow DSTCs with 76.1-mm diameter internal steel tubes, b) filled DSTCs with 101.6-mm diameter internal steel tubes

3.7. Effect of steel tube diameter

Figure 10 presents the stress-strain relationships of the specimens with different steel tube diameters. Fig. 10(a) illustrates the effect of changing the steel tube diameter from 76.1 mm (DSTC-5) to 101.6 mm (DSTC-1) on the stress-strain behavior of hollow NSC DSTCs. It is shown in the figure that the DSTC with a larger inner steel tube developed significantly higher ultimate stress (f'_{cu}) and strain (ε_{cu}) compared with its companion. A similar observation can be made through the comparison of the average values of f'_{cu} and ε_{cu} reported in Table 6 for the specimen pairs DSTC-1 & DSTC-2 and DSTC-5 & DSTC-6. Fig. 10(b) shows the effect of increasing steel tube diameter from 38.1 (DSTC-19) to 76.1 mm (DSTC-15) on the stress-strain behavior of hollow HSC DSTCs. As evident from the figure, the DSTC with a larger inner steel tube diameter once again exhibits a better performance than its companion. This observation is also supported by the one that can be made from the comparison of the average values of f'_{cu} and ε_{cu} reported in Table 6 for the specimen pairs DSTC-15 & DSTC-16 and DSTC-19 & DSTC-20. Fig. 10(c) illustrates the influence of changing steel tube diameter from 76.1 (DSTC-18) to 101.6 mm (DSTC-14) on the stress-strain behavior of filled HSC DSTCs. It is shown in the figure that the DSTC with a larger inner steel tube developed significantly higher ultimate stress (f'_{cu}) and strain (ε_{cu}) than its companion. This observation is also supported by the comparison of f'_{cu} and ε_{cu} values reported in Table 6 for DSTC-14 with the average values for the specimen pair DSTC-17 & DSTC-18. The aforementioned observations indicate in the diameter of the internal steel tube results in an increase in both the ultimate strength (f'_{cu}) and strain (ε_{cu}) of DSTCs. This influence has been observed to be independent of the concrete strength and presence/absence of concrete-filling inside the inner steel tube of DSTCs.

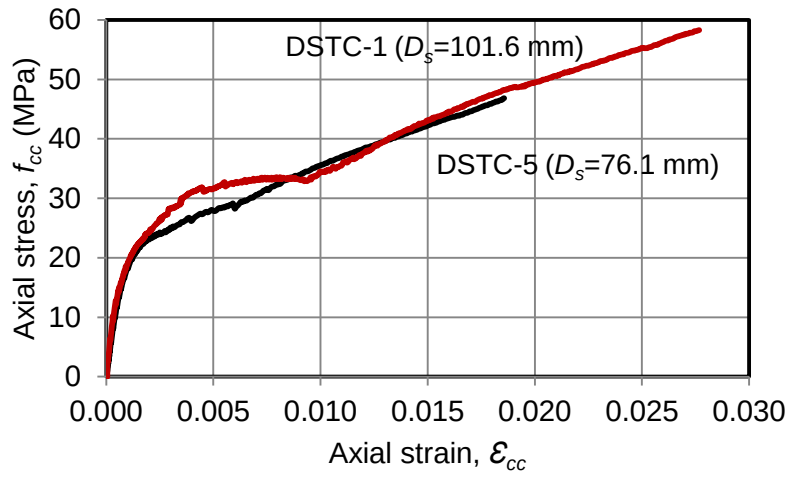

a)

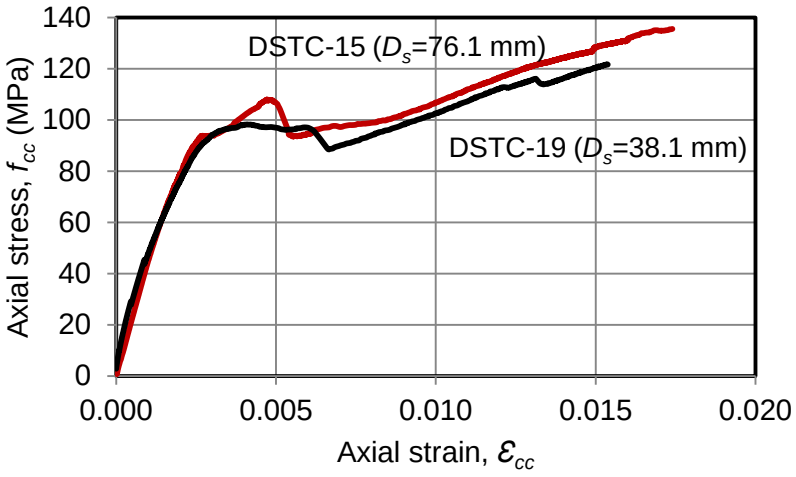

b)

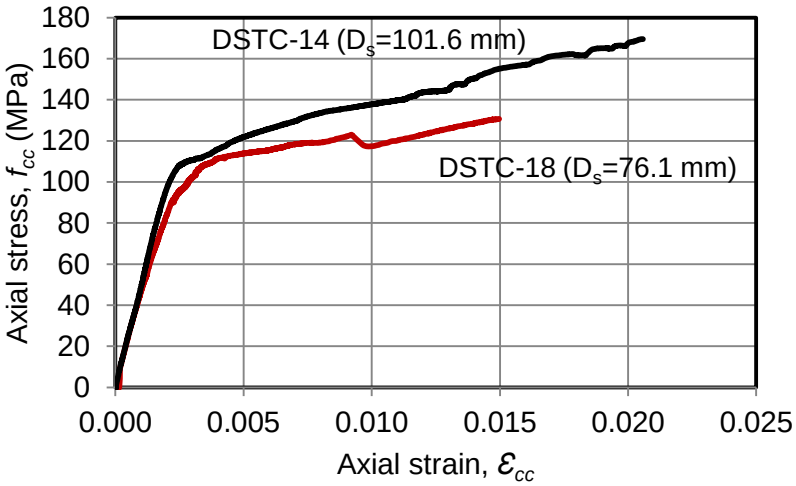

c)

Figure 10. Effect of steel tube diameter on stress-strain behavior of concrete in DSTCs: a) hollow NSC DSTC, b) hollow HSC DSTC, c) filled HSC DSTC

3.8. Effect of steel tube strength

Figure 11 illustrates the influence of the steel tube strength on the stress-strain behavior of concrete in DSTCs. As is shown in the figure, DSTC-22 with a NSS tube and DSTC-24 with a HSS tube developed almost identical ultimate stresses (f'_{cu}) and strains (ε_{cu}). The behavior of the companion DSTCs 23 and 24 showed some differences, which is believed to have been caused by minor manufacturing imperfections of DSTC-23. This resulted in slightly lower average ultimate stress and strain of the specimen pair DSTC 23 & 24 compared with those of the companion pair DSTC 21 & 22, as reported in Table 6. The influence of the steel tube strength was observed on DSTCs with small inner steel tubes, because of availability constraints for the HSS tubes. Therefore, additional research on DSTCs with larger inner tubes is required before a definitive conclusion can be drawn regarding the influence of the tube strength on axial compressive behavior of concrete in DSTCs.

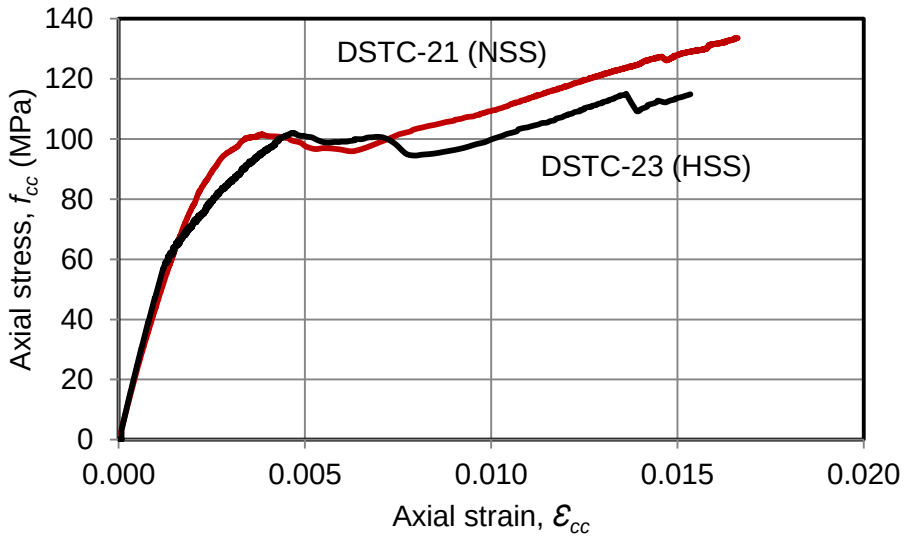

Figure 11. Effect of steel tube strength on stress-strain behavior of concrete in DSTCs

3.9. Effect of steel tube thickness

Figure 12 illustrates the influence of steel tube thickness on the stress-strain behavior of concrete in DSTCs. It is shown in Fig. 12 that increasing steel tube thickness from 1.6 mm in DSTC-21 to 3.2 mm in DSTC-19 leads to a decrease in f'_{cu} and ε_{cu}. This observation is also supported by the results reported in Table 6 for the specimen pairs DSTC-19 & DSTC-20 and DSTC-21 & DSTC-22. These observations are based on DSTCs with small diameter inner steel tubes and they are not in agreement with those reported previously in Wong et al. (2008) and Cheek et al. (2011), in which DSTCs with larger inner steel tubes were investigated. Therefore, further research, in which the steel tube slenderness ratio (D_s=t_s) is also studied as a key parameter, is required to better understand the influence of the steel tube thickness and how it varies with the slenderness of the tube.

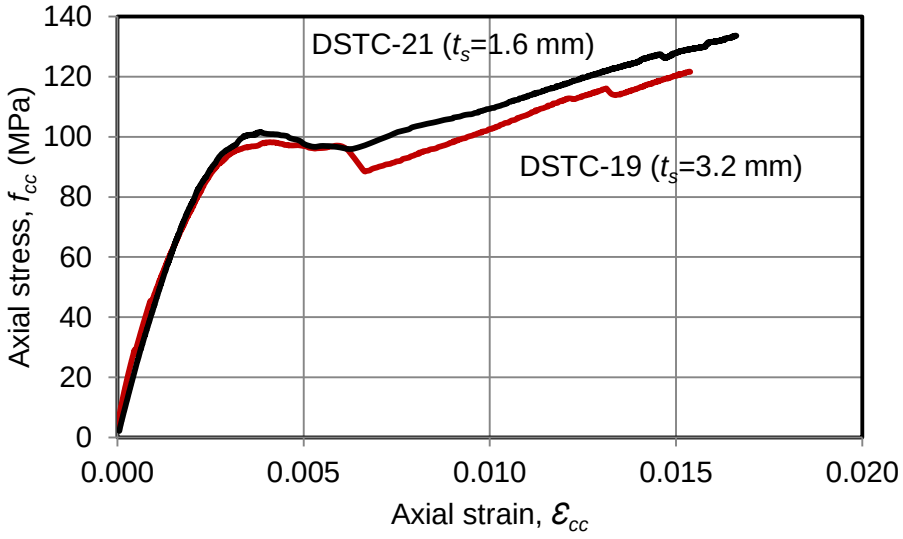

Figure 12. Effect of steel tube thickness on stress-strain behavior of concrete in DSTCs

3.10. Effect of concrete filling inner steel tube

The influence of concrete-filling the inner steel tube of DSTCs can be investigated by comparing the stress-strain curves of the NSC DSTCs [DSTC-1 (hollow) & DSTC-4

(filled)] and HSC DSTCs [DSTC-15 (hollow) & DSTC-17 (filled)] shown in Figs. 13(a and b), respectively. Fig. 13(a) shows that the filled NSC DSTC developed almost the same ultimate stress (f'_{cu}) and slightly lower ultimate strain (ε_{cu}) compared with the hollow NSC DSTC. As noted previously, because of manufacturing related problems, one of the filled specimens (i.e., DSTC-3) performed significantly worse than its nominally identical pair (i.e., DSTC-4), resulting in a lower average ultimate stress (f'_{cu}) for the filled DSTC pair, as shown in Table 6. The comparison of the stress-strain curves of the HSC DSTCs shown in Fig. 13(b) indicate that the difference between the behavior of filled and hollow DSTCs is not very significant, with the filled specimens developing slightly higher f'_{cu} and lower ε_{cu}. This observation is also supported by the average values of f'_{cu} and ε_{cu} reported in Table 6 for the specimen pairs DSTC-15 & DSTC-16 and DSTC-17 & DSTC-18. Additional tests are required to gain further insight into the influence of concrete filling the inner steel tube on the compressive behavior of DSTCs.

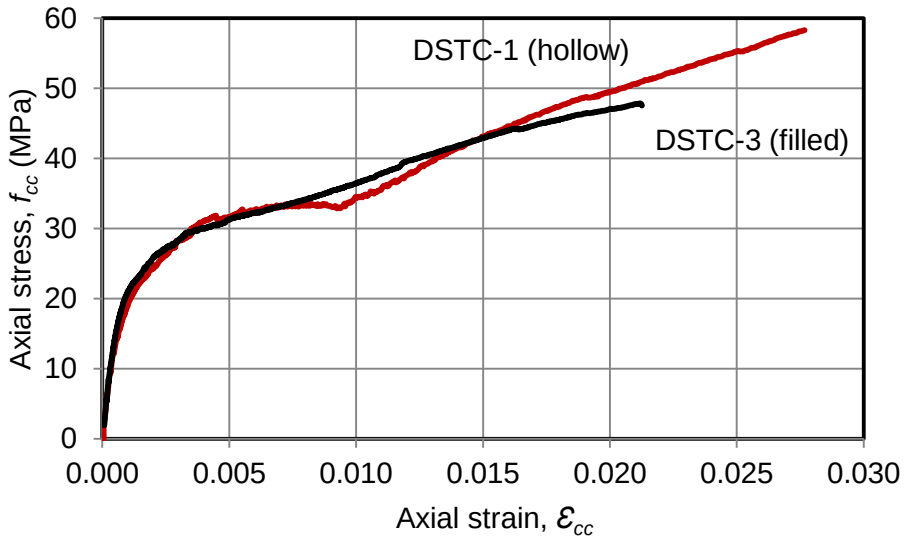

a)

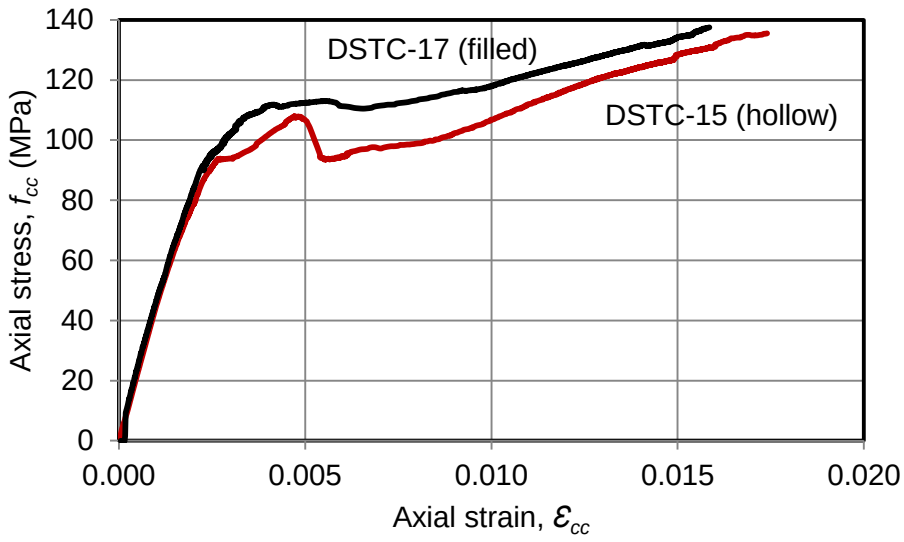

b)

Figure 13. Effect of concrete filling inner void on stress-strain behavior of concrete in DSTCs: a) NSC DSTCs, b) HSC DSTCs

4. CONCLUSIONS

This paper has presented the results of an experimental study on the axial compressive behavior of FRP-concrete-steel double-skin tubular columns. The experimental tests involved twenty-four normal-strength and high-strength concrete-filled DSTCs, designed and manufactured to investigate the behavior of concrete in DSTCs and the effect of the key parameters on the stress-strain relationship of concrete. The key parameters studied were concrete strength, steel tube diameter, steel tube thickness, steel tube strength, and provision (or absence) of concrete filling inside the inner steel tube. On the basis of the test results presented in this paper, the following conclusions can be drawn:

1. Concrete inside DSTCs demonstrates an almost monotonically ascending stress-strain curve, indicating that concrete in DSTCs is confined effectively by FRP and steel tubes.

2. FRP tube thickness has a significant influence on the stress-strain behavior of confined concrete in DSTCs. As expected, increasing the FRP tube thickness leads to an increase in the ultimate axial stress (f'_{cu}) and strain (ε_{cu}), and the second branch slope of the stress-strain curve of DSTCs.

3. For a given nominal confinement ratio (f_l/f'_c), an increase in the concrete strength results in a decrease in the ultimate axial strain (ε_{cu}) of DSTCs. The strength enhancement ratio (f_l/f'_c) also tends to decrease slightly with an increase in the concrete strength (f'_{cu}).

4. Increasing the inner steel tube diameter leads to an increase in the ultimate axial stress (f'_{cu}) and strain (ε_{cu}) of both hollow and filled DSTCs. This influence was found to be independent of concrete strength.

5. No clear influence of the strength of inner steel tube was evident on the ultimate axial stress (f'_{cu}) and strain (ε_{cu}) of the concrete in DSTCs. Further research on specimens with larger inner steel tubes is required to be able to draw a definitive conclusion on potential influence of inner steel tube strength.

6. Concrete filling of the inner steel tubes results in a slight decrease in the ultimate axial strain (ε_{cu}) of DSTCs. A slightly positive influence of concrete filling was observed on the ultimate axial stress (f'_{cu}) of DSTCs.

7. A clear conclusion cannot be drawn on the influence of the studied test parameters on the FRP tube hoop rupture strain ($\varepsilon_{h,rup}$). Further research is required to gain insight into how $\varepsilon_{h,rup}$ is influenced by the important parameters of DSTCs.

A clear conclusion cannot be drawn on the influence of the studied test parameters on the FRP tube hoop rupture strain ($\varepsilon_{h,rup}$). Further research is required to gain insight into how $\varepsilon_{h,rup}$ is influenced by the important parameters of DSTCs.

ACKNOWLEDGEMENTS

The authors would like to thank to Messrs. Kulbac, Mader, Wallent, and Whiting, who have undertaken the tests reported in this paper as part of their undergraduate theses. This research is part of an ongoing program at The University of Adelaide on FRP-concrete-steel composite columns.

REFFERENCES

Chaallal, O., Hassan, M., and Shahawy, M. (2003). "Confinement model for axially loaded short rectangular columns strengthened with fiber reinforced polymer wrapping." *ACI Struct. J.*, 100(2), 215–221.

Cheek, J., Formichella, N., Graetz, D., and Varasteh, S. (2011). "The behavior of ultra-high strength concrete in FRP confined concrete systems under axial compression." B.Sc. thesis, Civil Engineering, Univ. of Adelaide, Adelaide, SA, Australia.

Fam, A. Z., and Rizkalla, S. H. (2001). "Confinement model for axially loaded concrete confined by circular fiber-reinforced polymer tubes." *ACI Struct. J.*, 98(4), 451–461.

Fam, A. Z., Schnerch, D., and Rizkalla, S. (2005). "Rectangular filament wound GFRP tubes filled with concrete under flexural and axial loading: Experimental investigation." *J. Compos. Construct.*, 9(1), 25–33.

Hadi, M. N. S. (2006). "Behavior of FRP wrapped normal strength concrete columns under eccentric loading." *J. Compos. Struct.*, 72(4), 503–511.

Han, L. H., Tao, Z., Liao, F. Y., and Xu, Y. (2010). "Tests on cyclic performance of FRP-concrete-steel double-skin tubular columns." *Thin-Walled Struct.*, 48(6), 430–439.

Idris, Y., and Ozbakkaloglu, T. (2013). "Seismic behavior of high-strength concrete-filled FRP tube columns." *J. Compos. Construct.*, 17(6), 04013013.

Ilki, A., Peker, O., Karamuk, E., Demir, C., and Kumbasar, N. (2008). “FRP retrofit of low and medium strength circular and rectangular reinforced concrete columns.” *J. Mater. Civ. Eng.*, 20(2), 169–188.

Lam, L., and Teng, J. G. (2004). “Ultimate condition of fiber reinforced polymer-confined concrete.” *J. Compos. Construct.*, 8(6), 539–548.

Mirmiran, A., Shahawy, M., Samaan, M., El Echary, H., Mastrapa, J. C., and Pico, O. (1998). “Effect of column parameters on FRP-confined concrete.” *J. Compos. Construct.*, 2(4), 175–185.

Mohamed, H., and Masmoudi, R. (2010). “Axial load capacity of concrete-filled FRP tube columns: Experimental versus predictions.” *J. Compos. Construct.*, 14(2), 231–243.

Ozbakkaloglu, T. (2013a). “Axial compressive behavior of square and rectangular high-strength concrete-filled FRP tubes.” *J. Compos. Construct.*, 17(1), 151–161.

Ozbakkaloglu, T. (2013b). “Compressive behavior of concrete-filled FRP tube columns: Assessment of critical column parameters.” *Eng. Struct.*, 51, 151–161.

Ozbakkaloglu, T. (2013c). “Concrete-filled FRP tubes: Manufacture and testing of new forms designed for improved performance.” *J. Compos. Construct.*, 17(2), 280–291.

Ozbakkaloglu, T., and Akin, E. (2012). “Behavior of FRP confined normal-and high-strength concrete under cyclic axial compression.” *J. Compos. Construct.*, 16(4), 451–463.

Ozbakkaloglu, T., and Oehlers, D. J. (2008a). “Concrete-filled square and rectangular FRP tubes under axial compression.” *J. Compos. Construct.*, 12(4), 469–477.

Ozbakkaloglu, T., and Oehlers, D. J. (2008b). “Manufacture and testing of a novel FRP tube confinement system.” *Eng. Struct.*, 30(9), 2448–2459.

Ozbakkaloglu, T., and Saatcioglu, M. (2006). "Seismic behavior of high strength concrete columns confined by fiber-reinforced polymer tubes." *J. Compos. Construct.*, 10(6), 538–549.

Ozbakkaloglu, T., and Saatcioglu, M. (2007). "Seismic performance of square high-strength concrete columns in FRP stay-in-place formwork." *J. Struct. Eng.*, 133(1), 44–56.

Ozcan, O., Binici, B., and Ozcebe, G. (2010). "Seismic strengthening of rectangular reinforced concrete columns using fiber reinforced polymers." *Eng. Struct.*, 32(4), 964–973.

Rochette, P., and Labossiere, P. (2000). "Axial testing of rectangular column models confined with composites." *J. Compos. Construct.*, 4(3), 129–136.

Seible, F., Burgueño, R., Abdallah, M. G., and Nuismer, R. (1996). "Development of advanced composite carbon shell systems for concrete columns in seismic zones." *Proc., 11th World Conf. Earthquake Eng.*, Pergamon, Elsevier Science, Oxford.

Shao, Y., and Mirmiran, A. (2005). "Experimental investigation of cyclic behavior of concrete-filled FRP tubes." *J. Compos. Construct.*, 9(3), 263–273.

Tasdemir, M. A., Tasdemir, C., Jefferson, A. D., Lydon, F. D., and Barr, B. I. G. (1998). "Evaluation of strains at peak stresses in concrete: A three phase composite model approach." *Cement Concr. Res.*, 20(4), 301–318.

Teng, J. G., Yu, T., and Wong, Y. L. (2004). "Behavior of hybrid FRP-concrete-steel double-skin tubular columns." *2nd Int. Conf. on FRP Composites in Civil Engineering-CICE 2004*, A. A. Balkema, Leiden, The Netherlands, 811–818.

Teng, J. G., Yu, T., and Wong, Y. L. (2010). "Hybrid FRP-concrete-steel double-skin tubular structural members." *Proc., 5th Int. Conf. on FRP Composites in Civil Engineering*, Springer, Berlin, Heidelberg, 26–32.

Teng, J. G., Yu, T., Wong, Y. L., and Dong, S. L. (2005). "Innovative FRP-steel-concrete hybrid columns." *4th Int. Conf. on Advance in Steel Structure*, Elsevier, Oxford, UK, 545–554.

Teng, J. G., Yu, T., Wong, Y. L., and Dong, S. L. (2007). "Hybrid FRP concrete steel tubular columns: Concept and behavior." *Construct. Build. Mater*., 21(4), 846–854.

Wang, Z. Y., Wang, D. Y., Smith, S. T., and Lu, D. G. (2012). "CFRP confined square RC columns. I: Experimental investigation." *J. Compos. Construct*., 16(2), 150–160.

Wong, Y. L., Yu, T., Teng, J. G., and Dong, S. L. (2008). "Behavior of FRP-confined concrete in annular section columns." *Compos., Part B*, 39(3), 451–466.

Wu, Y. F., and Wei, Y. Y. (2010). "Effect of cross-sectional aspect ratio on the strength of CFRP-confined rectangular concrete columns." *Eng. Struct*., 32(1), 32–45.

Xie, P., Yu, T., Wong, Y. L., and Teng, J. G. (2011). "Compressive behavior of large scale hybrid FRP concrete steel double skin tubular columns." *Adv. Mater. Res*., 243–249, 1138–1144.

Yu, T., and Teng, J. G. (2010). "Hybrid FRP concrete-steel double-skin tubular columns with a square outer and a circular inner tube: stub column tests." *13th Int. Symp. on Tubular Structures*, CRC Press/Balkema, 629–636.

Yu, T., Wong, Y. L., and Teng, J. G. (2010). "Behavior of hybrid FRP-concrete-steel double-skin tubular columns subjected to eccentric compression." *Adv. Struct. Eng*., 13(5), 961–974.

Yu, T., Wong, Y. L., Teng, J. G., Dong, S. L., and Lam, E. S. S. (2006). "Flexural behavior of hybrid FRP-concrete-steel double-skin tubular members." *J. Compos. Construct*., 10(5), 443–452.

Paper 2 Compressive Behavior of Aramid FRP-Concrete-Steel Double-Skin Tubular Columns

Butje Alfonsius Louk Fanggi and Togay Ozbakkaloglu

School of Civil, Environmental, and Mining Engineering, University of Adelaide, 5000

Journal of Construction and Building Materials (Published)

Statement of Authorship

Title of Paper	Compressive Behavior of Aramid FRP-Concrete-Steel Double-Skin Tubular Columns
Publication Status	● Published ○ Accepted for publication ○ Submitted for publication ○ Publication style
Publication Details	Louk Fanggi, B.A., and Ozbakkaloglu, T. (2013). "Compressive behavior of aramid FRP-HSC-steel double-skin tubular columns." *Construction and Building Materials*. 48: 554-565.

Author Contributions

By signing the Statement of Authorship, each author certifies that their stated contribution to the publication is accurate and that permission is granted for the publication to be included in the candidate's thesis.

Name of Principal Author (Candidate)	Butje Alfonsius Louk Fanggi		
Contribution to the Paper	Review of literature, analysis data, and preparation of manuscript		
Signature		Date	28/07/2015

Name of Co-Author	Dr. Togay Ozbakkaloglu		
Contribution to the Paper	Research supervision and review of manuscript		
Signature		Date	28/07/2015

COMPRESSIVE BEHAVIOR OF ARAMID FRP-HSC-STEEL DOUBLE-SKIN TUBULAR COLUMNS

Butje Alfonsius LOUK FANGGI [1] and Togay OZBAKKALOGLU [2]

ABSTRACT

This paper presents the results of an experimental study on the behavior of fiber reinforced polymer (FRP)-concrete-steel double-skin tubular columns (DSTCs) under concentric compression. Influence of column parameters was investigated experimentally through the test of 16 normal- and high-strength concrete-filled DSTCs and six concrete-filled FRP tubes (CFFTs). The column parameters examined included the thickness of FRP tube; the concrete strength; the diameter, thickness, and shape of inner steel tube. The results of the experimental study show that concrete in a DSTC system is confined effectively by FRP and steel tubes. Both the normal- and high-strength concrete DSTCs tested in the present study exhibited a highly ductile compressive behavior. The results also show that increasing the inner steel tube diameter leads to an increase in the ultimate axial stress and strain of concrete in DSTCs. It is found that, for a given nominal confinement ratio, an increase in the concrete strength results in a decrease in the ultimate axial strain of DSTCs. It is also observed that DSTCs with square inner steel tube confined concrete ineffectively. In addition, it is found that concrete in DSTCs developed similar ultimate axial stresses but higher ultimate axial strains compared to concrete in companion CFFTs. The results of the present study and those from the previously reported studies are then compared with the only existing stress-strain model proposed for DSTCs. Finally, a new design-oriented

[1] PhD Candidate, School of Civil, Environmental and Mining Engineering University of Adelaide, Australia.
[2] (Corresponding author) Senior Lecturer, School of Civil, Environmental and Mining Engineering, University of Adelaide, Australia. Tel : + 618 8303 6477; Fax : +618 8303 4359; Email: togay.ozbakkaloglu@adelaide.edu.au

model that provides improved predictions of the ultimate conditions of concrete in DSTCs was proposed.

KEYWORDS: Fiber reinforced polymer (FRP); Concrete; High-strength concrete (HSC); Confinement; Composite Columns; Stress-strain relations; FRP tubes; Steel tubes; DSTCs.

1. INTRODUCTION

As was demonstrated in a recent review study [1], confinement of concrete with fiber reinforced polymer (FRP) composites has received a great deal of attention over the last two decades. A large number of experimental studies that have been reported on the axial compressive behavior of FRP-wrapped concrete specimens (e.g., [2-10]) and concrete-filled FRP tubes (CFFTs) (e.g. [11-22]) have demonstrated the effectiveness of FRP confinement in increasing the axial deformation capacity of concrete.

More recently, Teng et al. [23] proposed a new type of composite system in the form of FRP-concrete-steel double-skin tubular columns (DSTCs). This composite system consists of a steel tube inside, an FRP tube outside with concrete in between, and it produces high-performance structural members by combining the advantages of all three materials. A series of axial compression and flexure tests have been conducted by the research group lead by Teng [24-31] to investigate the performance of FRP-concrete-steel DST stub columns and beams. Following these studies, Han et al. [32] reported on the tests of eight DST beam-columns and Zhang et al. [33] reported on the tests of six DST columns that were tested under combined axial compression and lateral cyclic loading. The results of these early tests have demonstrated that the DST beam and column systems provide very effective confinement to concrete, which in turn leads to a highly ductile member behavior. These studies have also demonstrated that the

behavior of DSTCs is different from previously studied column forms, including CFFTs, concrete-filled steel tubes (CFSTs), and concrete filled steel double-skin tubes (CFSDS).

During the last two decades, the popularity of high-strength concrete (HSC) in the construction industry has been undergoing a steady growth due to the superior performance and economy offered by the material over normal-strength concrete (NSC) in a large number of structural engineering applications. The use of high-strength concrete in the construction of new composite columns such as CFFTs and DSTCs is particularly attractive because, as was demonstrated in recent studies [34-36], the combination of these high-strength materials results in high-performance structural members. However, the existing studies on DSTCs have so far focused on NSC, and only two studies have been reported to date on the axial compressive behavior of HSC DSTCs [28, 37]. Additional experimental studies are required to better understand and be able to model the compressive behavior of HSC DSTCs.

To contribute towards this end, this paper presents the results of an experimental program that was aimed at investigating the influence of critical columns parameters on the compressive behavior of HSC DSTCs manufactured with aramid FRP tubes. The results of the experimental program are first presented and followed by a discussion on the influence of the key parameters on the performance of the DSTCs.

2. EXPERIMENTAL PROGRAM

2.1 Test Specimens and Materials

A total of 16 DSTCs with circular external FRP tubes and circular or square internal steel tubes were prepared and tested under axial compression. In addition, six companion CFFTs were also manufactured and tested under the same conditions to establish relative performance of DSTCs with respect to CFFTs. The specimens had a

diameter of 152.5 mm, measured at the concrete core, and a height of 305 mm. The test parameters included the FRP thickness, concrete strength, and diameter, thickness and shape of the inner steel tube. Two nominally identical specimens were tested in the case of DSTCs and 3 identical specimens were tested in the case CFFTs for each unique specimen configuration. Details of the specimens are shown in *Table 1*.

DSTCs 1 to 8 were designed to investigate the effect of different FRP types, FRP thickness, and concrete strength. The diameter and thickness of the inner steel tubes of these specimens were 88.9 mm and 3.2 mm, respectively. To study the influence of FRP type, DSTCs 1 and 2 were manufactured using carbon FRP (CFRP), and the companion specimens, DSTCs 3 and 4, were manufactured using aramid FRP (AFRP). To study the influence of FRP tube thickness DSTCs 5 and 6, which were companion to DSTCs 3 and 4, were manufactured using 4 layers of AFRP. To study the influence of concrete strength, DSTCs 7 and 8 were manufactured using NSC as companions to HSC DSTCs 3 and 4. In addition, DSTCs 9 to 16 were designed to investigate the effect of steel tube parameters, namely the diameter, thickness, and shape. The thickness of the FRP tube and the concrete grade was kept constant in all of these specimens. Finally, 3 NSC and 3 HSC CFFTs were designed as companions to the DSTCs to establish the relative performance levels of DSTCs compared to CFFTs.

The specimens were prepared using NSC and HSC mixes with 49.8 MPa and 113.8 MPa average unconfined concrete compressive strengths that were attained during the period of testing. Both mixes consisted of crushed bluestone as the coarse aggregate, with a nominal maximum size of 10 mm. Silica fume was added to the HSC mix at 8% of the binder content by weight. The unconfined concrete strengths (f'_{co}) of the specimens at the day of testing are reported together with the corresponding axial strains

ε_{co} in *Table 1*. The ε_{co} values were established using the expression given by Tasdemir et al. [38].

Table 1. Details of test specimens

Specimen	Number of FRP layers	Strength of concrete, f'_{co} (MPa)	Strain at peak stress, $\mathcal{E}_{co}$ (%)	Steel tube diameter, D_s (mm)	Steel tube thickness, t_s (mm)	Steel tube section	Type of FRP
DSTC-1 DSTC-2	6	113.8	0.36	88.9	3.2	Circular	CFRP
DSTC-3 DSTC-4	4	113.8	0.36	88.9	3.2	Circular	AFRP
DSTC-5 DSTC-6	6	113.8	0.36	88.9	3.2	Circular	AFRP
DSTC-7 DSTC-8	3	49.8	0.24	88.9	3.2	Circular	AFRP
DSTC-9 DSTC-10	6	113.8	0.36	60.3	3.6	Circular	AFRP
DSTC-11 DSTC-12	6	113.8	0.36	88.9	5.5	Circular	AFRP
DSTC-13 DSTC-14	6	113.8	0.36	114.3	6.02	Circular	AFRP
DSTC-15 DSTC-16	6	113.8	0.36	89	3.5	Square	AFRP
CFFT-1 CFFT-2 CFFT-3	3	49.4	0.24	-	-	-	AFRP
CFFT-4 CFFT-5 CFFT-6	6	113.4	0.36	-	-	-	AFRP

In designing the FRP tubes, due consideration was given to the well-understood influence of the strength of concrete on its confinement demand [35 - 36]. This was done through the use of nominal confinement ratio (f_l /f'_{co}), calculated from Eq.1 assuming a uniform confinement distribution, as the performance criterion in establishing relative confinement levels of DSTCs with different concrete strengths.

$$\frac{f_l}{f'_{co}} = \frac{2E_f t_f \varepsilon_f}{D_f f'_c} \quad (1)$$

where, f_l is the confining pressure, E_f is the modulus of elasticity, t_f is the total nominal thickness and ε_f is the ultimate tensile strain of the fibers, and D_f is the internal diameter of the FRP tube.

Table 2. Measured properties of steel tubes

D_s (mm)	t_s (mm)	Grade (MPa)	Height (mm)	Peak axial load (kN)	Yield stress (MPa)	Peak stress (MPa)	Axial strain at peak (%)	Failure mode *
88.9	3.2	350	305	345.6	314.2	387.9	2.02	EF
60.3	3.6	350	305	337.0	459.4	526.4	2.85	G
88.9	5.5	350	305	710.6	407.7	493.1	3.06	EF
114.3	6.02	350	305	858.4	342.3	419.0	2.93	EF
89	3.5	350	305	539.9	461.8	491.6	0.80	L

Note: * EF= Elephant foot buckling, G= Global buckling, L=Local buckling

To establish the material properties of the steel tubes used in the DSTCs, axial compression tests were conducted on hollow steel tubes. The results of these tests are shown in *Table 2*. For each steel tube type three hollow tubes having the same height as the DSTC specimens were tested. As noted in *Table 2*, the 88.9-mm and 114.3-mm diameter steel tubes failed due to localized elephant foot buckling either at the top or the bottom of the specimen. On the other hand, the 60.3-mm diameter and the square steel tubes failed due to global and local buckling, respectively.

2.2 Specimen Preparation

The FRP tubes were formed using a manual wet lay-up process by wrapping epoxy resin impregnated carbon fiber sheets around precision-cut high-density styrofoam templates in the hoop direction. FRP sheets were provided with a 150 mm overlap to

prevent premature debonding failure. The FRP tubes with three layers of FRP were wrapped with a single FRP sheet continuously, whereas the tubes with four and six layers of FRP were wrapped by two FRP sheets, and therefore had two overlap regions. In these tubes the two overlaps were provided along the same region around the circumference of the tube. A thin polyester film was placed on the surface of the Styrofoam template to prevent bonding between the FRP tube and the template to allow easy removal of the template after the resin had dried. The properties of the unidirectional fibers sheets used in the manufacture of the FRP tubes are provided in *Table 3*. Both the manufacturer supplied properties and the ones obtained from the flat coupon test are provided in the table.

Table 3. Properties of fibers sheets used in test specimens

Type	Nominal thickness t_f (mm/ply)	Provided by manufacturers			Obtained from flat FRP coupon tests		
		Tensile strength f_f (MPa)	Ultimate tensile strain, ε_f (%)	Elastic modulus E_f (GPa)	Tensile strength f_{frp} (MPa)	Ultimate tensile strain, ε_{frp} (%)	Elastic modulus E_{frp} (GPa)
Aramid	0.200	2900	2.50	116.0	2663	2.12	125.7
Carbon	0.117	3800	1.55	240.0	3626	1.44	251.0

A formwork system was developed and used to support the tubes during the process of concrete pouring to ensure the FRP and steel tubes remained concentric. At the base, wooden spacers were used to hold the bottom of the FRP tube in place and nails were used to maintain the position of the steel tube relative to the FRP tube. At the top, a cap with three steel arms was used to maintain the position of the two tubes concentrically. Alignment was maintained by anchoring the top cap to the wooden base. The formwork is illustrated in *Fig.1*.

Figure 1. DSTC specimens before concrete pouring

2.3 Instrumentation and testing

For each specimens, four linear variable displacement transducers (LVDTs) were used to measure axial deformations of the specimens, which were mounted at the corners between the loading and supporting steel plates of the compression test machine, as shown in *Fig.2*. The recorded deformations were used in the calculation of the average axial strains along the height of the specimens. Four inner cage LVDTs were also placed in mid-height of the specimens to measure deformation of the middle part of 170 mm. In addition, FRP tubes of the specimens were instrumented at the mid-height with two unidirectional strain gauges with a gauge length of 20 mm to measure axial strains, which were used to validate LVDT measurements at the early stages of loading. FRP tube lateral strains were measured by three unidirectional strain gauges with 20-mm gauge lengths that were spaced equally around the perimeter at the mid-height of the specimen outside the overlap region. Axial and lateral strains of inner steel tubes were measured at the mid-height by two axially and two laterally oriented strain gauges with 5-mm gauge lengths.

The specimens were tested under concentric axial compression using a 5,000-kN capacity universal testing machine. During the initial elastic stage of the behavior, the loading was applied with load control at 3 kN per second, whereas displacement control was used at approximately 0.003 mm per second beyond the initial softening until specimen failure. Prior to testing, all specimens were capped at both ends to ensure uniform distribution of the applied pressure, and the load was applied only to the concrete core and inner steel tube through precision-cut high-strength steel loading discs placed at each end of the specimens. A data logger system was used to record strains, loads, and displacements of the test specimens simultaneously.

Figure 2. Test setup and instrumentation

3. TEST RESULTS

3.1 Failure modes

All of the specimens failed by rupture of the FRP tube in the hoop direction. The rupture of the FRP tubes was often localized and corresponded to the location of significant steel tube deformation inside the specimen. The failure modes of the specimens and locations of FRP rupture corresponding to regions of significant steel tube deformation are summarized in *Table 4*. DSTCs 1 and 2 experienced an early

failure due to elephant foot buckling of their inner steel tubes, which occurred at a lower axial deformation. These specimens are excluded from the discussions presented in the following sections.

Table 4. Failure modes of steel tubes in DSTCs

Specimen	D_s (mm)	t_s (mm)	Steel tube failure		FRP tube failure location
			Mode	Location	
DSTC-1	88.9	3.2	EF	Top	Top
DSTC-2			EF	Top	Top
DSTC-3	88.9	3.2	Rippling	Top & bottom	Top
DSTC-4			Rippling	Top & bottom	Middle
DSTC-5	88.9	3.2	Rippling	Top & bottom	Top
DSTC-6			Rippling	Global	Top half
DSTC-7	88.9	3.2	Rippling	Top & bottom	Top
DSTC-8			Rippling	Top & bottom	Top
DSTC-9	60.3	3.6	Rippling	Top & bottom	Top
DSTC-10			Rippling	Top	Top
DSTC-11	88.9	5.5	NA	NA	Middle
DSTC-12			Rippling	Top	Top
DSTC-13	114.3	6.02	Rippling	Top	Middle
DSTC-14			Rippling	N.A	Top
DSTC-15	89.0	3.5	L	Top	Top
DSTC-16			L	Top	Top

Note: * EF= Elephant foot buckling, G= global buckling, L= local buckling, NA= no observed deformation

3.2 Axial load capacities

Experimentally recorded axial load capacities of the DSTCs (P_T) are presented in *Table 5* together with axial capacities of the steel tubes (P_s), and unconfined concrete (P_{co}). The axial load capacities of the steel tubes (P_s) were determined from hollow steel tube tests, whereas the axial load capacities of unconfined concrete (P_{co}) were obtained by multiplying unconfined concrete strength by the area of the concrete cross-section. As evident from the $P_T/(P_s+P_{co})$ ratios shown in *Table 5*, except for DSTCs 1 and 2 that failed as a result of elephant foot buckling, the DSTCs with circular inner steel tubes developed significantly higher axial load capacities than the combined axial load

capacity of the unconfined concrete and steel tube, except DSTCs 15 and 16. On the other hand, DSTCs 15 and 16 that were manufactured with square inner steel tube developed a slightly lower axial load capacity than the combined axial load capacity of the unconfined concrete and steel tube.

Table 5. Axial load capacities of DSTCs

Specimen	Ultimate load of DSTC, P_T (kN)	Average P_T (kN)	Ultimate load of steel tube, P_s (kN)	Ultimate load of unconfined concrete section, P_{co} (kN)	$P_{s+}P_{co}$ (kN)	$P_{T/(}P_{s+}$ $P_{co)}$	$P_{cc/}P_{co}$
DSTC-1	1,624	1,623	346	1,372	1,718	0.94	0.93
DSTC-2	1,622						
DSTC-3	1,919	1,942	346	1,372	1,718	1.13	1.16
DSTC-4	1,965						
DSTC-5	2,247	2,249	346	1,372	1,718	1.31	1.39
DSTC-6	2,251						
DSTC-7	1,664	1,616	346	601	946	1.71	2.12
DSTC-8	1,567						
DSTC-9	2,745	2,764	337	1,754	2,091	1.32	1.39
DSTC-10	2,783						
DSTC-11	2,843	2,845	711	1,372	2,083	1.37	1.56
DSTC-12	2,846						
DSTC-13	2,331	2,279	858	911	1769	1.29	1.56
DSTC-14	2,228						
DSTC-15	1,482	1,414	540	1,177	1,717	0.82	0.74
DSTC-16	1,346						

3.3 Behavior of inner steel tube in DSTCs

Tables 2 and *4* provide the failure modes of hollow steel tubes and steel tubes in DSTCs, respectively. As indicated in these tables, the compressive behavior of the steel tubes inside the DSTCs was observed to be different from the behavior of hollow steel tubes in DSTCs, except for DSTCs 15 and 16. Just like the square hollow steel tubes, square inner steel tubes of DSTCs 15 and 16 experienced local buckling. A similar observation that the compressive behavior of the steel tubes inside the DSTCs was observed to be

different from the behavior of hollow steel tubes was also reported in Wong et al. [27] and Ozbakkaloglu and Louk Fanggi [37].

The FRP tube rupture locations corresponded to the regions of significant deformation on the steel tube as mentioned early. *Table 4* shows the location of FRP tube rupture corresponded to the location of significant deformation on the steel tube. As can be seen in *Table 4*, there are some differences in FRP tube rupture locations for two nominally identical specimens. For instance FRP tubes of companion specimens DSTCs 3 and 4 ruptured at different locations. The difference in the FRP tube rupture locations of these nominally identical specimens is believed to be caused by the sensitivity of the steel tubes to disturbances caused by the movement of surrounding concrete and that of the FRP tubes to slight imperfections. Similar observations were previously reported by Wong et al. [27] and Ozbakkaloglu and Louk Fanggi [37].

3.4 Axial stress-strain behavior of concrete inside DSTCs and CFFTs

The axial stress on the concrete inside the DSTCs was calculated by dividing the axial load resisted by the concrete (P_C) with the cross sectional area of the concrete section. The load applied to the concrete was determined by subtracting the axial load resisted by the steel tube (P_S) for a given axial strain from the total load resisted by the DSTC (P_T) at the same axial strain. The load acting on the steel tube was calculated by assuming that the load-strain behavior of the steel tubes inside a DSTC is similar to the load-strain behavior of the corresponding unconfined hollow steel tube obtained from a compression test. The ultimate axial stress (f'_{cu}) and strain (ε_{cu}) of the concrete inside the DSTCs reported in *Table 6* were calculated using the approach summarized in this section. For specimens exhibiting stress-strain curves with ascending second branches the compressive strength (f'_{cc}) corresponds to the ultimate axial stress (f'_{cu}), and in this

paper, the terms compressive strength (f'_{cc}) and strength enhancement ratio (f'_{cc}/f'_{co}) are used consistently in the discussions of the ultimate conditions of these specimens.

Table 6. Ultimate condition of concrete in DSTCs

Specimen	f_l/f'_{co}	f'_{cu} (MPa)	Avg. f'_{cu} (MPa)	f'_{cu}/f'_{co}	ε_{cu} (%)	Avg. ε_{cu} (%)	Avg. $\varepsilon_{cu}/\varepsilon_{co}$	$\varepsilon_{h,rup}$	Avg. $\varepsilon_{h,rup}$
DSTC-1*	0.31	109.3	109.5	0.96	0.86	0.87	2.42	0.10	0.10
DSTC-2*	0.31	109.8			0.88			0.10	
DSTC-3	0.27	130.6	132.4	1.16	2.89	2.90	8.09	1.39	1.37
DSTC-4	0.27	134.3			2.92			1.35	
DSTC-5	0.40	157.7	158.0	1.39	2.94	3.02	8.41	1.77	1.55
DSTC-6	0.40	158.3			3.10			1.32	
DSTC-7	0.46	109.4	105.3	2.12	4.22	4.01	16.88	1.83	1.73
DSTC-8	0.46	101.3			3.80			1.63	
DSTC-9	0.40	156.4	157.7	1.39	2.41	2.27	6.33	1.30	1.23
DSTC-10	0.40	159.0			2.13			1.15	
DSTC-11	0.40	176.8	177.0	1.56	3.21	3.09	8.60	1.26	1.27
DSTC-12	0.40	177.2			2.96			1.27	
DSTC-13	0.40	184.0	177.6	1.56	3.33	3.22	8.97	1.44	1.31
DSTC-14	0.40	171.2			3.11			1.18	
DSTC-15	0.40	91.1	84.5	0.74	1.96	1.93	5.37	NA**	0.08
DSTC-16	0.40	78.0			1.89			0.08	

*elephant foot buckling failure

**not recorded due to an instrumentation problem

Figures 3 and *4* present the stress-strain relationships of the concrete inside the DSTCs and CFFTs, respectively. As evident from *Figs. 3 and 4*, except for DSTCs 15 and 16 that were made of square inner steel tube, the specimens of the present study exhibited almost monotonically ascending stress-strain curves, indicating that the concrete was effectively confined. It can also be observed in *Figs. 3 and 4* that some of the specimens experienced a sudden drop in strength after the transition point between the initial ascending branch and the second branch that follows it. A similar behavior was previously observed in HSC-filled FRP tubes [19, 39, 40] and it can be attributed to the brittle nature of the high-strength concrete. As expected, the stress-strain behavior of the specimens along the second branch of the curve is influenced by the column parameters

of the DSTCs, including thickness of FRP tube; the concrete strength; diameter, thickness, and shape of inner steel tube. The influence of these parameters on the stress-strain behavior of DSTCs is discussed in the following sections on the basis of the results of the present study and those previously reported in Wong et al. [27] and Ozbakkaloglu and Louk Fanggi [37].

Table 7. Influence of FRP thickness

Source	Specimen	FRP type	D_s/t_s (mm)	f'_{co} (MPa)	f_l/f'_{co}	f'_{cc} (MPa)	f'_{cc}/f'_{co}	ε_{cu} (%)	$\varepsilon_{cu}/\varepsilon_{co}$
Present study	DSTC-3	AFRP	88.9/3.2	113.8	0.27	132.5	1.16	2.90	8.09
	DSTC-4								
	DSTC-5	AFRP	88.9/3.2	113.8	0.40	158.0	1.39	3.02	8.41
	DSTC-6								
Wong et al. [27]	D40-B1-I	GFRP	76.0/3.3	39.6	0.11	40.8	1.03	1.45	5.53
	D40-B1-II								
	D40-B2-I	GFRP	76.0/3.3	39.6	0.22	55.6	1.40	2.02	7.69
	D40-B2-II								
	D40-B3-1	GFRP	76.0/3.3	39.6	0.33	68.2	1.72	2.35	8.96
	D40-B3-II								
	D37-C1-I	GFRP	88.0/2.1	36.9	0.11	42.2	1.14	1.50	5.71
	D37-C1-II								
	D37-C2-I	GFRP	88.0/2.1	36.9	0.22	54.4	1.48	2.12	8.07
	D37-C2-II								
	D37-C3-I	GFRP	88.0/2.1	36.9	0.33	69.3	1.88	2.59	9.89
	D37-C3-II								
Ozbakkaloglu and Louk Fanggi [37]	DSTC-1	CFRP	101.6/3.2	37.0	0.32	60.4	1.63	2.63	12.72
	DSTC-2								
	DSTC-9	CFRP	101.6/3.2	37.0	0.96	116.6	3.15	5.09	24.62
	DSTC-10								

4. DISCUSSION

4.1 Effect of FRP tube thickness

To illustrate the influence of FRP thickness on the compressive strength (f'_{cc}) and ultimate axial strain (ε_{cu}), *Table 7* presents the relevant results of the present study together with those from CFRP-confined DSTCs reported in Ozbakkaloglu and Louk

Fanggi [37] and glass FRP (GFRP)-confined DSTCs reported in Wong et al. [27]. All the specimens had a nominal diameter of 150 mm and a height of 300 mm. It can be seen from *Table 7* that, as expected, increasing FRP thickness from 4 to 6 layers leads to an increase in both f'_{cc} and ε_{cu}. It should be noted, however, that the increase in axial strain was lower than anticipated. Similar observations on the influence of FRP tube thickness can also be made from the results of Wong et al. [27] and Ozbakkaloglu and Louk Fanggi [37].

4.2 Effect of concrete strength

As can be seen in *Table 8*, the companion NSC and HSC DSTCs in this present study were designed to have similar levels of confinement, which was established through the use of the nominal confinement ratio (f_l/f'_{co}). This enabled the investigation of the influence of concrete strength through the comparison of the compressive behavior of DSTCs with similar confinement levels at different concrete strengths. In calculating f_l, it was assumed that the confining pressure was uniform and the section was treated as a solid section, ignoring the influence of the inner void when applicable.

Table 8 presents the influence of concrete strength (f'_{co}) on the compressive strength (f'_{cc}) and ultimate axial strain (ε_{cu}) of the specimens of the present study, together with those from Ozbakkaloglu and Louk Fanggi [37]. It can be observed from *Table 8* that the NSC DSTCs developed higher strength and strain enhancement ratios (f'_{cc}/f'_{co}) and ($\varepsilon_{cu}/\varepsilon_{co}$) than HSC DSTCs. Similar observations can also be made from results of Ozbakkaloglu and Louk Fanggi [37], as presented in *Table 8*. Nevertheless, the results reported in *Table 8* indicate that HSC DSTCs can exhibit highly ductile behavior.

4.3 Effect of steel tube diameter

Table 9 illustrates the influence of inner steel tube diameter on f'_{cc} and ε_{cu}, as established through the results of the present and those reported in Wong et al. [27] and Ozbakkaloglu and Louk Fanggi [37]. The specimens of the present study that are included in this comparison (i.e., DSCTs 9-14) were designed to have similar D_s/t_s ratios. In addition to these specimens, DSTCs 5 and 6 were also included in *Table 9* for completeness. Comparison of the results of the specimens of the present study indicates that both f'_{cc} and ε_{cu} tend to increase with an increase in the steel tube diameter. Similar observation can be also made from results of Wong et al. [27] and Ozbakkaloglu and Louk Fanggi [37], which consistently show that DSTCs with larger steel tube diameters developed higher f'_{cc} and ε_{cu} than their companions. It is worthwhile noting that the specimens reported in *Table 9* cover three different types of FRP material (i.e. AFRP, CFRP, and GFRP) and a wide range of steel tube diameters.

Table 8. Influence of concrete strength, f'_{co}

Source	Specimen	FRP type	D_S/t_S (mm)	f'_{co} (Mpa)	f_l/f'_{co}	f'_{cc} (Mpa)	f'_{cc}/f'_{co}	ε_{cu} (%)	$\varepsilon_{cu}/\varepsilon_{co}$
Present study	DSTC-7	AFRP	88.9/3.2	49.8	0.46	105.3	2.12	4.01	16.88
	DSTC-8								
	DSTC-5	AFRP	88.9/3.2	113.8	0.40	158.0	1.39	3.02	8.41
	DSTC-6								
Ozbakkaloglu and Louk Fanggi [37]	DSTC-5	CFRP	76.1/3.2	36.9	0.32	47.3	1.28	1.87	9.03
	DSTC-6								
	DSTC-15	CFRP	76.1/3.2	105.8	0.33	128.8	1.22	1.64	4.72
	DSTC-16								

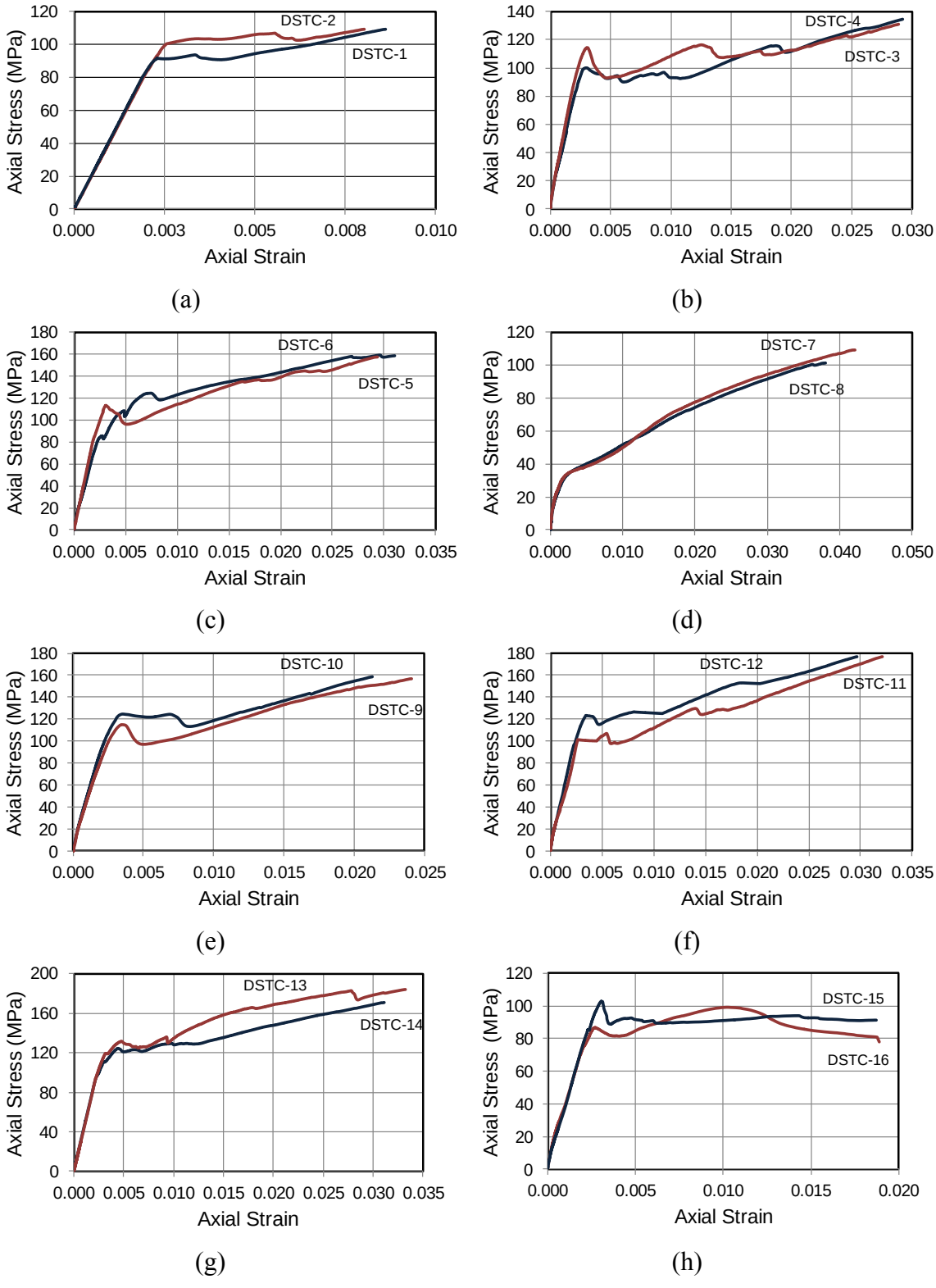

Figure 3. Axial stress-strain behavior of concrete in DSTCs: (a) 1&2, (b) 3&4, (c) 5&6, (d) 7&8, (e) 9&10, (f) 11&12, (g) 13&14, and (h) 15&16

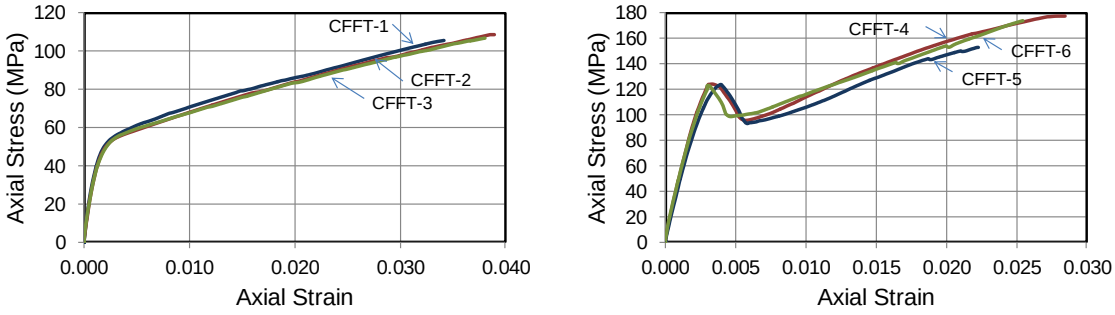

(a) (b)

Figure 4. Axial stress-strain behavior of concrete in CFFTs: (a) 1-3, (b) 4-6

4.4 Effect of steel tube thickness

Table 10 shows the influence of steel tube thickness on f'_{cc} and ε_{cu}, as established through the results of the present and those reported in Wong et al. [27] and Ozbakkaloglu and Louk Fanggi [37]. It can be seen in *Table 10* that increasing steel tube thickness from 3.2 mm in DSTCs 5 and 6 to 5.5 mm in DSTCs 11 and 12 lead to an increase in f'_{cc} and a slightly increase in ε_{cu}. This suggests that the increased stiffness of the inner steel tube results in an improvement on the compressive behavior of concrete in DSTCs. However, this observation is not supported with the one arises through the investigation of the results from Wong et al [27] and Ozbakkaloglu and Louk Fanggi [37]. The results of Wong et al. [27] suggest that ε_{cu} decreases slightly with an increase in steel tube thickness, and no clear influence of thickness is evident on f'_{cc}. The results of Ozbakkaloglu and Louk Fanggi [37] also points to a reduction in both f'_{cc} and ε_{cu} with an increase in tube thickness. It should be noted, however, that the DSTCs of Ozbakkaloglu and Louk Fanggi [37] had small inner steel tubes, and hence relative contribution of the steel tube parameters to the overall behavior of the DSTCs were low. The slight difference in the diameters of the companion specimens of Wong et al. [27] should also be noted. Nonetheless, the observations presented in this section indicate that no definitive conclusion can be drawn on the influence of steel tube

thickness on the compressive behavior of concrete in DSTCs, and further research is required to better understand this influence.

Table 9. Influence of steel tube diameter, D_s

Source	Specimen	FRP type	f'_{co} (MPa)	f_l/f'_{co}	D_s (mm)	t_s (mm)	f'_{cc} (Mpa)	f'_{cc}/f'_{co}	ε_{cu} (%)	$\varepsilon_{cu}/\varepsilon_{co}$
Present study	DSTC-9	AFRP	113.8	0.40	60.3	3.6	157.7	1.39	2.27	6.33
	DSTC-10									
	DSTC-5	AFRP	113.8	0.40	88.9	3.2	158.0	1.39	3.02	8.41
	DSTC-6									
	DSTC-11	AFRP	113.8	0.40	88.9	5.5	177.0	1.56	3.09	8.60
	DSTC-12									
	DSTC-13	AFRP	113.8	0.40	114.3	6.02	177.6	1.56	3.22	8.97
	DSTC-14									
Wong et al. [27]	D37-A2-I	GFRP	36.7	0.22	42	2.3	52.1	1.42	1.75	6.37
	D37-A2-II									
	D37-C2-I	GFRP	36.9	0.22	88	2.1	54.4	1.48	2.12	8.07
	D37-C2-II									
Ozbakkaloglu and Louk Fanggi [37]	DSTC-5	CFRP	36.9	0.32	76.1	3.2	47.3	1.28	1.87	9.03
	DSTC-6									
	DSTC-1	CFRP	37.0	0.32	101.6	3.2	60.4	1.63	2.63	12.72
	DSTC-2									
	DSTC-19	CFRP	106.2	0.33	38.1	3.2	117.6	1.11	1.52	4.38
	DSTC-20									
	DSTC-15	CFRP	105.8	0.33	76.1	3.2	128.8	1.22	1.64	4.72
	DSTC-16									

Table 10. Influence of steel tube thickness, t_s

Source	Specimen	FRP type	f'_{co} (MPa)	f_l/f'_{co}	D_s (mm)	t_s (mm)	f'_{cc} (MPa)	f'_{cc}/f'_{co}	ε_{cu} (%)	$\varepsilon_{cu}/\varepsilon_{co}$
Present study	DSTC-5	AFRP	113.8	0.40	88.9	3.2	158.0	1.39	3.02	8.41
	DSTC-6									
	DSTC-11	AFRP	113.8	0.40	88.9	5.5	177.0	1.56	3.09	8.60
	DSTC-12									
Wong et al. [27]	D37-C1-I	GFRP	36.9	0.11	88.0	2.1	42.2	1.14	1.50	5.71
	D37-C1-II									
	D40-B1-I	GFRP	39.6	0.11	76.0	3.3	40.8	1.03	1.45	5.53
	D40-B1-II									
	D37-C2-I	GFRP	36.9	0.22	88.0	2.1	54.4	1.48	2.12	8.07
	D37-C2-II									
	D40-B2-I	GFRP	39.6	0.22	76.0	3.3	55.6	1.40	2.02	7.69
	D40-B2-II									
	D37-C3-I	GFRP	36.9	0.33	88.0	2.1	69.3	1.88	2.59	9.89
	D37-C3-II									
	D40-B3-I	GFRP	39.6	0.33	76.0	3.3	68.2	1.72	2.35	8.96
	D40-B3-II									
Ozbakkaloglu and Louk Fanggi [37]	DSTC-21	CFRP	106.2	0.33	38.1	1.6	136.4	1.28	1.67	4.79
	DSTC-22									
	DSTC-19	CFRP	106.2	0.33	38.1	3.2	117.6	1.11	1.52	4.38
	DSTC-20									

4.5 Effect of inner steel tube shape

Figure 3(h) illustrates the stress-strain behavior of concrete inside the DSTCs with square inner steel tubes. It can be seen from the figure that concrete inside these DSTCs exhibited an overall descending second branch, which indicates that confinement efficiency of these DSTCs was lower than those at the DSTCs with circular inner tube. This is also evident from *Table 6* that the DSTCs with square inner steel tubes developed much lower f'_{cu} and ε_{cu} compared to the DSTCs with circular inner steel tube. This can be attributed to the ability of the circular tube to provide an internal restraint that prevents spalling or excessive expansion of concrete on the inner surface of the annular section. The square inner steel tube, on the other hand, is more prone to inward buckling, which results in loss of restraint for the inner surface of concrete annular

section along these regions. This in turn results in lower lateral resistant to concrete, which leads to reduce confinement efficiency of DSTC system.

4.6 Relative performance of DSTCs compared to CFFTs

Table 11 presents the comparison of the results from companion DSTCs and CFFTs. It can be seen from *Table 11* that NSC DSTCs developed similar f'_{cc} but significantly larger ε_{cu} than NSC CFFTs. Similar observation can also be made based on the results of the HSC specimens, except for DSTCs 9 and 10 with the smallest inner steel tube diameters, which developed similar f'_{cc} and ε_{cu} to the companion CFFTs. These observations indicate that the presence of the inner void does not compromise the performance of DSTCs; on the contrary, it has a beneficial influence on the axial deformation capacity of the composite system.

4.7 Comparison of DSTC test results with predictions of model by Yu et al. [44]

In this section, the results of the present study and those available from the literature (i.e. Wong et al. [27], Xie et al. [41], Ozbakkaloglu and Louk Fanggi [37], Albitar [42], and Ding et al. [43]) are compared with the predictions of the model by Yu et al. [44], which is the only existing stress-strain model of DSTCs. Because the database contained specimens with ultimate strains established using two different measurement methods (i.e. full-height LVDTs and mid-height LVTDs), the ultimate axial strains of the specimens in the database was scaled based on the relative values established in Ozbakkaloglu and Lim [45] to eliminate the influence of the measurement methods. In establishing the model predictions, the hoop strain reduction factor ($k_{\varepsilon,f}$) was taken as 0.630 and peak axial strain of unconfined concrete (ε_{co}) as 0.2% as recommended by the originators of the model. The details of the model can be found in the original paper, and hence are not discussed in this section. The accuracy and consistency of the model

were quantified using statistical indicators: the average absolute error (*AAE*), mean (*M*), and standard deviation (*SD*). The average absolute error (*AAE*), defined by Eq. (2), is used to establish the overall model accuracy. The mean (*M*), determined by Eq. (3), is used to describe the associated average overestimation or underestimation of the model, where an overestimation is represented by a mean value greater than 1. The standard deviation (*SD*), determined by Eq. (4), is used to establish the magnitude of the associated scatter for the model.

Table 11. Relative performance of DSTCs compared to CFFTs

Group	Column system	Specimen	f'_{co} (MPa)	D_s/t_s (mm)	f_l/f_{co}	f'_{cc} (MPa)	f'_{cc}/f'_{co}	ε_{cu} (%)	$\varepsilon_{cu}/\varepsilon_{co}$
NSC	DSTC	DSTC-7	49.8	88.9/3.2	0.46	105.3	2.12	4.01	16.88
		DSTC-8							
	CFFT	CFFT-1							
		CFFT-2	49.4	-	0.46	107.0	2.15	3.47	14.59
		CFFT-3							
HSC	DSTC	DSTC-5	113.8	88.9/3.2	0.40	158.0	1.39	3.02	8.41
		DSTC-6							
		DSTC-9	113.8	60.3/3.6	0.40	157.7	1.39	2.27	6.33
		DSTC-10							
		DSTC-11	113.8	88.9/5.5	0.40	177.0	1.56	3.09	8.60
		DSTC-12							
		DSTC-13	113.8	114.3/3.2	0.40	177.6	1.56	3.22	8.97
		DSTC-14							
	CFFT	CFFT-4							
		CFFT-5	113.4	-	0.40	166.6	1.47	2.44	6.80
		CFFT-6							

$$AAE = \frac{\sum_{i=1}^{n} \left| \frac{\mathrm{mod}_i - \exp_i}{\exp_i} \right|}{n} \tag{2}$$

$$M = \frac{\sum_{i=1}^{n} \left(\frac{\mathrm{mod}_i}{\exp_i} \right)}{n} \tag{3}$$

$$SD = \sqrt{\frac{\sum_{i=1}^{n}\left(\frac{\text{mod}_i}{\text{exp}_i} - \frac{\text{mod}_{avg}}{\text{exp}_{avg}}\right)^2}{n-1}} \quad (4)$$

where *mod* is the model prediction, *exp* is the experimental value, *n* is the total number of datasets and *avg* is the sample average.

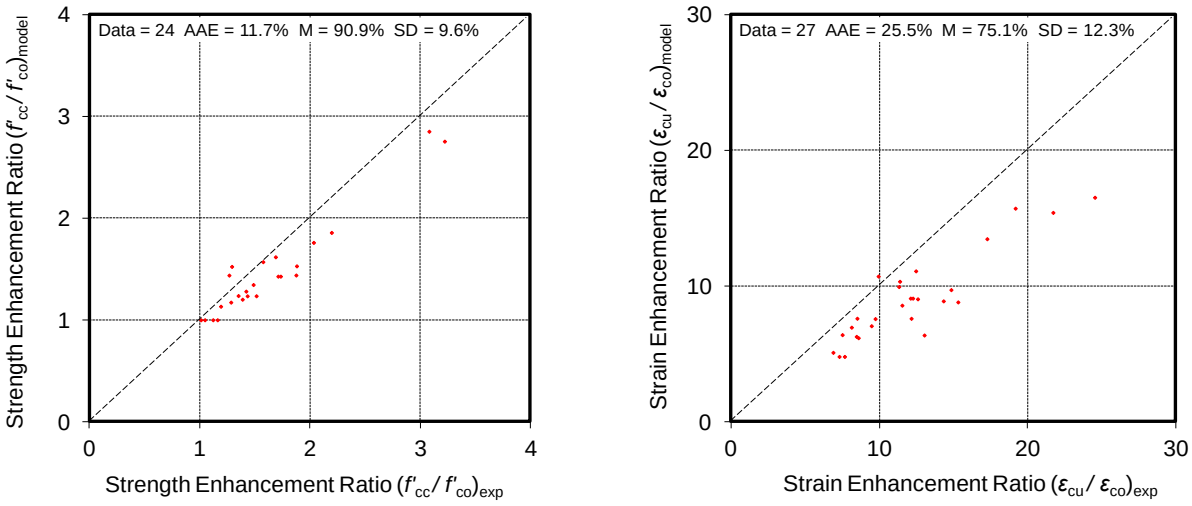

(a) (b)

Figure 5. Comparison of model predictions of Yu et al. [44] with experimental data from NSC DSTCs

Figures 5 and *6* show the distribution of model predictions across the full range of the axial strength and strain enhancement ratios (f'_{cc}/f'_{co} and $\varepsilon_{cu}/\varepsilon_{co}$) for NSC and HSC DSTCs, respectively. It can be seen from these figures that the model by Yu et al. [44] provides reasonably good predictions of the strength enhancement ratios, with a tendency to underestimate the compressive strength of NSC specimens and overestimate the strength of HSC specimens. On the other hand, as can be seen in *Figs.5 and 6*, the model significantly underestimates the strain enhancement ratios of both NSC and HSC DSTCs. This results in diminished model accuracy as evident from the higher AAE values in the prediction of the ultimate strains.

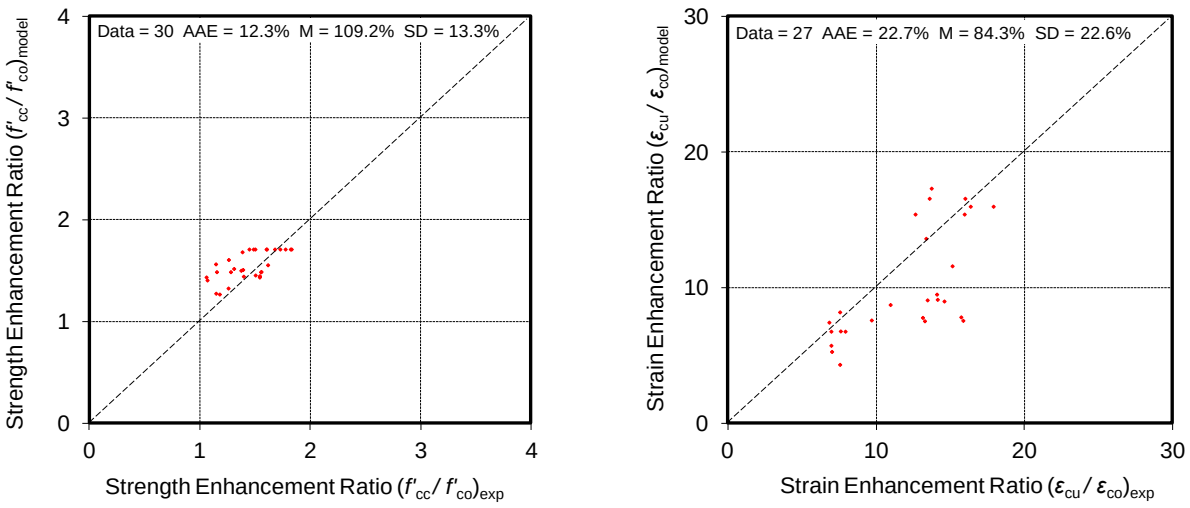

(a) (b)

Figure 6. Comparison of model predictions of Yu et al. [44] with experimental data from HSC DSTCs.

4.8 A new model for DSTCs

A new model to predict the ultimate conditions of concrete in DSTCs has been developed based on the complete database of tests results of DSTCs available in the literature and is presented in this section. This model is an extension of the model by Lim and Ozbakkaloglu [39], which was recently proposed for FRP-confined concrete with unconfined strengths up to 120 MPa. The following expressions are proposed for the prediction of the compressive strength (f'cc) and ultimate axial strain (εcu) of concrete in DSTCs.

$$f'_{cc} = c_1 f'_{co} + k_1 (f_{lu,a} - f_{lo}) \quad (5)$$

$$\varepsilon_{cu} = \left(c_2 \varepsilon_{co} + k_2 \left(\frac{K_1}{f'_{co}} \right)^{0.9} {\varepsilon_{h,rup}}^{1.35} \right) 1.28 \left(1 - \frac{D_s}{D} \right)^{-0.36} \quad (6)$$

where k_1 and k_2 respectively are the strength and strain enhancement ratios established specifically for each confinement method (i.e., FRP-wrapped concrete or CFFTs) and fiber type (e.g., carbon, glass or aramid) with average values recommended as k_1 = 3.2

and k_2 = 0.27. Based on marginal differences observed in the comparisons of the compressive strengths of the companion FRP-confined concrete and concrete in DSTCs, the expression proposed to predict the compressive strength of FRP-confined concrete in Lim and Ozbakkaloglu [39] (Eq. 5) is directly adopted here to predict the compressive strength of concrete in DSTCs. Based on the observation that the ultimate axial strains of concrete in DSTCs are consistently higher than those of FRP-confined concrete, and the difference in strain increases with an increase in the void ratio (D_s/D) of DSTCs, the equation given in Lim and Ozbakkaloglu [39] is modified to include the function $1.28\left(1-\frac{D_s}{D}\right)^{-0.36}$ and Eq.6 is proposed to predict the ultimate axial strain of concrete in DSTCs. In Eq. 6, c_2 is the concrete strength factor and is calculated from Eq. 7, and the void ratio (D_s/D) is the ratio between the inner diameter and the outer diameter of the annular concrete section. In the equation, the peak axial strain of unconfined concrete ε_{co} is to be determined using the expression proposed by Tasdemir et al. [38] (Eq. 8).

$$c_2 = 2 - \left(\frac{f'_{co} - 20}{100}\right) \text{ and } c_2 \geq 1 \tag{7}$$

$$\varepsilon_{co} = \left(-0.067 f'^{\,2}_{co} + 29.9 f'_{co} + 1053\right) \times 10^{-6} \tag{8}$$

To differentiate the specimens exhibiting stress-strain curves with ascending and descending second branches, a concept of confinement stiffness threshold introduced in Lim and Ozbakkaloglu [39] was adopted. The confinement stiffness threshold (K_{lo}) is the minimum stiffness of FRP confining shell required by the confined concrete to exhibit a stress-strain curve with an ascending second branch. It was previously shown that the confinement stiffness threshold (K_{lo}) changes with the unconfined concrete

strength (f'_{co}) and the relationship was defined as in Eq. 10 (Lim and Ozbakkaloglu [39]). In the proposed model, this boundary condition is used to distinguish the stress-strain curves of concrete in DSTCs. A value of K_l greater than K_{lo} represents a specimen having confinement stiffness above the minimum threshold, for which a full ascending second branch is expected. When the confinement stiffness (K_l) is lower than the threshold stiffness (K_{lo}), but the actual confining pressure ($f_{lu,a}$) at the ultimate condition is greater than the threshold confining pressure (f_{lo}), an ascending second branch with an initial loss of axial stress during the transition is expected. When the actual confining pressure ($f_{lu,a}$) is lower than the threshold confining pressure (f_{lo}), a full descending second branch is expected, and the proposed expression (Eq. 5) is not intended to predict the ultimate axial stress (f'_{cu}) of these specimens. The relationships between the threshold confining pressure (f_{lo}), initial peak stress (f'_{c1}), and the second transition stress (f'_{c2}), are discussed in detail in Lim and Ozbakkaloglu [39].

$$K_l = \frac{2E_f t_f}{D} \tag{9}$$

$$K_{lo} = f'^{\,1.65}_{co} \tag{10}$$

$$\text{if } K_l \geq K_{lo}, \qquad c_1 = \frac{f'_{c1}}{f'_{co}} = 1 + 0.0058\frac{K_l}{f'_{co}} \tag{11}$$

$$f_{lo} = f_{l1} = K_l \varepsilon_{l1}, \qquad \varepsilon_{l1} = \left(0.43 + 0.009\frac{K_l}{f'_{co}}\right)\varepsilon_{co} \tag{12}$$

$$\text{if } K_l < K_{lo}, \qquad c_1 = \frac{f'_{c2}}{f'_{co}} = \left(\frac{K_l}{f'^{\,1.6}_{co}}\right)^{0.2} \tag{13}$$

$$f_{lo} = f_{l2} = K_l \varepsilon_{l2}, \qquad \varepsilon_{l2} = 24\left(\frac{f'_{co}}{K_l^{1.6}}\right)^{0.4} \varepsilon_{co} \quad \text{where} \quad f_{lu,a} \geq f_{lo} \tag{14}$$

In the calculation of the actual confining pressure ($f_{lu,a}$), the hoop rupture strain $\varepsilon_{h,rup}$ is calculated through Eq.16 using hoop strain reduction factor $k_{\varepsilon,f}$ given in Eq.17, where f'_{co} and E_f are in MPa. The $k_{\varepsilon,f}$ expression was developed by Lim and Ozbakkaloglu [39] using the two large test databases of FRP-confined NSC and HSC presented in Ozbakkaloglu and Lim [45] and Lim and Ozbakkaloglu [39], respectively.

$$f_{lu,a} = \frac{2E_f t_f \varepsilon_{h,rup}}{D} \tag{15}$$

$$\varepsilon_{h,rup} = k_{\varepsilon,f} \varepsilon_f \tag{16}$$

$$k_{\varepsilon,f} = 0.9 - 2.3 f'_{co} \times 10^{-3} - 0.75 E_f \times 10^{-6} \; where \; 100{,}000MPa \leq E_f \leq 640{,}000MPa \tag{17}$$

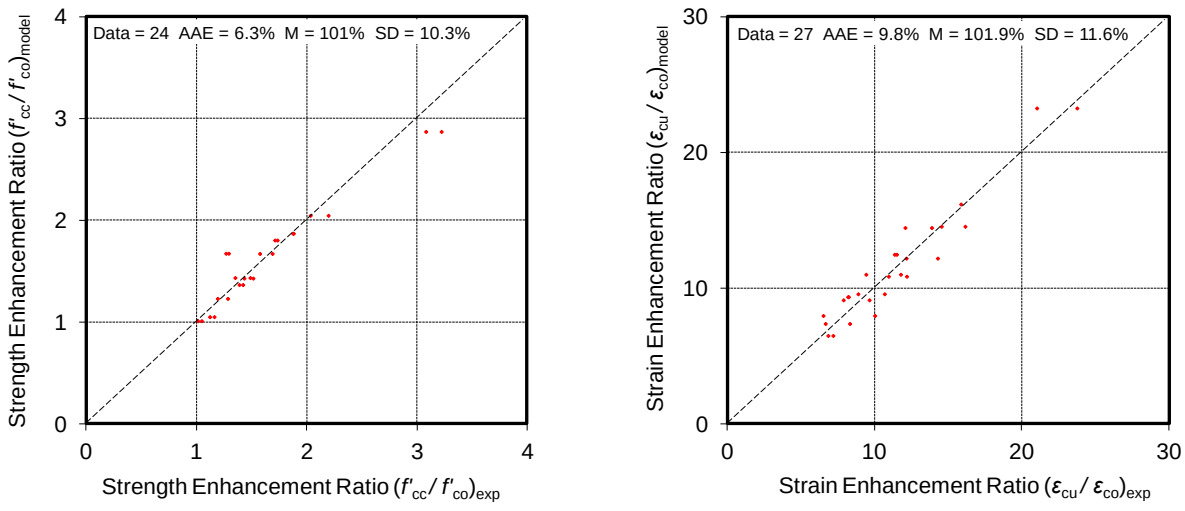

(a) (b)

Figure 7. Comparison of model predictions of the proposed model with experimental data from NSC DSTCs.

Figures 7 and *8* show the comparisons of the predictions of the proposed model with the experimental results from the database of NSC and HSC DSTCs, respectively. As evident from *Figs. 7* and *8*, the predictions of the proposed model is in close agreement with the test results, with AAEs below 12% in the predictions of both the strength and strain enhancement ratios (f'_{cc}/f'_{co} and $\varepsilon_{cu}/\varepsilon_{co}$). Comparison of the prediction statistics of the proposed model with those of the model by Yu et al. [44] showed in *Figs. 5* and *6* indicates that the proposed model provides improved performance in the prediction of the ultimate conditions of DSTCs.

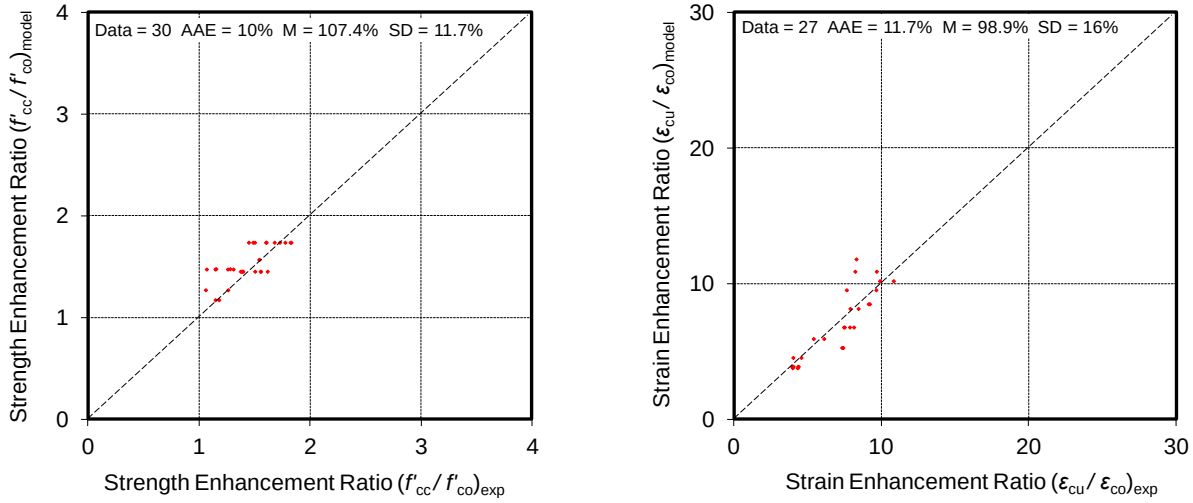

(a) (b)

Figure 8. Comparison of model predictions of the proposed model with experimental data from HSC DSTCs.

5. CONCLUSIONS

The first part of the paper has presented the results of an experimental study on the behavior of aramid FRP–HSC–steel double-skin tubular columns under axial compression. The experimental study involved design, manufacture and testing of 16

DSTCs and six companion CFFTs. Based on the test results and discussions presented in this paper, the following conclusions may be drawn:

1. Concrete inside DSTCs with circular inner steel tubes demonstrates almost monotonically ascending stress-strain curves, indicating that it is confined effectively by FRP and steel tubes. This is observed to be true for both NSC and HSC.
2. The thickness of FRP tube has a significant influence on the stress-strain behavior of confined concrete in DSTCs. As expected, increasing the FRP tube thickness leads to an increase in the compressive strength (f'_{cc}) and ultimate axial strain (ε_{cu}) of concrete in DSTCs.
3. For a given nominal confinement ratio (f_l/f'_{co}), an increase in the concrete strength results in a decrease in both the strength and strain enhancement ratios (f'_{cc}/f'_{co} and $\varepsilon_{cu}/\varepsilon_{co}$).
4. Increasing the inner steel tube diameter leads to a slight increase in the compressive strength (f''_{cc}) and a significant increase in the ultimate axial strain (ε_{cu}) of concrete in DSTCs.
5. It is observed that increased inner steel tube thickness leads to an increase in the compressive strength (f'_{cc}) and ultimate axial strain (ε_{cu}) of concrete in DSTCs. However, this observation is not consistent with the ones reported in previous studies, and additional studies are required to better understand this influence.
6. Concrete inside DSTCs with square inner steel tubes is confined less efficiently than concrete inside DSTCs with circular inner steel tubes.
7. It is observed that DSTCs develop larger ultimate axial strains than the companion CFFTs. This difference is found to be more significant for DSTCs with larger inner steel tube diameters.

In the final part of the paper, a new model is proposed to predict the ultimate conditions of concrete in DSTCs. The model was developed based on the complete database of tests results of DSTCs available in the literature, and it is applicable to both NSC and HSC DSTCs. It has been shown that the proposed model provides improved predictions of the ultimate conditions of concrete in DSTCs.

ACKNOWLEDGEMENTS

The authors would like to thank to Messrs. Cheek, Formichella, Graetz, and Varesteh, who have undertaken the tests reported in this paper as part of their undergraduate theses. This research is part of an ongoing program at The University of Adelaide on FRP-concrete-steel composite columns.

REFFERENCES

1. Ozbakkaloglu, T., Lim, J. C., and Vincent, T. (2013). "FRP-confined concrete in circular sections: Review and assessment of the stress-strain models." *Engineering Structures*, 49: 1068-1088.
2. Rochette, P., and Labossiere, P. (2000). "Axial testing of rectangular column models confined with composites." *J. Compos. Constr.*, ASCE, 4(3): 129-136.
3. Lam, L., and Teng, J. G. (2004). "Ultimate condition of fiber reinforced polymer-confined concrete." *J. Compos. Constr.*, ASCE, 8(6): 539-548.
4. Ilki, A., Peker, O., Karamuk, E., Demir, C., and Kumbasar, N. (2008). "FRP retrofit of low and medium strength circular and rectangular reinforced concrete columns." *J. Mater. Civ. Eng.*, 20(2): 169–188.
5. Cui, C., and Sheikh, S. A. (2010). "Experimental study of normal- and high-strength concrete confined with fiber-reinforced polymers." *Journal of Composites for Construction*, ASCE, 14(5), 553-561.

6. Kusumawardaningsih, Y., and Hadi, M. N. S. (2010). "Comparative behavior of hollow columns confined with FRP composites." *Composite Structures*, 93(1): 198-205.
7. Wu, Y. F., and Wei, Y. Y. (2010). "Effect of cross-sectional aspect ratio on the strength of CFRP-confined rectangular concrete columns." *Eng Struct.*, 32: 32-45.
8. Dai, J. G., Bai, Y. L., and Teng, J. G. (2011). "Behavior and modeling of concrete confined with FRP composites of large deformability." *J. Compos. Constr*., 15(6), 963-973.
9. Ozbakkaloglu, T., and Akin, E. (2012). "Behavior of FRP confined normal-and high-strength concrete under cyclic axial compression." *Journal of Composites for Construction,* ASCE, 16(4): 451-463.
10. Wang, Z. Y., Wang, D. Y., Smith, S. T., and Lu, D. G. (2012). "CFRP-confined square RC columns. I: Experimental investigation." *J. Compos. Constr.,* ASCE, 16(2): 150-160.
11. Mirmiran, A., Shahawy, M., Samaan, M., El Echary, H., Mastrapa, J. C., and Pico, O. (1998). "Effect of Column Parameters on FRP-confined Concrete." *Journal of Composites for Construction,* ASCE, 2(4): 175-185.
12. Fam, A. Z., and Rizkalla, S. H. (2001). "Confinement model for axially loaded concrete confined by circular fiber-reinforced polymer tubes." *ACI Structural Journal*, 98(4): 451-461.
13. Hong, W. K., and Kim, H. C. (2004). "Behavior of concrete columns confined by carbon composite tubes." *Canadian Journal of Civil Engineering*, 31(2): 178–188.
14. Fam, A. Z., Schnerch, D., and Rizkalla, S. (2005). "Rectangular Filament-Wound GFRP Tubes Filled with Concrete under Flexural and Axial Loading: Experimental Investigation." *Journal of Composites for Construction,* ASCE, 9(1): 25-33.
15. Ozbakkaloglu, T., and Oehlers, D. J. (2008). "Concrete-filled Square and Rectangular FRP Tubes under Axial Compression." *Journal of Composites for Construction,* ASCE, 12(4): 469-477.
16. Ozbakkaloglu, T., and Oehlers, D. J. (2008). "Manufacture and testing of a novel FRP tube confinement system." *Engineering Structures*, 30(9): 2448-2459.

17. Mohamed, H., and Masmoudi, R. (2010). “Axial Load Capacity of Concrete-Filled FRP Tube Columns: Experimental versus Predictions.” *J. Compos. Constr.,* ASCE, 14(2): 231-243.
18. Park, J. H., Jo, B. W., Yoon, S. J., and Park, S. K. (2011). “Experimental investigation on the structural behavior of concrete filled FRP tubes with/without steel re-bar.” *KSCE J. Civ. Eng*., 15(2): 337-345.
19. Ozbakkaloglu, T. (2013). “Axial compressive behavior of square and rectangular high-strength concrete-filled FRP tubes.” *Journal of Composites for Construction*, ASCE, 17(1): 151-161.
20. Ozbakkaloglu, T. (2013). “Compressive behavior of concrete-filled FRP tube columns: Assessment of critical column parameters.” *Engineering Structures*, 51: 151-161.
21. Ozbakkaloglu, T. (2013). “Concrete-filled FRP tubes: Manufacture and testing of new forms designed for improved performance.” *Journal of Composites for Construction*, ASCE, 17(2): 280-291.
22. Ozbakkaloglu, T., and Vincent, T. (2013). "Axial compressive behavior of high-strength concrete-filled FRP tubes." Journal of Composites for Construction, ASCE. 10.1061/(ASCE)CC.1943-5614.0000410
23. Teng, J. G., Yu, T., and Wong, Y. L. (2004). “Behavior of hybrid FRP-concrete-steel double-skin tubular columns.” *The 2nd International Conference on FRP Composites in Civil Engineering-CICE 2004,* Adelaide, Australia, 811-818.
24. Teng, J. G., Yu, T., Wong, Y. L., and Dong, S. L. (2005). “Innovative FRP-steel-concrete hybrid columns.” *4th International Conference on Advance in Steel Structure,* Shanghai, China, 545-554.
25. Yu, T., Wong, Y. L., Teng, J. G., Dong, S. L., and Lam, E. S. S. (2006). “Flexural Behavior of Hybrid FRP-Concrete-Steel Double-Skin Tubular Members.” *Journal of Composites for Construction,* ASCE, 10(5): 443-452.
26. Teng, J. G., Yu, T., Wong, Y. L., and Dong, S. L. (2007). “Hybrid FRP concrete steel tubular columns: concept and behavior.” *Construction and Building Materials*, 21: 846-854.

27. Wong, Y. L., Yu, T., Teng, J. G., and Dong, S. L. (2008). "Behavior of FRP-confined concrete in annular section columns." *Composites part B: Engineering*, 38: 451-466.
28. Teng, J. G., Yu, T., and Wong, Y. L. (2010). "Hybrid FRP-concrete-steel double-skin tubular structural members." *Proceedings, The Fifth International Conference on FRP Composites in Civil Engineering, 27-29 September, Beijing, China*, 26-32.
29. Yu, T., Wong, Y. L., and Teng, J. G. (2010). "Behavior of Hybrid FRP-Concrete-Steel Double-Skin Tubular Columns Subjected to Eccentric Compression." *Advances in Structural Engineering,* 13(5): 961-974.
30. Yu, T., and Teng, J. G. (2010). "'Hybrid FRP concrete-steel double skin tubular columns with a square outer and a circular inner tube: stub column tests". *13th International Symposium on tubular structures,* Hong Kong, China, 629-636.
31. Yu, T., Zhang, B., Cao, Y. B., and Teng, J. G. (2012). "Behavior of hybrid FRP-concrete-steel double-skin tubular columns subjected to cyclic axial compression." *Thin-Walled Structures*, 61: 196-203.
32. Han, L. H., Tao, Z., Liao, F. Y., and Xu, Y. (2010). "Tests on cyclic performance of FRP-concrete-steel double-skin tubular columns." *Thin-Walled Structures*, 48(6): 430-439.
33. Zhang, B., Teng, J. G., and Yu, T. (2012). "Behavior of hybrid double-skin tubular columns subjected to combined axial compression and cyclic lateral loading." *Sixth International Conference on FRP Composites in Civil Engineering*, Rome, Italy, 1-7.
34. Ozbakkaloglu, T., and Saatcioglu, M. (2006). "Seismic Behavior of High Strength Concrete Columns Confined by Fiber-Reinforced Polymer Tubes." *Journal of Composite Construction,* ASCE, 10(6): 538-549.
35. Ozbakkaloglu, T., and Saatcioglu, M. (2007). "Seismic Performance of Square High-Strength Concrete Columns in FRP Stay-in-Place Formwork." *Structural Engineering*, 133(1): 44-56.

36. Idris, Y., and Ozbakkaloglu, T. (2013). "Seismic Behavior of High-Strength Concrete-Filled FRP Tube Columns." *J. Compos. Constr*., 10.1061/(ASCE)CC.1943-5614.0000388.
37. Ozbakkaloglu, T., and Louk Fanggi, B. A. (2013). "Axial compressive behavior of FRP-concrete-steel double-skin tubular columns made of normal- and high-strength concrete." *Journal of Composites for Construction, ASCE,* doi*: 10.1061/(ASCE)CC.1943-5614.0000401*
38. Tasdemir, M. A., Tasdemir, C., Jefferson, A. D., Lydon, F. D., and Barr, B. I. G. (1998). "Evaluation of strains at peak stresses in concrete: A three-phase composite model approach." *Cement and Concrete Research*, 20: 301-318.
39. Lim, J. C., and Ozbakkaloglu, T. (2013). "Confinement model for FRP-confined high-strength concrete." *Journal of composites for constructions*, ASCE, doi: 10.1061/(ASCE)CC.1943-5614.0000376.
40. Vincent, T., and Ozbakkaloglu, T., (2013) "Influence of Concrete Strength and Confinement Method on Axial Compressive Behavior of FRP Confined High- and Ultra High-Strength Concrete." Composites Part B-Engineering, 50: 413-428.
41. Xie, P., Yu, T., Wong, Y. L., and Teng, J. G. (2011). "Compressive behavior of large scale hybrid FRP concrete steel double skin tubular columns." *Advanced Materials Research*, 243-249: 1138-1144.
42. Albitar, M. (2012). "Behavior of hybrid double-skin tubular columns under monotonic and cyclic axial compression." Master's Thesis, *The School of Civil, Environmental, and Mining Engineerin*g, The University of Adelaide, Adelaide.
43. Ding, Y., Rander, M., Reid, A., Singh, H. (2012). "Investigation into the use of GFRP in high strength concrete confinement systems." Honour's Thesis, *The School of Civil, Environmental, and Mining Engineerin*g, The University of Adelaide, Adelaide.
44. Yu, T., Teng, J. G., and Wong, Y. L. (2010). "Stress-strain behavior of concrete in hybrid FRP-concrete-steel double-skin tubular columns." *Journal of Structural Engineering, ASCE*, 136(4): 379-389.

45. Ozbakkaloglu, T., and Lim, J. C. (2013). “Axial compressive behavior of FRP-confined concrete: Experimental test database and new design-oriented model.” Composites part B. (Accepted).

Paper 3 FRP-HSC-Steel Composites Columns: Behavior under Monotonic and Cyclic Axial Compression

Togay Ozbakkaloglu and Butje Alfonsius Louk Fanggi

School of Civil, Environmental, and Mining Engineering, University of Adelaide, 5000

Journal of Materials and Structures (Published)

Statement of Authorship

Title of Paper	FRP-HSC-Steel Composites Columns: Behavior under Monotonic and Cyclic Axial Compression
Publication Status	● Published ○ Accepted for publication ○ Submitted for publication ○ Publication style
Publication Details	Ozbakkaloglu, T., and Louk Fanggi, B.A. (2015). "Behavior of FRP-HSC-steel composite tubular columns under monotonic and cyclic axial compression." *Materials and Structures*. 48: 1075-1093.

Author Contributions

By signing the Statement of Authorship, each author certifies that their stated contribution to the publication is accurate and that permission is granted for the publication to be included in the candidate's thesis.

Name of Principal Author	Dr. Togay Ozbakkaloglu		
Contribution to the Paper	Research supervision and review of manuscript		
Signature		Date	28/07/2015

Name of Co-Author (Candidate)	Butje Alfonsius Louk Fanggi		
Contribution to the Paper	Review of literature, analysis data, and preparation of manuscript		
Signature		Date	28/07/2015

FRP-HSC-STEEL COMPOSITE COLUMNS: BEHAVIOR UNDER MONOTONIC AND CYCLIC AXIAL COMPRESSION

Togay OZBAKKALOGLU [1] and Butje LOUK FANGGI [2]

ABSTRACT

This paper presents the results of an experimental study that was undertaken to investigate the effects of key parameters on the compressive behavior of fiber reinforced polymer (FRP)-concrete-steel composite columns. Performance parameters for the columns were investigated experimentally by testing 24 double-skin tubular columns (DSTCs), six concrete-filled FRP tubes (CFFTs), and two CFFTs with inner steel I-beams (I-CFFTs). The parameters examined included the loading patterns; concrete strength; diameter, thickness, and end condition of the inner steel tube in DSTCs, and influence of concrete-filling the inner steel tube. The results of the experimental study indicate that concrete-filling inner steel tubes of DSTCs results in an increase in the compressive strength and a slight decrease in the ultimate axial strain of concrete in DSTCs, compared to the values observed in companion specimens with hollow inner steel tubes. The new DSTC system developed in this study, which comprises dual-grade concretes, has been shown to exhibit superior performance compared to conventional normal-strength concrete (NSC) and high-strength concrete (HSC) DSTCs. The results also indicate that the ultimate axial stress and strain of concrete in filled DSTCs tend to increase with an increase in inner steel tube diameter. It was observed that increasing inner steel tube thickness leads to a slight increase in ultimate axial stress and strain of concrete in DSTCs. It was also observed that cyclically loaded NSC DSTCs developed similar strength and strain enhancement ratios

[1] (Corresponding author) Senior Lecturer, School of Civil, Environmental and Mining Engineering, University of Adelaide, Australia. Tel : + 618 8303 6477; Fax : +618 8303 4359; Email: togay.ozbakkaloglu@adelaide.edu.au

[2] PhD Candidate, School of Civil, Environmental and Mining Engineering University of Adelaide, Australia.

with monotonically loaded NSC DSTCs. On the other hand, a slightly increase strength and strain enhancement ratios was observed on HSC DSTCs in the presence of load cycles. Finally, it was found that the concrete in filled DSTCs exhibit slightly larger ultimate axial stress compared to those of the concretes in companion CFFTs and I-CFFTs.

KEYWORDS: Fiber reinforced polymer (FRP); Concrete; High-strength concrete (HSC), Confinement; Columns; FRP tubes; Steel tubes; DSTCs; Cyclic loading.

1. INTRODUCTION

As demonstrated in a recent review by Ozbakkaloglu et al. [1], the use of fiber reinforced polymer (FRP) composites as a confinement material has received a great deal of attention over the last two decades. Numerous experimental studies have been conducted to examine the performance of FRP composites in retrofitting existing concrete columns (e.g., [2-16]) and in the construction of new high-performance composite columns in the form of concrete-filled FRP tubes (CFFTs) (e.g., [17-31]).

More recently a new type of composite system was proposed by Teng et al. [32] in the form of FRP-concrete-steel double-skin tubular columns (DSTCs). This composite system consists of a steel tube inside a FRP tube with concrete in between, and combines the advantages of all three materials to achieve a high-performance structural member. A number of experimental studies on the axial compressive behavior of DSTCs have been reported in the literature [33-39]. The results of these studies demonstrated that concrete in DSTC is confined very efficiently, which in turn leads to a highly ductile member behavior. Along with the studies on DSTCs, a number of studies have also been carried out on a different type of FRP-concrete-steel composite system that comprises CFFTs with inner steel I-beams (referred to as I-CFFTs in this

paper). The results of the early studies on the compressive and flexural behavior of this composite system reported in Refs. [40-42] demonstrated some of its desirable properties, including a highly ductile behavior.

The use of high-strength concrete (HSC) in the construction of new composite columns such as CFFTs and DSTCs is attractive because, as was demonstrated in recent studies [22, 23, 29], the combination of these high-strength materials (i.e., HSC, steel and FRP) results in high-performance structural members. However, the existing studies on DSTCs and I-CFFTs have so far focused on normal-strength concrete (NSC), and only three studies have been reported to date on the axial compressive behavior of HSC DSTCs [34, 38, 39] and no studies on I-CFFTs made of HSC. The existing studies on DSTCs have also been concerned mainly with hollow DSTCs and only a single study investigated the influence of concrete-filling inner steel tubes [38]. Furthermore, most of the existing studies concerned on monotonically loaded DSTCs and only a single study investigated the axial cyclic behavior of DSTCs through the tests of 6 specimens [37].

As the first study in the literature that reports on the compressive behavior of aramid FRP-HSC-steel DSTCs with concrete-filled inner steel tubes, this paper presents the results of an experimental program that was aimed at addressing the outlined research gaps through the investigation of the behavior of DSTCs under monotonic and cyclic axial compression. In addition, to establish relative performances of the three aforementioned composite systems, the behavior of companion CFFTs and I-CFFTs was also experimentally investigated. The results of the experimental program are first presented and followed by a discussion on the influence of the key parameters on the behavior of FRP-HSC-steel composite columns.

2. EXPERIMENTAL PROGRAM

2.1 Test Specimens

A total of 24 DSTCs were prepared and tested using two different loading patterns: 18 DSTCs were tested under monotonic axial compression and six DSTCs were tested under cyclic axial compression. In addition, six companion CFFTs and two companion I-CFFTs were also manufactured and tested under the same loading conditions as the monotonically loaded DSTCs, to establish relative performance of DSTCs with respect to CFFTs and I-CFFTs. The specimens had a diameter of 152.5 mm, measured at the concrete core, and a height of 305 mm. The test parameters included the loading patterns; concrete strength; diameter, thickness, and end condition of the inner steel tubes, and presence (absence) of concrete-filling inside them. Two nominally identical specimens were tested in the case of DSTCs and I-CFFTs, and three identical specimens were tested in the case CFFTs for each unique specimen configuration. Details of the specimens are shown in Table 1.

In this study a new type of composite DSTC system that comprises concretes with two different grades was developed. The annular section of this column (i.e. the section between FRP and steel tubes) was filled with NSC, whereas the core inside the steel tube was filled with a higher grade concrete mix. The motivation behind the design of this system was the understanding that confinement demand of concrete increases with its strength. To make efficient use of the two confinement mechanism that exist in concrete-filled DSTCs, the higher grade concrete was placed inside the inner steel tube where it received the confining effects of both the steel and FRP tubes, whereas the section between the two tubes, which relied on the confinement of the FRP tube, was filled with NSC. To establish the relative performance of this new composite system,

dual-grade concrete DSTCs, DSTCs 3 and 4, were manufactured as companions to NSC DSTCs, DSTC-1 and 2, and HSC DSTCs, DSTC-5 and 6.

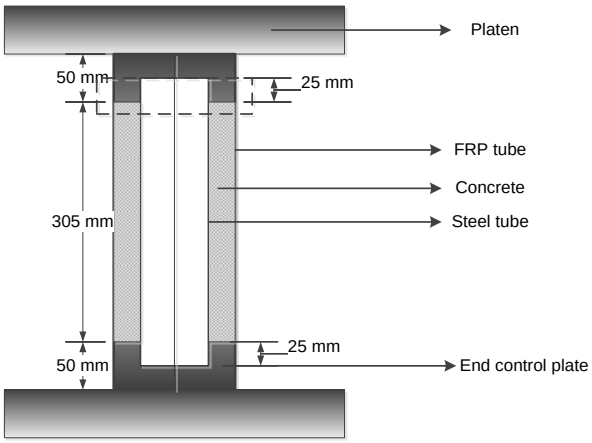

(a)

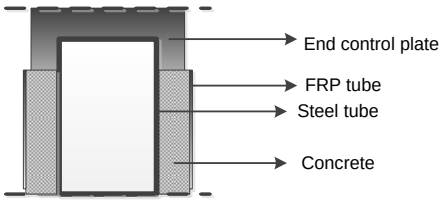

(b)

(c)

(d)

Figure 1. Specimens with special end control plates: (a) Illustration, (b) End detail, (c) Actual specimen, (d) End control plates

Table 1. Details of test specimens

Specimen	Number of FRP layers	Strength of concrete, f'_c (MPa)		Strain of peak stress, ε_{co} (%)	Steel tube diameter, D_s (mm)	Steel tube thickness, t_s (mm)	Type of FRP	Loading pattern	Specimen type
		Outer	Inner						
DSTC-1 DSTC-2	3	47.3	47.3	0.23	88.9	3.2	AFRP 1	Monotonic	Filled DSTC
DSTC-3 DSTC-4	6	47.3	104.6	0.28*	88.9	3.2	AFRP 1	Monotonic	Filled DSTC
DSTC-5 DSTC-6	6	104.6	104.6	0.32	88.9	3.2	AFRP 1	Monotonic	Filled DSTC
DSTC-7 DSTC-8	6	104.6	104.6	0.32	88.9	5.5	AFRP 1	Monotonic	Filled DSTC
DSTC-9 DSTC-10	6	104.6	104.6	0.32	60.3	3.6	AFRP 1	Monotonic	Filled DSTC
DSTC-11 DSTC-12	6	104.6	104.6	0.32	101.6	3.2	AFRP 1	Monotonic	Filled DSTC
DSTC-13 DSTC-14	6	104.6	104.6	0.32	114.3	6.02	AFRP 1	Monotonic	Filled DSTC
DSTC-15 DSTC-16	6	104.6	-	0.32	101.6	3.2	AFRP 1	Monotonic	Hollow DSTC
DSTC-17 DSTC-18	6	104.6	-	0.32	101.6	3.2	AFRP 1	Monotonic	Hollow DSTC
DSTC-1C DSTC-2C	3	42.5	42.5	0.22	88.9	3.2	AFRP 2	Cyclic	Filled DSTC
DSTC-3C DSTC-4C	6	82.4	82.4	0.29	88.9	3.2	AFRP 2	Cyclic	Filled DSTC
DSTC-5C DSTC-6C	6	82.4	82.4	0.29	60.3	3.6	AFRP 2	Cyclic	Filled DSTC
CFFT-1	3	49.4	-	0.24	-	-	AFRP 1	Monotonic	CFFT

CFFT-2 CFFT-3 CFFT-4 CFFT-5 CFFT-6	6	113.4	-	0.33	-	-	AFRP 1	Monotonic	CFFT
I-CFFT-1 I-CFFT-2	6	102.9	-	0.32	**d=125, b_f=65	t_f=8.5, t_w=5	AFRP 2	Monotonic	I-CFFT

* ε_{co} of DSTC-3 and 4 is calculated for an average concrete strength of 64.9 MPa, which was established based on cross-sectional areas of the two concrete mixes.

** Refer to Fig.2 for the details of steel I-beam.

To study the influence of inner steel tube thickness, two sets of companion specimens were manufactured with inner steel tubes with the same diameters but different thicknesses (i.e DSTC-5 and 6 and DSTC-7 and 8). To study the influence of inner steel tube diameter, while maintaining similar diameter-to-thickness ratios (D_s/t_s), three pairs of specimens were manufactured using 88.9-mm (DSTC-7 and 8), 60.3-mm (DSTC-9 and 10), and 114.3-mm (DSTC-13 and 14) inner steel tubes. In addition, to study the influence of inner steel tube diameter on the tubes having the same thickness, DSTC-11 and 12 were manufactured with 101.6-mm diameter steel tubes as companions to DSTC-5 and 6 with 88.9-mm diameter inner tubes. To study the influence of concrete-filling inner steel tubes, DSTC-15 and 16 were manufactured as companion hollow specimens to DSTC-11 and 12 with concrete-filled inner steel tubes. To investigate the influence of specimen end conditions, DSTC-17 and 18 were manufactured as companions to DSTC-15 and 16 and they were tested using special steel tube end conditions. The details of the end conditions used in DSTC-17 and 18 are illustrated in Fig. 1, and it involved the use of protruded steel tube end details (Fig.1c) together with a pair of precision-cut high-strength steel end plates (Fig. 1d), which encapsulated the protruded sections of the steel tubes.

Cyclically loaded specimens DSTC-1C to 6C were companion to monotonically loaded specimens DSTC-1 and 2, DSTC-5 and 6, and DSTC-9 and 10 and they were tested to investigate the effect of loading pattern on the compressive behavior of DSTCs. CFFTs consisted of an inner steel I-beam with a tapered flange, the geometric properties of which is shown in Fig. 2. Finally, six CFFTs and two I-CFFTs were designed as companions to the monotonically loaded DSTCs to establish relative performance levels of DSTCs compared to CFFTs and I-CFFTs. I-CFFTs consisted of an inner steel I-beam with a tapered flange, the geometric properties of which is shown in Fig. 2.

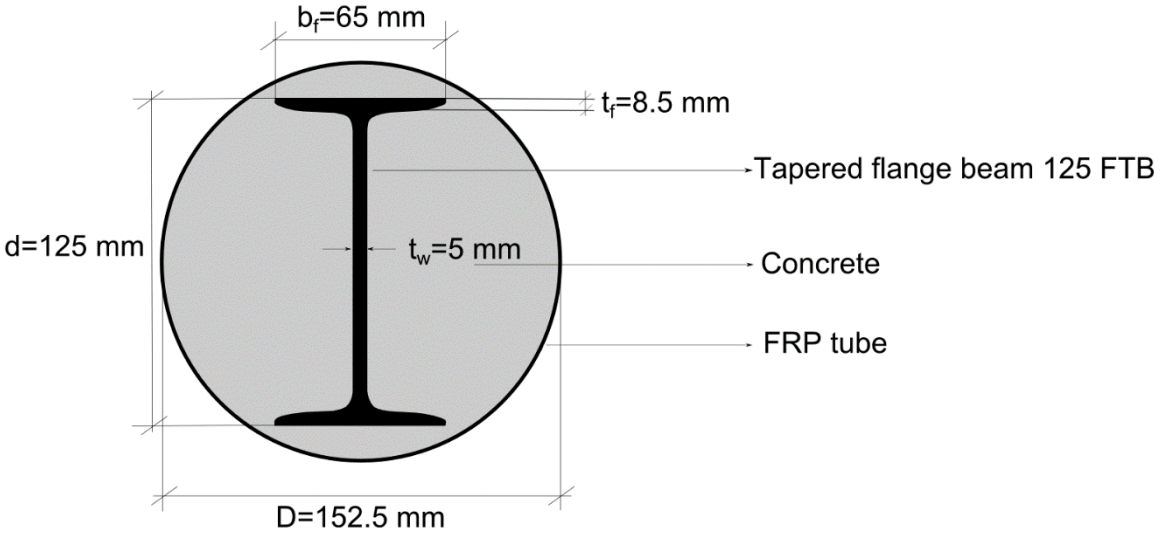

(a)

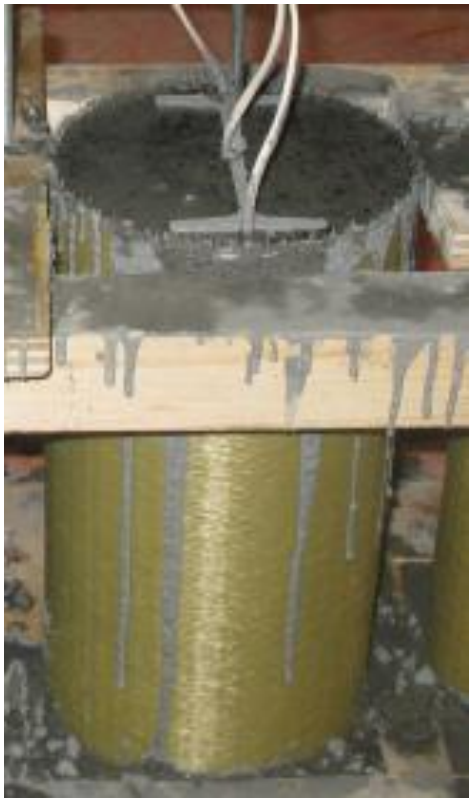

(b)

Figure 2. CFFT with inner steel I-beam: (a) Cross-section, (b) Actual specimen

2.2 Materials

The specimens were prepared using NSC and HSC mixes. All mixes consisted of crushed bluestone as the coarse aggregate, with a nominal maximum size of 10 mm. The average unconfined concrete strengths (f'_c) attained during the period of testing for the two NSC and three HSC mixes are shown in Table 1, together with the corresponding axial strains (ε_{co}) that were calculated using the expression given by Popovics [43].

In designing the FRP tubes, due consideration was given to the well-understood influence of the strength of concrete on its confinement demand [23, 13]. This was done through the use of the nominal confinement ratio (f_l / f'_c), calculated from Eq.1 established from statics assuming a uniform confinement distribution as the performance criterion in establishing relative confinement levels of DSTCs with different concrete strengths.

$$\frac{f_l}{f'_c} = \frac{2E_f t_f \varepsilon_f}{D_f f'_c} \tag{1}$$

where, f_l is the confining pressure, E_f is the modulus of elasticity, t_f is the total nominal thickness and ε_f is the ultimate tensile strain of the fibers, and D_f is the internal diameter of the FRP tube.

To establish the material properties of the steel tubes used in the DSTCs and the I-beam used in I-CFFTs, axial compression tests were conducted on hollow steel tubes and I beams. The heights of the hollow steel tubes were established based on their diameters. For tubes with diameters greater than 100 mm, three hollow tubes having the same height as those used in the DSTCs were tested. For tubes with diameters less than 100

mm, three hollow tubes with a height-to-diameter ratio of 3:1 were tested. The ratio was limited to 3:1 to prevent global buckling failure, based on the findings of previous research (e.g., [44]). For the steel I-beam, three specimens with the same height as those in I-CFFTs were tested. The results of the compression tests are shown in Table 2. All the steel tube specimens failed due to localized elephant foot buckling either at the top or bottom of the specimen as illustrated in Fig. 3, whereas the I-beam failed due to combined buckling of its web and flange sections at mid-height region.

Figure 3. Buckling of hollow steel tubes

2.3 Specimen Preparation

The FRP tubes were formed using a manual wet lay-up process by wrapping epoxy resin impregnated carbon fiber sheets around precision-cut high-density Styrofoam templates in the hoop direction. FRP sheets were provided with a 150 mm overlap to prevent premature debonding. The FRP tubes with three layers of FRP were wrapped with a single FRP sheet continuously, whereas the tubes with six layers of FRP were wrapped by two FRP sheets, with the resulting two overlap regions provided along the same area on the circumference of the tube. The properties of the unidirectional fiber

sheets used in the manufacture of the FRP tubes are provided in Table 3. Both the manufacturer-supplied properties and the ones obtained from the flat coupon test are provided in the table.

Table 2. Measured properties of steel tubes and I-beam

D_s (mm)	t_s (mm)	Grade (MPa)	Height (mm)	Peak axial load (kN)	Yield stress (MPa)	Peak stress (MPa)	Axial strain at peak (%)
60.3	3.6	350	181	246	319	384	3.34
88.9	3.2	350	267	348	320	404	2.43
88.9	5.5	350	267	711	408	493	3.06
101.6	3.2	350	305	382	310	387	2.09
114.3	6.0	350	305	1073	449	524	3.10
125 TFB		300+	305	740	396	443	5.45

TFB=Tapered flange beam

A formwork was developed and used to support the tubes during the process of concrete pouring to ensure the FRP and steel tubes remained concentric. At the base, wooden spacers were used to hold the bottom of the FRP tube in place and nails were used to maintain the position of the steel tube relative to the FRP tube. At the top, a cap with three steel arms was used to maintain the position of the two tubes concentrically. Alignment was maintained by anchoring the top cap to the wooden base. The formwork is illustrated in Fig. 4.

Table 3. Properties of fibers and FRP composites

Type	Weave	Density, ρ (g/cm^3)	Nominal thickness, t_f (mm/ply)	Provided by manufacturers			Obtained from flat FRP coupon tests*		
				Tensile strength, f_f (MPa)	Ultimate tensile strain, ε_f (%)	Elastic modulus, E_f (GPa)	Tensile strength, f_{frp} (MPa)	Ultimate tensile strain, ε_{frp} (%)	Elastic modulus, E_{frp} (GPa)
AFRP 1	Unidirectional	1.45	0.2	2900	2.50	116.0	2663	2.12	125.7
AFRP 2	Unidirectional	1.45	0.2	2600	2.20	118.2	2390	1.86	128.5

*Calculated based on nominal fibers thickness

Figure 4. Formwork used in manufacture of DSTC specimens

2.4 Instrumentation and testing

Axial deformations of the specimens were recorded with four linear variable differentiated transformers (LVDTs). These were mounted at the corners between the loading and supporting steel plates of the compression test machine, as shown in Fig. 5. The recorded deformations were used in the calculation of the average axial strains along the height of the specimens. In addition, four inner cage LVDTs were also placed in mid-height regions of the specimens to measure deformations along a gauge length of 170 mm. Furthermore, the FRP tube specimens were instrumented at mid-height with two unidirectional strain gauges with a gauge length of 20 mm to measure axial strain, which were used to validate LVDT measurements at early stage of loading. FRP tube lateral strains were measured by three unidirectional strain gauges with 20-mm gauge lengths. The gauges were spaced equally around the perimeter at the mid height of the specimen avoiding the overlap region. The axial and lateral strains of the inner steel tubes were measured mid-height by two axially and two laterally oriented strain gauges with 5-mm gauge lengths.

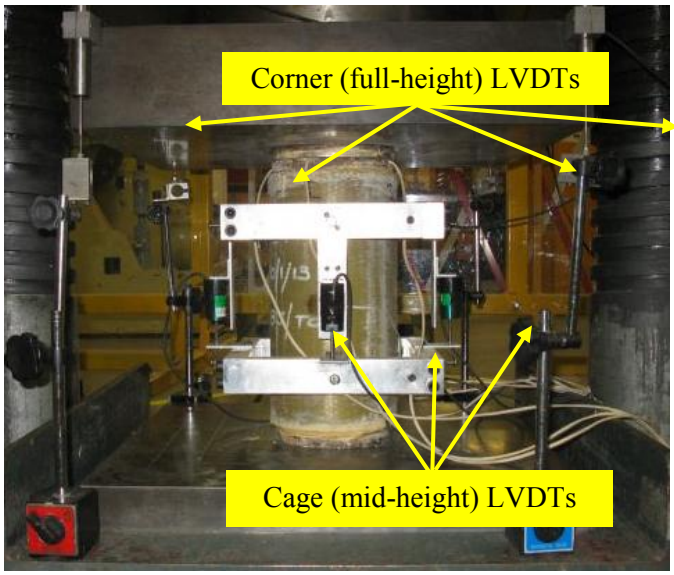

Figure 5. Test setup and instrumentation

The specimens were tested under axial compression using a 5,000-kN capacity universal testing machine. Prior to testing, the specimens were capped at both ends to ensure uniform distribution of the applied pressure, and the load was applied only to the concrete core and inner steel tube through 15-mm thick and 150-mm diameter precision-cut high-strength steel loading discs placed at each end of the specimens. The initial elastic portion of the monotonic and cyclic loading and the unloading/reloading cycles of the cyclic loading were performed with the load control at 5 kN per second, whereas displacement control was used at approximately 0.003 mm per second beyond initial softening for monotonic loading, and for the segments between each unloading/reloading curve for cyclic loading. Cyclically loaded specimens were subjected to a single unloading/reloading cycle that was applied at approximately 0.25% axial strain intervals. A small axial load of 50 kN was maintained during these cycles to prevent any undesired movement in the specimens. Test setup and instrumentation are shown in Fig. 5.

3. TEST RESULTS AND DISCUSSION

3.1 Failure modes

The failure mode of all specimens was rupture of FRP tubes in the hoop direction. It was observed that the rupture of hollow DSTC specimens was often localized and located at the end of the specimens (top or bottom). The location of the rupture of FRP was observed to correspond to the location of significant plastic deformation on inner steel tube, as shown in Fig. 6a. Moreover, it was observed that filled DSTCs, CFFTs, and I-CFFTs experienced more extensive FRP tube ruptures (than the companion hollow DSTCs), which were often initiated at the mid-height and extended towards the top and bottom of the specimens as illustrated in Figs. 6b to 6f. As illustrated by the comparison of Figs. 6b and 6c, filled DSTCs with smaller diameter inner steel tubes

often exhibited more global FRP tube failures compared to their counterparts with larger inner steel tubes.

3.2 Axial load capacities

Experimentally recorded axial load capacities of the DSTCs (P_T) are presented in Table 4 together with the axial capacities of the steel tubes (P_s), and unconfined concrete (P_{co}). The axial load capacities of the steel tubes (P_s) were determined from hollow steel tube tests, whereas the axial load capacities of unconfined concrete (P_{co}) were obtained by multiplying unconfined concrete strength by the area of the concrete cross-section. As evident from the $P_T/(P_s+P_{co})$ ratios shown in Table 4, the DSTC specimens developed significantly higher axial load capacities than the combined axial load capacity of the unconfined concrete and steel tube. This observation can be attributed to effects of confinement provided by FRP and steel tubes.

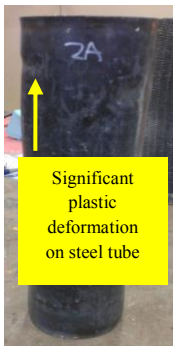

(a)

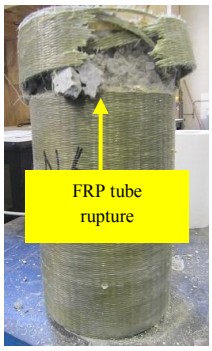

(b)


(c)


(d)


(e)


(f)


(g)

Figure 6. Failure mode specimens: (a) Hollow DSTC (DSTC-15), (b) Filled HSC DSTC with D_s=88.9 mm (DSTC-5), (c) Filled HSC DSTC with D_s=60.3 mm (DSTC-9), (d) filled NSC DSTC (DSTC-1), (e), (f) HSC CFFT (CFFT-2), (g) CFFT-IB (CFFT-IB-1)

Table 4. Axial load capacities of DSTCs

Specimen	Ultimate load of DSTC, P_T (kN)	Average P_T (kN)	Peak load of steel tube, P_s (kN)	Ultimate load of unconfined concrete section, P_{co} (kN)	P_s+P_{co} (kN)	$P_T/(P_s+P_{co})$
DSTC-1	2261	2239	348	823	1171	1.91
DSTC-2	2217					
DSTC-3	3844	3817	348	1130	1478	2.58
DSTC-4	3789					
DSTC-5	3534	3445	348	1820	2169	1.59
DSTC-6	3357					
DSTC-7	3713	3912	711	1760	2470	1.58
DSTC-8	4110					
DSTC-9	3496	3405	249	1843	2092	1.63
DSTC-10	3314					
DSTC-11	3816	3747	382	1807	2189	1.71
DSTC-12	3678					
DSTC-13	4293	4129	1074	1696	2771	1.49
DSTC-14	3964					
DSTC-15	2022	2022	382	1063	1445	1.40
DSTC-16	2021					
DSTC-17	2011	1925	382	1063	1445	1.33
DSTC-18	1839					
DSTC-1C	2072	2004	348	740	1088	1.84
DSTC-2C	1936					
DSTC-3C	3679	3746	348	1434	1782	2.10
DSTC-4C	3812					
DSTC-5C	3515	3574	249	1452	1701	2.10
DSTC-6C	3632					

3.3 Behavior of confined concrete in composite columns

3.3.1 FRP tube rupture strain

The average recorded hoop rupture strains ($\varepsilon_{h,rup}$) are given in Table 5 for all the specimens. A closer inspection of the $\varepsilon_{h,rup}$ values reported in the table allows a number of observations to be made on the influence of the important parameters on $\varepsilon_{h,rup}$. These observations are summarized in this section.

The influence of concrete filling inner steel tubes with different concrete grades on $\varepsilon_{h,rup}$ can be investigated through comparison of DSTC-1 and 2 and DSTC-5 and 6. It can be seen from Table 5 that the average hoop rupture strains recorded for NSC DSTCs is slightly larger than those for the companion HSC DSTCs. This observation indicates that hoop rupture strains ($\varepsilon_{h,rup}$) decrease with an increase in concrete strength. This finding is in agreement with that reported in past for CFFTs as described in Ozbakkaloglu and Akin [13] and Lim and Ozbakkaloglu [45], and it can be associated with the increased brittleness of HSC that results in the formation of more localized macro-cracks compared to the more evenly distributed micro-cracks observed in NSC.

To investigate the influence of inner steel tube thickness (t_s) on $\varepsilon_{h,rup}$, hoop rupture strains of the companion DSTCs with 3.2-mm (DSTC-5 and 6) and 5.5-mm (DSTC-7 and 8) tube thicknesses can be compared. It can be seen from Table 5 that the companion DSTCs developed almost identical hoop rupture strains, indicating that inner steel tube thickness has no important effect on $\varepsilon_{h,rup}$. Similar observation also can be made from Table 5 on the influence of inner steel tube diameter (D_s), where no clear influence of D_s on $\varepsilon_{h,rup}$ is evident from the comparison of the companion concrete-filled DSTCs (i.e. DSTC-5 to 14).

The effect of concrete-filling inner steel tube on $\varepsilon_{h,rup}$ can be investigated by comparing the companion filled (DSTC-11 and 12) and hollow DSTCs (DSTC-15 and 16). As can be seen from Table 5, hoop rupture strains of the filled DSTCs were significantly larger than those of the companion hollow DSTCs. The phenomenon can be explained by different failure locations of hollow and concrete-filled specimens. It was observed that failure of concrete-filled DSTCs was located at the middle region of the specimen, corresponding to the location of strain gauges placed on the FRP tube to measure hoop

strains. This resulted in larger hoop rupture strains of filled DSTCs compared to that of hollow DSTCs, which failed near one of the specimen ends away from the instrumented region.

Table 5. Ultimate condition of concrete in composite columns

Specimen	f_l/f'_c	f'_{cu} (MPa)	Avg. f'_{cu} (MPa)	f'_{cu}/f'_c	Avg. f'_{cu}/f'_c	ε_{cu} (%)	Avg. ε_{cu} (%)	$\varepsilon_{cu}/\varepsilon_{co}$	Avg. $\varepsilon_{cu}/\varepsilon_{co}$	$\varepsilon_{h,rup}$ (%)
DSTC-1	0.48	109.9	108.6	2.32	2.30	3.71	3.56	15.85	15.22	1.89
DSTC-2	0.48	107.4		2.27		3.41		14.59		
DSTC-3	0.70*	200.9	199.3	3.10	3.07	4.98	5.07	17.63	17.93	1.78
DSTC-4	0.70*	197.7		3.05		5.15		18.24		
DSTC-5	0.44	183.1	178.0	1.75	1.70	2.80	2.52	8.73	7.83	1.40
DSTC-6	0.44	172.9		1.65		2.23		6.94		
DSTC-7	0.44	179.0	190.5	1.71	1.82	2.73	3.05	8.50	9.49	1.56
DSTC-8	0.44	202.1		1.93		3.37		10.49		
DSTC-9	0.44	185.2	180.2	1.77	1.72	2.79	2.55	8.69	7.93	1.55
DSTC-10	0.44	175.2		1.67		2.31		7.18		
DSTC-11	0.44	198.7	194.7	1.90	1.86	3.09	2.99	9.61	9.32	1.65
DSTC-12	0.44	190.8		1.82		2.90		9.04		
DSTC-13	0.44	198.9	189.0	1.90	1.81	2.64	2.46	8.22	7.66	1.65
DSTC-14	0.44	179.2		1.71		2.28		7.11		
DSTC-15	0.44	161.4	161.3	1.54	1.54	3.46	3.48	10.77	10.82	1.02
DSTC-16	0.44	161.3		1.54		3.49		10.88		
DSTC-17	0.44	160.3	166.1	1.53	1.59	3.20	3.11	9.98	9.69	0.82
DSTC-18	0.44	171.9		1.64		3.02		9.40		
DSTC-1C	0.48	99.1	95.2	2.33	2.24	3.70	3.53	16.51	15.56	1.57
DSTC-2C	0.48	91.2		2.15		3.35		14.60		
DSTC-3C	0.50	191.4	195.3	2.32	2.37	3.29	3.35	11.27	11.46	1.13
DSTC-4C	0.50	199.1		2.42		3.40		11.64		
DSTC-5C	0.50	186.4	189.6	2.26	2.30	2.58	2.79	8.84	9.56	1.45
DSTC-6C	0.50	192.7		2.34		3.00		10.27		
CFFT-1	0.46	104.6	106.3	2.12	2.15	3.15	3.39	13.24	14.25	2.33
CFFT-2	0.46	107.9		2.18		3.55		14.92		
CFFT-3	0.46	106.3		2.15		3.47		14.58		
CFFT-4	0.40	177.1	167.7	1.56	1.48	2.80	2.50	8.44	7.54	1.60
CFFT-5	0.40	152.6		1.35		2.20		6.63		
CFFT-6	0.40	173.3		1.53		2.50		7.54		
I-CFFT-1	0.40	178.7	169.2	1.74	1.64	2.03	1.88	6.36	5.89	1.19
I-CFFT-2	0.40	159.7		1.55		1.73		5.42		

*Calculated based on an average concrete strength of 64.9 MPa

3.3.2 *Axial stress-strain behavior*

The axial stress on the concrete inside the DSTCs and I-CFFTs was calculated by dividing the axial load resisted by the concrete (P_c) with the net cross-sectional area of the concrete section. The load applied to the concrete was determined by subtracting the axial load resisted by the steel tube/section (P_s) for a given axial strain, from the total load resisted by the DSTC/I-CFFT (P_T) at the same axial strain. The load acting on the steel tube/section was calculated by assuming that the load-strain behavior of the steel tube/section inside a DSTC/I-CFFT is similar to the load-strain behavior of the corresponding unconfined steel tube/section obtained from a compression test. In addition, the load-axial strain relationships of steel tubes used in cyclically loaded specimens were generated from monotonic compression tests by assuming that the slope of the unloading/reloading path is the same as the elastic modulus of the steel tube. The ultimate axial stress (f'_{cu}) and strain (ε_{cu}) of the concrete inside the composite columns reported in Table 5 were calculated using the approach summarized in this section.

Figures 7 to 10 present the concrete stress-strain relationships for the specimens of the present study. As evident from these figures, all the specimens exhibited almost monotonically ascending stress-strain curves, indicating that the concrete inside the DSTCs, CFFTs, and I-CFFTs was effectively confined. It can also be observed in Figs. 7 to 4.10 that some of the HSC specimens experienced a sudden drop in strength after the transition point between the initial ascending branch and the second branch that follows it. Similar observations were previously reported in Refs. [26, 46, 47] for HSCFFTs, and this behavior can be attributed to the brittle nature of HSC, which results in formation of large cracks that leads to rapid and uncontrolled expansion. The sudden large damage sustained by HSC near the transition point of the stress-strain curve results in some decay in strength, which is subsequently recovered upon the full

activation of FRP tube confinement mechanism. As expected, the stress-strain behavior of the DSTC specimens along the second branch of the curve is influenced by the important parameters, including the concrete strength, diameter, thickness, and end condition of inner steel tube and presence (or absence) of concrete filling inside it. The influence of these parameters on the stress-strain behavior of DSTCs is discussed in the following sections, continued by discussion on the relative performance of DSTCs compared with those of CFFTs and I-CFFTs.

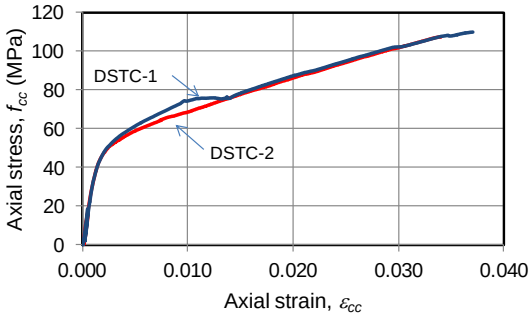

(b)

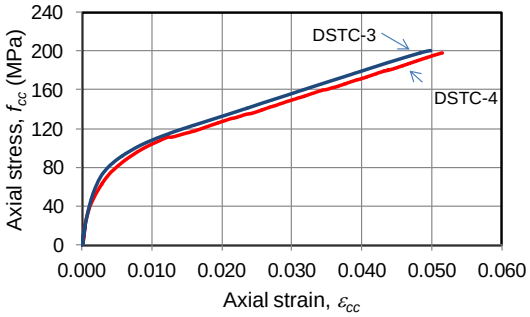

(b)

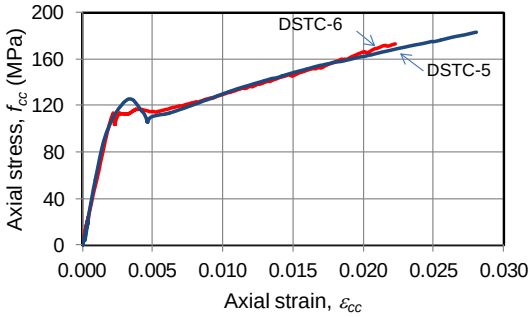

(c)

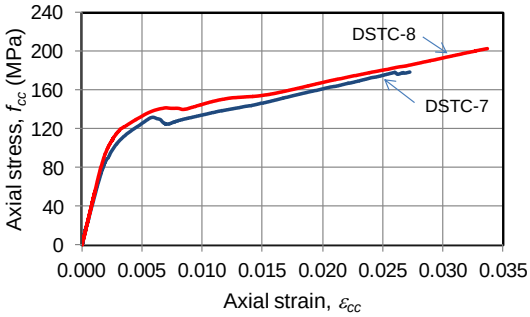

(d)

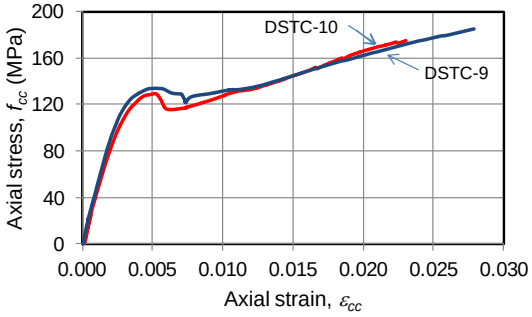

(e)

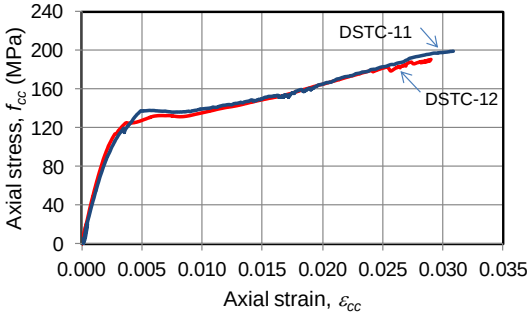

(f)

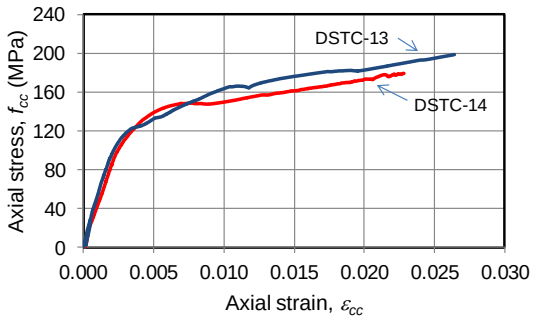

(g)

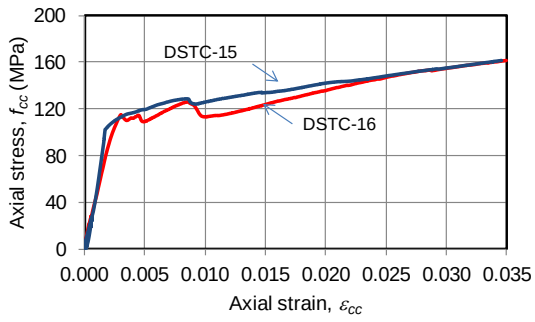

(h)

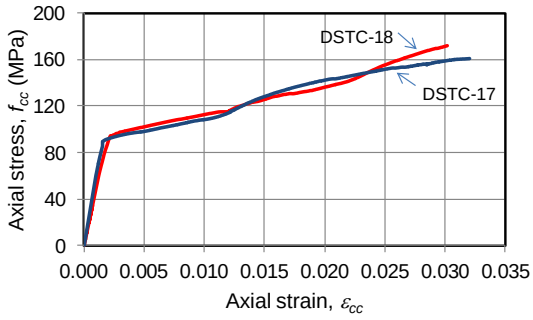

(i)

Figure 7. Axial stress-strain behavior of concrete in DSTCs: (a) 1&2, (b) 3&4, (c) 5&6, (d) 7&8, (e) 9&10, (f) 11&12, (g) 13&14, (h) 15&16, (i) 17&18

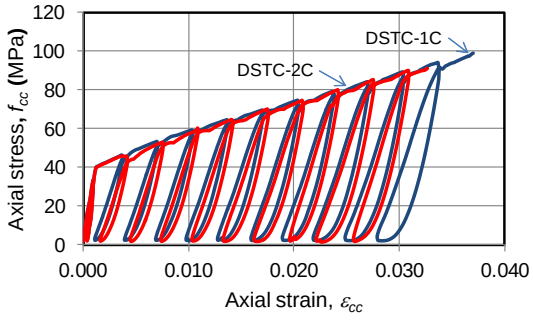

(a)

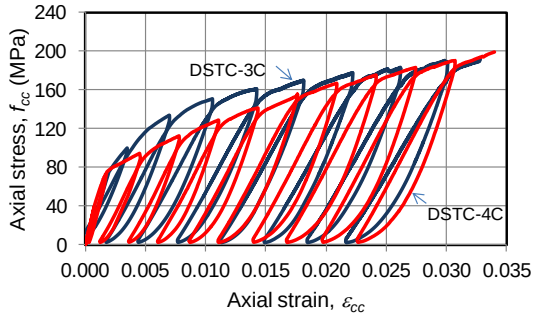

(b)

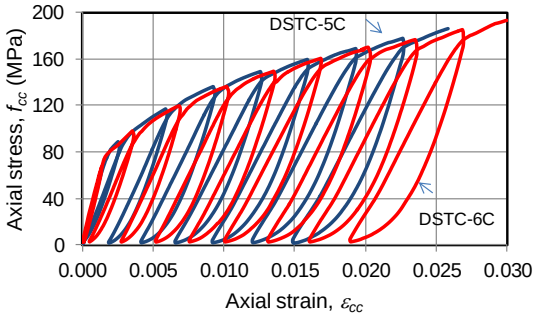

(c)

Figure 8. Stress-strain behavior of concrete in cyclically loaded DSTCs: (a) 1C&2C, (b) 3C&4C, (c) 5C&6C

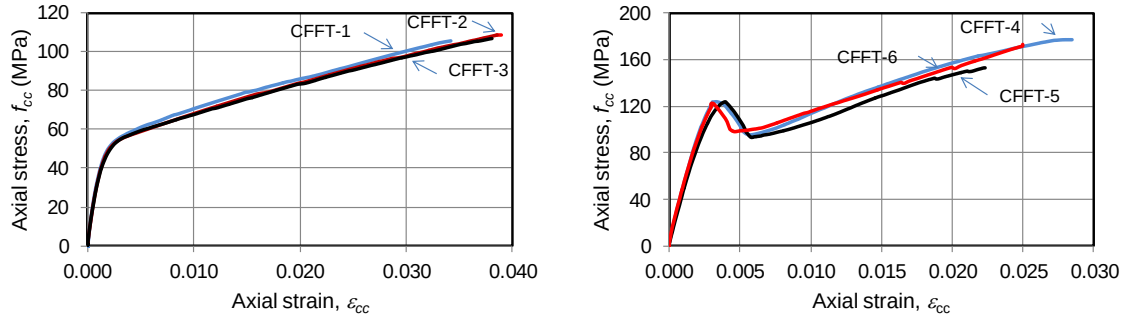

Figure 9. Axial stress-strain behavior of concrete in CFFTs: (a) 1-3, (b) 4-6

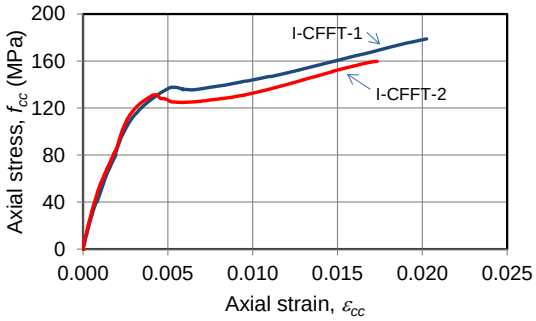

Figure 10. Axial stress-strain behavior of concrete in I-CFFTs

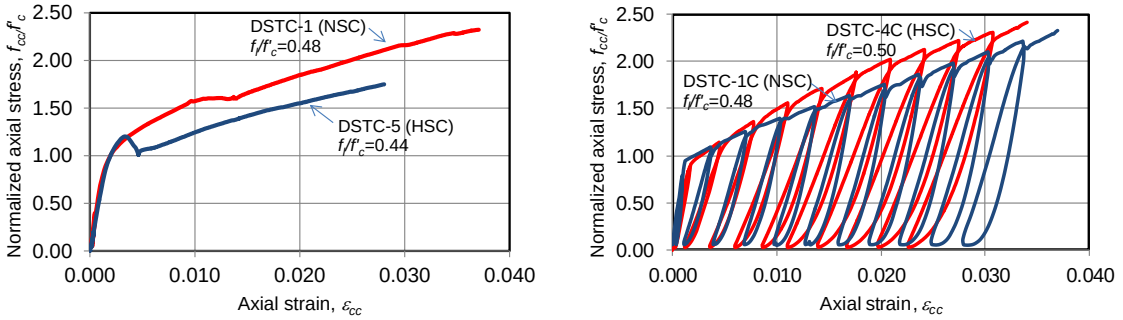

Figure 11. Influence of concrete strength: (a) specimens under monotonic loading, (b) specimens under cyclic loading

3.3.2.1 Effect of concrete strength

As can be seen in Table 5, the companion NSC and HSC DSTCs were designed to have similar levels of confinement, which was established through the use of the nominal confinement ratio (Eq. 1) as discussed previously. In calculating f_l it was assumed that the confining pressure was uniform and the section was treated as a solid section,

ignoring the influence of the inner void when applicable. To investigate the influence of concrete strength on DSTCs, the axial stress (f_{cc}) is normalized with unconfined concrete strength (f'_c) and is plotted against axial strain (ε_{cc}) as illustrated in Fig. 11.

Figure 11 illustrates the comparison of the normalized axial stress-axial strain curves of the companion NSC and HSC DSTCs for both monotonic and cyclic loading conditions. It can be seen from Fig. 11a that the NSC DSTC exhibited a larger ultimate strain (ε_{cu}) and strength enhancement ratio (f'_{cu}/f'_c) than the companion HSC DSTC. This observation is also supported by the one derived from the comparison of the average values of strength and strain enhancement ratios (f'_{cu}/f'_c and $\varepsilon_{cu}/\varepsilon_{co}$) reported in Table 5 for DSTC-1 and 2 and DSTC-5 and 6. The comparison of the stress-strain curves for cyclically loaded NSC and HSC DSTCs shown in Fig. 11b indicates that the HSC DSTCs developed slightly larger f'_{cu}/f'_c but lower ε_{cu} than the companion NSC DSTC (DSTC-1C). This observation is also supported by the average values of f'_{cu}/f'_c and $\varepsilon_{cu}/\varepsilon_{co}$ reported in Table 5 for DSTC-1C and 2C and DSTC-3C and 4C. These observations indicate that, for a given nominal confinement ratio, the strength enhancement ratio of concrete in DSTCs is not highly sensitive to the unconfined concrete strength. On the other hand, ultimate axial strains and resulting strain enhancement ratios tend to decrease with an increase in the unconfined concrete strength. Furthermore, the different observations derived from monotonically and cyclically loaded specimens on the influence of concrete strength on f'_{cu}/f'_c can be attributed to the differences in unconfined concrete strength (f'_c) and confinement ratio (f_l/f'_c) of those companion specimens. The cyclically loaded HSC specimens had a lower concrete strength (f'_c) than their monotonically loaded counterparts, which resulted in their having a higher f_l/f'_c. The combined influence of lower f'_c and higher f_l/f'_c, in turn, resulted in much

better performance of cyclically loaded HSC DSTCs compared to the companion monotonically loaded HSC DSTCs.

Figure 12 shows the comparison of the normalized stress-strain curve of the dual-grade concrete DSTC developed in this study with those of the companion NSC and HSC DSTCs. The superior performance of the new DSTC system is evident from Fig. 12, which illustrates the much higher strength and strain enhancements of concrete attained in the new system compared to those seen in conventional DSTCs. This observation is further supported by the comparison of the average values of strength and strain enhancement ratios (f'_{cu}/f'_c and $\varepsilon_{cu}/\varepsilon_{co}$) reported in Table 5 for the companion DSTC-1 to 6. An interesting observation from Table 5 is that the dual-grade concrete DSTCs developed higher ultimate axial stresses compared to the companion HSC DSTCs, despite their lower average unconfined concrete strength (i.e. 64.9 MPa versus 104.6 MPa). Furthermore, as indicated in Table 5, dual-grade DSTCs developed twice the ultimate axial strains (ε_{cu}) as those of the companion HSC DSTCs. These results demonstrate that the new composite system developed in this study, combines the benefits of NSC (i.e. low confinement demand) and HSC (i.e. high strength), which results in columns with extremely high axial load and deformation capacities. The new DSTC system owes its improved behavior to its efficient use of the two confinement mechanisms (i.e. one by steel tube and the other by FRP tube) that exists in concrete-filled DSTCs. Depending on the application, these benefits offered by dual-grade DSTCs might justify the more complex construction process involved in manufacturing these columns due to the use of two individual concrete mixes.

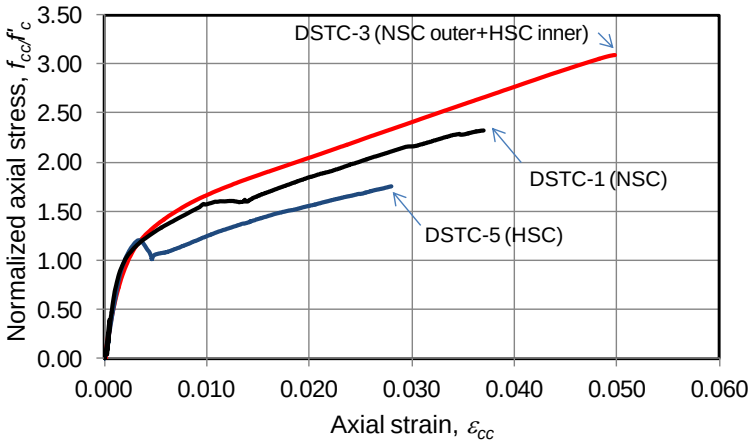

Figure 12. Influence of combining different grades of concrete

3.3.2.2 Effect of concrete-filling inner steel tube

Figure 13 presents the stress-strain relationships of specimens with and without concrete-filling inside their inner steel tubes. It can be seen from Fig. 13 that DSTC with concrete-filled inner steel tube (DSTC-12) developed larger ultimate axial stress (f'_{cu}) but lower ultimate strain (ε_{cu}) compared to the companion DSTC with a hollow inner steel tube (DSTC-16). This observation is also supported by the average values of f'_{cu} and ε_{cu} reported in Table 5 for the specimen pairs DSTC-11 and 12 and DSTC-15 and 16. The increase in the ultimate axial stress can be attributed to additional confinement effects provided by the inner steel tube to the core concrete. On the other hand, presence of concrete inside the steel tube results in an increased dilation rate of concrete for a given FRP tube stiffness, which in turn results in the failure of the FRP tubes at a lower ultimate axial strain (ε_{cu}). A Similar observation on the influence of concrete-filling inner steel tube was previously reported in Ozbakkaloglu and Louk Fanggi [38] for DSTCs fabricated by carbon FRP tubes.

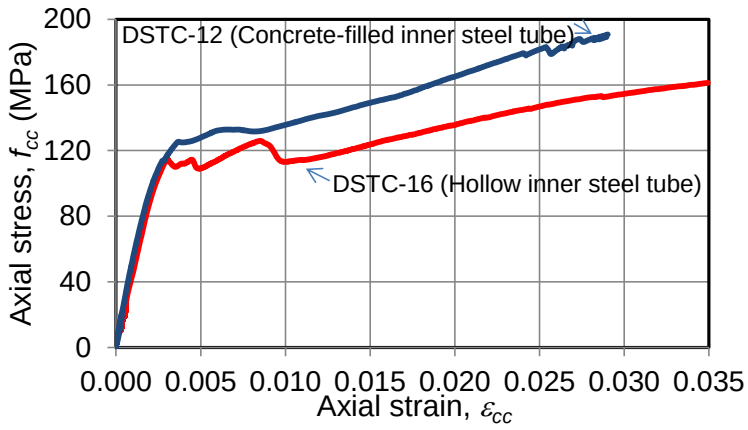

Figure 13. Influence of concrete filling inner steel tube

3.3.2.3 *Effect of steel tube diameter*

To illustrate the influence of inner steel tube diameter, Fig. 14 presents the stress-strain relationships of DSTCs with inner steel tubes having different diameters. Figure 14a shows the stress-strain curves of DSTCs with similar diameter-to-thickness ratios (D_s/t_s), whereas Fig. 14b shows the curves of DSTCs with the same steel tube thickness. It can be observed from Fig. 14a that increasing the diameter from 60.3 mm to 88.9 mm leads to an increase in both f'_{cu} and ε_{cu}, whereas increasing the diameter from 88.9 mm to 114.3 mm leads to no change in f'_{cu} but a decrease in ε_{cu}. The increase in the compressive strengths of concrete in DSTCs with 88.9-mm and 114.3-mm diameter inner steel tubes over that of DSTCs with 60.3-mm diameter tubes can be attributed to the increased confinement effects of the inner steel tube. Fig. 14b further illustrates that concrete in DSTCs with a larger inner steel tube developed higher f'_{cu} and ε_{cu} than those in the companion specimens having steel tubes with the same thickness but a smaller diameter. A similar observation was previously reported in Ozbakkaloglu and Louk Fanggi [38] for filled DSTCs fabricated with carbon FRP tubes.

These results indicate that, in general, both f'_{cu} and ε_{cu} of concrte-filled DSTCs tend to increase with an increase in inner steel tube diameter. However, the disagreement

between the observations on the influence of the tube diameter on ε_{cu}, from aforementioned comparisons of the specimens with similar D_s/t_s, points to the need for additional tests to gain further insight into this influence.

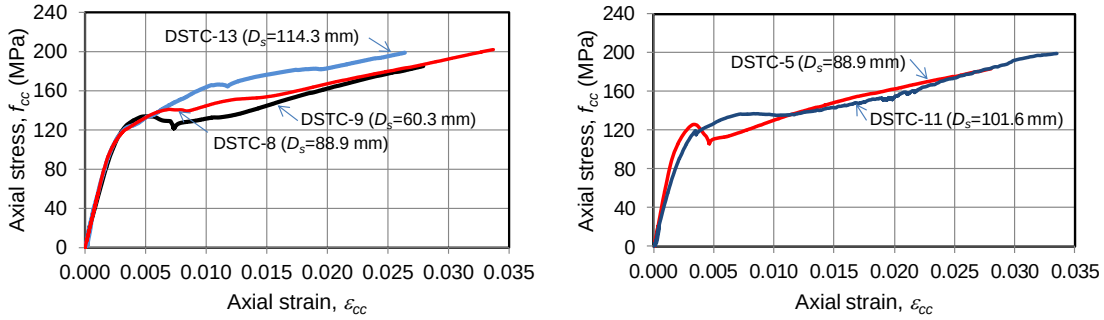

(a) (b)

Figure 14. Influence of inner steel tube diameter: (a) DSTCs with similar D_s/t_s ratios, (b) DSTCs with same inner steel tube thickness

Furthermore, the comparison of the results of the present study with those reported in Ozbakkaloglu and Louk Fanggi [38] indicates that the influence of the inner steel tube diameter on the ultimate axial strain of concrete (ε_{cu}) is more significant in hollow DSTCs than in filled DSTCs.

3.3.2.4 *Effect of steel tube thickness*

The influence of steel tube thickness can be investigated by comparing the stress-strain relationships of DSTC-5 (3.2 mm) and DSTC-8 (5.5 mm) as illustrated in Fig. 15. It can be seen in Fig. 15 that increasing steel tube thickness from 3.2 mm in DSTC-1 to 5.5 mm in DSTC-6 leads to a slight increase in f'_{cu} and ε_{cu}. This observation is also supported by the results reported in Table 5 for the specimen pairs DSTC-5 and 6 and DSTC-7 and 8. Furthermore, as can be seen in Fig. 15, the DSTC with a thinner inner steel tube exhibited a slight strength loss after initial peak strength, whereas the companion DSTC with a thicker tube did not experience any strength softening after its initial peak. The improved behavior of the DSTCs with thicker inner steel tubes can be

attributed to the increased level of confinement provided to the core concrete by the thicker steel tube.

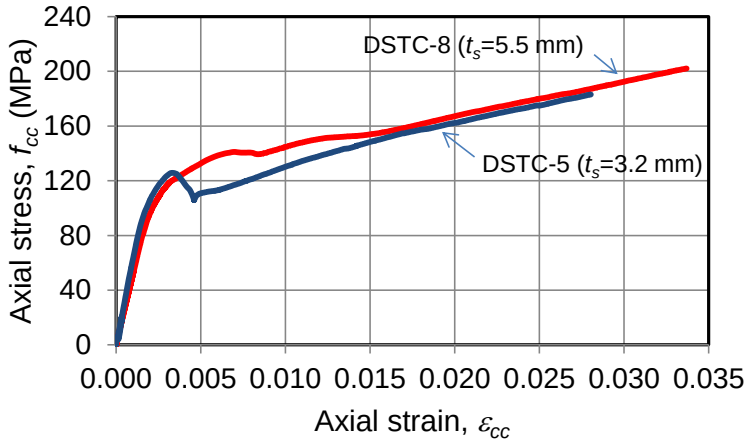

Figure 15. Influence of inner steel tube thickness

3.3.2.5 *Effect of steel tube end condition*

As previously reported in Ozbakkaloglu and Louk Fanggi [38], rupture of FRP tubes of DSTCs with hollow inner steel tubes observed to be localized at or near specimen ends. The location of the rupture of FRP was observed to correspond to the location of significant plastic deformation on inner steel tube. Two specimens of the present study were manufactured with special end condition details that were designed with the aim of preventing the local buckling of the inner steel tube at specimen ends. A similar end condition detail was previously used for FRP-confined steel tubular columns reported in Haedir and Zhao [48].

Figure 16 illustrates the influence of the steel tube end condition on the stress-strain behavior of concrete in hollow DSTCs. As can be seen in the figure, DSTC-18 with special end conditions developed similar f'_{cu} to and slightly lower ε_{cu} than DSTC-15 that was tested conventionally. This observation is also supported by the results reported in Table 5 for the specimen pairs DSTC-17 and 18 and DSTC-15 and 16. Furthermore, it

was observed that, both groups of the specimens failed at their ends and steel tube buckling occurred at the location of specimen failure. These observations indicate that the end condition investigated in this study provided no clear benefit to the overall behavior of hollow DSTCs.

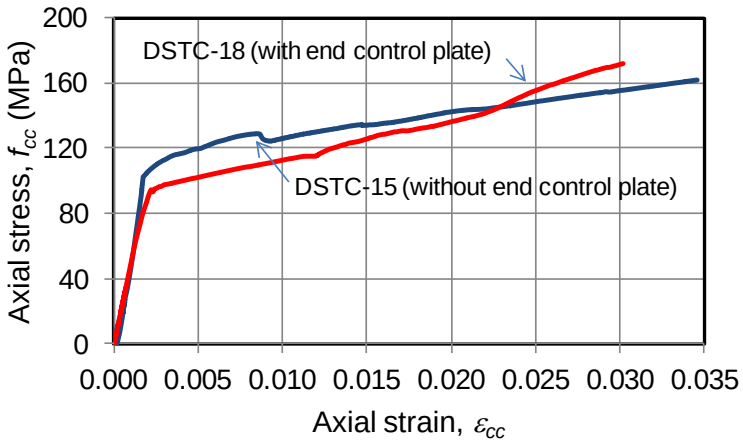

Figure 16. Influence of steel tube end condition

3.3.2.6 *Effect of loading pattern*

The influence of loading pattern on the compressive behavior of DSTCs can be investigated by comparing the stress-strain curves of the NSC DSTCs (DSTC-1 and 1C) and HSC DSTCs (DSTC-9 and 3C, and DSTC-5 and 4C) as shown in Figs. 17a to 17c, respectively. Because monotonically and cyclically loaded HSC DSTCs had slightly different nominal confinement ratios (f_l/f'_c), to enable a meaningful comparison between these specimens, strength and strain enhancement coefficients (k_1 and k_2) were calculated using Eqs. 2-3 and are shown in Fig. 17. These equations were used purely for comparison purposes, and hence simple equation forms were adopted.

$$k_1 = \left(\frac{f'_{cu}}{f'_c} - 1\right) / \frac{f_l}{f'_c} \tag{2}$$

$$k_2 = \left(\frac{\varepsilon_{cu}}{\varepsilon_{co}} - 2\right) / \frac{f_l}{f'_c} \tag{3}$$

It can be seen from Fig. 17a that the cyclically loaded NSC DSTC developed almost the same ultimate axial stress (f'_{cu}) and strain (ε_{cu}) as monotonically loaded NSC DSTC. This observation is also supported by the average values of strength and strain enhancement ratios (f'_{cu}/f'_c and $\varepsilon_{cu}/\varepsilon_{co}$) of DSTC-1 and 2 and the companion DSTC-1C and 2C as shown in Table 5. These findings are in agreement with those recently reported in Yu et al. [37], which stated that the ultimate conditions of the concrete in DSTCs subjected to cyclic axial compression were almost the same as those in the DSTCs subject to monotonic compression. As can be seen in Fig. 17a, however, that the envelope curve of the cyclically loaded DSTC corresponded to lower axial stresses than that observed on the curve of the monotonically loaded DSTC, which is caused by the lower f'_c of the cyclic specimen.

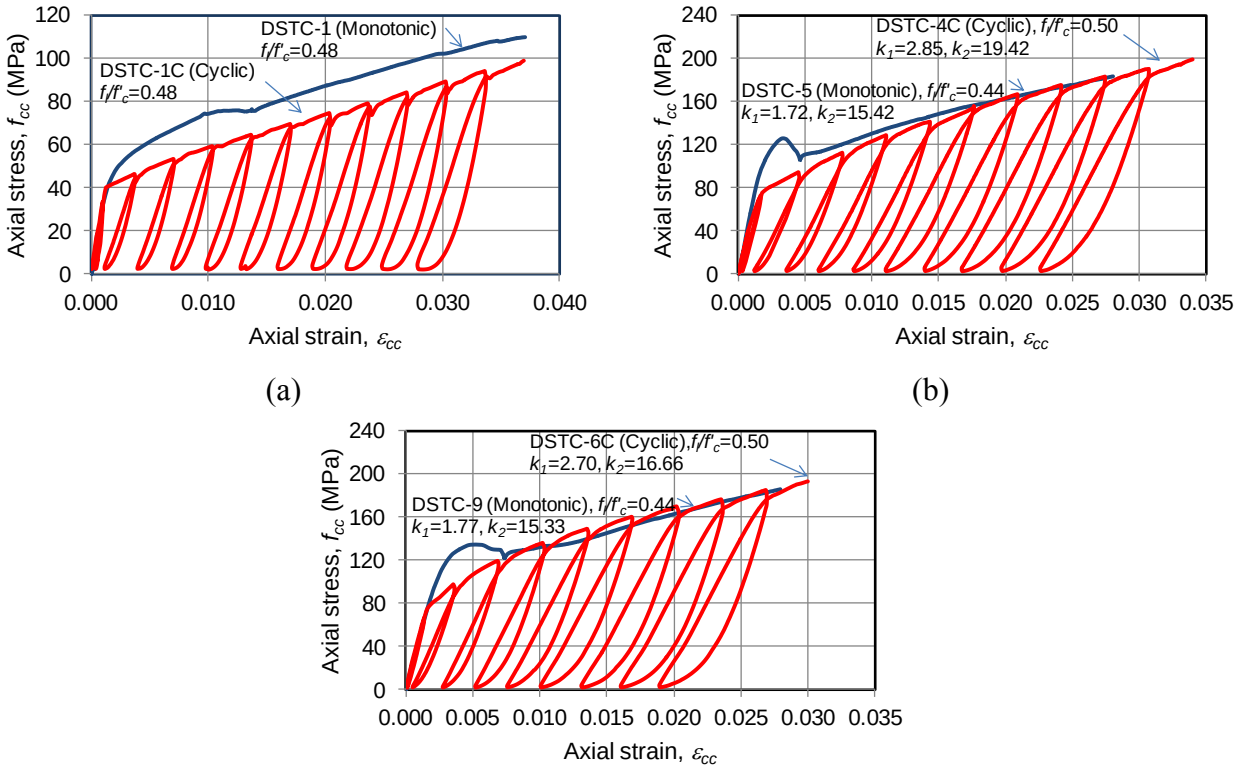

Figure 17. Influence of loading patterns: (a) NSC DSTCs with D_s=88.9 mm, (b) HSC DSTCs with D_s=88.9 mm, (c) HSC DSTCs with D_s=60.3 mm,

The stress strain curves of HSC DSTCs shown in Figs. 17b and 17c indicate that the cyclically loaded DSTCs developed similar envelope curves to the companion monotonically loaded DSTCs, but they exhibited slightly larger f'_{cu} and ε_{cu}. This observation is also supported by the higher values of strength and strain enhancement coefficients (k_1 and k_2) of the cyclically loaded specimens compared to the companion monotonically loaded specimens, as indicated in Figs. 17b and 17c. Similar improvements resulting from load cycles were reported previously for FRP-confined concrete specimens [13, 49, 50]. It is evident from the different observations reported herein for NSC and HSC specimens that additional experimental studies are required to gain further insight into the influence of load cycles on the compressive behavior of DSTCs.

3.3.2.7 Comparison of DSTCs, CFFTs, and I-CFFTs

To illustrate the relative performance of each composite system, Fig. 18 presents the stress-strain curves of concretes in the companion concrete-filled DSTC, CFFT and I-CFFT specimens made of HSC. As shown in the figure, the concretes in CFFT and I-CFFT developed similar ultimate stresses (f'_{cu}), whereas the ultimate axial stress of the concrete in filled DSTC was slightly higher. The increased compressive strength of the concrete in filled DSTCs can be attributed to additional confinement effects provided by the inner steel tube to the core concrete. Figure 18 also illustrates that the concrete in filled DSTC and CFFT developed similar ultimate axial strains (ε_{cu}), which were higher than that observed for the concrete in I-CFFTs. The observations suggest that the presence of an inner steel I-beam had no detrimental influence on the ultimate axial stress of concrete, but it resulted in a slight reduction in the overall axial deformation capacity of the column compared to the other two companion composite systems. The observations summarized in this section are also supported by the average values of

strength and strain enhancement ratios (f'_{cu}/f'_c and $\varepsilon_{cu}/\varepsilon_{co}$) reported in Table 5 for the companion specimens DSTC-9 and 10, CFFT-4 to 6, and I-CFFT-1 and 2. It might be worth noting that the discussion presented in this section is limited to the structural performance of the compared systems under axial compression and in a real world application there will most likely be additional considerations, which could one system more suitable over the others.

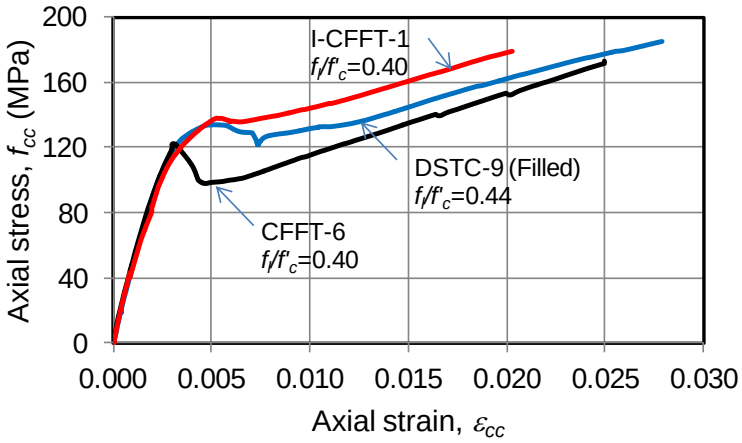

Figure 18. Comparison of different composite systems

4. CONCLUSIONS

This paper has presented the results of an experimental study on the behavior of FRP-HSC-steel composite columns subjected to monotonic and cyclic axial compression. The experimental study involved design, manufacture and testing of 24 filled and hollow DSTCs, six CFFTs, and two I-CFFTs to investigate the effect of key parameters on the stress-strain behavior of concrete in DSTCs. Based on the results and discussions presented in the paper, the following conclusions can be drawn:

1. A new form of DSTC developed in the present study that consists of NSC-filled annular section between FRP and steel tubes and HSC-filled inner core has been shown to exhibit superior performance compared to conventional NSC and HSC DSTCs. It has been demonstrated that the new composite system combines the

benefits of NSC (i.e. low confinement demand) and HSC (i.e. high strength), which results in columns with extremely high axial load and deformation capacities.

2. Concrete in DSTCs with concrete-filled inner steel tubes develop larger ultimate axial stresses (f'_{cu}) and lower ultimate strains (ε_{cu}) compared to concrete in companion DSTCs with hollow inner steel tubes.
3. Concretes in companion monotonically and cyclically loaded NSC DSTCs demonstrate similar strength and strain enhancement ratios (f'_{cu}/f'_c and $\varepsilon_{cu}/\varepsilon_{co}$). A slight influence of loading pattern has been observed for HSC DSTCs, with concrete in cyclically loaded DSTCs exhibiting slightly larger strength and strain enhancement ratios compared to concrete in monotonically loaded DSTCs.
4. Concrete in filled DSTCs develops slightly higher ultimate axial stress (f'cu) than concrete in CFFTs and I-CFFTs. The increased compressive strength of concrete in filled DSTCs can be attributed to additional confinement effects provided by the inner steel tube to the core concrete.

In addition to the above conclusions, the following observations are made on the influence of inner steel tube parameters on the compressive behavior of DSTCs. It should be noted that these influences were subtle and additional studies are required for their validation.

- Ultimate axial stress (f'_{cu}) and strain (ε_{cu}) of concrete in filled DSTCs tend to increase with an increase in inner steel tube diameter. However, the influence of the steel tube diameter on the ultimate axial strain (ε_{cu}) has been found to be less significant for concrete-filled DSTCs compared to DSTCs with a hollow inner core.
- Concrete in filled DSTCs with thicker inner steel tubes develop slightly larger ultimate axial stress (f'_{cu}) and strain (ε_{cu}) than concrete in DSTCs with thinner tubes.

This improved behavior can be attributed to the increased level of confinement provided to the core concrete by the steel tube with an increase in its thickness.

ACKNOWLEDGEMENTS

The authors would like to thank Mr. Albitar who has undertaken some of the tests reported in this paper as part of his Master thesis. This research is part of an ongoing program at The University of Adelaide on FRP-concrete-steel composite columns.

REFERENCES

1. Ozbakkaloglu, T., Lim, J. C., and Vincent, T. (2013). "FRP-confined concrete in circular sections: Review and assessment of the stress-strain models." *Engineering Structures*, 49: 1068-1088.
2. Lam, L., and Teng, J. G. (2004). "Ultimate condition of fiber reinforced polymer-confined concrete." *J. Compos. Constr.*, ASCE, 8(6): 539-548.
3. Campione, G. (2006). "Influence of FRP wrapping techniques on the compressive behavior of concrete prisms." *Cement and Concrete Composites*, 28(5): 497-505.
4. Lignola, G. P., Prota, A., Manfredi, G., and Cosenza E. (2007). "Experimental performance of RC hollow columns confined with CFRP." *Journal of Composite for Construction, ASCE*, 11(1): 42‑49.
5. Colomb, F., Tobbi, H., Ferrier, E., and Hamelin, P. (2008) "Seismic retrofit of reinforced concrete short columns by CFRP materials." *Composite Structures*, 82 (4): 475-487.
6. Ilki, A., Peker. O., Karamuk, E., Demir, C., and Kumbasar, N. (2008). "FRP retrofit of low and medium strength circular and rectangular reinforced concrete columns." *J. Mater. Civ. Eng.*, 20(2): 169–188.
7. Rousakis, T., and Karabinis, A. (2008). "Substandard reinforced concrete members subjected to compression: FRP confining effects." *Materials and Structures*, 41(9): 1595 – 1611.

8. Thermou, G. E., and Pantazopoulou, S. J. (2009) "Fiber-reinforced polymer retrofitting of predamaged substandard RC prismatic members." *Journal of Composites for Construction*, *ASCE,* 13 (6): 535-546.
9. Turgay, T., Polat, Z., Koksal, H.O., Doran, B., and Karakoç, C. (2010). "Compressive behavior of large-scale square reinforced concrete columns confined with carbon fiber reinforced polymer jackets." *Materials and Design*, 31 (1): 357-364.
10. Wu, Y. F., and Wei, Y. Y. (2010). "Effect of cross-sectional aspect ratio on the strength of CFRP-confined rectangular concrete columns." *Engineering Structures*, 32: 32-45.
11. De Luca, A., Nardone, F., Matta, F., Nanni, A., Lignola, G.P., and Prota, A. (2011). "Structural evaluation of full-scale FRP-confined reinforced concrete columns." *Journal of Composites for Construction*, *ASCE,* 15 (1): 112-123.
12. Abdelrahman, K., and El-Hacha, R. (2012). "Behavior of large-scale concrete columns wrapped with CFRP and SFRP sheets." *Journal of Composites for Construction*, *ASCE,* 16 (4): 430-439.
13. Ozbakkaloglu, T., and Akin, E. (2012). "Behavior of FRP confined normal-and high-strength concrete under cyclic axial compression." *Journal of Composites for Construction, ASCE*, 16(4): 451-463.
14. Realfonzo, R., and Napoli, A. (2012). "Results from cyclic tests on high aspect ratio RC columns strengthened with FRP systems." *Construction and building materials*, 37: 606-620.
15. Wang, Z. Y., Wang, D. Y., Smith, S. T., and Lu, D. G. (2012). "Experimental testing and analytical modeling of CFRP-confined large circular RC columns subjected to cyclic axial compression." *Engineering Structures,* 40: 64-74.
16. Vincent, T., and Ozbakkaloglu, T. (2013). "Influence of Concrete Strength and Confinement Method on Axial Compressive Behavior of FRP Confined High- and Ultra High-Strength Concrete." *Composites Part B-Engineering*, 50: 413-428.
17. Seible, F., Burgueño, R., Abdallah, M. G., and Nuismer, R. (1996). "Development of advanced composite carbon shell systems for concrete columns in seismic

zones." *Proc., 11th World Conf. Earthquake Engineering*, Pergamon, Elsevier Science, Oxford, Paper No. 1375.

18. Mirmiran, A., Shahawy, M., Samaan, M., El Echary, H., Mastrapa, J. C., and Pico, O. (1998). "Effect of Column Parameters on FRP-confined Concrete." *Journal of Composites for Construction, ASCE*, 2(4): 175-185.
19. Fam, A. Z., and Rizkalla, S. H. (2001). "Confinement model for axially loaded concrete confined by circular fiber-reinforced polymer tubes." *ACI Structural Journal*, 98(4): 451-461.
20. Fam, A. Z., Schnerch, D., and Rizkalla, S. (2005). "Rectangular Filament-Wound GFRP Tubes Filled with Concrete under Flexural and Axial Loading: Experimental Investigation." *Journal of Composites for Construction, ASCE*, 9(1): 25-33.
21. Zhu, Z., Ahmad, I., and Mirmiran, A. (2006). "Seismic performance of concrete-filled FRP tube columns for bridge substructure." *Journal of Bridge Engineering*, ASCE, 11(3): 359-370.
22. Ozbakkaloglu, T., and Saatcioglu, M. (2006). "Seismic Behavior of High Strength Concrete Columns Confined by Fiber-Reinforced Polymer Tubes." *Journal of Composite Construction, ASCE*, 10(6): 538-549.
23. Ozbakkaloglu, T., and Saatcioglu, M. (2007). "Seismic Performance of Square High-Strength Concrete Columns in FRP Stay-in-Place Formwork." *Structural Engineering*, 133(1): 44-56.
24. Ozbakkaloglu, T., and Oehlers, D. J. (2008). "Concrete-filled Square and Rectangular FRP Tubes under Axial Compression." *Journal of Composites for Construction, ASCE*, 12(4): 469-477.
25. Ozbakkaloglu, T., and Oehlers, D. J. (2008). "Manufacture and testing of a novel FRP tube confinement system." *Engineering Structures*, 30(9): 2448-2459.
26. Ozbakkaloglu, T. (2013). "Axial Compressive Behavior of Square and Rectangular High-Strength Concrete-Filled FRP Tubes." *Journal of Composites for Construction, ASCE*, 17(1): 151-161.

27. Ozbakkaloglu, T. (2013). “Concrete-filled FRP Tubes: Manufacture and Testing of New Forms Designed for Improved Performance.” *Journal of Composites for Construction, ASCE*, 17(2): 280-281.
28. Ozbakkaloglu, T. (2013). “Compressive behavior of concrete-filled FRP tube columns: Assessment of critical column parameters.” *Engineering Structures*, 51: 151-161.
29. Idris, Y., and Ozbakkaloglu, T. (2013). "Seismic Behavior of High-Strength Concrete-Filled FRP Tube Columns." *J. Compos. Constr.*, doi: 10.1061/(ASCE)CC.1943-5614.0000388.
30. Vincent, T., and Ozbakkaloglu, T. (2013). “Influence of fiber orientation and specimen end condition on axial compressive behavior of FRP-confined concrete.” *Construction and building materials*, 47: 814–826.
31. Fam, A. Z., and Rizkalla, S. H. (2001). “Behavior of axially loaded concrete-filled circular Fiber Reinforced Polymer Tubes.” *ACI Structural Journal*, 98(3): 280-289.
32. Teng, J. G., Yu, T., and Wong, Y. L. (2004). “Behaviour of hybrid FRP-concrete-steel double-skin tubular columns.” *The 2nd International Conference on FRP Composites in Civil Engineering-CICE 2004,* Adelaide, Australia, 811-818.
33. Teng, J. G., Yu, T., Wong, Y. L., and Dong, S. L. (2007). “Hybrid FRP concrete steel tubular columns: concept and behavior.” *Construction and building materials*, 21: 846-854.
34. Wong, Y. L., Yu, T., Teng, J. G., and Dong, S. L. (2008). “Behaviour of FRP-confined concrete in annular section columns.” *Composites part B: Engineering*, 38: 451-466.
35. Teng, J. G., Yu, T., and Wong, Y. L. (2010). “Hybrid FRP-concrete-steel double-skin tubular structural members.” *Proceedings, The Fifth International Conference on FRP Composites in Civil Engineerind (CICE), 27-29 September, Beijing, China*, 26-32.
36. Yu, T., Wong, Y. L., and Teng, J. G. (2010). “Behavior of Hybrid FRP-Concrete-Steel Double-Skin Tubular Columns Subjected to Eccentric Compression.” *Advances in Structural Engineering,* 13(5): 961-974.

37. Yu, T., Zhang, B., Cao, Y. B., and Teng, J. G. (2012). “Behavior of hybrid FRP-concrete-steel double-skin tubular columns subjected to cyclic axial compression.” *Thin-Walled Structures*, 61: 196-203.
38. Ozbakkaloglu, T., and Louk Fanggi, B. A. (2013). “Axial compressive behavior of FRP-concrete-steel double-skin tubular columns made of normal- and high-strength concrete.” *Journal of Composites for Construction, ASCE.* doi: 10.1061/(ASCE)CC.1943-5614.0000401.
39. Louk Fanggi, B.A., and Ozbakkaloglu, T. (2013). “Compressive behavior of aramid FRP-HSC-Steel double-skin tubular columns.” *Construction and Building Materials*, 48: 554-565.
40. Karimi, K., Tait, M. J., and El-Dakhakhni, W. W. (2011). “Testing and modelling of a novel FRP-encased steel-concrete composite column.” *Composite Structures,* 93: 1463-1473.
41. Karimi, K., Tait, M. J., and El-Dakhakhni, W. W. (2012). “Influence of slenderness on the behaviour of a FRP-encased steel-concrete composite column.” *Journal of Composite for Construction, ASCE*, 16(1), 100-109.
42. Zakaib, S., and Fam, A. (2012). “Flexural performance and moment connection of concrete concrete-filled GFRP tube-encased steel I-sections.” *Journal of Composites for Construction, ASCE*, 16(5): 604-613.
43. Popovics, S. (1973). “A numerical approach to the complete stress-strain curves of concrete." *Cement and Concrete Research,* 3(5): 583-599.
44. Han, L. H., Zhao, X. L., and Tao, Z. (2001). “Tests and mechanics model of concrete-filled SHS stub columns, columns, and beam-columns.” *Steel Comp. Struct.,* 1(1): 51-74.
45. Lim, J., and Ozbakkaloglu, T. (2013). "Confinement Model for FRP-Confined High-Strength Concrete." *Journal of Composite for Construction*, *ASCE*. doi:10.1061/(ASCE)CC.1943-5614.0000376.
46. Ozbakkaloglu, T. (2013). "Behavior of Square and Rectangular Ultra High-Strength Concrete-Filled FRP Tubes under Axial Compression." *Composites Part B*. 54: 97-111.

47. Ozbakkaloglu, T., and Vincent, T. (2013). "Axial compressive behavior of high-strength concrete-filled FRP tubes." *Journal of Composites for Construction, ASCE*. Doi:10.1061/(ASCE)CC.1943-5614.0000410.
48. Haedir, J., and Zhao, X. L. (2011). "Design of short CFRP-reinforced steel tubular columns." *Journal of Constructional Steel Research,* 67: 497-509.
49. Lam, L., Teng, J. G., Cheung, Y., and Xiao, Y. (2006). "FRP-confined concrete under axial cyclic compression." *Cement and concrete composites*, 28: 949-958.
50. Demir, C., Kolcu, K., and Ilki, A. (2010). "Effects of loading rate and duration on axial behavior of concrete confined by fiber-reinforced polymer sheets." *Journal of Composites for Construction, ASCE*, 14(2): 146-151.

Paper 4 Behavior of Hollow and Concrete-Filled FRP-HSC and FRP-HSC-Steel Composite Columns Subjected to Concentric Compression

Butje Alfonsius Louk Fanggi and Togay Ozbakkaloglu

School of Civil, Environmental, and Mining Engineering, University of Adelaide, 5000

Journal of Advanced in Structural Engineering (Published)

Statement of Authorship

Title of Paper	Behavior of Hollow and Concrete-Filled FRP-HSC and FRP-HSC-Steel Composite Columns Subjected to Concentric Compression
Publication Status	● Published ○ Accepted for publication ○ Submitted for publication ○ Publication style
Publication Details	Louk Fanggi, B.A., and Ozbakkaloglu, T. (2015). "Behavior of Hollow and Concrete-Filled FRP-HSC and FRP-HSC-Steel Composite Columns Subjected to Concentric Compression." *Advanced in Structural Engineering*. 18(5): 715-738.

Author Contributions

By signing the Statement of Authorship, each author certifies that their stated contribution to the publication is accurate and that permission is granted for the publication to be included in the candidate's thesis.

Name of Principal Author (Candidate)	Butje Alfonsius Louk Fanggi		
Contribution to the Paper	Review of literature, analysis data, and preparation of manuscript		
Signature		Date	28/07/2015

Name of Co-Author	Dr. Togay Ozbakkaloglu		
Contribution to the Paper	Research supervision and review of manuscript		
Signature		Date	28/07/2015

BEHAVIOR OF HOLLOW AND CONCRETE-FILLED FRP-HSC AND FRP-HSC-STEEL COMPOSITE COLUMNS SUBJECTED TO CONCENTRIC COMPRESSION

B.A. LOUK FANGGI[1] and T. OZBAKKALOGLU[2]

ABSTRACT

This paper presents an experimental study that was undertaken to investigate the effects of key parameters on the compressive behavior of fiber reinforced polymer (FRP)-concrete-steel composite columns that were manufactured with S-Glass FRP tubes. A total of 24 hollow and concrete-filled double-skin tubular columns (DSTCs), two concrete-filled FRP tubes (CFFTs), and six CFFTs with inner voids (H-CFFTs) were prepared and tested. The parameters examined included the inner steel tube diameter, influence of concrete-filling the inner steel tube, and the loading pattern. The results indicate that concrete-filling the inner steel tubes of DSTCs results in an increase in the compressive strength of confined concrete in DSTCs, compared to that of the companion specimens with hollow inner steel tubes. It was observed that cyclically loaded DSTCs exhibited slightly higher strength and strain enhancements compared to their monotonically loaded counterparts. The results also indicate that H-CFFTs perform significantly worse than DSTCs and CFFTs and their performance further degrades with an increase in the diameter of inner void. Comparison of the results from DSTCs and CFFTs indicate that both hollow and concrete-filled DSTCs exhibit improved compressive behavior compared to those of the companion CFFTs.

[1] PhD Candidate, School of Civil, Environmental and Mining Engineering, University of Adelaide, SA 5005 Australia.
[2] (Corresponding author) Senior Lecturer, School of Civil, Environmental and Mining Engineering, University of Adelaide, SA 5005 Australia. Tel : + 618 8313 6477; Fax : +618 8313 4359; Email: togay.ozbakkaloglu@adelaide.edu.au

KEYWORDS: Fiber reinforced polymer (FRP), High-strength concrete (HSC), Columns, Confinement, FRP tubes, Steel tubes, DSTCs.

1. INTRODUCTION

Over the last two decades, the use of fiber reinforced polymer (FRP) composites as a confinement material has received a great deal of attention as demonstrated in a recent review by Ozbakkaloglu *et al*. (2013). Two main subjects that researchers focusing on were in: 1) the performance of FRP composites in retrofitting existing concrete columns (e.g., Lam and Teng 2004, Campione 2006, Lignola *et al*. 2007, Colomb *et al*. 2008, Ilki *et al*. 2008, Rousakis and Karabinis 2008, Thermou and Pantazopoulou 2009, Turgay *et al*. 2010, Wu and Wei 2010, De Luca *et al*. 2011, Abdelrahman and El-Hacha 2012, Ozbakkaloglu and Akin, 2012, Realfonzo and Napoli 2012, Wang *et al*. 2012, Vincent and Ozbakkaloglu 2013a) and 2) the construction of new high-performance composite columns in the form of concrete-filled FRP tubes (CFFTs) (e.g., Seible *et al*. 1996, Mirmiran *et al*. 1998, Fam and Rizkalla 2001, Fam *et al*. 2005, Zhu *et al*. 2006, Ozbakkaloglu and Saatcioglu 2006, 2007, Idris and Ozbakkaloglu 2013, Ozbakkaloglu 2013a,b,c,d, Vincent and Ozbakkaloglu 2013b, Lim and Ozbakkaloglu 2014a, Ozbakkaloglu and Vincent 2014, Vincent and Ozbakkaloglu 2014). More recently a new type of composite system was proposed by Teng *et al*. (2004) in the form of FRP-concrete-steel double-skin tubular columns (DSTCs). This composite system consists of a steel tube inside a FRP tube with concrete in between, and combines the advantages of all three materials to achieve a high-performance structural member. A large number of experimental studies have recently been undertaken on the axial compressive behavior of DSTCs by groups led by Teng in Hong Kong (Teng *et al*. 2004, Teng *et al*. 2007, Wong *et al*. 2008, Teng *et al*. 2010, Yu *et al*. 2010, Yu *et al*. 2012) and the second author in Australia (Ozbakkologlu and Louk Fanggi 2013, Louk Fanggi and

Ozbakkaloglu 2013). The results of these studies demonstrated that concrete in DSTC is confined very efficiently, which in turn leads to a highly ductile member behavior.

The use of high-strength concrete (HSC) in the construction of new composite columns such as CFFTs and DSTCs is attractive because, as was demonstrated in recent studies (Ozbakkaloglu and Saatcioglu 2006, 2007, Lim and Ozbakkaloglu 2014a), the combination of these high-strength materials (i.e., HSC, steel and FRP) results in high-performance structural members. However, the existing studies on DSTCs has so far focused on normal-strength concrete (NSC), and only two specimen tests have been reported to date on the axial compressive behavior of HSC DSTCs made of glass FRP tubes (Teng *et al*. 2010). Likewise, majority of the existing studies on DSTCs have focused on hollow DSTCs and only single study reported the influence of concrete-filling inner steel tubes (Ozbakkologlu and Louk Fanggi 2013). Finally, most of the existing studies were concerned with monotonically loaded DSTCs and only a single study investigated the axial cyclic behavior of DSTCs through the tests of 6 specimens (Yu *et al*. 2012).

This paper presents the results of an experimental program that was aimed at addressing the outlined research gaps through the investigation of the behavior of HSC DSTCs manufactured with S-glass FRP tubes and tested under monotonic and cyclic axial compression. In addition, the behavior of companion solid and hollow concrete-filled FRP tubes (CFFTs and H-CFFTs) was also experimentally investigated to establish relative performances of DSTCs to CFFTs and H-CFFTs. The results of the experimental program are first presented and followed by a discussion on the influence of the important parameters on the compressive behavior of FRP-HSC-steel composite columns.

2. EXPERIMENTAL PROGRAM

2.1. Test Specimens

A total of 32 specimens that were confined with FRP tubes that were fabricated using S-glass fibers were prepared and tested under concentric compression. 24 of the specimens were DSTCs with hollow or concrete filled inner steel tubes and they were tested using two different loading patterns: 20 DSTCs were tested under monotonic axial compression and four DSTCs were tested under cyclic axial compression. In addition, six companion H-CFFTs and two companion CFFTs were manufactured and tested under the same loading conditions as the monotonically loaded DSTCs, to establish relative performance of DSTCs with respect to CFFTs and H-CFFTs. The specimens had a diameter (D) of 152.5 mm, measured at the concrete core, and a height of 305 mm. The test parameters included the loading pattern, diameter of the inner steel tubes, and presence (absence) of concrete-filling inside them. Two nominally identical specimens were tested for each unique specimen configuration. Details of the specimens are shown in Table 1.

To study the influence of inner steel tube diameter (D_s), while maintaining similar diameter-to-thickness ratios (D_s/t_s) on hollow DSTC specimens, DSTCs 1 and 2 were manufacturing with 60.3-mm diameter steel tubes as companions to DSTCs 9 and 10 with 114.3-mm diameter inner tubes. In addition, to study the influence of inner steel tube diameter on the tubes having the same thickness, three pairs of specimens were manufactured using 76.1-mm (DSTCs 3 and 4), 88.9-mm (DSTCs 5 and 6), and 101.6-mm (DSTCs 7 and 8) inner steel tubes. To study the influence of concrete-filling inner steel tubes and the effect of inner tube parameters on the behavior of these specimens, concrete-filled DSTCs 11 to 20 were designed as companion to hollow DSTCs 1 to 10. Filled DSTCs 11 to 20 were analogous to hollow DSTCs 1 to 10 and they were

designed to investigate the same parameters as the ones studied for hollow DSTC specimens. Furthermore, to study the influence of loading pattern, cyclically loaded specimens DSTCs 1C to 4C were designed as companion to monotonically loaded specimens DSTCs 5 and 6 and DSTCs 15 and 16. Finally, six H-CFFTs and two CFFTs were designed as companions to the monotonically loaded DSTCs to establish relative performance levels of DSTCs compared to H-CFFTs and CFFTs.

2.2.Materials

Two HSC mixes were used in the manufacture of the specimens. The mix consisted of crushed bluestone as the coarse aggregate with a nominal maximum size of 10 mm, and silica fume added at 8% of the binder content by weight. To determine the compressive strength of the unconfined concrete, three plain concrete cylinders with a diameter of 100 mm and height of 200 mm were tested in accordance with ASTM C39 (2010) for each concrete mix.in parallel to testing of DSTC, H-CFFT, and CFFT specimens. The average unconfined concrete strengths (f'_c) attained during the period of testing are shown in Table 1, together with the corresponding axial strains (ε_{co}) that were calculated using the expression given by Popovics (1973). As evident from Table 1, test day strength of the mix used in the manufacture of the monotonically loaded specimens was approximately 15% higher than that of the cyclically loaded specimens.

Table 1. Details of test specimens

Specimen	Number of FRP layers	Strength of concrete, f'_c (MPa)	Strain at peak stress, ε_{co} (%)	External diameter of inner steel tube or void, D_s (mm)	Steel tube thickness, t_s (mm)	Specimen type	Loading pattern
DSTC-1	6	96.2	0.31	60.3	3.6	Hollow DSTC	Monotonic
DSTC-2							
DSTC-3	6	96.2	0.31	76.1	3.2	Hollow DSTC	Monotonic
DSTC-4							
DSTC-5	6	96.2	0.31	88.9	3.2	Hollow DSTC	Monotonic
DSTC-6							
DSTC-7	6	96.2	0.31	101.6	3.2	Hollow DSTC	Monotonic
DSTC-8							
DSTC-9	6	96.2	0.31	114.3	6.0	Hollow DSTC	Monotonic
DSTC-10							
DSTC-11	6	96.2	0.31	60.3	3.6	Filled DSTC	Monotonic
DSTC-12							
DSTC-13	6	96.2	0.31	76.1	3.2	Filled DSTC	Monotonic
DSTC-14							
DSTC-15	6	96.2	0.31	88.9	3.2	Filled DSTC	Monotonic
DSTC-16							
DSTC-17	6	96.2	0.31	101.6	3.2	Filled DSTC	Monotonic
DSTC-18							
DSTC-19	6	96.2	0.31	114.3	6.0	Filled DSTC	Monotonic
DSTC-20							
DSTC-1C	6	82.4	0.29	88.9	3.2	Hollow DSTC	Cyclic
DSTC-2C							
DSTC-3C	6	82.4	0.29	88.9	3.2	Filled DSTC	Cyclic
DSTC-4C							
H-CFFT-1	6	96.2	0.31	60.3	-	Hollow-CFFT	Monotonic
H-CFFT-2							
H-CFFT-3	6	96.2	0.31	88.9	-	Hollow-CFFT	Monotonic
H-CFFT-4							
H-CFFT-5	6	96.2	0.31	114.3	-	Hollow-CFFT	Monotonic
H-CFFT-6							
CFFT-1	6	96.2	0.31	-	-	CFFT	Monotonic
CFFT-2							

In designing the FRP tubes, due consideration was given to the well-understood influence of the strength of concrete on its confinement demand (Ozbakkaloglu and Akin 2012, Ozbakkaloglu and Saatcioglu 2007). This was done through the use of the nominal confinement ratio (f_{lu}/f'_c), calculated from Eqn.1 assuming a uniform confinement distribution, as the performance criterion in establishing relative confinement levels of DSTCs with different concrete strengths.

$$\frac{f_{lu}}{f'_c} = \frac{2E_f t_f \varepsilon_{fu}}{D_f f'_c} \tag{1}$$

where, f_{lu} is the ultimate confining pressure, E_f is the modulus of elasticity, t_f is the total nominal thickness and ε_{fu} is the ultimate tensile strain of the fibers, and D_f is the internal diameter of the FRP tube.

To establish the material properties of the steel tubes used in the DSTCs, axial compression tests were conducted on hollow steel tubes. The heights of the hollow steel tubes were established based on their diameters. For tubes with diameters greater than 100 mm, three hollow tubes having the same height as those used in the DSTCs were tested. For tubes with diameters less than 100 mm, three hollow tubes with a height-to-diameter ratio of 3:1 were tested. The tests were conducted using a universal testing machine with axial strains obtained from four LVDTs mounted along the full height of the specimens and two unidirectional strain gauges with a gauge length of 5 mm attached at mid-height of the steel tubes. All the steel tube specimens failed due to localized elephant foot buckling either at the top or bottom of the specimen. In all tubes, the axial strains obtained from strain gauges and LVDTs remained consistent until an axial strain of around 0.015, beyond which localized deformations started to become

evident. The results of the compression tests are shown in Table.2, where the axial strains were obtained from LVDTs. In addition, tensile tests on steel coupons were conducted for each steel tube type, with three coupons that were cut from each steel tube along the longitudinal direction and tested in accordance with AS 1391 (1991). The results of the coupons tests are supplied in Table.3.

Table 2. Measured properties of steel tubes from compression tests

D_s (mm)	t_s (mm)	Height (mm)	Peak axial load (kN)	Axial strain at peak (%)	Failure mode*
60.3	3.6	181	246	3.34	EF
76.1	3.2	228	312	2.34	EF
88.9	3.2	267	348	2.43	EF
101.6	3.2	305	382	2.09	EF
114.3	6.0	305	1073	3.10	EF

* EF = Elephant foot buckling

Table 3. Material properties of steel tubes obtained from coupon tests

D_s (mm)	t_s (mm)	Elastic modulus E_s (MPa)	Yield stress f_y (MPa)	Ultimate stress f_u (MPa)
60.3	3.6	203.8	325.5	386.2
76.1	3.2	200.6	359.4	432.5
88.9	3.2	199.8	334.3	415.2
101.6	3.2	198.7	318.3	385.4
114.6	6.0	201.4	446.4	510.3

2.3.Specimen Preparation

The FRP tubes were formed using a manual wet lay-up process by wrapping epoxy resin impregnated S-Glass fiber sheets around precision-cut high-density Styrofoam templates in the hoop direction. FRP sheets were provided with a 150-mm overlap to prevent premature debonding. The FRP tubes were wrapped with two FRP sheets (each with a length to provide 3 layers of confinement), with the resulting two overlap regions

provided along the same area on the circumference of the tube. The material properties of the unidirectional fiber sheets used in the manufacture of the FRP tubes are provided in Table 4. The table reports both the manufacturer-supplied fiber properties and the properties of the FRP composites obtained from coupon tests undertaken in accordance with ASTM D3039 (2008). Five flat coupon specimens were manufactured using a wet layup technique in a custom-built high-precision mold. Each coupon was instrumented with four 20 mm strain gauges placed at mid-height, two on each side, for the measurement of the longitudinal strains. The coupon specimens were tested using a screw-driven tensile test machine under a constant cross-head movement rate, and they exhibited a nearly perfectly linear elastic behavior until their rupture near mid-height. The material properties of the FRP composites established from the coupon tests and calculated based on the nominal fiber thickness are shown in Table 4. As evident from the table, the average tensile strength obtained from the coupon tests was similar to that supplied by the manufacturer. On the other hand, the elastic modulus of the FRP composite obtained from the coupon tests was higher than that supplied by the manufacturer for the fibers, with this increase attributable to the contribution of the epoxy resin, consistent with that would be predicted by the simple rule of mixtures.

Table 4. Properties of fibers and FRP composites

Type	Nominal thickness, t_f (mm/ply)	Provided by manufacturers			Obtained from flat FRP coupon tests*		
		Tensile strength, f_f (MPa)	Ultimate tensile strain, ε_f (%)	Elastic modulus, E_f (GPa)	Tensile strength, f_{frp} (MPa)	Ultimate tensile strain, ε_{frp} (%)	Elastic modulus, E_{frp} (GPa)
S-Glass	0.2	3040	3.50	86.9	3055	3.21	95.3

*Calculated based on nominal fiber thickness

A formwork was developed and used to support the tubes during the process of concrete pouring to ensure the FRP and steel tubes remained concentric. Wooden spacers were used to hold the bottom and top of the FRP tube in place, and nails were placed at the base of the setup to maintain the position of the steel tube relative to the FRP tube. Concentric positioning of the tubes was maintained through the use of a wooden cap with steel bars anchored in that was connected to the wooden frame. The formwork is illustrated in Figure 1.

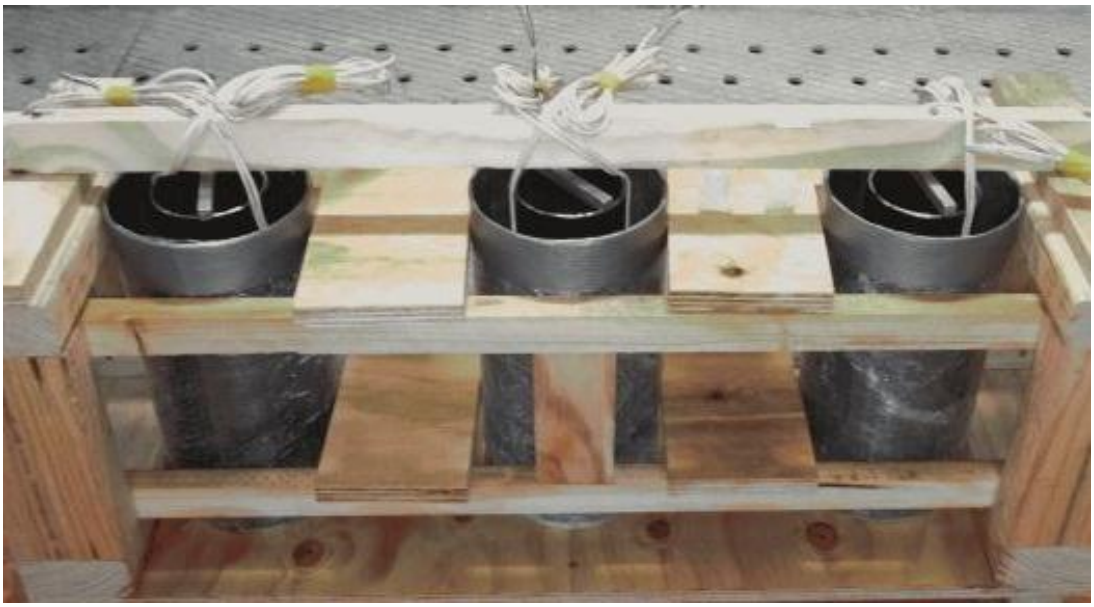

Figure 1. Formwork used in manufacture of DSTC specimens

2.4. Instrumentation and testing

For each specimen, four linear variable differentiated transformers (LVDTs) were used to measure axial deformation of the specimens, which where were mounted at the corners between the loading and supporting steel plates of the compression test machine (LVDTs 1-4 in Figure 1). The recorded deformations were used in the calculation of the average axial strains along the entire height of the specimens (referred to in this paper as AFL). In addition to the four full heights LVDTs, four inner cage LVDTs were placed at mid-height regions of the specimens (LVDTs 5-8 in Figure 1) to measure the average

axial strains within a gauge length of 170 mm (referred to as AML). The specimens were also instrumented at their mid-height with two unidirectional strain gauges with a gauge length of 20 mm placed on FRP tube to measure axial strains (referred to as ASG). The axial strains shown in Figures. 6 to 13 were obtained from the full-height LVDTs after correcting the initial part of the behavior for the additional displacements, caused by closure of the gaps in the setup, based on the data supplied from axial strain gauges and mid-height LVDTs. Strains on FRP tube along the hoop direction were measured by three unidirectional strain gauges having a gauge length of 20 mm, which were spaced at an equal distance around the perimeter of the specimen at mid-height avoiding the overlap region. The axial and lateral strains of the inner steel tubes were measured at mid-height by two axially and two laterally oriented strain gauges with a 5-mm gauge length.

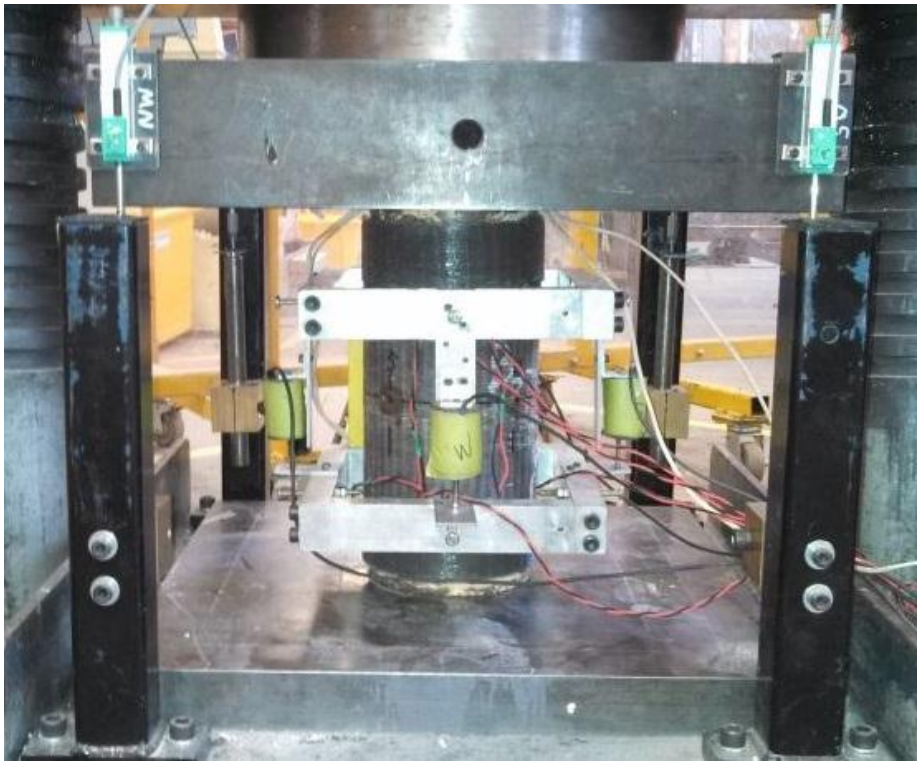

(a) Specimen before testing

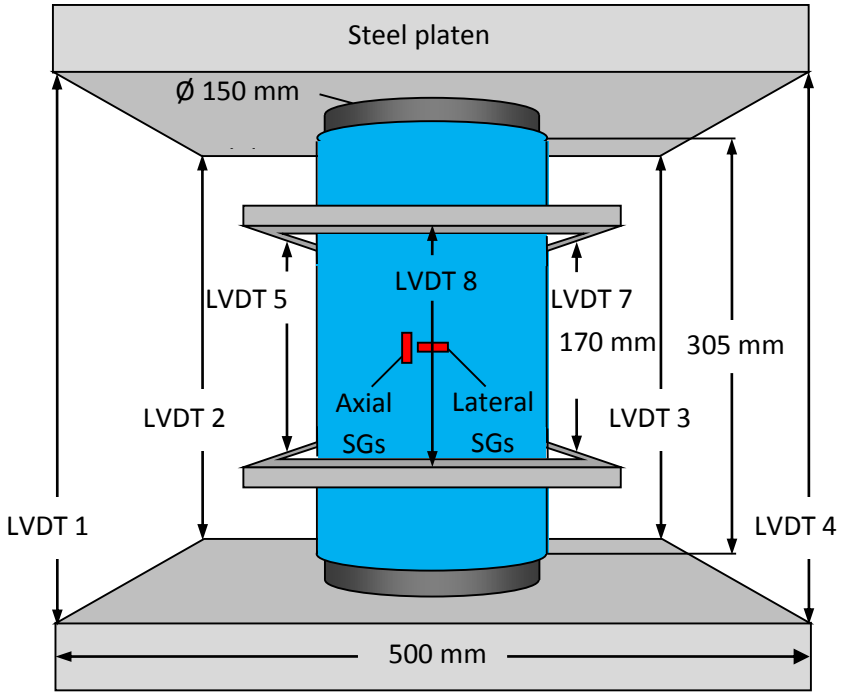

(b) Technical illustration

Figure 2. Test setup and instrumentation

The specimens were tested under axial compression using a 5000-kN capacity universal testing machine. The initial elastic portion of the monotonic and cyclic loading and the unloading/reloading cycles of the cyclic loading were performed with the load control at 5 kN per second, whereas displacement control was used at approximately 0.003 mm per second beyond initial softening for monotonic loading, and for the segments between each unloading/reloading curve for cyclic loading. Prior to testing, a capping process was completed at both ends of all specimens to ensure uniform distribution of the applied pressure, and the load was applied only to the concrete core and inner steel tube through 15-mm thick and 150-mm diameter precision-cut high-strength steel loading discs placed at each end of the specimens. Loading was applied monotonically for 20 DSTCs, six H-CFFTs, and two CFFT until failure, whereas, cyclic compression involving unloading and reloading cycles was applied at approximately 0.25% axial

strain intervals for the remaining 4 DSTC specimens. These specimens were subjected to a single unloading/reloading cycle at each prescribed axial strain level. A small axial load of at least 35 kN was maintained at the end of each unloading cycle to prevent any undesired movement in the specimen. Test setup and instrumentation are shown in Figure 2. A data logger system was used to simultaneously record strains, loads, and displacements of the test specimens at intervals of approximately one second.

3. TEST RESULTS AND DISCUSSION

3.1 Failure modes

Representative photos showing the failure modes of a group of selected specimens are shown in Figure 3, with the photos illustrating the inner steel tubes of the hollow and concrete-filled DSTCs after the removal of the concrete and FRP tube are supplied in Figure 4. As can be seen in Figure 4, the condition of the inner steel tube by the time of the failure of the specimen varied significantly among the DSTCs. It can also be seen in Figure 4 that steel tubes of hollow DSTCs exhibited one of the three different conditions at the end of testing, namely: i) local inward buckling (Figure 4(c) and 4(d)), ii) local "elephant's foot" type outward buckling (Figure 4(e)) and iii) no buckling with the original form maintained (Figures 4(a) and 4(b)). It is also evident from Figure 4 that steel tubes of concrete-filled DSTCs experienced localized bulging, with an increase in the extent of lateral expansion observed with an increase in the tube diameter (D_s). Influences of these observed failure modes of inner steel tubes on FRP tube hoop rupture strains and compressive behavior of DSTCs are discussed in detail later in the paper.

(a) DSTC-1 (Hollow, D_s = 60.3 mm)

(b) DSTC-9 (Hollow, D_s = 114.3 mm)

(c) DSTC-12 (Filled, D_s = 60.3 mm)

(d) DSTC-17 (Filled, D_s = 101.6 mm)

(e) CFFT-2

(f) H-CFFT-4 (D_s = 88.9 mm)

Figure 3. Specimen failure modes

The ultimate failure mode of all specimens was rupture of FRP tubes in the hoop direction, except for hollow CFFTs with an inner void diameter of 114.3 mm (i.e. H-CFFT-5 and 6), which experienced a failure that was governed by crushing of concrete at inner surface of the annular section. It was observed that the FRP tube rupture of hollow DSTCs with inner steel tube diameters (D_s) of 88.9, 101.6, and 114.3 mm were often localized and occurred at one of the specimen ends, as shown in Figure 3(b). It also was observed that hollow DSTCs with D_s of 60.3 and 76.1 mm exhibited a more

extensive FRP tube rupture than that seen in hollow DSTCs with larger inner steel tubes, as is evident from the comparison of Figures 3(a) and 3(b). CFFTs and filled DSTCs with D_s of 60.3 and 76.1 mm both exhibited extensive FRP tube failures (similar to that seen in the companion hollow DSTCs with the same inner tube diameters), which often initiated at the mid-height and extended towards the top and bottom of the specimens as illustrated in Figures 3(c) and 3(e). Filled DSTCs with D_s of 88.9, 101.6, and 114.3 mm, on the other hand, had more localized failure regions that were shifted towards one of the specimen ends (Figure 3(d)), though the extent of the FRP tube damage they experienced was significantly larger than those of the companion hollow DSTCs with the same D_s. The failure mode of H-CFFTs with D_s = 60.3 mm resembled that of solid CFFTs, whereas H-CFFTs with D_s = 88.9 mm exhibited a more localized FRP tube rupture (Figure 3(f)) without a similar explosive failure that was observed in their solid counterparts. As noted previously, hollow CFFTs with D_s = 114.3 mm did not experience an FRP tube rupture and their failure was governed by crushing of concrete at inner surface of the annular section. Upon inspection of the failed specimens, it was found that concrete at the inner surface of the H-CFFTs with D_s of 88.9 and 114.3 mm experienced significant damage by the time of failure, indicating that concrete crushing at inner surface contributed to the failure of both specimen pairs, albeit to a greater extent in the latter pair. These observed differences in the failure modes of hollow CFFTs can be explained by differences in the levels of hoop stresses experienced on the unsupported inner concrete surfaces of these specimens, the relative magnitude of which is to theoretically increase, for a given outer pressure, with an increase in the diameter of the void section.

3.2. Axial load capacities

Experimentally recorded axial load capacities of the DSTCs (P_T) are presented in Table 4 together with the axial capacities of the steel tubes (P_s), and unconfined concrete (P_{co}). The axial load capacities of the steel tubes (P_s) were determined from hollow steel tube tests, whereas the axial load capacities of unconfined concrete (P_{co}) were obtained by multiplying unconfined concrete strength by the area of the concrete cross-section. The individual contributions of unconfined concrete section and hollow steel tube to the axial load carrying capacity was graphically illustrated previously in Wong *et al*. (2008), where it was also shown that the total load capacity obtained through the summation of these two loads was significantly lower than the axial load capacity of the corresponding DSTC. As evident from the $P_T/(P_s+P_{co})$ ratios shown in Table 5, the results of the present study are in support of those reported in Wong *et al*. (2008), and they show that DSTC specimens of the present study developed significantly higher axial load capacities than the combined axial load capacity of the unconfined concrete section and steel tube. This increase is a result of the confinement provided by the FRP tubes in the case of hollow DSTCs, or by both FRP and steel tubes in the case of concrete-filled DSTCs.

3.3. Behavior of confined concrete in composite columns

3.3.1 FRP tube rupture strain

The average recorded hoop rupture strain ($\varepsilon_{h,rup}$) of each specimen pair is given in Table 6, with strains recorded by individual hoop strain gages of all specimens supplied in Table 7. A closer inspection of the $\varepsilon_{h,rup}$ values reported in Table 6 allows a number of observations to be made on the influence of the important parameters on hoop rupture strains. These observations are summarized in this section.

Table 5. Axial load capacities of DSTCs

Specimen	Ultimate load of DSTC, P_T (kN)	Average P_T (kN)	Peak load of steel tube, P_s (kN)	Ultimate load of unconfined concrete section, P_{co} (kN)	P_s+P_{co} (kN)	$P_T/(P_s+P_{co})$
DSTC-1	2940	2774	246	1482	1728	1.60
DSTC-2	2608					
DSTC-3	2741	2705	312	1320	1632	1.66
DSTC-4	2668					
DSTC-5	2212	2282	348	1160	1508	1.51
DSTC-6	2352					
DSTC-7	1798	1824	382	977	1359	1.34
DSTC-8	1850					
DSTC-9	2367	2291	1073	770	1843	1.24
DSTC-10	2215					
DSTC-11	3579	3446	246	1695	1941	1.77
DSTC-12	3313					
DSTC-13	3409	3507	312	1687	1999	1.75
DSTC-14	3605					
DSTC-15	3683	3549	348	1674	2022	1.75
DSTC-16	3415					
DSTC-17	3567	3620	382	1662	2044	1.77
DSTC-18	3672					
DSTC-19	4213	4133	1073	1560	2633	1.57
DSTC-20	4053					
DSTC-1C	2355	2269	348	995	1343	1.69
DSTC-2C	2183					
DSTC-3C	3416	3319	348	1436	1784	1.86
DSTC-4C	3221					

Investigation of the hoop rupture strains of hollow DSTCs in Table 6 indicates that the specimens are natural separated into two groups according to their $\varepsilon_{h,rup}$. DSTCs with inner steel tube diameters (D_s) of 60.3 and 76.1 mm (i.e. DSTCs 1-4), which formed the first group, exhibited hoop rupture strains that were significantly larger than those of the specimens of the second group with steel tube diameters of 88.9, 101.6 and 114.3 mm (i.e. DSTCs 5-10). The lower hoop rupture strains of the DSTCs in the second group

can be attributed to the more localized failure region formations observed in these specimens, as discussed previously. The local buckling experienced by the inner steel tubes of DSTCs 5-10 near one of the specimen ends (refer to Figure 4) resulted in stress concentrations on FRP tubes of these specimens leading to their localized failure away from the mid-height region where the hoops strains were measured. Steel tubes of DSTCs 1-4, on the other hand, experienced no local buckling and, in turn, FRP tubes of these specimens were not subjected local stress concentrations, which resulted in an earlier FRP tube rupture in DSTCs 5-10. The implications of these observed differences in the failure modes of inner steel tubes on the axial compressive behavior of hollow DSTCs are discussed in detail in the following sections.

(a) Hollow D_s/t_s=60.3/3.6 (DSTC-1)

(b) Hollow D_s/t_s=76.1/3.2 (DSTC-3)

(c) Hollow D_s/t_s=88.9/3.2 (DSTC-5)

(d) Hollow D_s/t_s=101.6/3.2 (DSTC-8)

(e) Hollow D_s/t_s=114.3/6.0 (DSTC-9)

(f) Filled D_s/t_s=60.3/3.6 (DSTC-11) (g) Filled D_s/t_s=76.1/3.2 (DSTC-14) (h) Filled D_s/t_s=88.9/3.2 (DSTC-15) (i) Filled D_s/t_s=101.6/3.2 (DSTC-17) (j) Filled D_s/t_s=114.3/6.0 (DSTC-20)

Figure 4. Inner steel tube deformations

The comparison of hoop rupture strains of filled DSTCs illustrates a similar influence of D_s on $\varepsilon_{h,rup}$ to that seen in hollow DSTCs, with an increase in D_s leading to a slight decrease in $\varepsilon_{h,rup}$. Once again, this reduction is attributable to the increased plastic deformations experienced by inner steel tubes with larger diameters, which took the form of bulging at one of the specimen ends in filled DSTCs (refer to Figure 4) that resulted in the failure of the FRP tube at a region that corresponded to these deformations. However, the reduction seen in filled DSTCs was much more subtle than that observed in hollow DSTCs, and filled DSTCs with D_s of 88.9, 101.6 and 114.3 mm (i.e. DSTCs 15-20) developed significantly higher hoop rupture stains than those of their hollow counterparts with the same D_s (i.e. DSTCs 5-10). These observations indicate that, in DSTCs with D_s of 88.9, 101.6 and 114.3 mm, buckling of hollow inner steel tubes had a more detrimental influence on the compressive behavior of hollow DSTCs than that caused by bulging of concrete-filled inner steel tubes on the behavior of filled DSTCs. Nonetheless, these observations show that in both hollow and filled DSTCs plastic deformations experienced by steel tubes might result in reductions in

hoop rupture strains on the FRP tube through a mechanism that leads to a localized failure of the FRP tube due to stress concentrations.

Table 6. Ultimate condition of concrete in composite columns

Specimen	f_{lu}/f'_c	f'_{cu} (MPa)	Avg. f'_{cu} (MPa)	f'_{cu}/f'_c	*Avg.* f'_{cu}/f'_c	ε_{cu} (%)	Avg. ε_{cu} (%)	$\varepsilon_{cu}/\varepsilon_{co}$	Avg. $\varepsilon_{cu}/\varepsilon_{co}$	*Avg.* $\varepsilon_{hup,rup}$ (%)
DSTC-1	0.50	175.3	164.8	1.82	1.71	3.51	3.15	11.30	10.12	1.86
DSTC-2		154.2		1.60		2.78		8.95		
DSTC-3	0.50	176.1	173.4	1.83	1.80	3.94	3.77	12.68	12.14	1.76
DSTC-4		170.8		1.78		3.60		11.59		
DSTC-5	0.50	154.6	160.4	1.61	1.67	2.99	3.26	9.63	10.49	0.89
DSTC-6		166.2		1.73		3.53		11.36		
DSTC-7*	0.50	139.3	144.5	1.45	1.50	2.50	3.03	8.05	9.75	0.80
DSTC-8		144.5		1.50		3.03		9.75		
DSTC-9	0.50	161.6	161.6	1.68	1.68	3.18	3.18	10.24	10.24	1.02
DSTC-10*		143.0		1.49		2.77		8.92		
DSTC-11	0.50	189.5	182.0	1.97	1.89	3.64	3.42	11.72	10.99	1.95
DSTC-12		174.6		1.81		3.19		10.27		
DSTC-13	0.50	175.8	181.4	1.83	1.89	3.09	3.43	9.95	11.03	1.85
DSTC-14		187.0		1.94		3.76		12.10		
DSTC-15	0.50	179.2	185.4	1.86	1.93	2.88	3.19	9.27	10.27	1.74
DSTC-16		191.6		1.99		3.50		11.27		
DSTC-17	0.50	184.3	187.4	1.92	1.95	3.24	3.28	10.43	10.56	1.63
DSTC-18		190.5		1.98		3.32		10.69		
DSTC-19	0.50	194.0	188.9	2.02	1.96	3.37	3.20	10.85	10.30	1.66
DSTC-20		183.9		1.91		3.03		9.75		
DSTC-1C	0.58	166.5	159.3	2.02	1.93	4.50	3.99	15.41	13.80	1.60
DSTC-2C		152.1		1.85		3.48		12.19		
DSTC-3C	0.58	176.3	170.7	2.14	2.07	3.10	2.96	10.69	10.20	1.65
DSTC-4C		165.1		2.00		2.81		9.69		
H-CFFT-1	0.50	131.2	130.9	1.36	1.36	2.94	2.97	9.46	9.56	1.83
H-CFFT-2		130.6		1.36		3.00		9.66		
H-CFFT-3	0.50	77.2	66.1	0.80	0.69	2.15	2.17	6.92	6.99	0.52
H-CFFT-4		54.9		0.57		2.19		7.05		
H-CFFT-5	0.50	41.9	51.2	0.44	0.53	0.50	0.42	1.61	1.34	0.14
H-CFFT-6		60.5		0.63		0.33		1.06		
CFFT-1	0.50	153.0	163.7	1.59	1.70	2.44	2.71	7.86	8.71	1.85
CFFT-2		174.3		1.81		2.97		9.56		

* Premature failure. The marked specimens were excluded in the calculation of the average values

The comparison of $\varepsilon_{h,rup}$ of hollow and filled DSTCs with inner steel tube diameters of 60.3 and 76.1 mm shown in Table 6 indicate that the hoop rupture strains of these specimens were not influenced by the presence of concrete filling inside the steel tube. As noted previously, in specimens with D_s of 60.3 and 76.1 mm, inner steel tubes of hollow DSTCs exhibited no local buckling and those of filled DSTCs experienced only a slight bulging. Therefore, these observations indicate that, in DSTCs with inner steel tubes that do not undergo local buckling or significant local bulging, companion hollow and filled DSTCs develop comparable hoop rupture strains, with magnitudes larger than those seen in DSTCs with inner steel tubes that exhibit the said deformations.

In addition to the summarized observations on DSTCs, it can also been seen from Tables 6 and 5.7 that CFFTs and H-CFFTs with D_s = 60.3 mm developed similar hoop rupture strains to those of the hollow and filled DSTCs with D_s of 60.3 and 76.1 mm. This can be explained by the similar failure modes observed in these specimens, as discussed previously. Conversely, $\varepsilon_{h,rup}$ of the hollow DSTCs with inner void diameters of 88.9 and 114.3 mm were much lower than those of the solid CFFTs and H-CFFTs with a D_s of 60.3 mm. Observed differences in the hoop rupture strains of these specimens can be explained by different failure modes experienced by these specimens, as previously discussed in Section 3.1.

3.3.2 Influence of axial strain measurement methods

Based on the investigation of the behavior of FRP-confined concrete specimens, it was previously reported in Ozbakkaloglu and Lim (2013) that the recorded ultimate axial strain (ε_{cu}) is highly sensitive to the instrumentation arrangement used in the measurement of these strains. It was demonstrated that higher axial strains were obtained from full-height LVDTs mounted on the steel loading platens of the

compression machines compared to those from the LVDTs mounted along the mid-height region of the specimens and the strain gauges attached on the surface of the specimens. It was further demonstrated in Lim and Ozbakkaloglu (2014b) that this effect is more pronounced in HSC specimens than in NSC specimens.

Table 7. Variation of hoop rupture strains around perimeter of specimens

Specimens	SG1 (%)	SG2 (%)	SG3 (%)	Average (%)
DSTC-1	2.00	1.98	1.85	1.94
DSTC-2	1.55	1.99	1.76	1.77
DSTC-3	1.54	1.67	1.75	1.65
DSTC-4	2.09	1.65	1.85	1.86
DSTC-5	0.85	0.73	1.49	1.03
DSTC-6	0.45	0.81	0.98	0.75
DSTC-7	1.07	0.60	1.60	1.09
DSTC-8	0.97	0.55	0.89	0.80
DSTC-9	0.68	1.18	1.21	1.02
DSTC-10	0.89	0.85	0.90	0.88
DSTC-11	1.71	2.15	2.06	1.97
DSTC-12	1.63	1.85	2.28	1.92
DSTC-13	1.51	1.95	1.80	1.75
DSTC-14	1.54	2.09	2.19	1.94
DSTC-15	1.61	1.89	1.65	1.72
DSTC-16	1.49	1.89	1.91	1.76
DSTC-17	1.40	1.49	1.73	1.54
DSTC-18	1.51	1.67	1.97	1.72
DSTC-19	1.70	1.77	1.75	1.74
DSTC-20	1.27	1.54	1.90	1.57
DSTC-1C	1.79	1.31	1.87	1.66
DSTC-2C	1.16	2.05	1.42	1.54
DSTC-3C	1.96	1.35	1.72	1.68
DSTC-4C	1.88	1.49	1.50	1.62
H-CFFT-1	2.21	1.34	2.06	1.87
H-CFFT-2	1.86	1.66	1.85	1.79
H-CFFT-3	0.58	0.71	0.67	0.65
H-CFFT-4	0.45	0.40	0.28	0.38
H-CFFT-5	0.07	0.05	0.09	0.07
H-CFFT-6	0.17	0.25	0.23	0.22
CFFT-1	1.51	1.82	1.68	1.67
CFFT-2	2.09	1.88	2.14	2.04

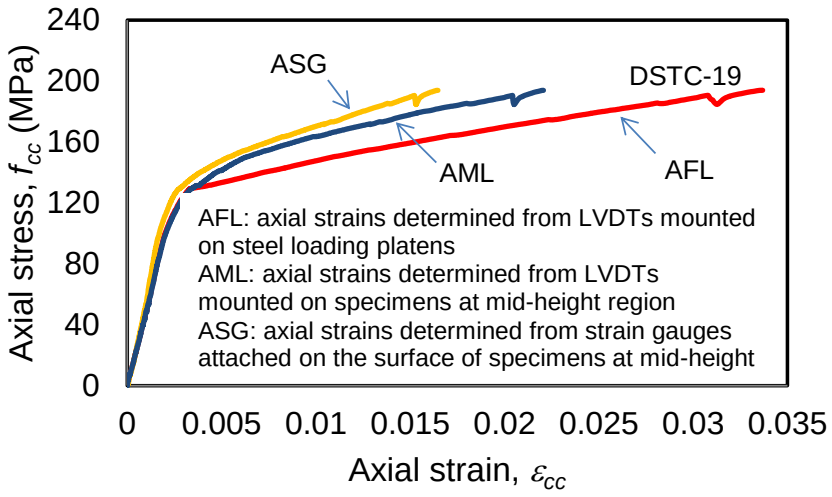

Figure 5. Influence of instrumentation arrangements on axial stress-strain curves

Figure 5 compares the stress-strain curves of a specimen of the present study with axial strains obtained from: i) full-height LVDTs (AFL), ii) LVDTs mounted along the mid-height region of the specimen (AML), and iii) strain gauges attached on the surface of the FRP tube at mid-height (ASG). As illustrated in Figure 5, there are significant differences in the strains obtained from different measurement methods along the second branch of the stress-strain relationships. Table 8 shows the ultimate axial strains (ε_{cu}) recorded using these three different instrumentation arrangements for all the specimens of the present study. For the DSTC specimens, the average ratios of the axial strains recorded by the mid-height LVDTs (AML) and strain gauges (ASG) to that of the full-height LVDTs (AFL) are established as 0.57 and 0.44, respectively. This observation indicates that the axial strains of HSC DSTCs are influenced by the instrumentation arrangement used in measuring these strains. The observed differences can be attributed to nonuniform inelastic deformations of the specimens along their heights caused by the presence of localized regions of higher plasticity. Therefore, for the most accurate interpretation of the results, it is recommended that in future studies axial strains of test specimens be obtained using a combination of strain measurement

methods, as it was done in the present study. In this approach, during the initial stages of loading, the measurements from axial strain gauges or mid-height LVDTs are used, as they are highly reliable until the initial peak on the axial stress-strain curve. However, beyond the initial peak, both measurement methods become sensitive to localized effects, and hence corner LVDTs are used in this region as they provide a more accurate representation of the overall axial behavior of the specimen, which is free of localized effects.

3.3.3. Axial stress-strain behavior

The axial stress of concrete inside the DSTCs was calculated by dividing the axial load resisted by the concrete (P_c) with the net cross-sectional area of the concrete section. The load applied to the concrete was determined by subtracting the axial load resisted by the steel tube (P_s) for a given axial strain, from the total load resisted by the DSTC (P_T) at the same axial strain. The load acting on the steel tube was calculated by assuming that the load-strain behavior of the steel tube inside a DSTC is similar to that of the corresponding unconfined steel tube obtained from a hollow tube compression test. When the axial strain of strain of a DSTC specimen exceeded the axial strain that corresponded to the peak axial load (P_s) of the hollow steel tube, it was assumed that the inner steel tube maintained this load capacity (P_s) until the failure of the specimen. This is because in a DSTC specimen the buckling of the steel inner tube is prevented or delayed by lateral restraint provided by surrounding concrete, and the decrease in the load carried by the tube may be expected to be limited. The load-axial strain relationships of steel tubes used in cyclically loaded specimens were generated from monotonic compression tests by assuming that the slope of the unloading/reloading path is the same as the elastic modulus of the steel tube. It is worth noting that, as previously discussed in Yu *et al*. (2012), when the steel tube and concrete of a DSTC are axially

strained to a level that is larger than the yield strain of steel, the plastic strain component of the concrete is generally smaller than that of the steel tube because the nonlinearity of concrete is largely due to degradation in stiffness, whereas that of steel depends almost solely on plasticity. As a result, during the unloading cycle, the steel tube reaches zero stress before the axial load reduces to zero, and a subsequent reduction in the axial load might result in the development of tensile stresses in the steel tube if the bond between the inner steel tube and concrete is maintained. In the present study, the development of tensile stresses in inner steel tube was not allowed with the assumption of bond slip at the concrete-steel tube interface. However, it is recommended that future studies on cyclically loaded DSTCs have a close look into this part of the behavior with the aim of gaining further insight into the nature of the said interaction. The ultimate axial stresses (f'_{cu}) and strains (ε_{cu}) of concrete reported in Table 6 and concrete axial stress-strain relationships shown in Figures 5 to 13 were established using the approach summarized in this section and Section 3.3.2.

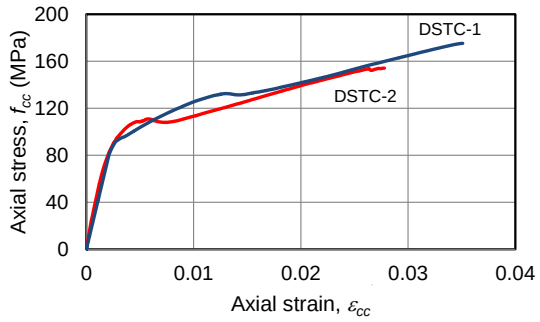

(a) DSTC-1&2

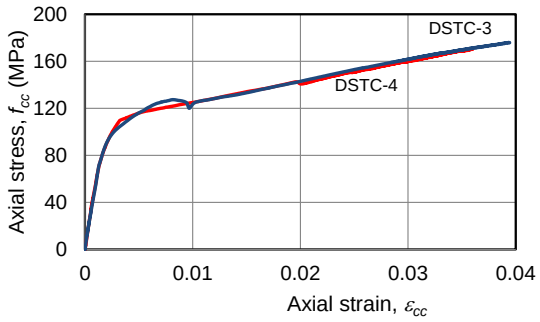

(b) DSTC-3&4

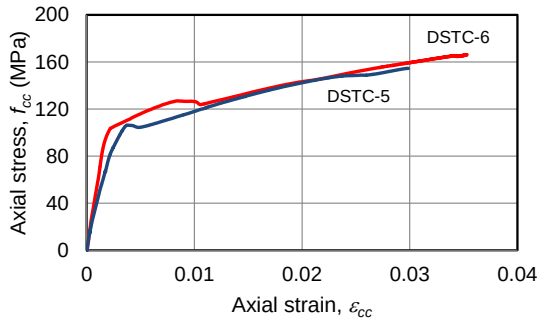

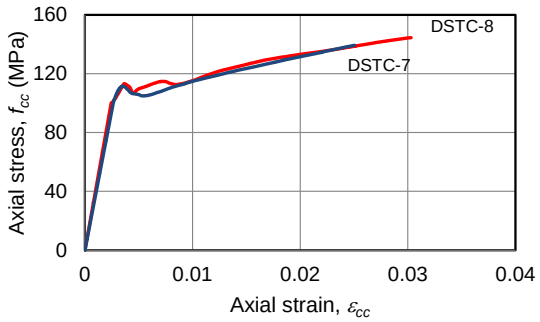

(c) DSTC-5&6

(d) DSTC-7&8

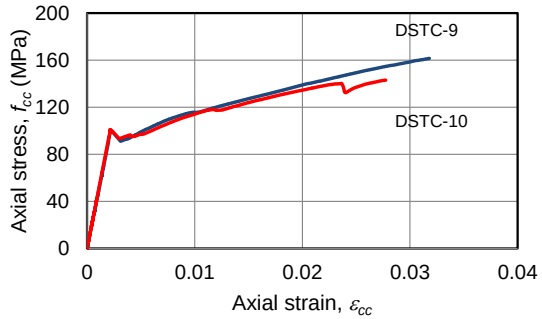

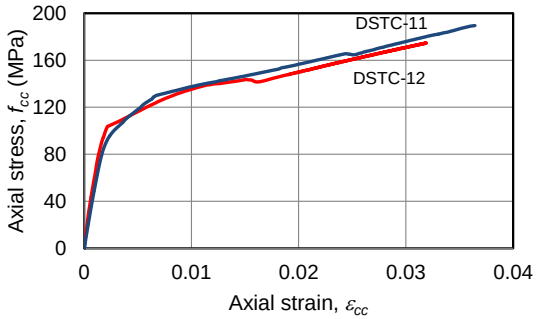

(e) DSTC-9&10

(f) DSTC-11&12

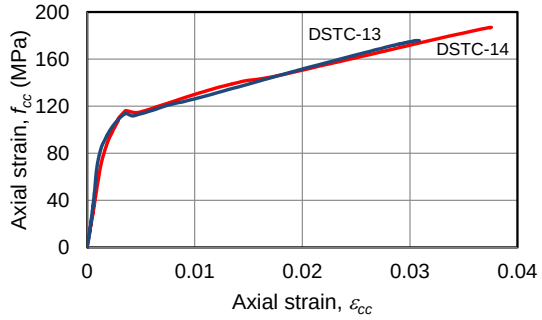

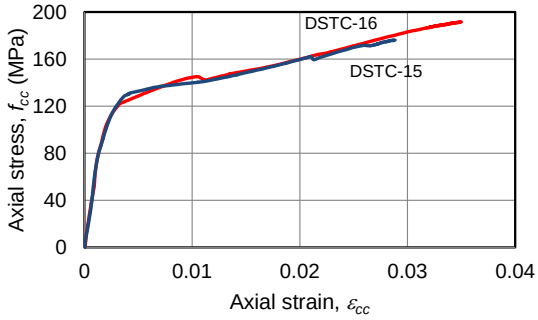

(g) DSTC-13&14

(h) DSTC-15&16

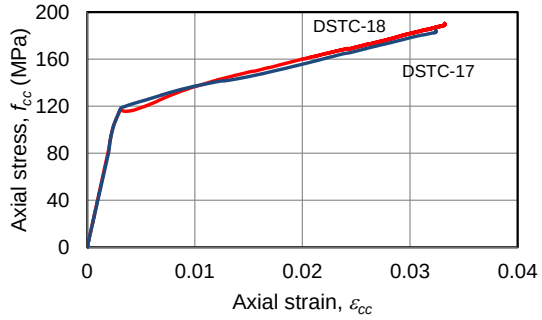

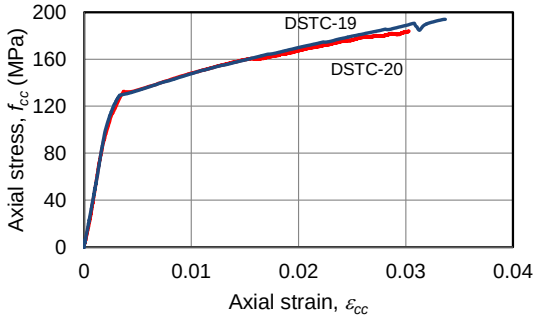

(i) DSTC-17&18

(j) DSTC-19&20

Figure 6. Axial stress-strain behavior of concrete in DSTCs

Table 8. Comparison of ultimate axial strains determined from different instrumentation arrangements

Specimen	ε_{cu} (%)			Average ε_{cu} (%)			Differences	
	AFL	AML	ASG	AFL	AML	ASG	AML/AFL	ASG/AFL
DSTC-1	3.51	1.35	1.29	3.15	1.27	0.97	0.40	0.31
DSTC-2	2.78	1.18	0.65					
DSTC-3	3.94	2.50	2.19	3.77	2.34	1.91	0.62	0.51
DSTC-4	3.60	2.18	1.62					
DSTC-5	2.99	1.67	1.22	3.26	1.78	1.84	0.54	0.56
DSTC-6	3.53	1.88	2.46					
DSTC-7*	2.50	1.78	1.32	3.03	1.27	1.49	0.42	0.49
DSTC-8	3.03	1.27	1.49					
DSTC-9	3.18	2.12	0.72	3.18	2.12	0.72	0.67	0.23
DSTC-10*	2.77	2.33	0.98					
DSTC-11	3.64	1.56	1.79	3.42	1.46	1.52	0.43	0.45
DSTC-12	3.19	1.35	1.25					
DSTC-13	3.09	0.45**	1.72	3.43	1.94	1.70	0.57	0.50
DSTC-14	3.76	1.94	1.68					
DSTC-15	2.88	1.58	0.99	3.19	1.72	1.26	0.54	0.39
DSTC-16	3.50	1.86	1.53					
DSTC-17	3.24	1.23	1.42	3.28	1.41	1.18	0.43	0.36
DSTC-18	3.32	1.59	0.94					
DSTC-19	3.37	2.21	1.65	3.20	2.01	1.49	0.63	0.47
DSTC-20	3.03	1.81	1.33					
DSTC-1C	4.50	3.02	-	3.99	2.91	-	0.73	-
DSTC-2C	3.48	2.79	-					
DSTC-3C	3.10	2.49	-	2.96	2.36	-	0.80	-
DSTC-4C	2.81	2.22	-					
H-CFFT-1	2.94	1.04	1.34	2.97	1.69	1.73	0.57	0.58
H-CFFT-2	3.00	2.33	2.11					
H-CFFT-3	2.15	0.74	0.47	2.17	0.74	0.47	0.34	0.22
H-CFFT-4	2.19	0.24**	0.32**					
H-CFFT-5	0.50	0.28	0.22	0.42	0.22	0.18	0.52	0.42
H-CFFT-6	0.33	0.15	0.13					
CFFT-1	2.44	0.30**	1.20	2.71	0.84	1.37	0.31	0.50
CFFT-2	2.97	0.84	1.53					

AFL: axial strains determined from LVDTs mounted on steel loading platens
AML: axial strains determined from LVDTs mounted on specimens
ASG: axial strains determined from strain gauges attached on the surface of specimens
* Premature failure. The marked specimens were excluded in the calculation of the average values.
** Encountered instrumentation problems. The marked values were excluded from the calculations.

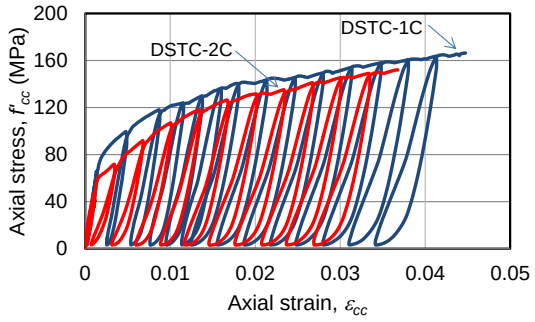

(a) DSTC-1C&2C

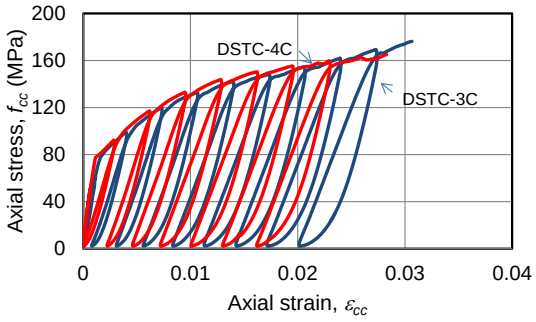

(b) DSTC-3C&4C

Figure 7. Stress-strain behavior of concrete in cyclically loaded DSTCs

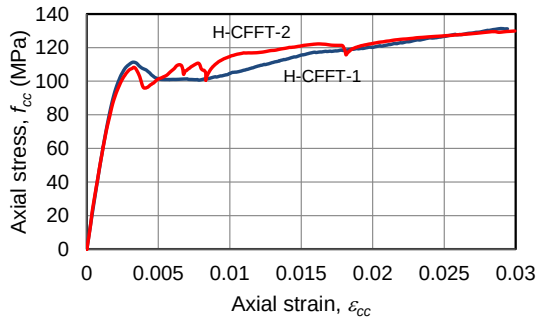

(a) H-CFFTs with inner void diameter of 60.3 mm

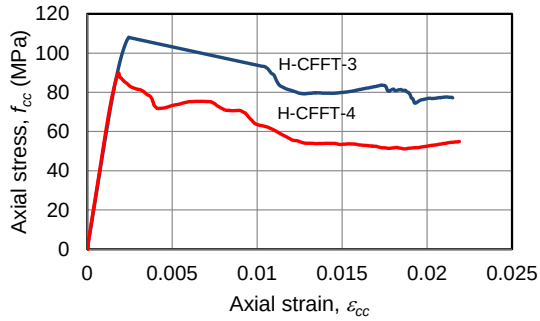

(b) H-CFFTs with inner void diameter of 88.9 mm

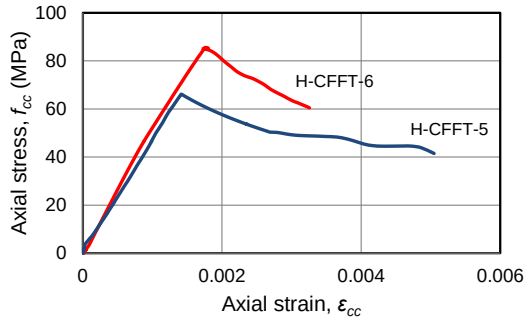

(c) H-CFFTs with inner diameter of 114.3 mm

Figure 8. Axial stress-strain behavior of concrete in H-CFFTs

Figures 6 to 9 present the concrete stress-strain relationships for the specimens of the present study. As evident from these figures, except for H-CFFTs with large inner void diameter (H-CFFT-3 to 6), all the specimens exhibited almost monotonically ascending stress-strain curves, indicating that the concrete inside the DSTCs, CFFTs, and H-CFFTs was effectively confined. It can also be observed in these figures that most of the specimens experienced a sudden drop in strength or a plateau region immediately after

the transition point between the initial ascending branch and the second branch that follow it. A similar behavior was also observed in FRP-confined HSC specimens, and as was recently discussed in detail in Refs (Ozbakkaloglu 2013d, Lim and Ozbakkaloglu 2014c) and this is attributable to the brittle nature of the high-concrete strength. It can be seen in Figure 8 that there were significant differences between the axial stress-strain curves of the companion hollow CFFTs, H-CFFT-3 and 4 and H-CFFT-5 and 6. Visual observation of these specimens after testing revealed that the specimens that exhibited lower compressive strengths (i.e. H-CFFT-4 and 5) failed near their top portions with an isolated failure region. On the other hand, their counterparts with higher strengths (i.e. H-CFFT-3 and 6) exhibited larger failure regions that extended from one of the specimen ends toward the specimen mid-height. This observation suggest that the lower capacities of the former group can be attributed to the stress concentrations experienced by these specimens at their ends, which resulted in the formation of a weaker region near one of the specimen ends.

As expected, the stress-strain behavior of the DSTC specimens along the second branch of the curve is influenced by the important parameters, including the loading pattern, the diameter of inner steel tube and presence (or absence) of concrete filling inside it. The influence of these parameters on the stress-strain behavior of DSTCs is discussed in the following sections, continued by discussion on the relative performance of DSTCs compared with those of CFFTs and H-CFFTs.

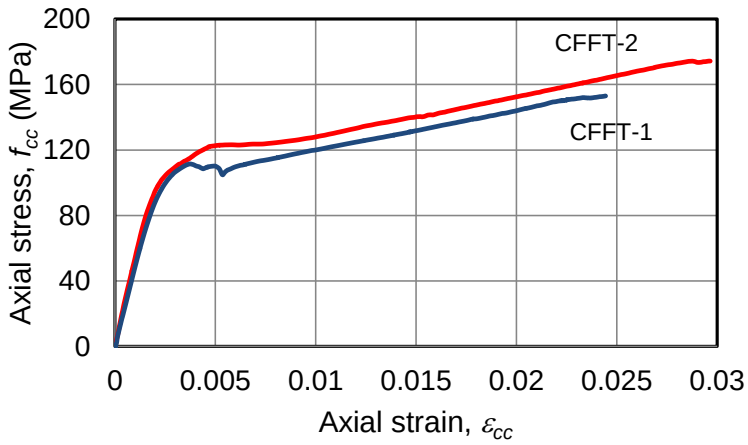

Figure 9. Axial stress-strain behavior of concrete in CFFTs

3.3.4. Effect of steel tube diameter

Figure 10 illustrates the stress-strain relationships of DSTCs with different inner steel tube diameters (D_s). For clarity of presentation, two sets of charts were supplied for both hollow (Figures 10(a) and 10(b)) and concrete-filled (10(c) and 10(d)) DSTCs, with the first chart showing the curves of specimens with similar D_s/t_s ratios and the second chart those of specimens with the same inner steel tube thickness (t_s). At first glance, both the curves shown in Figure 10 and results tabulated in Table 6 indicate that the ultimate axial stress (f'_{cu}) and strain (ε_{cu}) of the hollow DSTCs of the present study were not significantly influenced by the inner steel tube diameter. Likewise, no clear influence of D_s was evident on ε_{cu} of the filled DSTCs, whereas an increase in D_s resulted in an increase in their f'_{cu}. These observations on the influence of D_s in hollow DSTCs do not agree with those previously reported in Refs. (Wong *et al*. 2008, Ozbakkaloglu and Louk Fanggi 2013, Louk Fanggi and Ozbakkaloglu 2013), where it was shown that D_s influences the ultimate conditions of concrete in hollow DSTCs and ε_{cu} increases with an increase in D_s. Therefore, to understand the reasons behind the noted differences in observations, a closer investigation of the results of the present study is required. In this process it will also be important to clearly establish the role of the inner steel tube that might play in the eventual failure of the DSTC. By the time of

DSTC failure, as a result of the interactions among the influential parameters, such as D_s/t_s, confining pressure (fl_u) and void ratio (D_s/D), as illustrated in Section 3.1, inner steel tube would have experienced one of the three conditions: i) local inward buckling, ii) local outward buckling, or iii) no local buckling. In the context of the overall DSTC behavior, it is important to distinguish the first two steel tube failure modes from the third one, as the former leads to a steel tube-induced failure of the DSTC, whereas in the latter case the failure is caused by the system dilation of the DSTC (referred to as dilation-based failure). In a steel tube-induced failure, FRP tube experiences a localized failure (at a region along its height that corresponds to the local buckling region of inner steel tube) that is caused by stress concentrations that result from buckling of the inner tube. In a dilation-based failure, on the other hand, FRP tube is free from localized stresses exerted by inner steel tube and its failure is governed by the overall dilation behavior of the DSTC, with the failure occurring when the hoop rupture strain of the FRP tube is reached. Therefore, the steel tube-induced failure can be considered an early failure mode, in which the full capacity of the FRP tube could not be develop as a result of its early local failure under stress concentrations.

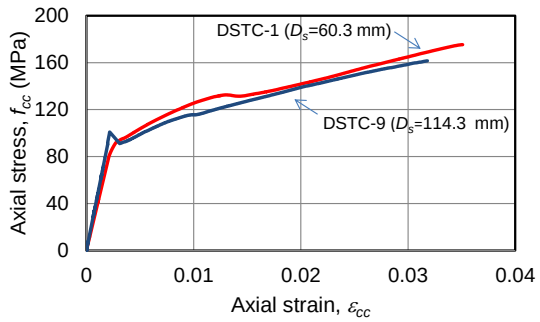

(a) Hollow DSTCs with similar D_s/t_s ratios

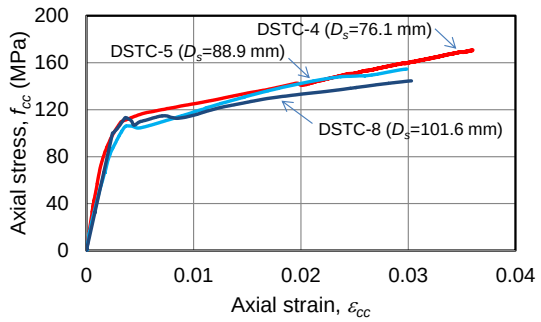

(b) Hollow DSTCs with same inner steel tube thickness

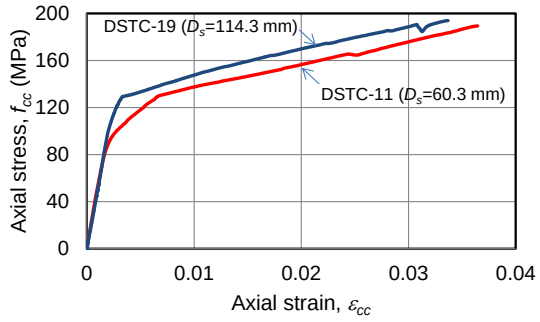

(c) Filled DSTCs with similar D_s/t_s ratios

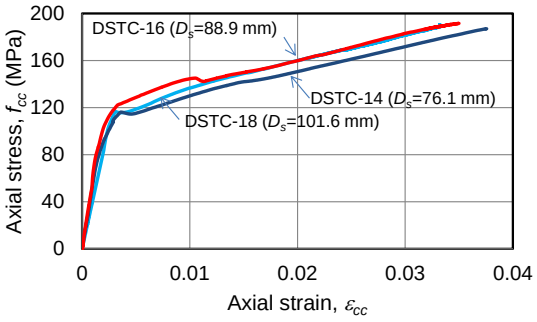

(d) Filled DSTCs with same inner steel tube thickness

Figure 10. Influence of inner steel tube diameter (D_s)

If the results of the presents study are to be investigated with due consideration given to the failure modes established in this section, a number of important observations can be made on the influence of D_s on ε_{cu} of hollow DSTCs. For example, the comparison of the average ε_{cu} of the DSTC pairs 1&2 and 3&4 shows that ε_{cu} increased from 3.15% to 3.77% with an increase in D_s from 60.3 to 76.1 mm. As was previously shown in Figure 3, inner steel tubes of these specimens were free from local buckling. This observation indicates that, in hollow DSTCs that exhibit dilation-based failure, ε_{cu} increases with an increase in D_s. The comparison of the ultimate axial stresses (f'_{cu}) of the same specimen pairs shows that an increase in D_s also resulted in an increase in f'_{cu}. However, as evident from Table 6, the increase in f'_{cu} was less significant than that in ε_{cu}, which can be attributed to the reduced slope of the second branch of the stress-strain relationship with an increase in D_s. A similar observation on the reduced second branch slope of hollow DSTCs with larger inner steel tubes was previously noted in Ref. (Wong *et al.* 2008). Both the increase in ε_{cu} and decrease in the second branch slope can be attributed to the decrease in the system dilation rate of hollow DSTCs with an increase in D_s. This reduction results in a slower development of confining pressures applied by the FRP tube, which explains both the lower rate of strength gains and higher ultimate axial strains seen in DSTCs with a larger D_s.

Comparisons of the ultimate axial strains (ε_{cu}) of the hollow DSTCs with inner steel tube diameters (D_s) of 88.9, 101.6 and 114.3 mm (i.e. DSTCs 5-10) with that of the hollow DSTCs with D_s = 76.1 mm (i.e. DSTCs 3 and 4) indicate that all of the specimen pairs in the former group exhibited a lower average ε_{cu} than that of the latter DSTC pair. This observation becomes meaningful only after noting that DSTCs 5-10 all experienced a steel tube-induced failure, which was initiated by the inward (in DSTCs 5-8) or outward buckling (in DSTC 9 and 10) of the inner steel tube, as was previously shown in Figure 4. The steel tube governed failure modes of these specimens resulted in their earlier failure compared to that of DSTCs 3 and 4 that exhibited a dilation-based failure, as discussed previously. The effects of the different failure modes of these specimens can also be seen in their hoop rupture strains shown in Tables 6 and 7, with DSTCs 5-10 developing significantly lower $\varepsilon_{h,rup}$ compared to those of DSTCs 1-4, due to localized failures experienced by the former specimens that corresponded to one of their ends. Furthermore, as to be expected in stress-strain curves with ascending second branches, reduced ε_{cu} of DSTCs 5-10 also translated into their lower ultimate axial stresses (f'_{cu}). The decrease in f'_{cu} was particularly pronounced in specimens with D_s of 88.9 and 101.6 mm due to the combined effect of the reduced second branch slope and ε_{cu}. The higher steel tube stiffness (t_s/D_s) of DSTCs 9 and 10 with D_s = 114.3 mm appears to have compensated to some extent for the reduction in the second branch slope that resulted from an increase in D_s, and as a result further decrease in f'_{cu} was not seen in these specimens over those observed in DSTCs 5-8. A similar influence of steel tube stiffness on the second branch slope of concrete in hollow DSTCs was previously noted in Ref. (Louk Fanggi and Ozbakkaloglu 2013), and these observations suggest that an increase in tube stiffness leads to an increase in the rate of dilation of the DSTC system.

Comparisons of the results from the concrete-filled DSTCs indicate that D_s had only a minor influence on ε_{cu} of these specimens. However, a clear understanding of the influence of this parameter requires the understanding of the two confinement mechanisms that are present in filled DSTCs, together with their interaction with each other. That is, as far as the dilation behavior is concerned, filled DSTCs can be seen as two discrete systems that interact with each other, namely: i) a concrete-filled inner steel tube and ii) an FRP-confined annular concrete section. Diameter of inner steel tube (D_s) affects both confinement mechanisms and their resulting dilation behaviors. It is easy to visualize that D_s, together with t_s, have a direct influence on the behavior of the core concrete inside the steel tube, and confinement pressures exerted on this section varies with the stiffness of inner steel tube (t_s/D_s). Likewise, as discussed previously for hollow DSTCs, D_s affects the behavior of the FRP-confined annular concrete section, with a change in D_s resulting in a change in the dilation behavior of this section. In addition to its influence on these two confinement mechanism, D_s also affects relative areas of the core and annular concrete sections, thereby influencing the interaction between the dilation behaviors of steel tube-confined core and FRP tube-confined annular concrete sections. Therefore, combined influences of these two confinement mechanisms and their interaction with one another determine the resulting influence of D_s on the dilation behavior of filled DSTCs. In addition, as discussed previously, D_s also influences the failure mode of the inner steel tube, and hence the effect of this on the failure condition of DSTCs will also have to be considered in establishing the cumulative effect of D_s on the system behavior and resulting ultimate axial strain (ε_{cu}). It should be apparent from the above summary that D_s has a complex influence on the behavior of concrete-filled DSTCs, as it affects the behavior through a number of different but interrelated mechanisms.

Comparisons of the results of the filled DSTCs in Table 6 and Figure 10 indicate a very slight decrease in the ultimate axial strain (ε_{cu}) with an increase in D_s. However, in interpreting this observation, the failure modes of inner steel tubes need to be considered. As discussed previously, filled DSTCs with inner steel tubes of 88.9 mm or larger diameters experienced more extensive inner steel tube deformations that resulted in an earlier rupture of their FRP tubes due to localized stress concentrations, as was reflected in their hoop rupture strains (refer to Table 6). Therefore, the results indicate that the lower ε_{cu} of these specimens were contributed by the earlier FRP tube failure they experienced, and hence this reduction in ε_{cu} cannot be directly attributed to the changes in the sectional dilation behavior of the filled DSTCs with D_s. As should be clear from the discussion presented in this section, additional focused analytical and experimental studies are required to gain further insight into the complex influence of D_s on the dilation behavior of filled DSTCs.

Comparisons of the ultimate axial stresses (f'_{cu}) of the filled DSTCs of the present study show that in general an increase in D_s resulted in an increase in f'_{cu}. This increase can be explained by an increase in the relative contribution of the confinement provided by inner steel tube to the load carrying capacity of the DSTC, with this contribution can be represented by the steel tube reinforcement ratio ($\rho_s = t_s.D_s/D$). An increase in ρ_s, resulting from an increase in t_s, D_s or both, would lead to an increase in the second branch slope of the stress-strain relationship of filled DSTCs. As can be seen from the comparison of ε_{cu} and f'_{cu} of DSTCs 11-20, owing to an increase in their second branch slopes, even with their slightly lower ε_{cu}, specimens with larger D_s developed higher f'_{cu} than their counterparts with smaller inner steel tubes.

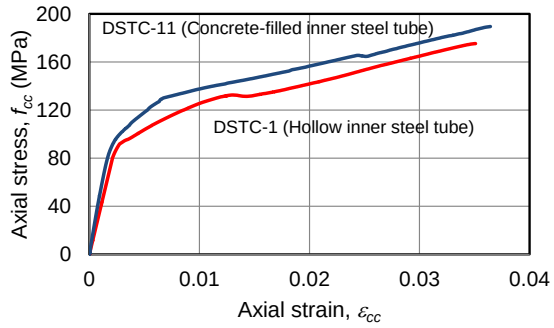

(a) DSTCs with D_s= 60.3 mm

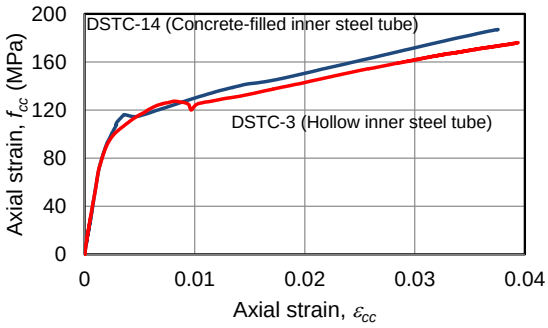

(b) DSTCs with D_s= 76.1 mm

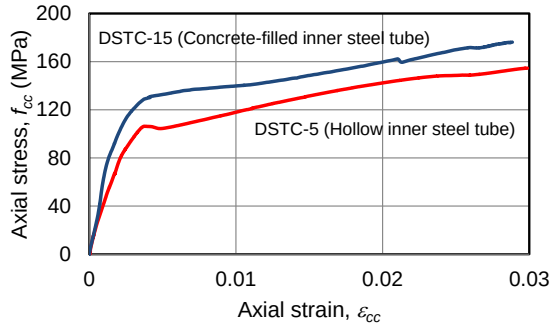

(c) DSTCs with D_s= 88.9 mm

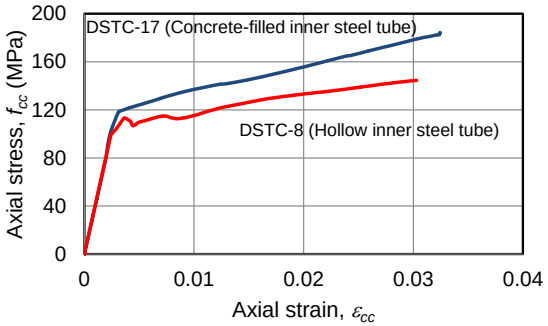

(d) DSTCs with D_s= 101.6 mm

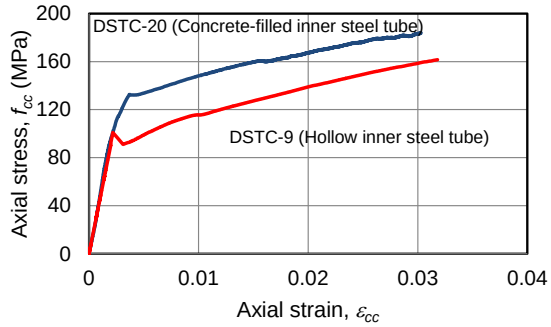

(e) DSTCs with D_s= 114.3 mm

Figure 11. Influence of concrete-filling inner steel tube

3.3.5. Effect of concrete-filling inner steel tube

Figure 11 presents the comparison of stress-strain relationships of the companion hollow and concrete-filled DSTCs. It can be seen from Figure 11 and Table 6 that DSTCs with concrete-filled inner steel tubes developed higher ultimate axial stresses (f'_{cu}) than those of DSTCs with hollow inner steel tubes. This observation is in agreement with that reported in Ozbakkaloglu and Louk Fanggi (2013) on monotonically loaded DSTCs manufactured with carbon FRP tubes, and the increase in

f'_{cu} can be attributed to the additional confinement provided by the inner steel tube to the core concrete. It can also be observed from Figure 11 and Table 6 that the concrete-filled DSTCs developed almost the same ultimate axial strains (ε_{cu}) as those of the hollow DSTCs. This observation does not agree with that reported in Ref. (Ozbakkaloglu and Louk Fanggi 2013), where it was found that hollow DSTCs developed higher ε_{cu} than those of the companion concrete-filled DSTCs. To explain this discrepancy, a closer investigation of the results is required. As far as the dilation behavior of DSTCs are concerned, it would be reasonable to expect that, everything else being the same, concrete filling the inner steel tube would result in an increase in the system dilation rate of the DSTC. Therefore, if the FRP tubes of the companion filled and hollow DSTCs were to fail at a same hoop rupture strain ($\varepsilon_{h,rup}$), it would be expected that the hollow DSTCs would develop a higher ε_{cu} than that of the filled DSTCs. However, as discussed previously, hollow DSTCs of the present study with larger inner steel tubes (i.e. DSTCs 5-10), for which the dilation behavior is expected to differ sufficiently from that of the corresponding filled DSTC, exhibited significantly lower hoop rupture strains than those of the companion filled DSTCs. Therefore, earlier failure of these specimens caused by stress concentrations on their FRP tubes resulted in an early termination of their axial load-displacement behaviors, before a global failure of the FRP tube was reached. These observations provide an explanation as to why these hollow DSTCs were not able to develop higher ultimate axial strains than those of their concrete-filled counterparts, as would have been expected if only the sectional dilation behavior of the specimens were to be considered. These observations also, once again, point to the complex interactions that are present among a number of different mechanisms that influence the compressive behavior of DSTCs.

3.3.6. Effect of loading pattern

The influence of loading pattern on the compressive behavior of hollow and filled DSTCs is illustrated in Figures 12(a) and 12(b), respectively. As can be seen in these figures, the envelope curves of cyclically loaded DSTCs were slightly different than the curves of corresponding monotonically loaded specimen due to differences in the unconfined concrete strengths (f'_c) of these specimens. The change in f'_c affected both the brittleness of concrete and nominal confinement ratio (f_{lu}/f'_c), both of which have significant influences on the behavior of confined concrete. Therefore, to enable a meaningful comparison between monotonically and cyclically loaded DSTCs, strength and strain enhancement coefficients (k_1 and k_2) of these specimens were established using Eqns. 2 and 3, respectively. The values of k_1 and k_2 are also shown in Figure 12.

$$k_1 = \left(\frac{f'_{cu}}{f'_c} - 1\right) / \frac{f_{lu}}{f'_c} \tag{2}$$

$$k_2 = \left(\frac{\varepsilon_{cu}}{\varepsilon_{co}} - 2\right) / \frac{f_{lu}}{f'_c} \tag{3}$$

It can be seen from Figure 12(a) that cyclically loaded hollow DSTCs developed slightly higher strength and strain enhancement ratios (k_1 and k_2) than those of the monotonically loaded hollow DSTCs. A similar observation on the strength enhancement ratio (k_1) of concrete-filled DSTCs can also be made based on the comparison of the curves shown in Figure 12(b). Figure 12(b) also indicates that cyclically loaded filled DSTCs developed a similar strain enhancement ratio (k_2) to that of their monotonically loaded counterparts. The final observation is in agreement with the one reported in Yu *et al*. (2012) for hollow DSTCs, where it was stated that the ultimate conditions of the concrete in DSTCs under cyclic axial compression were almost the same as those of concrete in DSTCs subjected to monotonic compression. It

is worth noting that the slightly better overall performance of the cyclically loaded DSTCs of the present study might have been contributed by the lower unconfined concrete strength of these specimens compared to that of their monotonically loaded counterparts.

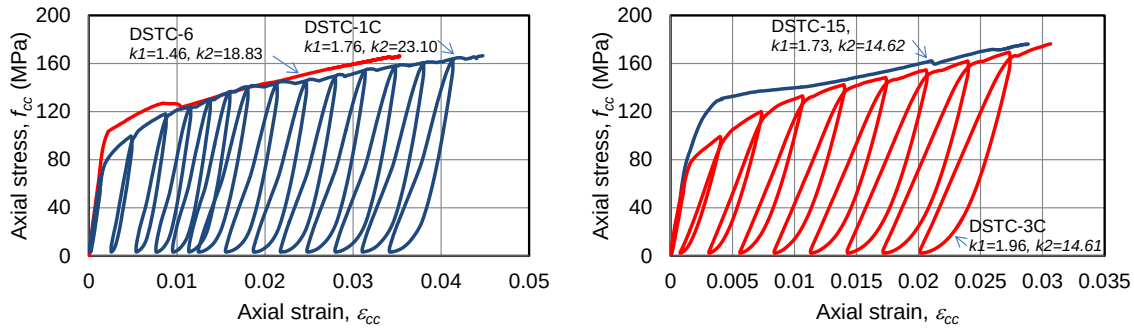

(a) Hollow DSTCs (b) Filled DSTCs

Figure 12. Influence of loading pattern on DSTCs with D_s= 88.9 mm

3.3.7. Comparison of DSTCs, CFFTs and H-CFFTs

To illustrate the relative performance of each composite system, Figure 13 presents the stress-strain curves of concretes in the companion H-CFFT, hollow DSTC, filled DSTC, and CFFT specimens. Figures 13(a), 13(b) and 13(c), respectively, show the stress-strain curves of DSTCs and H-CFFTs with D_s of 60.3 mm, 88.9 mm, and 114.3 mm together with the curves of a companion CFFT. As illustrated in Figure 13, H-CFFTs performed significantly worse that both CFFTs and DSTCs. As evident from the figure, the performance of these specimens further degraded with an increase in the diameter of inner void. Figure 13 also illustrates that both hollow and concrete-filled DSTCs developed higher ultimate axial strains (ε_{cu}) than the companion CFFTs. Furthermore, as can be seen from Figure 13, filled DSTCs also developed higher ultimate axial stresses (f'_{cu}) than CFFTs, whereas hollow DSTCs and CFFTs exhibited similar f'_{cu} values. Higher ultimate axial stresses seen in filled DSTCs compared to those in CFFTs can be attributed to the additional confinement received by core concrete inside the steel

tube, which creates a mechanism where the concrete inside the steel tube is confined by both the steel tube and FRP tube. These additional confinement effects in turn results in an increase in the load carrying capacity of the DSTC and the average strength of concrete calculated based on this capacity. Similar ultimate axial stresses seen in companion hollow DSTCs and CFFTs resulted from the combined influence of the previously mentioned opposing effects of inner steel tube diameter on the second branch slope of stress-train relationship of concrete and its ultimate axial strain (ε_{cu}) in a hollow DSTC. These observations indicate that the presence of an inner steel tube effectively compensates for the removed core concrete in hollow DSTCs, an the annular concrete section in a hollow DSTCs is confined with similar efficiency to that experienced by concrete in a companion solid CFFT.

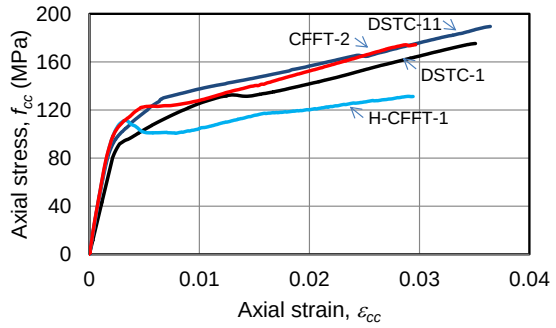

(a) Inner void or D_s= 60.3 mm

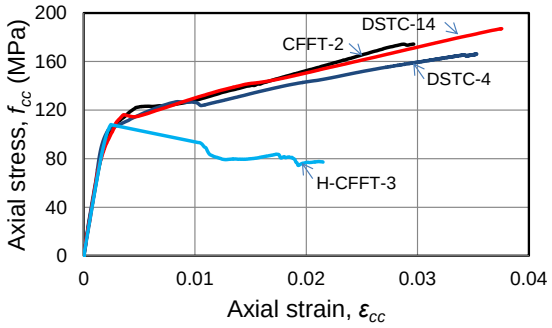

(b) Inner void or D_s= 88.9 mm

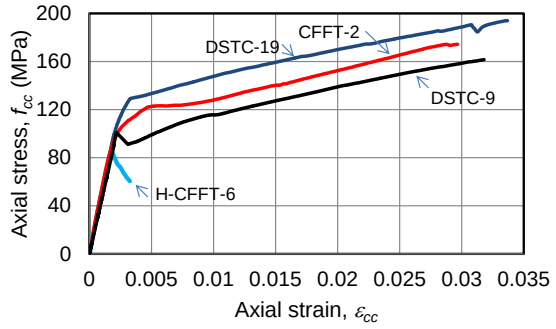

(c) Inner void or D_s= 114.3 mm

Figure 13. Comparison of different composite systems

4. CONCLUSIONS

This paper has presented the results of an experimental study on the behavior of FRP-HSC-steel composite columns subjected to concentric compression. The experimental study involved design, manufacture, and testing of 24 hollow and concrete- filled DSTCs, six H-CFFTs, and two CFFTs to investigate the effect of key parameters on the stress-strain behavior of concrete in DSTCs. Based on the results and discussions presented in this paper, the following conclusions can be drawn:

- The ultimate axial strains (ε_{cu}) of HSC DSTCs are highly sensitive to the method used in the measurement of these strains. Higher axial strains are obtained from LVDTs that measure the displacements along the entire height of the specimen than mid-height region LVDTs and axial strain gauges.
- Diameter of inner steel tube (D_s) is a major parameter that affects the behavior of both hollow and filled DSTCs significantly through its influences on both the dilation behavior and failure mode of the DSTC system. An increase in D_s results in a decrease in the second branch slope of stress-strain curves of hollow DSTCs and an increase in that of concrete-filled DSTCs. In addition, an increase in D_s increases the likelihood of a steel tub- induced early failure in hollow DSTCs and to a lesser extent in filled DSTCs.
- FRP tube hoop rupture strains ($\varepsilon_{h,rup}$) of both hollow and concrete-filled DSTCs are influenced by inner steel tube diameter (D_s), and they decrease with an increase in D_s. This is caused by the change in the failure mode of inner steel tube with D_s, with more significant reductions in $\varepsilon_{h,rup}$, resulting from an increase in D_s, observed in hollow DSTCs than in filled DSTCs.
- Concrete in filled DSTCs develops higher ultimate axial stresses (f'_{cu}) and strains (ε_{cu}) than concrete in CFFTs. The superior behavior of concrete in filled DSTCs over

CFFTs can be attributed to additional confinement effects provided by the inner steel tube to the core concrete. Furthermore, it has been shown that H-CFFTs perform significantly worse than DSTCs and CFFTs, and their performance further degrades with an increase in the diameter of inner void.

- It has been observed that cyclically loaded DSTCs exhibit slightly larger strength and strain enhancement ratios (k_1 and k_2) than those of the companion monotonically loaded DSTCs.

The results of the present study also confirm the following findings that were previously reported in Refs. Ozbakkaloglu and Louk Fanggi (2013) and Louk Fanggi and Ozbakkaloglu (2013), respectively:

- DSTCs with concrete-filled inner steel tubes develop higher ultimate axial stresses (f'_{cu}) than those of DSTCs with hollow inner steel tubes, and the increase in f'_{cu} can be attributed to the additional confinement provided by the inner steel tube to the core concrete.
- Concrete in hollow DSTCs develops similar ultimate axial stresses (f'cu) to and larger ultimate axial strains (εcu) than concrete in companion CFFTs, which results from a change in the system dilation behavior.

On the other hand, the findings of the present study as to the influence of concrete filling inner steel tube on the ultimate axial strain (ε_{cu}) are not in agreement with that reported in Ref. (Ozbakkaloglu and Louk Fanggi 2013), with no major influence of concrete filling found in the present study as opposed to a decrease in ε_{cu} reported in Ref. (Ozbakkaloglu and Louk Fanggi 2013). It has been shown that this difference can be attributed to steel tube-induced early failures experienced by the hollow DSTCs of the present study. The findings of present study, therefore, highlights the importance of

interpreting the experimental results of DSTCs with due consideration given to the failure mechanism associated with the obtained result.

ACKNOWLEDGEMENTS

The authors would like to thank Messrs. Ding, Rander, Reid, and Singh who have undertaken some of the tests reported in this paper as part of their Honour's theses. This research is part of an ongoing program at The University of Adelaide on FRP-concrete-steel composite columns.

REFFERENCES

Abdelrahman, K., and El-Hacha, R. (2012). "Behavior of large-scale concrete columns wrapped with CFRP and SFRP sheets", *Journal of Composites for Construction*, *ASCE,* Vol. 16, No. 4, pp. 430-439.

ASTM C39/C39M-10 (2010). *Standard test method for compressive strength of cylindrical concrete specimens*, (ASTM), West Conshohocken, PA.

ASTM D3039/D3039M-08 (2008). *Standard test method for tensile properties of polymer matrix composites materials*, (ASTM), West Conshohocken, PA.

Australian Standard AS 1391-1991 (1991). *Methods for tensile testing for metals*, (AS), Homebush, NSW 2014.

Campione, G. (2006). "Influence of F RP wrapping techniques on the compressive behavior of concrete prisms", *Cement and Concrete Composites*, Vol. 28, No. 5, pp. 497-505.

Colomb, F., Tobbi, H., Ferrier, E., and Hamelin, P. (2008). "Seismic retrofit of reinforced concrete short columns by CFRP materials", *Composite Structures*, Vol. 82, No. 4, pp. 475-487.

De Luca, A., Nardone, F., Matta, F., Nanni, A., Lignola, G.P., and Prota, A. (2011). "Structural evaluation of full-scale FRP-confined reinforced concrete columns", *Journal of Composites for Construction*, *ASCE,* Vol. 15, No. 1, pp. 112-123.

Fam, A. Z., and Rizkalla, S. H. (2001). “Confinement model for axially loaded concrete confined by circular fiber-reinforced polymer tubes”, *ACI Structural Journal*, Vol. 98, No. 4, pp. 451-461.

Fam, A. Z., Schnerch, D., and Rizkalla, S. (2005). “Rectangular Filament-Wound GFRP Tubes Filled with Concrete under Flexural and Axial Loading: Experimental Investigation”, *Journal of Composites for Construction, ASCE*, Vol. 9, No. 1, pp. 25-33.

Idris, Y., and Ozbakkaloglu, T. (2013). "Seismic Behavior of High-Strength Concrete-Filled FRP Tube Columns", *Journal of Composites for Construction, ASCE,* Vol. 17, No. 6, pp. 04013013.

Ilki, A., Peker. O., Karamuk, E., Demir, C., and Kumbasar, N. (2008). “FRP retrofit of low and medium strength circular and rectangular reinforced concrete columns”, *J. Mater. Civ. Eng.*, Vol. 20, No. 2, pp. 169–188.

Lam, L., and Teng, J. G. (2004). “Ultimate condition of fiber reinforced polymer-confined concrete”, *J. Compos. Constr.*, *ASCE*, Vol. 8, No. 6, pp. 539-548.

Lignola, G. P., Prota, A., Manfredi, G., and Cosenza E. (2007). “Experimental performance of RC hollow columns confined with CFRP”, *Journal of Composite for Construction, ASCE*, Vol. 11, No. 1, pp. 42 – 49.

Lim, J., and Ozbakkaloglu, T. (2014a). “Hoop strains in FRP-confined concrete columns: experimental observations”, *Materials and structures*, doi: 10.1617/s11527-014-0358-8.

Lim, J. C., Ozbakkaloglu, T. (2014b). “Influence of silica fume on stress-strain behavior of FRP-confined HSC”, *Construction and Building Materials*, Vol. 63, pp. 11-24.

Lim, J.C., and Ozbakkaloglu, T. (2014c). “Confinement model for FRP-confined high-strength concrete”, *Journal of Composites for Construction, ASCE*, Vol. 18, No. 4, pp. 04013058.

Louk Fanggi, B.A., and Ozbakkaloglu, T. (2013). “Compressive behavior of aramid FRP-HSC-Steel double-skin tubular columns”, *Construction and Building Materials*, Vol. 48, pp. 554-565.

Mirmiran, A., Shahawy, M., Samaan, M., El Echary, H., Mastrapa, J. C., and Pico, O. (1998). "Effect of Column Parameters on FRP-confined Concrete", *Journal of Composites for Construction, ASCE*, Vol. 2, No. 4, pp. 175-185.

Ozbakkaloglu, T. (2013a). "Axial Compressive Behavior of Square and Rectangular High-Strength Concrete-Filled FRP Tubes", *Journal of Composites for Construction, ASCE*, Vol. 17, No. 1, pp. 151-161.

Ozbakkaloglu, T. (2013b). "Concrete-filled FRP Tubes: Manufacture and Testing of New Forms Designed for Improved Performance", *Journal of Composites for Construction, ASCE*, Vol. 17, No. 2, pp. 280-281.

Ozbakkaloglu, T. (2013c). "Compressive behavior of concrete-filled FRP tube columns: Assessment of critical column parameters", *Engineering Structures*, Vol. 51, pp. 151-161.

Ozbakkaloglu, T. (2013d). "Behavior of square and rectangular ultra high-strength concrete-filled FRP tubes under axial compression", *Composites Part B: Engineering*, Vol. 54, pp. 97-111.

Ozbakkaloglu, T., and Akin, E. (2012). "Behavior of FRP confined normal-and high-strength concrete under cyclic axial compression." *Journal of Composites for Construction, ASCE*, Vol. 16, No. 4, pp. 451-463.

Ozbakkaloglu, T. and Lim, J. C. (2013). "Axial Compressive Behavior of FRP-Confined Concrete: Experimental Test Database and a New Design-Oriented Model", *Composites Part B: Engineering,* Vol. 55, pp. 607-634.

Ozbakkaloglu, T., and Louk Fanggi, B. A. (2013). "Axial compressive behavior of FRP-concrete-steel double-skin tubular columns made of normal- and high-strength concrete", *Journal of Composites for Construction, ASCE.* doi: 10.1061/(ASCE)CC.1943-5614.0000401.

Ozbakkaloglu, T., and Saatcioglu, M. (2006). "Seismic Behavior of High Strength Concrete Columns Confined by Fiber-Reinforced Polymer Tubes", *Journal of Composite Construction, ASCE*, Vol. 10, No. 6, pp. 538-549.

Ozbakkaloglu, T., and Saatcioglu, M. (2007). “Seismic Performance of Square High-Strength Concrete Columns in FRP Stay-in-Place Formwork”, *Structural Engineering*, Vol. 133, No. 1, pp. 44-56.

Ozbakkaloglu, T., Lim, J. C., and Vincent, T. (2013). “FRP-confined concrete in circular sections: Review and assessment of the stress-strain models”, *Engineering Structures*, Vol. 49, pp. 1068-1088.

Ozbakkaloglu, T. and Vincent, T. (2014). "Axial Compressive Behavior of Circular High-Strength Concrete-Filled FRP Tubes", *J. Compos. Constr*., Vol. 18, No. 2, pp. 04013037.

Popovics, S. (1973). “A numerical approach to the complete stress-strain curves of concrete", *Cement and Concrete Research,* Vol. 3, No. 5, pp. 583-599.

Realfonzo, R., and Napoli, A. (2012). “Results from cyclic tests on high aspect ratio RC columns strengthened with FRP systems”, *Construction and building materials*, Vol. 37, pp. 606-620.

Rousakis, T., and Karabinis, A. (2008). “Substandard reinforced concrete members subjected to compression: FRP confining effects”, *Materials and Structures*, Vol. 41, No. 9, pp. 595 – 1611.

Seible, F., Burgueño, R., Abdallah, M. G., and Nuismer, R. (1996). “Development of advanced composite carbon shell systems for concrete columns in seismic zones”, *Proc., 11th World Conf. Earthquake Engineering*, Pergamon, Elsevier Science, Oxford, Paper No. 1375.

Teng, J. G., Yu, T., and Wong, Y. L. (2004). “Behaviour of hybrid FRP-concrete-steel double-skin tubular columns”, *The 2nd International Conference on FRP Composites in Civil Engineering-CICE 2004,* Adelaide, Australia, pp. 811-818.

Teng, J. G., Yu, T., Wong, Y. L., and Dong, S. L. (2007). “Hybrid FRP concrete steel tubular columns: concept and behavior”, *Construction and building materials*, Vol. 21, pp. 846-854.

Teng, J. G., Yu, T., and Wong, Y. L. (2010). "Hybrid FRP-concrete-steel double-skin tubular structural members", *Proceedings, The Fifth International Conference on FRP Composites in Civil Engineerind (CICE),* 27-29 September, Beijing, China, pp. 26-32.

Thermou, G. E., and Pantazopoulou, S. J. (2009) "Fiber-reinforced polymer retrofitting of predamaged substandard RC prismatic members", *Journal of Composites for Construction*, *ASCE,* Vol. 13, No. 6, pp. 535-546.

Turgay, T., Polat, Z., Koksal, H.O., Doran, B., and Karakoç, C. (2010). "Compressive behavior of large-scale square reinforced concrete columns confined with carbon fiber reinforced polymer jackets", *Materials and Design*, Vol. 31, No. 1, pp. 357-364.

Vincent, T., and Ozbakkaloglu, T. (2013a). "Influence of Concrete Strength and Confinement Method on Axial Compressive Behavior of FRP Confined High- and Ultra High-Strength Concrete", *Composites Part B-Engineering*, Vol. 50, pp. 413-428.

Vincent, T., and Ozbakkaloglu, T. (2013b). "Influence of fiber orientation and specimen end condition on axial compressive behavior of FRP-confined concrete", *Construction and Building materials*, Vol. , pp. 814–826.

Vincent, T., and Ozbakkaloglu, T. (2014). "Influence of slenderness on stress-strain behavior of concrete-filled FRP tubes: experimental study", *Journal of Composites for Construction, ASCE*, doi: 10.1061/(ASCE)CC.1943-5614.0000489.

Wang, Z. Y., Wang, D. Y., Smith, S. T., and Lu, D. G. (2012). "Experimental testing and analytical modeling of CFRP-confined large circular RC columns subjected to cyclic axial compression", *Engineering Structures,* Vol. 40, pp. 64-74.

Wong, Y. L., Yu, T., Teng, J. G., and Dong, S. L. (2008). "Behaviour of FRP-confined concrete in annular section columns", *Composites part B: Engineering*, Vol. 38, pp. 451-466.

Wu, Y. F., and Wei, Y. Y. (2010). "Effect of cross-sectional aspect ratio on the strength of CFRP-confined rectangular concrete columns", *Engineering Structures*, Vol. 32, pp. 32-45.

Yu, T., Wong, Y. L., and Teng, J. G. (2010). "Behavior of Hybrid FRP-Concrete-Steel Double-Skin Tubular Columns Subjected to Eccentric Compression", *Advances in Structural Engineering,* Vol. 13, No. 5, pp. 961-974.

Yu, T., Zhang, B., Cao, Y. B., and Teng, J. G. (2012). "Behavior of hybrid FRP-concrete-steel double-skin tubular columns subjected to cyclic axial compression", *Thin-Walled Structures*, Vol. 61, pp. 196-203.

Zhu, Z., Ahmad, I., and Mirmiran, A. (2006). "Seismic performance of concrete-filled FRP tube columns for bridge substructure", *Journal of Bridge Engineering*, ASCE, Vol. 11, No. 3, pp. 359-370.

Paper 5 Behavior of FRP-HSC and FRP-HSC-Steel Double-Skin Tubular Columns under Cyclic Axial Compression

Mohammad Albitar, Togay Ozbakkaloglu and Butje Alfonsius Louk Fanggi

School of Civil, Environmental, and Mining Engineering, University of Adelaide, 5000

Journal of Composites for Construction, ASCE (Published)

Statement of Authorship

Title of Paper	Behavior of FRP-HSC and FRP-HSC-Steel Double-Skin Tubular Columns under Cyclic Axial Compression
Publication Status	● Published ○ Accepted for publication ○ Submitted for publication ○ Publication style
Publication Details	Albitar, M., Ozbakkaloglu, T., and Louk Fanggi, B.A. (2015). "Behavior of FRP-HSC-Steel double-skin tubular columns under cyclic axial compression." *Journal of Composites for Construction*. 19(2): 04014041.

Author Contributions

By signing the Statement of Authorship, each author certifies that their stated contribution to the publication is accurate and that permission is granted for the publication to be included in the candidate's thesis.

Name of Principal Author	Mohammad Albitar		
Contribution to the Paper	Review of literature, analysis data, and preparation of manuscript		
Signature		Date	28/07/2015

Name of Co-Author	Dr. Togay Ozbakkaloglu		
Contribution to the Paper	Research supervision and review of manuscript		
Signature		Date	28/07/2015

Name of Co-Author (Candidate)	Butje Alfonsius Louk Fanggi		
Contribution to the Paper	analysis data and edit of manuscript		
Signature		Date	28/07/2015

BEHAVIOR OF FRP-HSC-STEEL DOUBLE-SKIN TUBULAR COLUMNS UNDER CYCLIC AXIAL COMPRESSION

Mohammad ALBITAR [1], Togay OZBAKKALOGLU [2],
and Butje Alfonsius LOUK FANGGI [3]

ABSTRACT

This paper presents an experimental study on the behavior of fiber-reinforced polymer (FRP)-concrete-steel double-skin tubular columns (DSTCs) under cyclic axial compression. The experimental program included 30 DSTCs, 22 of which were manufactured using a high-strength concrete (HSC). The key parameters considered were the FRP type, FRP tube thickness, concrete strength, inner steel tube diameter and presence (absence) of concrete filling inside the steel tube. The results show that both normal- and high-strength concrete DSTCs exhibit a highly ductile behavior under cyclic axial compression. However, for a given nominal confinement ratio, hollow HSC DSTCs tend to develop lower strength and strain enhancement ratios than their normal-strength concrete (NSC) counterparts. It is found that the residual plastic strain of concrete in DSTCs is linearly related to the envelope unloading strain, and this relationship is not influenced significantly by any of the test parameters investigated in this study. The results also show that DSTCs manufactured with aramid FRP tubes exhibit a slightly higher stress enhancement and a slightly lower strain enhancement ratio than the companion DSTCs manufactured with S-glass FRP tubes. It is observed that concrete-filling inner steel tubes results in an increase in the compressive strength of confined concrete in DSTCs. On the other hand, hollow DSTCs develop slightly higher ultimate axial strains than the

[1, 3] PhD Candidate, School of Civil, Environmental and Mining Engineering, University of Adelaide, SA 5005 Australia.
[2] (Corresponding author) Senior Lecturer, School of Civil, Environmental and Mining Engineering, University of Adelaide, SA 5005 Australia. Tel : + 618 8313 6477; Fax : +618 8313 4359; Email: togay.ozbakkaloglu@adelaide.edu.au

companion concrete-filled DSTCs. The experimental results are subsequently compared with predictions from a model developed for confined concrete in monotonically loaded hollow DSTCs. The comparison suggests that the model provides reasonably accurate predictions of the ultimate conditions of concrete in hollow DSTCs.

KEYWORDS: Fiber reinforced polymer (FRP); Concrete; High-strength concrete (HSC); Columns; Confinement; Steel tubes; Cyclic loading; DSTCs.

1. INTRODUCTION

As demonstrated in a recent review by Ozbakkaloglu et al. (2013), confining concrete with fiber-reinforced polymer (FRP) composites have become increasingly popular in the construction industry over the past two decades. The advantages of using FRP as a concrete confinement material, such as strength-to-weight ratio and corrosion resistance have provided increased impetus for research into two main research directions: (i) the use of FRP composites in retrofitting existing concrete columns (e.g., Lam and Teng 2004; Lignola et al. 2007; Wu and Wei 2010; Wang et al. 2012; Vincent and Ozbakkaloglu 2013a,b), and (ii) the construction of new high-performance composite columns in the form of concrete-filled FRP tubes (CFFTs) (e.g., Seible et al. 1996; Fam and Rizkalla 2001; Ozbakkaloglu and Saatcioglu 2007; Idris and Ozbakkaloglu 2013; Ozbakkaloglu 2013a,b; Ozbakkaloglu and Vincent 2013).

Following from the research on CFFTs, FRP-concrete-steel double-skin tubular columns (DSTCs), a new type of composite system that was originally proposed by Teng et al. (2004), has received significant recent research attention. One of the most important features of this composite system is that, through full utilization of the benefits of the three constituent materials, it can be designed to exhibit extremely high structural performance levels. Other important advantages offered by this system over

other column systems were discussed in detail in Teng et al. (2007). A large number of experimental studies have recently been undertaken on DSTCs by groups led by Teng in Hong Kong (Yu et al. 2006; Teng et al. 2007; Wong et al. 2008; Teng et al. 2010; Yu et al. 2010, 2012) and the second author in Australia (Ozbakkaloglu and Louk Fanggi 2013a, 2013b; Louk Fanggi and Ozbakkaloglu 2013; Ozbakkaloglu and Idris 2013). These studies have clearly shown some of the performance advantages of DSTCs under different loading conditions.

As was recently demonstrated in Ozbakkaloglu and Idris (2013), DSTCs exhibit extremely high performance levels under simulated seismic loading. Given the suitability of DSTCs for use in the seismic design of new structures, it is of particular importance to understand the behavior of DSTCs subjected to cyclic loading. However, the studies on the comprehensive behavior of DSTCs have so far focused on the behavior under monotonic loading, and only two studies investigated the behavior of DSTCs under cyclic axial compression (Yu et al. 2012; Ozbakkaloglu and Louk Fanggi 2013b), with each studying only three pairs of specimens. Likewise, high-strength concrete (HSC) is particularly suitable for use in the construction of DSTCs in the development of high-performance structural members. On the other hand, apart from the two specimen pairs reported in Ozbakkaloglu and Louk Fanggi (2013b), no information is currently available on the behavior of HSC DSTCs under cyclic axial compression.

This paper presents the results of the first comprehensive experimental study in literature on the behavior of FRP-HSC-steel DSTCs under cyclic axial compression. The specimens were manufactured with aramid and S-glass FRP (AFRP and GFRP) tubes, and additional normal-strength concrete (NSC) specimens were also tested as part of the experimental program to establish relative performances of NSC and HSC

DSTCs. The experimental results are first presented and followed by a discussion on the influence of the important parameters on the cyclic compressive behavior of FRP-concrete-steel composite DSTCs.

2. EXPERIMENTAL PROGRAM

2.1. Test specimens and materials

A total of 30 DSTCs were designed, manufactured and tested under cyclic axial compression. All the specimens had a diameter of 152.5 mm, measured at the concrete core, and a height of 305 mm. The test parameters included concrete strength (i.e., NSC and HSC), FRP type (i.e., AFRP and GFRP) and thickness, inner steel tube diameter and whether the inner steel tube was concrete-filled or hollow. Two nominally identical specimens were tested for each unique specimen configuration. Details of the specimens are shown in *Table 1*.

Table 1. Details of test specimens

Specimen	Number of FRP layers	Concrete strength, f'_c (MPa)	Strain at peak stress, ε_{co} (%)	Steel tube diameter, D_s (mm)	Steel tube thickness, t_s (mm)	Type of DSTC	Type of FRP
DSTCs 1C & 2C	3	42.5	0.22	60.3	3.6	Hollow	AFRP
DSTCs 3C & 4C	3	42.5	0.22	88.9	3.2	Hollow	AFRP
DSTCs 5C & 6C	3	42.4	0.22	114.3	6.02	Hollow	AFRP
DSTCs 7C & 8C	6	82.4	0.29	60.3	3.6	Hollow	AFRP
DSTCs 9C & 10C	6	82.4	0.29	88.9	3.2	Hollow	AFRP
DSTCs 11C & 12C	6	82.4	0.29	114.3	6.02	Hollow	AFRP
DSTCs 13C & 14C	6	82.4	0.29	60.3	3.6	Hollow	GFRP
DSTCs 15C & 16C	6	82.4	0.29	88.9	3.2	Hollow	GFRP
DSTCs 17C & 18C	6	82.4	0.29	114.3	6.02	Hollow	GFRP
DSTCs 19C & 20C	3	42.5	0.22	88.9	3.2	Filled	AFRP
DSTCs 21C & 22C	6	82.4	0.29	60.3	3.6	Filled	AFRP
DSTCs 23C & 24C	6	82.4	0.29	88.9	3.2	Filled	AFRP
DSTCs 25C & 26C	6	82.4	0.29	114.3	6.02	Filled	AFRP
DSTCs 27C & 28C	9	82.4	0.29	88.9	3.2	Filled	AFRP
DSTCs 29C & 30C	6	82.4	0.29	88.9	3.2	Filled	GFRP

To investigate the influence of steel tube diameter (D_s), specimens were manufactured with three different steel tubes with diameters (D_s) of 60.3 mm, 88.9 mm and 114.3 mm, as can be seen in *Fig. 1*. The selected diameters satisfied the following conditions: i) they were sufficiently different from each other, and ii) they were large enough to have influence on the overall response, yet they allowed sufficient space for concrete to ensure its proper placement in the DSTC. To investigate the influence of unconfined concrete strength (f'_c), two different concrete grades were used (i.e., f'_c = 42.5 and 82.4 MPa). In addition, concrete-filled DSTCs were manufactured as companion to hollow DSTCs to investigate the influence of concrete-filling inner steel tube. To investigate the influence of FRP types, two types of FRP were used, namely aramid FRP and S-glass FRP, where letter "S" refers to the type of glass fibers, which exhibit superior mechanical properties than those of the more common E-glass fibers. Furthermore, two additional DSTCs with a thicker AFRP tube (i.e., DSTCs 27 and 28) were manufactured to investigate the influence of FRP tube thickness.

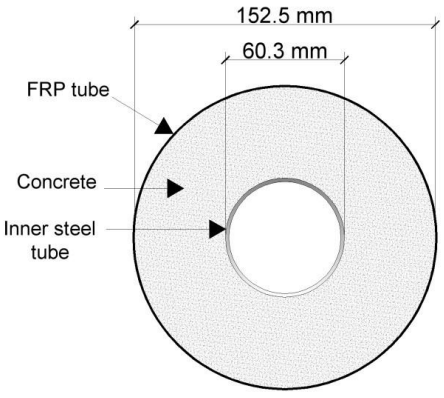

(a)

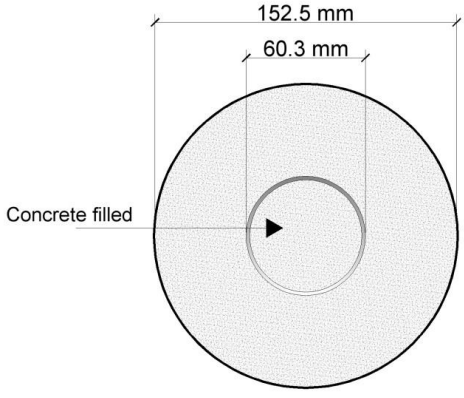

(b)

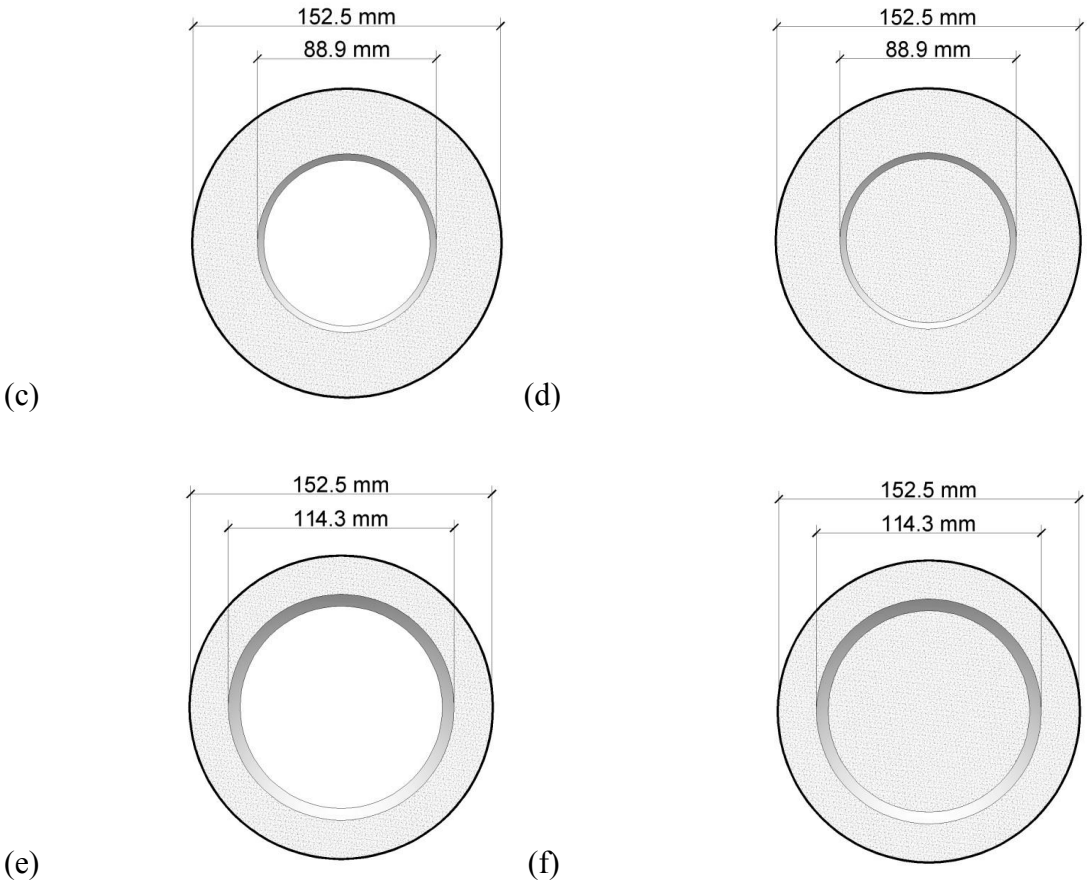

Figure 1. Geometric dimension of the specimens: (a) hollow DSTCs with D_s = 60.3 mm; (b) filled DSTCs with D_s = 60.3 mm; (c) hollow DSTCs with D_s = 88.9 mm; (d) filled DSTCs with D_s = 88.9 mm; (e) hollow DSTCs with D_s = 114.3 mm; (f) filled DSTCs with D_s = 114.3 mm

The specimens were manufactured using two different unconfined compressive strengths with 42.5 MPa and 82.4 MPa test day strengths attained for NSC and HSC mixes, respectively. Both mixes consisted of crushed bluestone as the coarse aggregate, with a nominal maximum size of 10 mm. The water/cement (*w/c*) ratio in the NSC mixture was 0.55, whereas the HSC included silica fume and superplasticiser with a *w/c* ratio of 0.3. *Table 1* reports the unconfined concrete strength f'_c of each specimen at the day of testing, together with the corresponding axial strain ε_{co} calculated using the expression given by Popovics (1973) shown in *Eq.1*.

$$\varepsilon_{co} = 0.000937 \sqrt[4]{f'_c} \quad (1)$$

where f'_c is in MPa.

In designing the FRP tubes, due consideration was given to the well-understood influence of the strength of concrete on its confinement demand (Ozbakkaloglu and Saatcioglu 2006; Ozbakkaloglu and Akin 2012). This was done through the use of nominal confinement ratio (f_{lu}/f'_c), calculated from *Eq.2* assuming a uniform confinement distribution and treating the section as a solid section, as the performance criterion in establishing relative confinement levels of DSTCs with different concrete strengths. This resulted in FRP tubes of NSC specimens receiving 3 layers of FRP, whereas the tubes of HSC specimens received 6 layers of FRP.

$$\frac{f_{lu}}{f'_c} = \frac{2E_f t_f \varepsilon_{fu}}{D_f f'_c} \quad (2)$$

where f_{lu} is the ultimate confining pressure, E_f is the modulus of elasticity, t_f is the total nominal thickness, ε_{fu} is the ultimate tensile strain of the fibers and D_f is the internal diameter of the FRP tube.

The FRP tubes were formed using a manual wet lay-up process by wrapping epoxy resin impregnated fiber sheets around precision-cut high-density Styrofoam templates in the hoop direction. In order to prevent premature debonding, FRP sheets were provided with a 150-mm overlap. The three-layer tubes of the NSC specimens were wrapped with a single FRP sheet continuously, whereas the six-layer tubes of the HSC DSTCs were wrapped by two FRP sheets, with the resulting two overlap regions provided at the same region around the perimeter of the tube. The properties of the unidirectional fiber sheets used in the manufacture of the tubes are provided in *Table 2*. Both the

manufacturer-supplied properties and the ones obtained from the flat coupon tests, in which the coupon specimens were loaded in accordance with ASTM standard D3039M-08 (ASTM 2008), are given in the table.

Table 2. Properties fibers and FRP composites used in test specimen

Type	Nominal thickness, t_f (mm/ply)	Provided by manufacturers			Obtained from flat FRP coupon tests		
		Tensile strength, f_f (MPa)	Ultimate tensile strain, ε_f (%)	Elastic modulus, E_f (GPa)	Tensile strength, f_{frp} (MPa)	Ultimate tensile strain, ε_{frp} (%)	Elastic modulus, E_{frp} (GPa)
Aramid	0.2	2600	2.2	118.2	2390	1.86	128.5
S-Glass	0.2	3040	3.5	86.9	3055	3.21	95.3

A formwork was developed to support the columns during the process of concrete pouring to ensure the FRP and steel tubes remained concentric, as illustrated in *Fig. 2*. At the base, wooden spacers were used to hold the bottom of the FRP tube in place and nails were used to maintain the position of the steel tube relative to the FRP tube. At the top, a cap with three steel arms was used to maintain the concentric relationship of the different parts of the column. Alignment was maintained by anchoring the top cap to the wooden base.

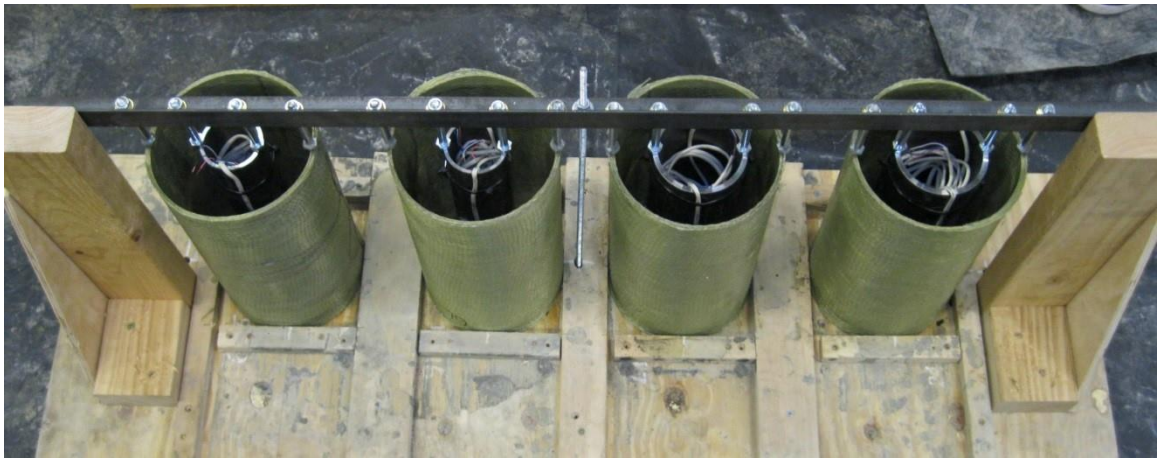

Figure 2. DSTC specimens before concrete pouring

To establish the material properties of the steel tubes used in the DSTCs, axial compression tests were conducted on hollow steel tubes. The heights of the tubes were based on their diameters. For tubes with diameters greater than 100 mm, three hollow tubes having the same height as those used in the DSTCs were tested. For tubes with diameters less than 100 mm, three hollow tubes with a height-to-diameter ratio of 3:1 were tested. The material properties of steel tubes obtained from the compression tests are given in *Table 3*. All the steel tube specimens failed due to localized elephant's foot buckling either at the top or bottom of the specimen.

Table 3. Measured properties of steel tubes

D_s (mm)	t_s (mm)	Peak axial load (P_s) (kN)	Yield stress (MPa)	Peak stress (MPa)	Axial strain at peak (%)	Failure Mode*
60.3	3.6	246	319	384	3.34	EF
88.9	3.2	348	320	404	2.43	EF
114.3	6.02	1073	449	524	3.10	EF

*EF=Elephant's foot buckling

2.2. Instrumentation and testing

A total of eight linear variable displacement transformers (LVDTs) were used to measure axial deformation of the specimens, as illustrated in *Fig. 3*. To measure the average axial deformation along the entire height of the specimen, four LVDTs were mounted at the corners between the loading and supporting steel plates of the compression test machine. To measure the average axial deformation along the mid-height region within a gauge length of 170 mm, four inner cage LVDTs were placed at the mid-height regions of the specimens. FRP tube lateral strains were measured by three unidirectional strain gauges with a gauge length of 20 mm that were spaced equally around the perimeter at the mid-height of the specimen outside the overlap

region. Axial and lateral strains of inner steel tubes were measured at the mid-height by two axially and two laterally oriented strain gauges with 5 mm gauge length.

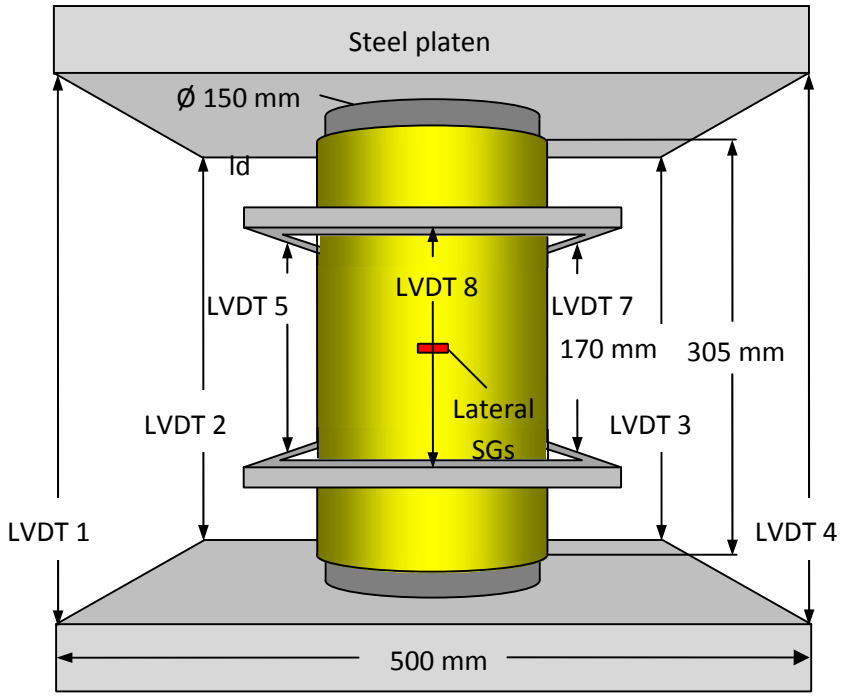

Figure 3. Test setup and instrumentation

The specimens were tested under axial compression using a 5000 kN-capacity universal testing machine. Initial elastic portion and the unloading/reloading cycles of the cyclic loading were performed with load control at 5-kN per second, whereas displacement control was used at approximately 0.003 mm per second beyond initial softening and for the segments between each unloading/reloading curve. Before testing, all specimens were capped at both ends with a thin layer of high-strength capping material to ensure uniform distribution of the applied pressure. The load was applied directly to the concrete core and inner steel tube thorough the use of two precision-cut high-strength steel disks with a 150 mm diameter and 15 mm thickness. The specimens were subjected to cyclic compression involving unloading and reloading cycles at approximately 0.25% axial strain intervals, with a single cycle applied at each

prescribed axial strain level. A small axial load of 50 kN was maintained during the unloading/reloading cycles to prevent any undesired movement in the specimen.

3. TEST RESULTS

3.1. Failure modes

The failure modes of the DSTC specimens are shown in *Fig. 4*. All the DSTCs failed due to the rupture of their FRP tubes. Different failure progressions were observed in DSTCs with AFRP and GFRP tubes. DSTCs manufactured with AFRP tubes experienced a sudden failure with vertical cuts on the FRP tubes, as shown in *Figs. 4a* to *4c*. In contrast, DSTCs manufactured with GFRP tubes showed a progressive failure of the FRP tube, as illustrated in *Figs. 4d* to *4f*. As evident from comparison of *Figs. 4a and 4b* and *Figs. 4d and 4e*, hollow specimens with smaller inner steel tubes showed more extensive FRP tube rupture than the companions DSTCs with larger inner steel tubes. Likewise, as illustrated in *Fig.4*, filled DSTCs experienced a more extensive tube rupture than their hollow counterparts. Moreover, FRP tube rupture locations of filled DSTCs often corresponded to the mid-height of the specimens (*Figs. 4c* and *4f*), whereas the tubes of the majority of the hollow DSTCs ruptured near one of the specimen ends (*Figs. 4a&b* and *4d&e*).

(a) (b) (c)

(d) (e) (f)

Figure 4. Failure modes of DSTCs: (a) hollow AFRP, *Ds* = 60.3 mm, (b) hollow AFRP, *Ds* = 88.9 mm, (c) filled AFRP, *Ds* = 88.9 mm, (d) hollow GFRP, *Ds* = 60.3 mm, (e) hollow GFRP, *Ds* = 88.9 mm, (f) filled GFRP, *Ds* = 88.9 mm

Table S 1, which is available online in the ASCE Library (www.ascelibrary.org), presents the failure mode of the steel tube and the failure locations of both the inner steel and outer FRP tubes. As shown in this table, most of the FRP tubes ruptured in locations that corresponded with the regions of significant deformation in the steel tube. A similar observation was previously reported in Louk Fanggi and Ozbakkaloglu (2013) for DSTCs under monotonic axial compression.

3.2. Axial load capacities

Experimentally recorded axial load capacities of the DSTCs (P_T) are presented in *Table S 2*, which is available online in the ASCE Library (www.ascelibrary.org), together with the axial capacities of the steel tubes (P_s), and unconfined concrete (P_{co}). The axial load capacities of the steel tubes (P_s) were determined from hollow steel tube tests (i.e. peak load in *Table 3*), whereas the axial load capacities of unconfined concrete (P_{co}) were obtained by multiplying unconfined concrete strength by the area of the concrete cross-section. The $P_T/(P_s+P_{co})$ ratios shown in *Table S 2* indicate that the DSTC specimens

developed significantly higher axial load capacities than the combined axial load capacities of the unconfined concrete and steel tubes. This is due to the confinement effect of FRP and steel tubes on concrete, which is discussed in detail in the following sections.

Table S 1. Failure modes of steel tubes in DSTCs

Specimen	Steel tube diameter, D_s (mm)	Steel tube thickness, t_s (mm)	Steel tube failure		FRP tube failure location
			Mode	Location	
DSTC 1C	60.3	3.6	Rippling	Upper part	Upper part
DSTC 2C			Rippling	Middle	Full height
DSTC 3C	88.9	3.2	Rippling	Middle	Lower part
DSTC 4C			Buckling	Middle	Upper to mid
DSTC 5C	114.3	6.02	Buckling	Lower part	Lower part
DSTC 6C			Elephant foot	Upper part	Upper part
DSTC 7C	60.3	3.6	N/A	N/A	Middle
DSTC 8C			N/A	N/A	Middle
DSTC 9C	88.9	3.2	N/A	N/A	Middle
DSTC 10C			N/A	N/A	Middle
DSTC 11C	114.3	6.02	N/A	N/A	Middle
DSTC 12C			N/A	N/A	Middle
DSTC 13C	60.3	3.6	Buckling	Middle	Full height
DSTC 14C			Rippling	Middle	Middle
DSTC 15C	88.9	3.2	Rippling	Upper part	Upper part
DSTC 16C			Rippling	Middle	Middle
DSTC 17C	114.3	6.02	Buckling	Upper part	Upper part
DSTC 18C			Buckling	Upper part	Upper part
DSTC 19C	88.9	3.2	N/A	N/A	Full height
DSTC 20C			N/A	N/A	Full height
DSTC 21C	60.3	3.6	N/A	N/A	Middle
DSTC 22C			N/A	N/A	Upper part
DSTC 23C	88.9	3.2	N/A	N/A	Upper part
DSTC 24C			N/A	N/A	Upper part
DSTC 25C	114.3	6.02	N/A	N/A	Middle
DSTC 26C			N/A	N/A	Middle
DSTC 27C	88.9	3.2	N/A	N/A	Upper part
DSTC 28C			N/A	N/A	Upper part
DSTC 29C	88.9	3.2	N/A	N/A	Middle
DSTC 30C			N/A	N/A	Upper part

N/A indicates no failure.

Table S 2. Axial load capacities of DSTCs

Specimen	Axial load capacity of DSTC, P_T (kN)	Average P_T (kN)	Average axial load capacity of steel tube, P_s (kN)	Average axial load capacity of unconfined concrete section, P_{co} (kN)	P_s+P_{co} (kN)	$P_T/(P_s+P_{co})$
DSTC 1C	1722	1762	246	655	901	1.96
DSTC 2C	1802					
DSTC 3C	1587	1570	348	512	860	1.82
DSTC 4C	1553					
DSTC 5C	1873	1882	1073	340	1414	1.33
DSTC 6C	1891					
DSTC 7C	2893	2915	246	1271	1517	1.92
DSTC 8C	2937					
DSTC 9C	2132	2172	348	995	1343	1.62
DSTC 10C	2212					
DSTC 11C	2367	2349	1073	660	1734	1.36
DSTC 12C	2331					
DSTC 13C	2799	2819	246	1271	1517	1.86
DSTC 14C	2838					
DSTC 15C	2355	2269	348	995	1343	1.69
DSTC 16C	2182					
DSTC 17C	2440	2363	1073	660	1734	1.36
DSTC 18C	2285					
DSTC 19C	2072	2004	348	740	1088	1.84
DSTC 20C	1936					
DSTC 21C	3515	3573	246	1454	1700	2.10
DSTC 22C	3632					
DSTC 23C	3679	3746	348	1436	1784	2.06
DSTC 24C	3814					
DSTC 25C	4266	4306	1073	1338	2412	1.79
DSTC 26C	4346					
DSTC 27C	4403	4344	348	1436	1784	2.44
DSTC 28C	4284					
DSTC 29C	3416	3319	348	1436	1784	1.86
DSTC 30C	3221					

4. DISCUSSION

4.1. FRP tube hoop rupture strains

Table 4 shows the hoop rupture strains ($\varepsilon_{h,rup}$) of the specimens, which were averaged from the three strain gauges placed outside the overlap region. It is evident from the

results shown in Table 4 that the NSC DSTCs developed larger hoop rupture strains ($\varepsilon_{h,rup}$) than the companion HSC DSTCs. This observation is in agreement with that previously reported on DSTCs under monotonic axial compression (Ozbakkaloglu and Louk Fanggi 2013a). The influence of concrete strength (f'_c) on $\varepsilon_{h,rup}$ was first noted in Ozbakkaloglu and Akin (2012) for FRP-confined concrete, and the reduction in $\varepsilon_{h,rup}$ with an increase in f'_c can be attributed to the change in concrete cracking patterns as was previously discussed in Lim and Ozbakkaloglu (2013).

The effect of concrete-filling inner steel tube on hoop rupture strain ($\varepsilon_{h,rup}$) can be investigated through comparison of the hollow and concrete-filled DSTCs shown in *Table 4*. It can be observed from the table that filled DSTCs developed larger rupture strains than those of the companions hollow DSTCs. This phenomenon can be explained by the location of failure of these specimens, which corresponded to the mid-height of the filled DSTC specimens where $\varepsilon_{h,rup}$ was recorded. By contrast, the hollow DSTC specimens failed near one of the specimen ends, away from the location where $\varepsilon_{h,rup}$ was recorded. Again, this observation is in agreement with those reported in Ozbakkaloglu and Louk Fanggi (2014) and Louk Fanggi and Ozbakkaloglu (2013) for DSTCs tested under monotonic axial compression. It can also be seen from *Table 4* that DSTCs manufactured with GFRP tubes developed higher $\varepsilon_{h,rup}$ than the companions DSTCs manufactured with AFRP tubes, owing to the larger ultimate tensile strain of S-glass fibers, as previously shown in *Table 2*.

Table 4. Ultimate condition of concrete in DSTCs

Specimens	f_{lu}/f'_c	f'_{cu} (MPa)	Avg. f'_{cu} (MPa)	Avg. f'_{cu}/f'_c	ε_{cu} (%)	Avg. ε_{cu} (%)	Avg. $\varepsilon_{cu}/\varepsilon_{co}$	$\varepsilon_{h,rup}$ (%)	Avg. $\varepsilon_{h,rup}$ (%)
DSTC 1C	0.48	95.8	98.4	2.31	3.67	3.84	17.5	1.60	1.57
DSTC 2C	0.48	101.0			4.01			1.54	
DSTC 3C	0.48	102.8	101.4	2.38	3.99	3.90	17.7	1.36	1.35
DSTC 4C	0.48	100.0			3.80			1.33	
DSTC 5C	0.48	100.0	100.1	2.36	4.17	4.07	18.5	1.48	1.37
DSTC 6C	0.48	102.2			3.96			1.25	
DSTC 7C	0.50	171.8	173.2	2.10	2.85	2.95	10.2	0.96	0.97
DSTC 8C	0.50	174.6			3.05			0.97	
DSTC 9C	0.50	147.9	151.2	1.83	2.96	2.95	10.1	0.60	0.77
DSTC 10C	0.50	154.5			2.93			0.94	
DSTC 11C	0.50	161.6	159.4	1.93	3.68	3.57	12.3	0.89	0.79
DSTC 12C	0.50	157.2			3.46			0.69	
DSTC 13C	0.58	165.7	167.0	2.02	3.58	3.54	12.2	1.11	1.20
DSTC 14C	0.58	168.2			3.50			1.28	
DSTC 15C	0.58	166.5	159.3	1.93	4.50	3.99	13.8	1.66	1.60
DSTC 16C	0.58	152.1			3.48			1.54	
DSTC 17C	0.58	170.8	161.1	1.95	4.55	4.17	14.4	1.34	1.34
DSTC 18C	0.58	151.4			3.78			1.01	
DSTC 19C	0.48	99.1	95.2	2.24	3.70	3.53	16.0	1.64	1.56
DSTC 20C	0.48	91.2			3.35			1.48	
DSTC 21C	0.50	185.5	188.8	2.29	2.58	2.79	9.6	1.38	1.45
DSTC 22C	0.50	192.1			3.00			1.51	
DSTC 23C	0.50	191.4	195.3	2.37	3.29	3.35	11.5	1.65	1.57
DSTC 24C	0.50	199.1			3.40			1.49	
DSTC 25C	0.50	196.9	199.4	2.42	3.23	3.19	11.0	1.03	1.12
DSTC 26C	0.50	201.8			3.15			1.20	
DSTC 27C	0.74	233.0	229.6	2.78	3.99	3.77	13.0	1.29	1.30
DSTC 28C	0.74	226.2			3.54			1.30	
DSTC 29C	0.58	176.3	170.7	2.07	3.10	2.96	10.2	1.68	1.65
DSTC 30C	0.58	165.1			2.81			1.62	

4.2. Axial stress-strain behavior of concrete inside DSTCs

The axial stress experienced by the concrete inside the DSTCs can be defined as the load resisted by the annular concrete section divided by its cross-sectional area. The

applied load on the confined concrete was determined by subtracting the axial load resisted by steel tube for a given axial strain, from the total load resisted by the DSTC at the same axial strain. The load acting on the steel tube was determined based on the results of hollow steel tube compression tests, assuming that the load-strain behavior of the steel tube inside a DSTC is similar to that of the corresponding hollow steel tube. The concrete load at failure was then divided by the cross sectional area of the concrete section to determine the ultimate axial stress on the concrete (f'_{cu}) inside the DSTCs. When the axial strain of a DSTC specimen exceeded the axial strain that corresponded to the peak axial load (P_s) of the hollow steel tube, it was assumed that the inner steel tube maintained this load capacity (P_s) until the failure of the specimen. This is because in a DSTC specimen the buckling of the steel inner tube is prevented or delayed by the restraint provided by the concrete, and the decrease in the load carried by the tube may be expected to be limited. *Table 4* provides the ultimate conditions of the concrete in the DSTCs, including the ultimate axial stress (f'_{cu}) and strain (ε_{cu}), whereas *Fig. 5* shows the stress-strain relationships of the concrete inside the DSTCs. It is worth noting that these deduced stress-strain curves for the concrete in the DSTCs have included any beneficial effect that may arise as a result of the steel tube being restrained by the concrete and hence carrying a higher load at the same axial strain. Nonetheless, this effect is believed to be small (Teng et al 2007; Ozbakkaloglu and Louk Fanggi 2013b). As illustrated by *Fig. 5*, the stress-strain behavior of concrete in DSTCs was influenced by the investigated parameters, including concrete strength, the thickness of the FRP tube, the properties of the inner steel tube and the presence (or absence) of concrete-filling inside it. The influence of these parameters on the unloading-reloading behavior and ultimate conditions of concrete in DSTCs is discussed in the following sections.

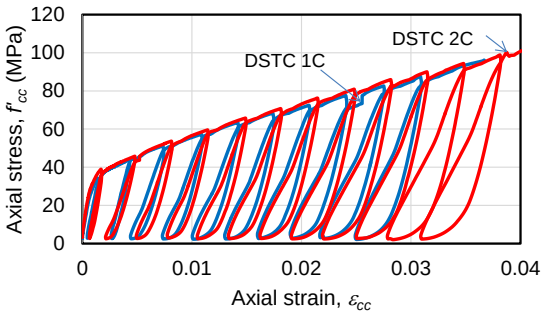
DSTC 1C
DSTC 2C
Axial stress, f'_{cc} (MPa)
Axial strain, ε_{cc}

(a)

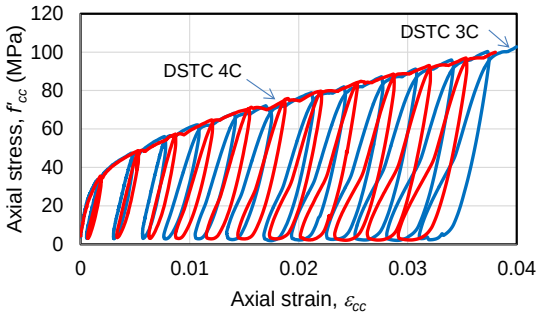
DSTC 4C
DSTC 3C
Axial stress, f'_{cc} (MPa)
Axial strain, ε_{cc}

(b)

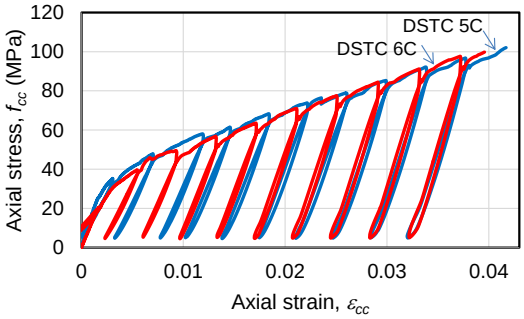
DSTC 6C
DSTC 5C
Axial stress, f_{cc} (MPa)
Axial strain, ε_{cc}

(c)

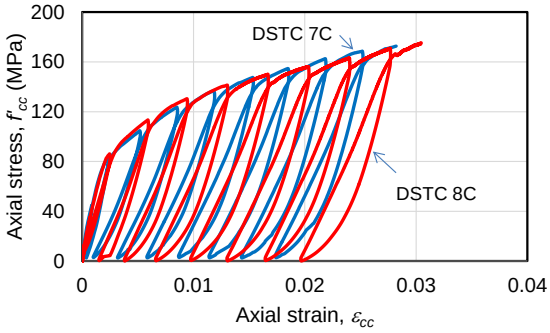
DSTC 7C
DSTC 8C
Axial stress, f'_{cc} (MPa)
Axial strain, ε_{cc}

(d)

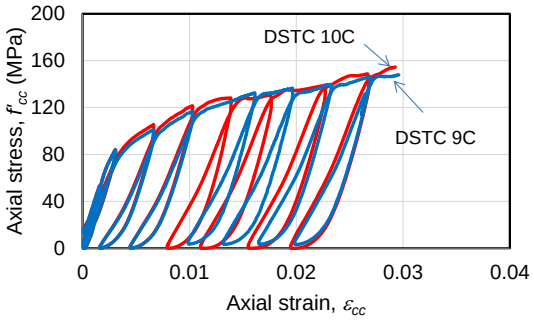
DSTC 10C
DSTC 9C
Axial stress, f'_{cc} (MPa)
Axial strain, ε_{cc}

(e)

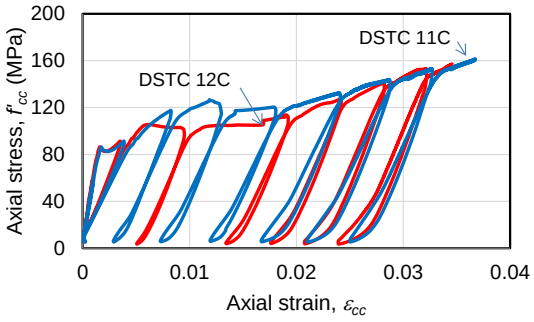
DSTC 12C
DSTC 11C
Axial stress, f'_{cc} (MPa)
Axial strain, ε_{cc}

(f)

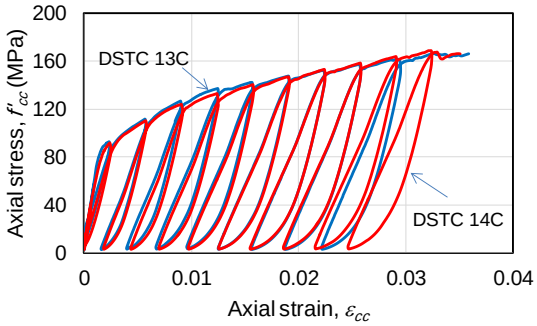
DSTC 13C
DSTC 14C
Axial stress, f'_{cc} (MPa)
Axial strain, ε_{cc}

(g)

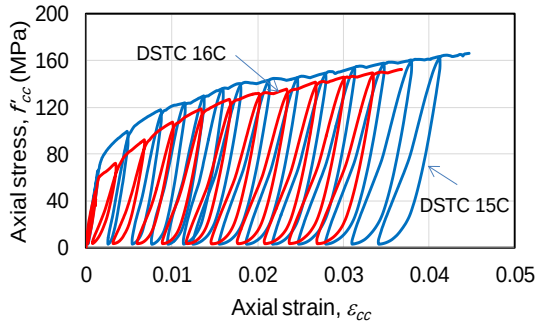
DSTC 16C
DSTC 15C
Axial stress, f'_{cc} (MPa)
Axial strain, ε_{cc}

(h)

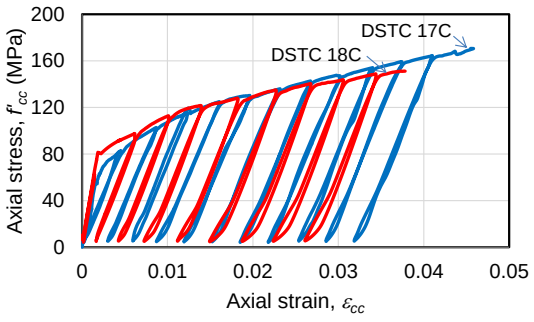
DSTC 18C
DSTC 17C
Axial stress, f'_{cc} (MPa)
Axial strain, ε_{cc}

(i)

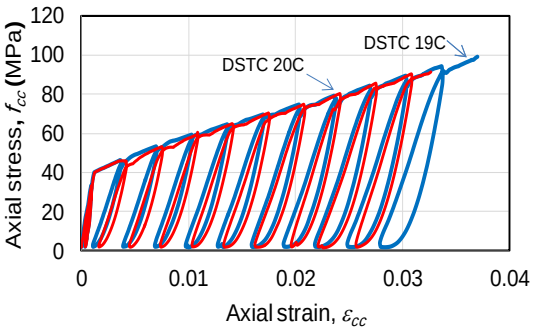
DSTC 20C
DSTC 19C
Axial stress, f'_{cc} (MPa)
Axial strain, ε_{cc}

(j)

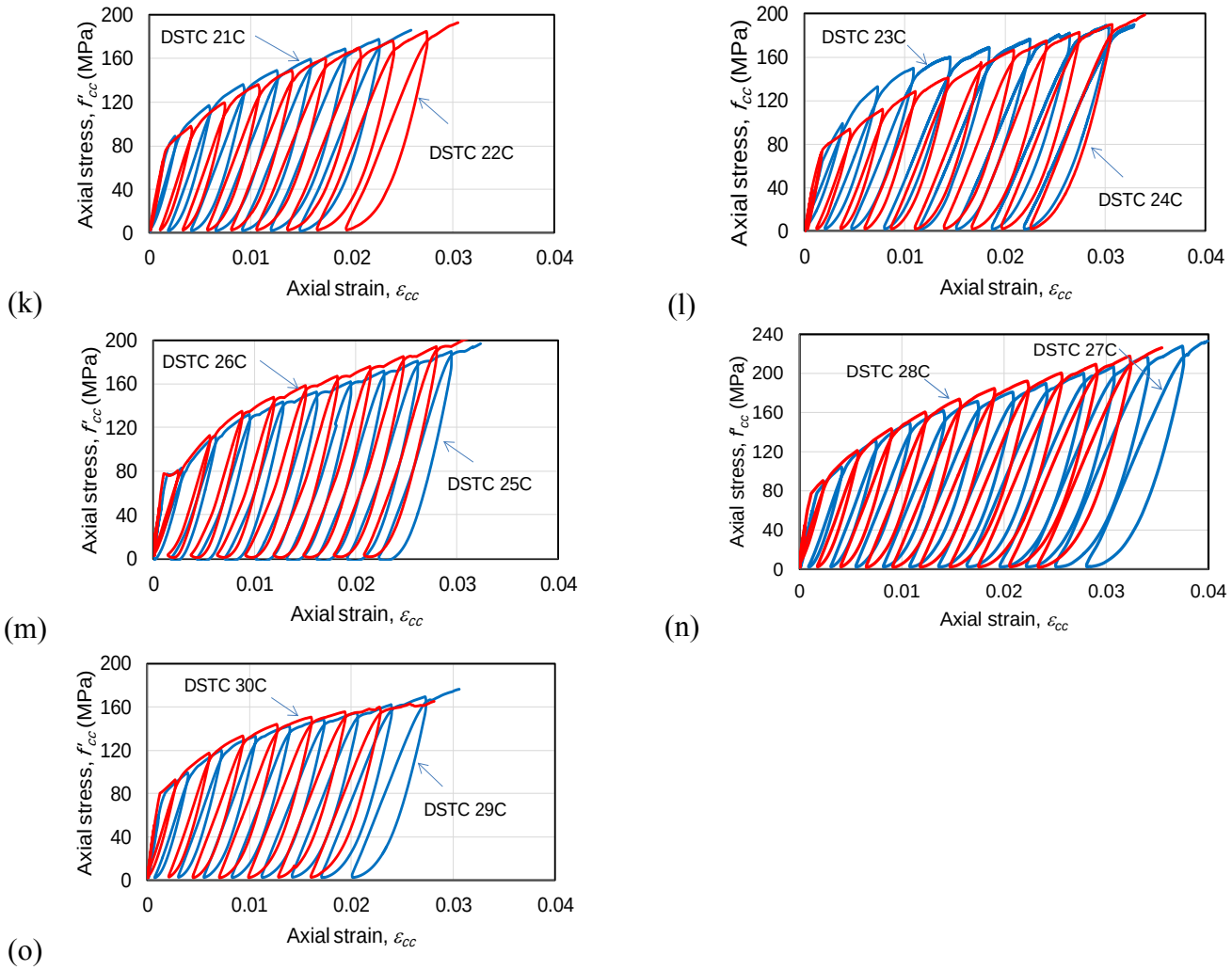

Figure 5. Cyclic axial stress-strain behavior of concrete in DSTCs:
(a) – (o) DSTCs 1C to 30C

4.3. Unloading and reloading paths and the plastic strain

To define the complete axial stress-strain response of concrete in cyclically loaded DSTCs, in addition to an envelope curve that represents the upper boundary of the response, unloading and reloading paths are required. An unloading path is defined as the stress-strain path traced by the concrete as its axial strain reduces, and a reloading path is defined as the stress-strain path traced by concrete as its axial strain increases from a starting point on an unloading path (Lam and Teng 2009; Ozbakkaloglu and Akin 2012). Unloading may be from a point on the envelope curve or from a point on a reloading curve (i.e., before reaching the envelope curve on the reloading path). All the specimens of the present study were unloaded from their envelope curves; thus, in this

paper the term "unloading" refers to envelope-curve unloading. The axial strain at the starting point of unloading path is referred to as the envelope unloading strain, $\varepsilon_{un,env}$.

An unloading path intersects the axial strain axis at a strain value that is referred to as the residual plastic strain, ε_{pl}. The residual plastic strain of concrete can be defined as the residual axial strain of the material when it is unloaded to the zero stress, and its accurate determination is of vital importance in describing complete stress-strain behavior of cyclically loaded specimens. As a result, the relationship between $\varepsilon_{un,env}$ and ε_{pl} has been investigated in a number of studies on unconfined, steel-confined, and FRP-confined concrete (e.g., Bahn and Hsu 1998; Sakai and Kawashima 2006; Lam et al. 2006; Abbasnia and Ziaadiny 2010; Ozbakkaloglu and Akin 2012). Lam et al. (2006) demonstrated that the relationship between unloading strains $\varepsilon_{un,env}$ and plastic strains ε_{pl} was linear for carbon FRP (CFRP)-confined NSC cylinders for $\varepsilon_{un,env} \geq 0.0035$. This observation was then supported by those reported in Ozbakkaloglu and Akin (2012) based on a comprehensive experimental study on CFRP-confined HSC and AFRP-confined NSC and HSC cylinders.

The relationships between the envelope unloading strain $\varepsilon_{un,env}$ and the estimated plastic strain ε_{pl} of the specimens of the present study are shown in *Fig. 6* separately for AFRP-confined NSC, AFRP-confined HSC, and GFRP-confined HSC DSTCs. As noted previously, the unloading curves of the specimens were terminated just before they reached zero stress; therefore, the plastic strains were estimated by extending the unloading curves to cross the axial-strain axis. *Fig. 6* illustrates that, just like it was observed in FRP-confined concrete, the residual plastic strain of concrete in DSTCs is linearly related to the envelope unloading strain. A closer inspection of the relationships

shown in *Fig.6* allows a number of important observations to be made on the influence of the studied specimen parameters on $\varepsilon_{un,env}$-ε_{pl} relationships.

First, it can be observed from *Figs. 6(a)-6(c)* that the trend-lines of the companion hollow and concrete-filled specimens with the same concrete strength and confinement material almost coincide, which suggests that concrete-filling inner steel tubes has little to no influence on the residual plastic strains of concrete in DSTCs. Furthermore, comparison of the trend-line equations of NSC and HSC DSTCs with AFRP external tubes in *Figs. 6(a)* and *6(b)* indicates that the trend-line equation does not change significantly with the unconfined concrete strength. Likewise, a closer inspection of the $\varepsilon_{un,env}$-ε_{pl} relationships of the specimens in each group consisting of companion specimens with different inner steel tube diameters indicate that the inner steel tube diameter has only a slight influence on the trend-line expressions of both hollow and concrete-filled DSTCs. Finally, comparison of the trend-lines of HSC DSTCs manufactured with AFRP and GFRP external tubes in *Figs. 6(b)* and *6(c)* indicates that the trend-line equation is not affected significantly by the type of FRP material.

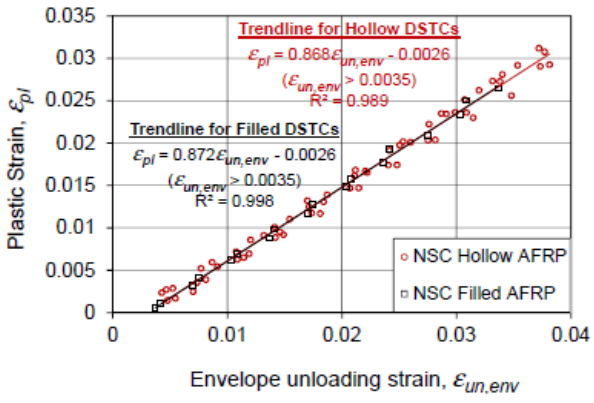

(a)

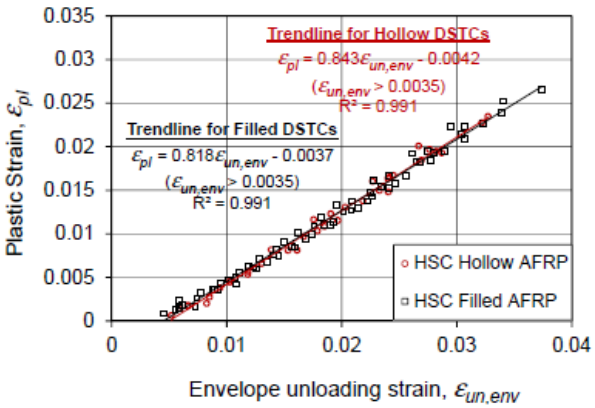

(b)

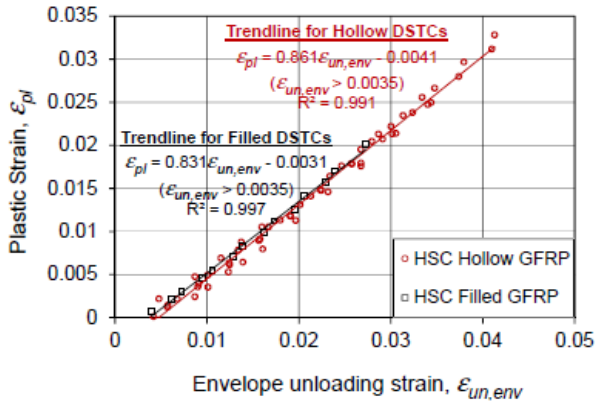

(c)

Figure 6. Plastic strain-envelope unloading strain relationships of test specimens: (a) NSC AFRP, (b) HSC AFRP, (c) HSC GFRP

To summarize, the results of the present study indicate that none of the four important specimen parameters investigated in the present study (i.e., concrete strength, FRP type, inner steel tube diameter, and presence/absence of a concrete filling inside inner steel tube) has significant influence on the relationship between the unloading strain $\varepsilon_{un,env}$ and residual plastic strain ε_{pl} of concrete in DSTCs. Among these findings, the ones on the influence of concrete strength and FRP type on the unloading-reloading behavior of concrete in DSTCs are in agreement with those reported in Ozbakkaloglu and Akin (2012) on the behavior of FRP-confined concrete.

4.4. Ultimate condition

4.4.1. Influence of unconfined concrete strength

To examine the influence of concrete strength on the axial stress-strain behavior of concrete inside a DSTC, the companion NSC and HSC DSTCs were designed to have similar levels of confinement, which was calculated through the use of the nominal confinement ratio (f_{lu}/f'_c) presented in *Eq. 2*, where f_{lu} is the lateral confining pressure at failure. Similar confinement ratios of different strength concretes allowed the effects of concrete strength on the behavior of the DSTCs to be examined.

Table 5 shows the influence of concrete strength (f'_c) on the ultimate axial stress (f'_{cu}) and strain (ε_{cu}) of concrete inside DSTCs. The results demonstrate that the hollow NSC DSTCs developed larger strength and strain enhancement ratios (f'_{cu}/f'_c and $\varepsilon_{cu}/\varepsilon_{co}$) than their HSC counterparts. Similar observations on the influence of concrete strength were previously reported for CFFTs in Ozbakkaloglu and Vincent (2013) and DSTCs in Louk Fanggi and Ozbakkaloglu (2013) that were under monotonic axial compression. Nevertheless, as evident from *Table 5*, both NSC and HSC DSTCs of the present study exhibited a highly ductile behavior under cyclic axial compression, as marked by the large ultimate axial strains of the specimens.

Table 5. Influence of concrete strength, f'_c

Group	Specimens	f'_c (MPa)	D_s/t_s (mm)	f_{lu}/f'_c	f'_{cu} (MPa)	f'_{cu}/f'_c	ε_{cu} (%)	$\varepsilon_{cu}/\varepsilon_{co}$
AFRP hollow	DSTCs 1C & 2C	42.5	60.3/3.6	0.48	98.4	2.31	3.84	17.5
	DSTCs 7C & 8C	82.4	60.3/3.6	0.50	173.2	2.10	2.95	10.2
	DSTCs 3C & 4C	42.5	88.9/3.2	0.48	101.4	2.38	3.90	17.7
	DSTCs 9C & 10C	82.4	88.9/3.2	0.50	151.2	1.83	2.95	10.1
	DSTCs 5C & 6C	42.5	114.3/6.02	0.48	100.1	2.36	4.07	18.5
	DSTCs 11C & 12C	82.4	114.3/6.02	0.50	159.4	1.93	3.57	12.3
AFRP filled	DSTCs 19C & 20C	42.5	88.9/3.2	0.48	95.2	2.24	3.53	16.0
	DSTCs 23C & 24C	82.4	88.9/3.2	0.50	195.3	2.37	3.35	11.5

The comparison of the results of concrete-filled DSTCs in *Table 5* leads to an interesting observation that the filled HSC DSTCs exhibited a slightly higher f'_{cu}/f'_c than the companions NSC DSTCs. The improved behavior of the HSC DSTCs can be attributed to the beneficial influence of the additional confinement provided by the inner steel tube in addressing the increased confinement demand of HSC. It might be worth noting, however, that NSC concrete-filled specimens (i.e. DSTCs 19C&20C) exhibited

lower than anticipated load carrying capacities, which contributed to the lower strength enhancement ratios observed in these specimens.

4.4.2. Effect of FRP tube material

The effect of FRP confinement on the behavior of the specimens was determined by investigating relative performances of the companion DSTCs manufactured with AFRP and GFRP tubes. *Table 6.6* presents the influence of the different types of FRP on the ultimate stress (f'_{cu}) and strain (ε_{cu}) of concrete inside DSTCs. As shown in *Table 6*, DSTCs manufactured with AFRP and GFRP tubes had slightly different nominal confinement ratios (f_{lu}/f'_c). Therefore, in order to enable a meaningful comparison, the stress and strain enhancement coefficients (k_1 and k_2) were calculated using *Eqs. 3* and *4*. Because these equations were used solely for comparison purposes, simple equation forms, which are used commonly also for FRP-confined concrete (Ozbakkaloglu et al. 2013), were adopted.

$$k_1 = \left(\frac{f'_{cu}}{f'_c} - 1\right) \Big/ \frac{f_{lu}}{f'_c} \quad (3)$$

$$k_2 = \left(\frac{\varepsilon_{cu}}{\varepsilon_{co}} - 2\right) \Big/ \frac{f_{lu}}{f'_c} \quad (4)$$

It can be seen from *Table 6* that hollow DSTCs manufactured with AFRP tubes developed slightly higher k_1 and slightly lower k_2 than the companions DSTCs confined with GFRP tubes. This observation is consistent with the one reported in Lim and Ozbakkaloglu (2013) for FRP-confined concrete, where based on a large experimental test database it was demonstrated that an increase in fiber elastic modulus (E_f) resulted in an increase in k_1 and a decrease in k_2. Filled DSTCs manufactured with GFRP tubes, on the other hand, had lower k_1 and k_2 values than the companion filled DSTCs manufactured with AFRP tubes. It might be worth noting, however, that the former

specimens exhibited lower performance levels than anticipated, and hence additional tests are required to determine if this observation has any broader implications.

Table 6. Influence of FRP type

Group	Specimens	FRP type	D_s/t_s (mm)	f_{lu}/f'_c	f'_{cu} (MPa)	f'_{cu}/f'_c	ε_{cu} (%)	$\varepsilon_{cu}/\varepsilon_{co}$	k_1	k_2
HSC hollow	DSTCs 7C & 8C	AFRP	60.3/3.6	0.50	173.2	2.10	2.95	10.2	2.23	16.3
	DSTCs 13C & 14C	GFRP		0.58	167.0	2.02	3.54	12.2	1.78	17.6
	DSTCs 9C & 10C	AFRP	88.9/3.2	0.50	151.2	1.83	2.95	10.1	1.67	16.3
	DSTCs 15C & 16C	GFRP		0.58	159.3	1.93	3.99	13.8	1.61	20.3
	DSTCs 11C & 12C	AFRP	114.3/6.02	0.50	159.4	1.93	3.57	12.3	2.03	20.6
	DSTCs 17C & 18C	GFRP		0.58	161.1	1.95	4.17	14.4	1.65	21.3
HSC filled	DSTCs 23C & 24C	AFRP	88.9/3.2	0.50	195.3	2.37	3.35	11.5	2.73	19.1
	DSTCs 29C & 30C	GFRP		0.58	170.7	2.07	2.96	10.2	1.84	14.1

4.4.3. Effect of FRP tube thickness

To illustrate the influence of FRP tube fiber thickness on the ultimate axial stress (f'_{cu}) and strain (ε_{cu}), *Table 7* presents the results from the two specimen pairs. As expected, an increase in the AFRP tube fiber thickness from 1.2 mm to 1.8 mm led to an increase in both f'_{cu} and ε_{cu} and resulting strength and strain enhancement ratios (f'_{cu}/f'_c and $\varepsilon_{cu}/\varepsilon_{co}$). On the other hand, as illustrated in *Table 7*, the specimens with thicker FRP tubes developed slightly lower strength and strain enhancement coefficients (k_1 and k_2) than their companions, indicating that the increase in the ultimate axial stress and strain was not directly proportional to the increase in nominal confinement ratio (f_{lu}/f'_c) resulting from the increase in FRP tube thickness.

Table 7. Influence of FRP tube thickness

Group	Specimens	FRP tube fiber thickness (mm)	D_s/t_s (mm)	f_{lu}/f'_c	f'_{cu} (MPa)	f'_{cu}/f'_c	ε_{cu} (%)	$\varepsilon_{cu}/\varepsilon_{co}$	k_1	k_2
HSC filled AFRP	DSTCs 23C&24C	1.2	88.9/3.2	0.50	195.3	2.37	3.35	11.5	2.73	19.1
	DSTCs 27C&28C	1.8	88.9/3.2	0.74	229.6	2.78	3.77	13.0	2.41	14.7

4.4.4. Effect of inner steel tube diameter

To illustrate the influence of inner steel tube diameter (D_s) *Table 8* presents the results from four different specimen groups. Each group shown in *Table 8* consisted of three DSTCs with different inner steel tube sizes. It can be seen from the table that an increase in D_s led to an increase in the ultimate axial strains (ε_{cu}) of the hollow DSTCs. It can also be seen from *Table 8* that the increase in D_s had no significant influence on the ultimate axial stress (f'_{cu}) of the hollow NSC DSTCs. On the other hand, as evident from the table, an increase in D_s resulted in a decrease in f'_{cu} of the hollow HSC DSTCs. This final observation is not in agreement with those previously reported in Wong et al. (2008), Ozbakkaloglu and Louk Fanggi (2013a) and Louk Fanggi and Ozbakkaloglu (2013) for monotonically loaded hollow DSTCs, where it was found that f'_{cu} increased slightly with an increase in D_s.

The results shown in *Table 8* also illustrate that, in filled DSTCs, an increase in D_s resulted in an increase in both f'_{cu} and ε_{cu}. This observation can be attributed to the increase in the additional confinement effects provided by the inner steel tube to the core concrete with an increase in D_s, and it is in support of the findings previously reported in Ozbakkaloglu and Louk Fanggi (2013a, 2013b) for monotonically loaded concrete-filled DSTCs.

Table 8. Influence of steel tube diameter, D_s

Group	Specimens	D_s/t_s (mm)	f_{lu}/f'_c	Avg. f'_{cu} (MPa)	Avg. f'_{cu}/f'_c	Avg. ε_{cu} (%)	Avg. $\varepsilon_{cu}/\varepsilon_{co}$
NSC hollow AFRP	DSTCs 1C & 2C	60.3/3.6	0.48	98.4	2.31	3.84	17.5
	DSTCs 3C & 4C	88.9/3.2	0.48	101.4	2.38	3.90	17.7
	DSTCs 5C & 6C	114.3/6.02	0.48	100.1	2.36	4.07	18.5
HSC hollow AFRP	DSTCs 7C & 8C	60.3/3.6	0.50	173.2	2.10	2.95	10.2
	DSTCs 9C & 10C	88.9/3.2	0.50	151.2	1.83	2.95	10.1
	DSTCs 11C & 12C	114.3/6.02	0.50	159.4	1.93	3.57	12.3
HSC hollow GFRP	DSTCs 13C & 14C	60.3/3.6	0.58	167.0	2.02	3.54	12.2
	DSTCs 15C & 16C	88.9/3.2	0.58	159.3	1.93	3.99	13.8
	DSTCs 17C & 18C	114.3/6.02	0.58	161.1	1.95	4.17	14.4
HSC filled AFRP	DSTCs 21C & 22C	60.3/3.6	0.50	188.8	2.29	2.79	9.6
	DSTCs 23C & 24C	88.9/3.2	0.50	195.3	2.37	3.35	11.5
	DSTCs 25C & 26C	114.3/6.02	0.50	199.4	2.42	3.19	11.0

4.4.5. Effect of concrete-filling inner steel tube

Table 9 presents the comparison between paired hollow and concrete-filled DSTCs. The results shown in the table indicates that, except for the AFRP-confined NSC specimens where, as noted previously, the concrete-filled DSTCs developed lower than anticipated axial load capacities, DSTCs with filled inner steel tubes exhibited a higher ultimate axial stress (f'_{cu}) than that of the companion DSTCs with hollow inner steel tubes. The increase in f'_{cu} in the concrete-filled DSTCs can be attributed to aforementioned confinement effects provided by the inner steel tube to the core concrete. The results shown in *Table 9* also indicate that hollow DSTCs developed higher ultimate axial strains (ε_{cu}) compared to the companions concrete-filled DSTCs. Both of these observations are in agreement with those previously reported in Ozbakkaloglu and Louk Fanggi (2013b), where the influence of concrete-filling on the behavior of monotonically loaded DSTCs was investigated.

Table 9. Influence of concrete-filling inner steel tube

Group	Specimens	DSTC type	D_s/t_s (mm)	f_{lu}/f'_c	f'_{cu} (MPa)	f'_{cu}/f'_c	ε_{cu} (%)	$\varepsilon_{cu}/\varepsilon_{co}$
NSC AFRP	DSTCs 3C & 4C	Hollow	88.9/3.2	0.48	101.4	2.38	3.90	17.7
	DSTCs 19C & 20C	Filled	88.9/3.2	0.48	95.2	2.24	3.53	16.0
HSC AFRP	DSTCs 7C & 8C	Hollow	60.3/3.6	0.50	173.2	2.10	2.95	10.2
	DSTCs 21C & 22C	Filled	60.3/3.6	0.50	188.8	2.29	2.79	9.6
	DSTCs 9C & 10C	Hollow	88.9/3.2	0.50	151.2	1.83	2.95	10.1
	DSTCs 23C & 24C	Filled	88.9/3.2	0.50	195.3	2.37	3.35	11.5
	DSTCs 11C & 12C	Hollow	114.3/6.02	0.50	159.4	1.93	3.57	12.3
	DSTCs 25C & 26C	Filled	114.3/6.02	0.50	199.4	2.42	3.19	11.0
HSC GFRP	DSTCs 15C & 16C	Hollow	88.9/3.2	0.58	159.3	1.93	3.99	13.8
	DSTCs 29C & 30C	Filled	88.9/3.2	0.58	170.7	2.07	2.96	10.2

5. Comparison of experimental results with Louk Fanggi and Ozbakkaloglu's model (2013)

Louk Fanggi and Ozbakkaloglu (2013) proposed a model to predict the compressive strength (f'_{cc}) and ultimate axial strain (ε_{cu}) of concrete in monotonically loaded hollow DSTCs. The model is described by the following expressions:

$$f'_{cc} = c_1 f'_c + k_1 (f_{lu,a} - f_{lo}) \tag{5}$$

$$\varepsilon_{cu} = \left(c_2 \varepsilon_{co} + k_2 \left(\frac{K_l}{f'_{co}} \right)^{0.9} \varepsilon_{h,rup}{}^{1.35} \right) 1.28 \left(1 - \frac{D_s}{D} \right)^{-0.36} \tag{6}$$

In *Eqs. 5* and *6*, k_1 and k_2, respectively, are the strength and strain enhancement ratios with recommended values of $k_1 = 3.2$ and $k_2 = 0.27$. In the calculation of the actual confining pressure ($f_{lu,a}$) in *Eq. 7*, the hoop rupture strain $\varepsilon_{h,rup}$ is established through *Eq. 8* based on the hoop strain reduction factor $k_{\varepsilon,f}$ given in *Eq. 9*. The confinement stiffness (K_l) of the FRP tube is calculated by *Eq. 10* and the threshold confinement stiffness (K_{lo}) is established from *Eq. 11*. Depending on the relationship between K_l and K_{lo}, strength

multiplier (c_1) and threshold confining pressure (f'_{lo}) in *Eq. 5* is calculated using either *Eqs. 12* and *13* or *Eqs. 14* and *15*. In *Eq. 6*, the concrete strength factor (c_2) is calculated from *Eq. 16*, the peak axial strain of unconfined concrete (ε_{co}) is determined by *Eq. 17*, and the void ratio (D_s/D) is the ratio of the inner to outer diameter of the annular concrete section.

$$f_{lu,a} = \frac{2E_f t_f \varepsilon_{h,rup}}{D} \tag{7}$$

$$\varepsilon_{h,rup} = k_{\varepsilon,f}\varepsilon_f \tag{8}$$

$$k_{\varepsilon,f} = 0.9 - 2.3f'_{co} \times 10^{-3} - 0.75E_f \times 10^{-6} \quad \text{where } 100{,}000\text{MPa} \leq E_f \leq 640{,}000\text{MPa} \tag{9}$$

$$K_{\mathrm{l}} = \frac{2E_f t_f}{D} \tag{10}$$

$$K_{lo} = {f'_c}^{1.65} \tag{11}$$

$$\text{if } K_{\mathrm{l}} \geq K_{\mathrm{lo}}, \qquad c_1 = 1 + 0.0058\frac{K_{\mathrm{l}}}{f'_{\mathrm{c}}} \tag{12}$$

$$f_{\mathrm{lo}} = K_{\mathrm{l}}\varepsilon_{\mathrm{l1}}, \qquad \varepsilon_{\mathrm{l1}} = \left(0.43 + 0.009\frac{K_{\mathrm{l}}}{f'_{\mathrm{c}}}\right)\varepsilon_{\mathrm{co}} \tag{13}$$

$$\text{if } K_{\mathrm{l}} < K_{\mathrm{lo}}, \qquad c_1 = \left(\frac{K_{\mathrm{l}}}{{f'_{\mathrm{c}}}^{1.6}}\right)^{0.2} \tag{14}$$

$$f_{\mathrm{lo}} = K_{\mathrm{l}}\varepsilon_{\mathrm{l2}}, \qquad \varepsilon_{\mathrm{l2}} = 24\left(\frac{f'_{\mathrm{c}}}{K_{\mathrm{l}}^{1.6}}\right)^{0.4}\varepsilon_{\mathrm{co}} \quad \text{where} \quad f_{\mathrm{lu,a}} \geq f_{\mathrm{lo}} \tag{15}$$

$$c_2 = 2 - \left(\frac{f'_c - 20}{100}\right) \; and \; c_2 \geq 1 \tag{16}$$

$$\varepsilon_{\mathrm{co}} = \left(-0.067{f'_{\mathrm{c}}}^2 + 29.9f'_{\mathrm{c}} + 1053\right) \times 10^{-6} \quad \text{where f'c is in MPa} \tag{17}$$

In Egs. (11), (14)-(17) f'_c, K_l, K_{lo} are in MPa. Because Louk Fanggi and Ozbakkaloglu model was intended for hollow DSTCs and hence does not allow for the additional confinement provided by the inner steel to core concrete, in the model calculations of f'_{cc} in concrete-filled DSTCs, the increase in the load carrying capacity of core concrete due to the confinement provided by the inner steel tube (i.e. $\lambda.P_s$) was accounted for through the use of an augmentation factor (λ), the value of which was established based on experimental results as 0.27 in Sakino et al. (2004).

Table 10 shows comparisons of model predictions with experimental results. It might be worth noting that, because the concrete stress-strain curves of all of the specimens of the present study exhibited an ascending type of second branches, the compressive strengths (f'_{cc}) corresponded to their ultimate axial stresses (f'_{cu}). It can be seen from *Table 10* that for hollow HSC DSTCs the model predictions are in good agreement with the experimental results. In general, the model slightly underestimates f'_{cc} and ε_{cu} of hollow NSC DSTCs and very slightly overestimates f'_{cc} and ε_{cu} of hollow HSC DSTCs. However, comparison of the model predictions with the results from concrete-filled DSTCs indicate that, except for those of the specimens that developed lower than expected f'_{cc} as noted previously (i.e. DSTCs 19&20 and 29C&30C), the model

underestimates the compressive strength of concrete in filled DSTCs even when the additional confinement provided by the inner steel tube is considered. On the other hand, the comparisons in *Table 10* indicate that, except for a single case caused by the lower than expected ε_{cu} of DSTCs 29C&30C, model predictions of ε_{cu} of the concrete-filled DSTCs are in reasonably good agreement with the experimental results.

Table 10. Comparisons of test results with predictions of Louk Fanggi And Ozbakkaloglu's model (2013)

Group	Specimens	Experimental		Prediction		Experimental / Prediction	
		$(f'_{cc})_{exp.}$ (MPa)	$(\varepsilon_{cu})_{exp.}$ (%)	$(f'_{cc})_{model}$ (MPa)	$(\varepsilon_{cu})_{model}$ (%)	$(f'_{cc})_{exp.}/(f'_{cc})_{model}$	$(\varepsilon_{cu})_{exp.}/(\varepsilon_{cu})_{model}$
NSC hollow AFRP	DSTCs 1C & 2C	98.4	3.84	91.6	3.12	1.07	1.23
	DSTCs 3C & 4C	101.4	3.90	91.6	3.56	1.11	1.10
	DSTCs 5C & 6C	100.1	4.07	91.6	4.28	1.09	0.95
HSC hollow AFRP	DSTCs 7C & 8C	173.2	2.95	164.9	2.80	1.05	1.05
	DSTCs 9C & 10C	151.2	2.95	164.9	3.20	0.92	0.92
	DSTCs 11C & 12C	159.4	3.57	164.9	3.84	0.97	0.93
HSC hollow GFRP	DSTCs 13C & 14C	167.0	3.54	165.5	3.76	1.01	0.94
	DSTCs 15C & 16C	159.3	3.99	165.5	4.30	0.96	0.93
	DSTCs 17C & 18C	161.1	4.17	165.5	5.16	0.97	0.81
NSC filled AFRP	DSTCs 19C & 20C	95.2	3.53	97.0	3.56	0.98	0.99
HSC filled AFRP	DSTCs 21C & 22C	188.8	2.79	168.7	2.80	1.12	1.00
	DSTCs 23C & 24C	195.3	3.35	170.3	3.20	1.15	1.05
	DSTCs 25C & 26C	199.4	3.19	182.8	3.84	1.09	0.83
	DSTCs 27C & 28C	229.6	3.77	208.8	4.28	1.10	0.88
HSC filled GFRP	DSTCs 29C & 30C	170.7	2.96	170.9	4.30	1.00	0.69

These results illustrate that the Louk Fanggi and Ozbakkaloglu model that was proposed for monotonically loaded hollow DSTCs provides accurate estimates of the ultimate conditions (i.e. f'_{cc} and ε_{cu}) of concrete in hollow DSTCs subjected to cyclic axial compression. The results also illustrate that the additional confinement provided

by the steel tube is not sufficient to describe the increase in the compressive strength of concrete in filled DSTCs, suggesting that FRP confinement also contributes to the load carrying capacity of inner concrete-filled steel tubes. Therefore, a model that is capable of taking all of these effects into account to accurately predict the compressive strength (f'_{cc}) of concrete in filled DSTCs is required. To this end, research is currently underway at the University of Adelaide where additional concrete-filled DSTCs are being tested.

6. CONCLUSIONS

This paper has presented the results of an experimental study that was undertaken to investigate the behavior of FRP-concrete-steel DSTCs under cyclic axial compression. The following conclusions can be drawn based on the results and discussions reported in this paper.

1. DSTCs exhibit a very ductile behavior under cyclic axial compression, whether constructed from NSC or HSC, and whether had a concrete-filled or hollow inner steel tube.
2. The residual plastic strain of concrete in DSTCs is linearly related to the envelope unloading strain, and this relationship is not influenced significantly by: (i) unconfined concrete strength, (ii) FRP type, (iii) diameter of the inner steel tube, and (iv) presence/absence of a concrete filling inside the steel tube.
3. Hollow HSC DSTCs develops lower strength and strain enhancement ratios (f'_{cu}/f'_c and $\varepsilon_{cu}/\varepsilon_{co}$) than their NSC counterpart. Concrete-filled HSC DSTCs, on the other hand, exhibit a similar strength enhancement and ultimate axial strain level to the companion filled NSC DSTCs.
4. For a given nominal confinement ratio (f'_{lu}/f'_c), specimens manufactured with AFRP tubes exhibit a slightly higher strength enhancement and slightly lower strain

enhancement than companion DSTCs manufactured with GFRP tubes. This is due to the larger elastic modulus and lower tensile rupture strain of the aramid fibers compared to the S-glass fibers.

5. As expected, an increase in the FRP tube thickness results in an increase in the strength and strain enhancement ratios (f'_{cu}/f'_c and $\varepsilon_{cu}/\varepsilon_{co}$). On the other hand, it is observed that the strength and strain enhancement coefficients (k_1 and k_2) slightly decrease with an increase in the confinement ratio (f'_{lu}/f'_c).
6. Increasing the diameter of the inner steel tube results in an increase of the ultimate axial strain of concrete (ε_{cu}) in both hollow and concrete-filled DSTCs. An increase in the tube diameter also leads to an increase in the ultimate axial stress (f'_{cu}) of concrete in filled DSTCs.
7. DSTCs with hollow inner steel tubes demonstrate larger axial strains (ε_{cu}) than the companion concrete-filled DSTCs. DSTCs with concrete-filled inner steel tubes, on the other hand, develop higher ultimate axial stresses (f'_{cu}) than DSTCs with hollow inner steel tubes.
8. Specimens with concrete-filled inner steel tubes exhibit higher hoop rupture strains ($\varepsilon_{h,rup}$) than the companion hollow specimens. Likewise, NSC DSTCs exhibit higher hoop rupture strains ($\varepsilon_{h,rup}$) than their HSC counterparts.

This paper has also presented comparisons between the test results and predictions of Louk Fanggi and Ozbakkaloglu's model (2013), which was originally proposed for monotonically loaded hollow DSTCs. The comparisons indicate that the model provides reasonably accurate predictions of the compressive strength and ultimate strain (f'_{cc} and ε_{cu}) of concrete in hollow DSTCs. However, due to not allowing for the additional confinement provided by inner steel tube to core concrete, the model underestimates the compressive strength of concrete in DSTCs with concrete-filled inner steel tubes. The

research is ongoing at the University of Adelaide with the aim of developing an accurate model of concrete-filled DSTCs.

SUPLEMENTAL DATA

Table S1 and S2 are available online in the ASCE Library (http://www.ascelibrary.org/).

REFERENCES

Abbasnia, R., and Ziaadiny, H. (2010). "Behavior of concrete prisms confined with FRP composites under axial cyclic compression." *Engineering Structures*, 32(3), 648–655.

ASTM (2008). "Standard test method for tensile properties of polymer matrix composites materials". D3039-M-08, West Conshohocken, PA.

Bahn, B. Y., Hsu, and Cheng-Tzu T. (1998). "Stress-strain behavior of concrete under cyclic loading." *ACI Materials Journal*, 95(2), 178–193.

Fam, A. Z., and Rizkalla, S. H. (2001). "Confinement model for axially loaded concrete confined by circular fiber-reinforced polymer tubes." *ACI Structural Journal*, 98(4): 451–461.

Idris, Y., and Ozbakkaloglu, T. (2013). "Seismic performance of square high-strength concrete columns in FRP stay-in-place formwork." *Journal of Composites for Construction, ASCE*, 17(6), doi/abs/10.1061/(ASCE)CC.1943–5614.0000388.

Lam, L., and Teng, J. G. (2004). "Ultimate condition of fiber reinforced polymer-confined concrete." *Journal of Composites for Construction*, 8(6): 539–548.

Lam, L., and Teng, J. G. (2009). "Stress-strain model for FRP-confined concrete under cyclic axial compression." *Engineering Structures*, 31(2): 308–321.

Lam, L., Teng, J. G., Cheung, Y., and Xiao, Y. (2006). "FRP-confined concrete under axial cyclic compression." *Cement and Concrete Composites*, 8(10), 949–958.

Lignola, G. P., Prota, A., Manfredi, G., and Cosenza, E. (2007). "Experimental performance of RC hollow columns confined with CFRP." *Journal of Composites for Construction, ASCE*, 11(1): 42–49.

Lim, J., and Ozbakkaloglu, T. (2013). "Confinement model for FRP-confined high-strength concrete," *Journal of Composites for Construction, ASCE*, doi:10.1061/(ASCE)CC.1943–5614.0000376.

Louk Fanggi, B. A., and Ozbakkaloglu, T. (2013). "Compressive behavior of hollow aramid FRP-HSC-steel double-skin tubular columns." *Construction and Building Materials*, 48: 554–565.

Ozbakkaloglu, T. (2013a). "Concrete-filled FRP Tubes: Manufacture and Testing of New Forms Designed for Improved Performance." *Journal of Composites for Construction, ASCE*, 17(2): 280–281.

Ozbakkaloglu, T. (2013b). "Behavior of square and rectangular ultra high-strength concrete-filled FRP tubes under axial compression." *Composites Part B: Engineering*, 54: 97–111.

Ozbakkaloglu, T., and Akin, E. (2012). "Behavior of FRP-confined normal- and high-strength concrete under cyclic axial compression." *Journal of Composites for Construction. ASCE*. 16(4): 451–463.

Ozbakkaloglu, T., and Idris, Y. (2013). "Seismic behavior of FRP-high-strength concrete-steel double skin tubular columns." *Journal of Structural Engineering*, *ASCE*. doi: 10.1061/(ASCE) ST.1943–541X.0000981.

Ozbakkaloglu, T., and Louk Fanggi, B.A. (2013a). "Axial compressive behavior of FRP-concrete-steel double-skin tubular columns made of normal- and high-strength concrete." *Journal of Composites for Construction. ASCE*, doi:10.1061/(ASCE)CC.1943–5614.0000401.

Ozbakkaloglu, T., and Louk Fanggi, B.A. (2013b). "FRP-HSC-Steel composite columns: behavior under monotonic and cyclic axial compression." *Materials and Structures*, doi: 10.1617/s11527-013-0216-0.

Ozbakkaloglu, T., Lim, J. C., and Vincent, T. (2013). "FRP-confined concrete in circular sections: Review and assessment of the stress-strain models." *Engineering Structures*, 49: 1068–1088.

Ozbakkaloglu, T., and Saatcioglu, M. (2007). "Seismic performance of square high-strength concrete columns in FRP stay-in-place formwork." *Journal of Structural Engineering*, 133(1): 44–56.

Ozbakkaloglu, T. and Vincent, T. (2013). "Axial Compressive Behavior of Circular High-Strength Concrete-Filled FRP Tubes." *Journal of Composites for Construction, ASCE*, doi:10.1061/(ASCE)CC.1943–5614.0000410.

Popovics, S. (1973). "A numerical approach to the complete stress-strain curves of concrete." *Cement and Concrete Research,* 3(5): 583–599.

Sakai, J., and Kawashima, K. (2006). "Unloading and reloading stress strain model for confined concrete." *Journal of Structural Engineering*, 132(1), 112–122.

Sakino, K., Nakahara, H., Morino, S., and Nishiyama, I. (2004). "Behavior of centrally loaded concrete-filled steel-tube short columns." *Journal of Structural Engineering*, *ASCE*, 130 (2): 180–188.

Seible, F., Burgueño, R., Abdallah, M. G., and Nuismer, R. (1996). "Development of advanced composite carbon shell systems for concrete columns in seismic zones." *Proc., 11th World Conf. Earthquake Engineering, Pergamon, Elsevier Science, Oxford, Paper No. 1375*.

Teng, J. G., Yu, T., and Wong, Y. L. (2004). "Behaviour of hybrid FRP-concrete-steel double-skin tubular columns." *The 2nd International Conference on FRP Composites in Civil Engineering- CICE 2004*, Adelaide, Australia, 811–818.

Teng, J. G., Yu, T., Wong, Y. L., and Dong, S. L. (2007). "Hybrid FRP concrete steel tubular columns: concept and behavior." *Construction and Building Materials*, 21: 846–854.

Teng, J. G., Yu, T., and Wong, Y. L. (2010). "Hybrid FRP-concrete-steel double-skin tubular structural members." Proceedings, *The Fifth International Conference on FRP Composites in Civil Engineerind (CICE)*, 27-29 September, Beijing, China, 26–32.

Vincent, T., and Ozbakkaloglu, T. (2013a). "Influence of Concrete Strength and Confinement Method on Axial Compressive Behavior of FRP Confined High- and Ultra High-Strength Concrete." *Composites Part B-Engineering*, 50: 413–428.

Vincent, T., and Ozbakkaloglu, T. (2013b). "Influence of fiber orientation and specimen end condition on axial compressive behavior of FRP-confined concrete." *Construction and Building Materials*, 47: 814–826.

Wang, Z. Y., Wang, D. Y., Smith, S. T., and Lu, D. G. (2012). "Experimental testing and analytical modeling of CFRP-confined large circular RC columns subjected to cyclic axial compression." *Engineering Structures*, 40: 64–74.

Wong, Y. L., Yu, T., Teng, J. G., and Dong, S. L. (2008). "Behavior of FRP-confined concrete in annular section columns." *Composites Part B: Engineering*, 38: 451–466.

Wu, Y. F., and Wei, Y. Y. (2010). "Effect of cross-sectional aspect ratio on the strength of CFRP-confined rectangular concrete columns." *Engineering Structures*, 32: 32–45.

Yu, T., Wong, Y. L., and Teng, J. G. (2010). "Behavior of Hybrid FRP-Concrete-Steel Double-Skin Tubular Columns Subjected to Eccentric Compression." *Advances in Structural Engineering*, 13(5) 961–974.

Yu, T., Wong, Y. L., Teng, J. G., Dong, S. L., Lam, S. S. (2006). "Flexural behaviour of hybrid FRP- concrete-steel double skin tubular members." *Journal of Composites for Construction, ASCE*, 10(5): 443–52.

Yu, T., Zhang, B., Cao, YB., and Teng, JG. (2012). "Behavior of hybrid FRP-concrete-steel double-skin tubular columns subjected to cyclic axial compression." *Thin-Walled Structures*, 61: 196–203.

Paper 6 Square FRP-HSC-Steel Composite Columns: Behavior under Axial Compression

Butje Alfonsius Louk Fanggi and Togay Ozbakkaloglu

School of Civil, Environmental, and Mining Engineering, University of Adelaide, 5000

Journal of Engineering Structures (Published)

Statement of Authorship

Title of Paper	Square FRP-HSC-Steel Composite Columns: Behavior under Axial Compression
Publication Status	● Published ○ Accepted for publication ○ Submitted for publication ○ Publication style
Publication Details	Louk Fanggi, B.A., and Ozbakkaloglu, T. (2015). "Square FRP-HSC-steel composite columns: Behavior under Axial Compression." *Engineering Structures*. 92: 156-171.

Author Contributions

By signing the Statement of Authorship, each author certifies that their stated contribution to the publication is accurate and that permission is granted for the publication to be included in the candidate's thesis.

Name of Principal Author (Candidate)	Butje Alfonsius Louk Fanggi		
Contribution to the Paper	Review of literature, analysis data, and preparation of manuscript		
Signature		Date	28/07/2015

Name of Co-Author	Dr. Togay Ozbakkaloglu		
Contribution to the Paper	Research supervision and review of manuscript		
Signature		Date	28/07/2015

SQUARE FRP-HSC-STEEL COMPOSITE COLUMNS: BEHAVIOR UNDER AXIAL COMPRESSION

Butje Alfonsius LOUK FANGGI [1] and Togay OZBAKKALOGLU [2]

ABSTRACT

This paper presents an experimental study, which investigated the compressive behavior of square fiber reinforced polymer (FRP)-concrete composite columns through the tests of 40 column specimens. 24 FRP-concrete-steel double-skin tubular columns (DSTCs), four concrete-filled FRP tubes (CFFTs), and 12 CFFTs with inner voids (H-CFFTs) were tested under axial compression. The majority of the specimens were manufactured using high-strength concrete (HSC). The key parameters examined included the influence of the strength of the concrete, cross-sectional shape (i.e. circular and square) and dimension of the inner steel tube, and presence (or absence) of a concrete filling inside the steel tube. The results of the DSTCs with circular inner steel tubes indicate that concrete-filling inner tubes results in an increase in the ultimate axial stress but a decrease in the ultimate axial strain of concrete compared to those seen in DSTCs with hollow inner steel tubes. It is observed that concrete in hollow DSTCs manufactured with square inner steel tubes develop significantly lower ultimate axial stresses and strains than concrete in companion hollow DSTCs with circular inner steel tubes. It is found, however, that the performance of these specimens improves dramatically when the square inner steel tube is filled with concrete. Comparisons of the results indicate that concrete in filled DSTCs develops larger ultimate axial stresses and strains than concrete in companion CFFTs. Finally, the results demonstrate that H-CFFTs perform

[1] PhD Candidate, School of Civil, Environmental and Mining Engineering University of Adelaide, Australia.

[2] (Corresponding author) Senior Lecturer, School of Civil, Environmental and Mining Engineering, University of Adelaide, SA 5005 Australia. Tel : + 618 8303 6477; Fax : +618 8303 4359; Email: togay.ozbakkaloglu@adelaide.edu.au

significantly worse than DSTCs and CFFTs, and their performance further degrade as the diameter of the inner void increases.

KEYWORDS: Fiber reinforced polymer (FRP); Concrete; High-strength concrete (HSC); Columns; Confinement; FRP tubes; Steel tubes; Square DSTCs.

1. INTRODUCTION

As was demonstrated in a recent review by Ozbakkaloglu et al. [1], the use of fiber reinforced polymer (FRP) composites as a confinement material has received a great deal of attention over the last two decades. The success attained in using FRP as a concrete confinement material has provided increased impetus for research into two main research directions: (i) the use of FRP composites in retrofitting existing concrete columns (e.g., [2-16]) and ii) the construction of new high-performance composite columns in the form of concrete-filled FRP tubes (CFFTs) (e.g., [17-28]).

Following from the research on CFFTs, FRP-concrete-steel double-skin tubular columns (DSTCs), a new type of composite system that was originally proposed by Teng et al. [29], has received significant recent research attention. This composite column system relies on the same FRP tube confinement mechanism that is present in CFFTs, and through the combination of the advantages of the three constituent materials it can be designed to exhibit extremely high structural performance levels. A large number of experimental studies have recently been undertaken on DSTCs by groups led by Teng in Hong Kong [30-35] and the second author in Australia [36-42]. These studies have clearly shown some of the performance advantages of DSTCs under different loading conditions. However, apart from eight test results reported on the compressive behavior of square DSTCs in Ref. [35], all of the previous studies have been concerned with circular DSTCs.

The superior structural engineering properties of high-strength concrete (HSC) over normal-strength concrete (NSC) makes it an attractive alternative for use in the in the construction of new composite columns such as CFFTs and DSTCs. As demonstrated in Refs. [22, 26], new high-performance structural members can be developed through the combination of these high-strength materials (i.e., HSC, steel and FRP). Although a number of recent studies have investigated the compressive behavior of circular HSC DSTCs [36-38], to date no study has been reported on the behavior of square HSC DSTCs under axial compression. In addition, the only existing study on square DSTCs [35] focused on DSTCs with hollow circular inner steel tubes, and to date no study has investigated square DSTCs with concrete-filled inner steel tubes or DSTCs with square inner and outer tubes.

As the first study in literature that reports on the axial compressive behavior of square FRP-HSC-steel DSTCs, this paper presents the results of an experimental program that was aimed at addressing the outlined research gaps through the investigation of the influences of: i) concrete strength, ii) cross-sectional shape of inner steel tube, and iii) concrete-filling inner steel tube. In addition, the behaviors of companion solid and hollow square concrete-filled FRP tubes (CFFTs and H-CFFTs) were also experimentally investigated to establish the relative performances of DSTCs to CFFTs and H-CFFTs. The results of the experimental program are first presented and followed by a discussion on the influence of the investigated parameters on the compressive behavior of square FRP-HSC-steel composite columns.

2. EXPERIMENTAL PROGRAM

2.1. Test Specimens

A total of forty specimens were designed, manufactured, and tested under axial compression. Twenty-four of the specimens were DSTCs with hollow or concrete-filled inner steel tubes, four were CFFTs and the remaining twelve were H-CFFTs. The majority of the specimens were constructed using HSC, but a small group NSC specimens were also manufactured to investigate the influence of concrete strength on the compressive behavior of the composite columns. Three and eight layers of aramid fiber sheets were used to confine the NSC and HSC specimens, respectively. All specimens had a 305 mm height and a 152 mm square cross-section (measured inside the FRP tube) with a corner radius of 30 mm. The test parameters included the presence (or absence) of concrete-filling inside the steel tubes, concrete strength, the cross-sectional shape (i.e. square or circular) and dimension of the inner steel tube. Furthermore, two pairs of CFFTs and six pairs of H-CFFTs were designed as companions to DSTCs to establish the relative performance levels of DSTCs compared to CFFTs and H-CFFTs. Two nominally identical specimens were tested for each unique specimen configuration. Details of the specimens are shown in Table 1 and Fig. 1.

2.1. Materials

The specimens were prepared using HSC and NSC mixes, which consisted of crushed bluestone as the coarse aggregate with a nominal maximum size of 10 mm. Silica fume was added to the HSC mix at 8% of the binder content by weight. The average unconfined concrete strengths (f'_c) attained during the period of testing are shown in Table 1, together with the corresponding axial strains (ε_{co}) that were calculated using the expression given by Popovics [43].

Axial compression tests were conducted on hollow steel tubes to establish the material properties of the steel tubes used in the DSTCs. The heights of the hollow steel tubes were established based on their diameters. For tubes with diameters greater than 100 mm, three hollow tubes having the same height as those used in the DSTCs were tested, whereas for tubes with diameters less than 100 mm, three hollow tubes with a height-to-diameter ratio of 3:1 were tested. The results of these tests are shown in Table 2.

2.3. Specimen Preparation

Preparation of the specimens started with the manufacture of FRP tubes. The tubes were formed using a manual wet lay-up process by wrapping epoxy resin impregnated aramid fiber sheets around precision-cut, high-density Styrofoam templates. The FRP sheets were provided with a 150 mm overlap to prevent premature debonding. The FRP tubes with three layers of FRP were wrapped with a single FRP sheet continuously, whereas the tubes with eight layers of FRP were wrapped using two FRP sheets (each with a length to provide four layers of confinement). The two overlapping joins of the 8-layer tubes were positioned in the same region. The properties of the unidirectional aramid fiber sheets used in the manufacture of the FRP tubes are shown in Table 3. Both the manufacturer-supplied properties and the ones obtained from the flat coupon tests, which were performed in accordance with ASTM standard D3039M-08 (ASTM 2008) are given in the table.

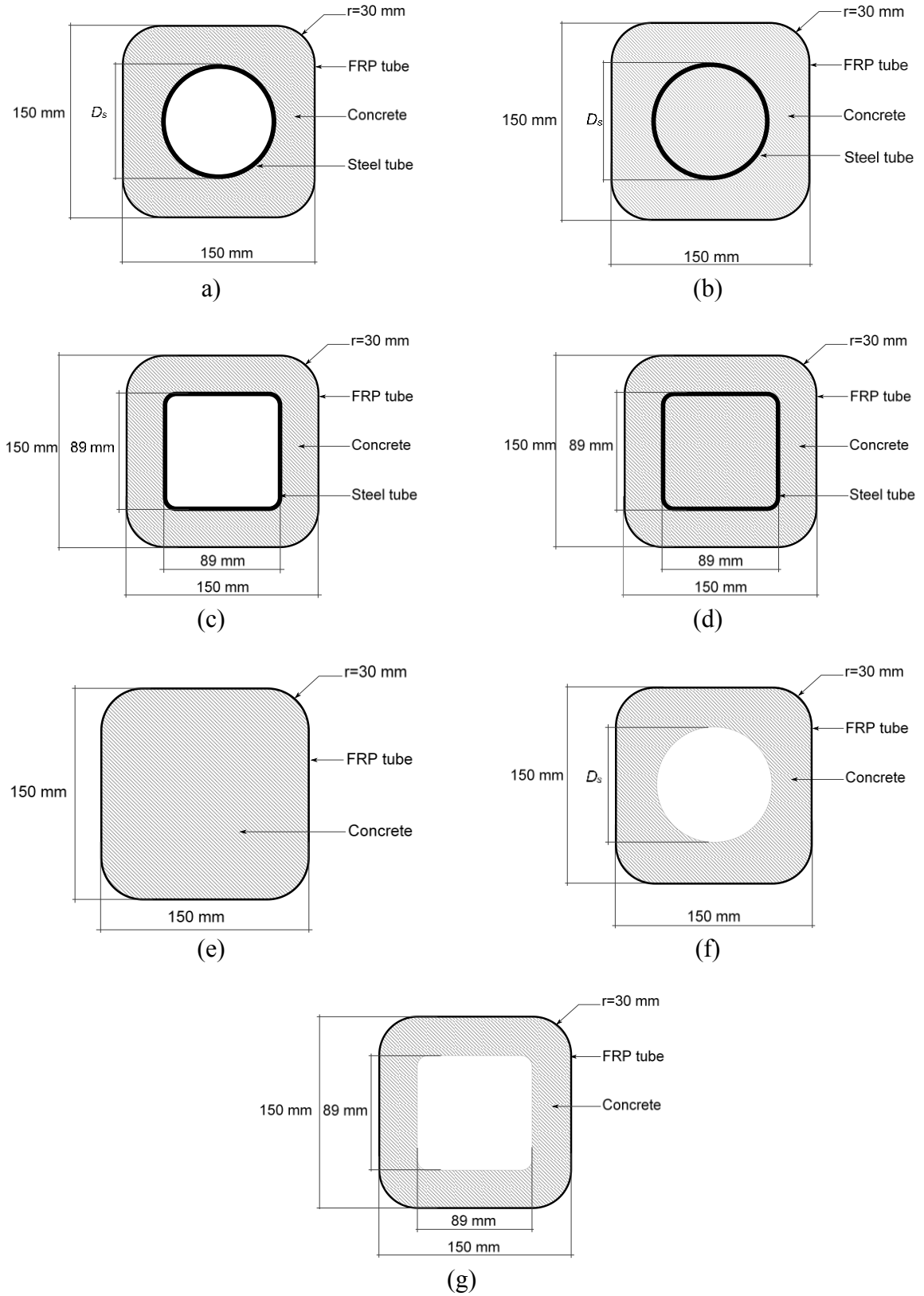

Figure 1. Cross-section of specimens: (a) Hollow HSC DSTC-1&2 (D_s=60.3 mm), Hollow HSC DSTC-4&5 (D_s=88.9 mm), Hollow HSC DSTC-9&10 (D_s=114.3 mm), Hollow NSC DSTC-13&14 (D_s=88.9 mm), (b) Filled HSC DSTC-3&4 (D_s=60.3 mm), Filled HSC DSTC-7&8 (D_s=88.9 mm), Filled HSC DSTC-11&12 (D_s=114.3 mm), Filled NSC DSTC-15&16 (D_s=88.9 mm), (c) Hollow HSC DSTC-17&18 (square inner tube), Hollow NSC DSTC-21&22 (square inner tube), (d) Filled HSC DSTC-19&20 (square inner tube), Filled NSC DSTC-23&24 (square inner tube), (e) HSC CFFT-1&2, NSC CFFT-3&4, (f) HSC H-CFFT-1&2 (D_s=60.3 mm), HSC H-CFFT-3&4 (D_s=88.9 mm), NSC H-CFFT-7&8 (D_s=88.9 mm), (g) HSC H-CFFT-9&10 (square inner void), NSC H-CFFT-11&12 (square inner void)

Table 1. Details of test specimens

Specimens	Number of FRP layers	Strength of concrete, f'_c (MPa)	Strain at peak stress, ε_{co} (%)	Inner section	External diameter of inner steel tube or void section, D_s (mm)	Steel tube thickness, t_s (mm)	Specimen type
DSTC-1&2	8	98.2	0.31	Circle	60.3	3.6	Hollow DSTC
DSTC-3&4	8	98.2	0.31	Circle	60.3	3.6	Filled DSTC
DSTC-5&6	8	98.2	0.31	Circle	88.9	3.2	Hollow DSTC
DSTC-7&8	8	98.2	0.31	Circle	89.9	3.2	Filled DSTC
DSTC-9&10	8	98.2	0.31	Circle	114.3	6.02	Hollow DSTC
DSTC-11&12	8	98.2	0.31	Circle	114.3	6.02	Filled DSTC
DSTC-13&14	3	47.0	0.23	Circle	88.9	3.2	Hollow DSTC
DSTC-15&16	3	47.0	0.23	Circle	88.9	3.2	Filled DSTC
DSTC-17&18	8	98.2	0.31	Square	89	3.5	Hollow DSTC
DSTC-19&20	8	98.2	0.31	Square	89	3.5	Filled DSTC
DSTC-21&22	3	47.0	0.23	Square	89	3.5	Hollow DSTC
DSTC-23&24	3	47.0	0.23	Square	89	3.5	Filled DSTC
CFFT-1&2	8	98.2	0.31	-	-	-	CFFT
CFFT-3&4	3	47.0	0.23	-	-	-	CFFT
H-CFFT-1&2	8	98.2	0.31	Circle	60.3	-	Hollow CFFT
H-CFFT-3&4	8	98.2	0.31	Circle	88.9	-	Hollow CFFT
H-CFFT-5&6	8	98.2	0.31	Circle	114.3	-	Hollow CFFT
H-CFFT-7&8	3	47.0	0.23	Circle	88.9	-	Hollow CFFT
H-CFFT-9&10	8	98.2	0.31	Square	89	-	Hollow CFFT
H-CFFT-11&12	3	47.0	0.23	Square	89	-	Hollow CFFT

Table 2. Measured properties of steel tubes

D_s (mm)	t_s (mm)	Section figure	Height	Peak axial load (kN)	Yield stress (Mpa)	Peak stress	Axial strain at peak (%)	Failure mode*
60.3	3.6	Circle	181	246	319	384	3.34	EF
88.9	3.2	Circle	267	348	320	404	2.43	EF
114.3	6.02	Circle	305	1073	449	524	3.10	EF
89	3.5	Square	305	540	462	492	0.80	L

EF= Elephant foot buckling, L= Local Buckling

To support the tubes and ensure that they remained concentric during the process of concrete pouring, a formwork was developed and used as illustrated in Fig. 2. At the base, wooden spacers were used to hold the bottom of the FRP tube in place and nails were used to maintain the position of the steel tube relative to the FRP tube. At the top, a cap with two steel arms was used to maintain the position of the interior and exterior tubes concentrically. Alignment was maintained by anchoring the top cap to the wooden base.

Table 3. Properties of fiber and FRP composites

Type	Nominal thickness, t_f (mm/ply)	Provided by manufacturer			Obtained from flat FRP coupon tests*		
		Tensile strength, f_f (MPa)	Ultimate tensile strain, ε_f (%)	Elastic modulus, E_f (GPa)	Tensile strength, f_{frp} (MPa)	Ultimate tensile strain, ε_{frp} (%)	Elastic modulus, E_{frp} (GPa)
AFRP	0.2	2600	2.2	118.2	2390	1.86	128.5

Figure 2. Formwork used in fabrication of DSTCs

2.4 Instrumentation and testing

Axial deformations of the specimens were recorded with four linear variable displacement transformers (LVDTs), which were mounted at the corners between the loading and supporting steel plates of the compression test machine, as shown in Fig. 3. In addition, four inner cage LVDTs were also placed in mid-height regions of the specimens to measure deformations along a gauge length of 175 mm. The specimens were also instrumented at their mid-heights with six unidirectional strain gauges with a gauge length of 10 mm to measure FRP tube lateral strains. Four of these gauges were installed at the mid-span of each face of the specimen and the remaining two gauges were installed on opposite corners of the specimens. The axial and lateral strains of the inner steel tubes were measured at mid-height by two axially and two laterally oriented strain gauges with 5 mm gauge lengths.

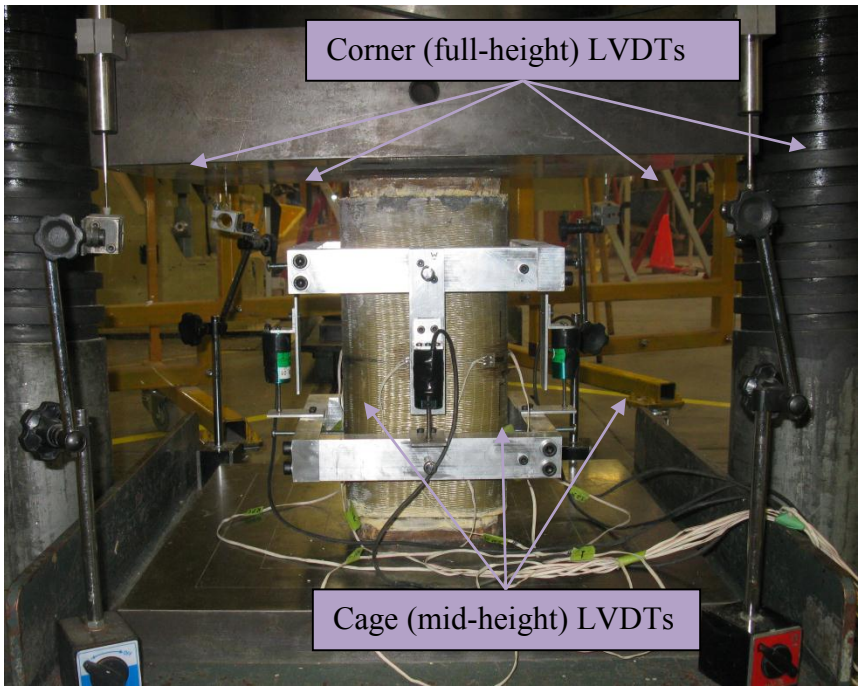

Figure 3. Test setup and instrumentation

The specimens were tested under axial compression using a 5000-kN capacity universal testing machine. During the initial elastic stage, the loading was applied with load control at 3 kN per second, whereas displacement control was approximately 0.003 mm per second beyond the initial softening until specimen failure. Prior to testing, a capping process was completed at both ends of all specimens to ensure uniform distribution of the applied pressure, and the load was applied only to the concrete core or, in the case of DSTCs, concrete and inner steel tube, through precision-cut high-strength steel loading discs placed at each end of the specimens. A data acquisition system was used to record the strains, loads and displacements of the test specimens simultaneously.

3. TEST RESULTS AND DISCUSSION

3.1. Failure modes

All of the specimens failed due to the rupture of the FRP tubes near one of the specimen corners, which was more extensive in concrete-filled DSTCs than the companion hollow DSTCs, as illustrated in Fig. 4. It was also observed that hollow DSTCs with

smaller inner steel tubes experienced more severe FRP tube rupture than the companion specimen with larger inner steel tube diameters, as can be seen from comparison of Figs. 4a and 4c. Furthermore, more severe rupture was experienced by both hollow and filled DSTCs composed of HSC than the companion NSC DSTCs, as illustrated in Figs. 4c to 4f. This was also the case for CFFT specimens, as can be seen in Figs. 4g and 4h. In general, CFFTs were observed to experience more severe FRP tube rupture than that experienced by both hollow and concrete-filled DSTCs (Figs. 4a to 4h). It was also observed that H-CFFTs with larger circular or square voids exhibited localized FRP tube ruptures (Figs. 4i and 4j) without the explosive failure that was observed in their solid counterparts. At the end of testing, it was found that concrete at the inner surface of all H-CFFT specimens had experienced significant damage by the time of failure.

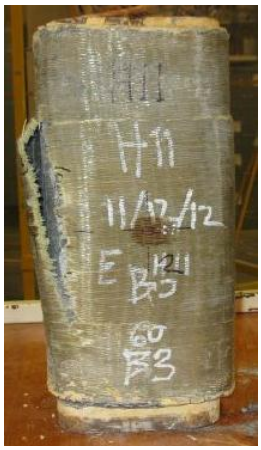

(a)

(b)


(c)

(d)


(e)

(f)

(g)


(h)

(i) (j)

Figure 4. Failure mode of specimens: (a) Hollow HSC DSTC with D_s=60.3 mm (DSTC-1), (b) Filled HSC DSTC with D_s=60.3 mm (DSTC-3), (c) Hollow HSC DSTC with D_s=88.9 mm (DSTC-6), (d) Filled HSC DSTC with D_s=88.9 mm (DSTC-8), (e) Hollow NSC DSTC with D_s=88.9 mm (DSTC-14), (f) Filled NSC DSTC with D_s=88.9 mm (DSTC-16), (g) HSC CFFT (CFFT-1), (h) NSC CFFT (CFFT-3), (i) HSC H-CFFT with circular inner void (H-CFFT-3), (j) HSC H-CFFT with square inner void (H-CFFT-9)

3.2. Axial load capacities

The recorded axial load capacities of the DSTCs (P_T) as recorded during testing are presented in Table 4, together with the axial capacities of the steel tubes (P_s) and unconfined concrete (P_{co}). The axial load capacities of the steel tubes (P_s) were determined from hollow steel tube tests, whereas the axial load capacities of unconfined concrete (P_{co}) were obtained by multiplying unconfined concrete strength by the area of the concrete cross-section. As evident from the $P_T/(P_s+P_{co})$ ratios shown in Table 4, apart from H-CFFTs with larger circular and square inner voids, all specimens developed higher axial load capacities than the combined axial load capacities of the unconfined concrete and steel tube.

3.3. Interaction between steel and FRP tubes

As illustrated in Fig. 5, the location of FRP tube rupture often corresponded to the regions of significant deformations on the inner steel tube. As can be seen from the Figs. 5a and 5c inside DSTCs, larger circular inner steel tubes experienced more severe

plastic deformations than their smaller counterparts. The most significant inner steel tube deformations were observed in DSTCs with square inner steel tubes due to tendency of the square inner steel tube to experience inward buckling, as shown in Fig. 5d.

3.4.Behavior of confined concrete in composite columns

3.4.1 FRP tube rupture strain

The recorded hoop rupture strains ($\varepsilon_{h,rup}$) of all specimens are given in Table 5. Unlike in circular section, concrete in square sections is not subjected to nearly uniform confining pressure, and the pressure provided by the FRP tube varies around the perimeter of the cross-section. To provide some insight into the distribution of the hoop rupture strains around the perimeter of the square specimens at ultimate, the hoop rupture strains along the spans $(\varepsilon_{h,rup})_{span}$ and corners $(\varepsilon_{h,rup})_{corner}$ also reported in Table 5. A closer inspection of the $\varepsilon_{h,rup}$ values reported in the table allows a number of observations to be made on the influence of the important parameters on the hoop rupture strains. These observations are summarized in this section. The effect of filling the inner steel tube with concrete on $\varepsilon_{h,rup}$ can be investigated by comparing the companion hollow and concrete-filled DSTCs. It can be seen from Table 5 that filled DSTCs experienced larger $\varepsilon_{h,rup}$ than hollow DSTCs, regardless of the strength of concrete or the shape of the inner tube. Table 5 also illustrates the influence of concrete strength on $\varepsilon_{h,rup}$. As can be seen from the table for both hollow and filled DSTCs, as well as CFFTs, NSC specimens had higher $\varepsilon_{h,rup}$ than their HSC counterparts. This observation suggests that the hoop rupture strains decrease with an increase in concrete strength, which accords with observations previously reported in Ozbakkaloglu and

Akin [13] and Lim and Ozbakkaloglu [44] for circular CFFTs and Louk Fanggi and Ozbakkaloglu [37] for circular DSTCs.

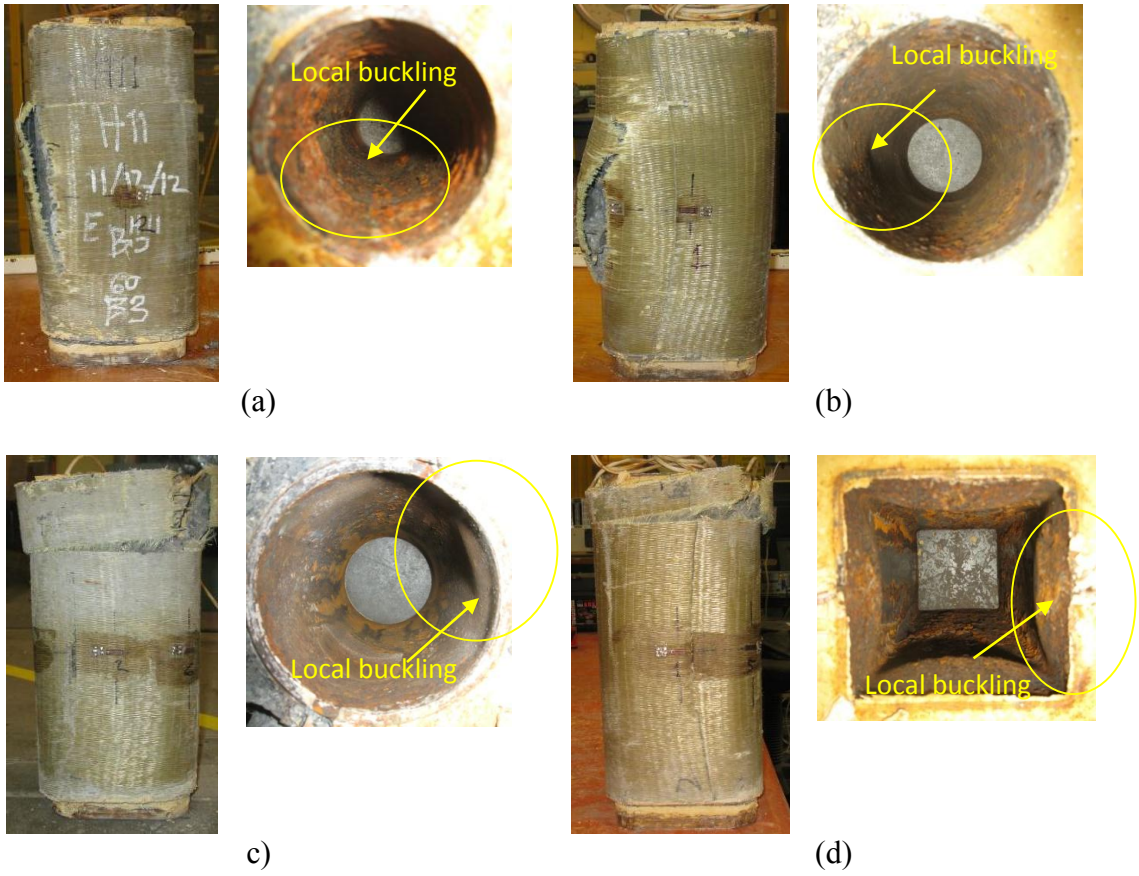

Figure.5. Interaction between damage regions of FRP and steel tubes: (a) DSTC-1, (b) DSTC-5, (c) DSTC-10, (d) DSTC-18

Table 4. Axial load capacities of DSTCs

Specimen	Specimen peak load, P_T (kN)	Average P_T (kN)	Peak load of steel tube, P_s (kN)	Ultimate load of unconfined concrete section, P_{co} (kN)	P_s+P_{co} (kN)	$P_T/(P_s+P_{co})$
DSTC-1	2516	2512	246	1856	2102	1.19
DSTC-2	2507					
DSTC-3	3080	3088	246	2071	2317	1.33
DSTC-4	3096					
DSTC-5	2174	2229	348	1523	1871	1.19
DSTC-6	2284					
DSTC-7	3134	3091	348	2049	2397	1.29
DSTC-8	3048					
DSTC-9	2490	2497	1073	1131	2204	1.13
DSTC-10	2505					
DSTC-11	3968	3909	1073	1934	3007	1.30
DSTC-12	3851					
DSTC-13	1422	1381	348	729	1077	1.28
DSTC-14	1340					
DSTC-15	2013	2002	348	981	1329	1.51
DSTC-16	1990					
DSTC-17	1936	1923	540	1356	1896	1.01
DSTC-18	1910					
DSTC-19	3201	3236	540	2016	2556	1.27
DSTC-20	3270					
DSTC-21	1279	1261	540	649	1189	1.06
DSTC-22	1242					
DSTC-23	2084	2128	540	965	1505	1.41
DSTC-24	2173					
CFFT-1	2722	2678	-	2134	2134	1.26
CFFT-2	2634					
CFFT-3	1664	1652	-	1021	1021	1.62
CFFT-4	1640					
H-CFFT-1	2244	2237	-	1856	1856	1.21
H-CFFT-2	2230					
H-CFFT-3	1234	1488	-	1523	1523	0.98
H-CFFT-4	1742					
H-CFFT-5	1097	1096	-	1131	1131	0.97
H-CFFT-6	1095					
H-CFFT-7	885	870	-	729	729	1.19
H-CFFT-8	854					
H-CFFT-9	1343	1240	-	1356	1356	0.91
H-CFFT-10	1138					
H-CFFT-11	728	728	-	729	729	1.00
H-CFFT-12*	304					

*Premature failure. The specimen was excluded from calculations of P_T average

Table 5. Ultimate condition of concrete in composite columns

Specimen	f'_{lu}/f'_c	f'_{cu} (MPa)	Avg. f'_{cu} (MPa)	f'_{cu}/f'_c	*Avg.* f'_{cu}/f'_c	ε_{cu} (%)	Avg. ε_{cu} (%)	$\varepsilon_{cu}/\varepsilon_{co}$	Avg. $\varepsilon_{cu}/\varepsilon_{co}$	$\varepsilon_{hup,rup}$ (%)	*Avg.* $\varepsilon_{hup,rup}$ (%)	$(\varepsilon_{hup,rup})_{span}$ (%)	*Avg.* $(\varepsilon_{hup,rup})_{span}$ (%)	$(\varepsilon_{hup,rup})_{corner}$ (%)	*Avg.* $(\varepsilon_{hup,rup})_{corner}$ (%)
DSTC-1	0.42	121.4	121.2	1.24	1.23	1.91	1.81	6.07	5.75	0.89	0.96	0.94	1.00	0.63	0.81
DSTC-2	0.42	121.0		1.23		1.71		5.43		1.03		1.06		0.98	
DSTC-3	0.42	135.1	135.6	1.38	1.38	2.50	2.34	7.94	7.42	0.96	1.02	1.10	1.14	0.69	0.76
DSTC-4	0.42	136.1		1.39		2.17		6.89		1.07		1.17		0.82	
DSTC-5	0.42	112.7	118.7	1.15	1.21	1.92	2.26	6.10	7.16	0.67	0.74	0.60	0.82	0.82	0.60
DSTC-6	0.42	124.8		1.27		2.59		8.22		0.81		1.04		0.37	
DSTC-7	0.42	134.1	131.9	1.37	1.34	1.90	2.01	6.01	6.35	0.80	0.76	1.05	0.95	0.48	0.47
DSTC-8	0.42	129.6		1.32		2.11		6.70		0.72		0.85		0.46	
DSTC-9	0.42	122.9	123.5	1.25	1.26	3.26	3.41	10.35	10.81	0.47	0.56	0.66	0.75	0.20	0.25
DSTC-10	0.42	124.2		1.26		3.55		11.27		0.65		0.83		0.30	
DSTC-11	0.42	148.0	144.5	1.51	1.47	2.39	2.52	7.73	8.15	0.88	0.85	0.94	1.01	0.62	0.49
DSTC-12	0.42	141.1		1.44		2.65		8.57		0.83		1.07		0.35	
DSTC-13	0.33	69.3	66.6	1.47	1.42	4.11	3.87	17.63	16.60	0.13	0.78	0.16	0.91	0.07	0.53
DSTC-14	0.33	64.0		1.36		3.63		15.56		0.14		0.17		0.09	
DSTC-15	0.33	79.8	79.3	1.70	1.69	3.70	3.61	15.87	15.49	0.88	1.07	0.84	1.15	0.97	0.93
DSTC-16	0.33	78.7		1.67		3.52		15.09		0.74		0.94		0.33	
DSTC-17	0.42	101.1	94.9	1.03	0.97	1.55	1.56	4.92	4.94	0.68	0.13	0.77	0.17	0.51	0.08
DSTC-18	0.42	88.7		0.90		1.56		4.95		0.88		1.05		0.55	
DSTC-19	0.42	129.6	131.3	1.32	1.34	1.89	2.12	6.00	6.72	1.04	0.81	1.12	0.89	0.89	0.65
DSTC-20	0.42	133.0		1.35		2.34		7.43		1.10		1.17		0.97	
DSTC-21	0.33	43.2	42.0	0.92	0.89	2.52	2.52	10.80	10.78	0.39	0.36	0.41	0.39	0.35	0.30
DSTC-22	0.33	40.7		0.87		2.51		10.76		0.34		0.36		0.24	
DSTC-23	0.33	75.2	77.4	1.60	1.65	3.35	3.50	14.36	15.01	1.07	1.06	1.24	1.19	0.72	0.80
DSTC-24	0.33	79.6		1.69		3.65		15.65		1.05		1.13		0.88	

CFFT-1	0.42	125.3	123.3	1.28	1.26	1.71	1.74	5.43	5.53	1.07	1.04	1.18	1.18	0.69	0.67
CFFT-2	0.42	121.2		1.23		1.77		5.62		1.01		1.18		0.64	
CFFT-3	0.33	76.6	76.0	1.63	1.62	3.11	3.26	13.33	13.99	1.49	1.39	1.76	1.76	0.94	0.76
CFFT-4	0.33	75.5		1.61		3.41		14.63		1.29		1.76		0.58	
H-CFFT-1	0.42	109.1	113.0	1.11	1.15	1.71	2.19	5.43	6.94	0.79	0.86	0.88	0.88	0.61	0.83
H-CFFT-2	0.42	116.9		1.19		2.66		8.45		0.93		0.88		1.05	
H-CFFT-3	0.42	79.6	80.5	0.81	0.82	3.47	2.63	11.02	8.34	0.44	0.47	0.57	0.59	0.17	0.17
H-CFFT-4	0.42	81.3		0.83		1.78		5.65		0.51		0.60		0.17	
H-CFFT-5	0.42	70.3	65.8	0.72	0.67	1.00	1.03	3.18	3.26	0.04	0.03	0.05	0.04	0.03	0.03
H-CFFT-6	0.42	61.2		0.62		1.05		3.33		0.03		0.03		0.03	
H-CFFT-7	0.33	48.2	47.2	1.03	1.00	3.22	3.22	13.81	13.78	0.40	0.36	0.47	0.43	0.26	0.25
H-CFFT-8	0.33	46.2		0.98		3.21		13.76		0.33		0.38		0.24	
H-CFFT-9	0.42	57.5	58.6	0.59	0.60	1.54	1.49	4.89	4.73	0.03	0.12	0.03	0.03	0.03	0.03
H-CFFT-10	0.42	59.7		0.61		1.44		4.57		0.21		0.03		0.02	
H-CFFT-11	0.33	28.8	28.8	0.61	0.61	2.63	2.63	11.28	11.28	0.05	0.05	0.06	0.06	0.04	0.04
H-CFFT-12*	0.33	-		-		-		-		-		-		-	

*Premature failure. The specimen was excluded from calculations of averages

Table 5 further illustrates that hollow DSTCs with square inner tubes recorded much lower $\varepsilon_{h,rup}$ than did the companion DSTCs with circular inner tubes. On the other hand, as evident from Table 5, when the DSTC was filled with concrete, the cross-sectional shape of the inner steel tube had no major influence on $\varepsilon_{h,rup}$. In addition, an increase in inner steel tube diameter (D_s) resulted in a decrease in $\varepsilon_{h,rup}$ for hollow DSTCs. However, when the DSTC specimens were filled with concrete, D_s had no major effect on $\varepsilon_{h,rup}$. As evident from Table 5, a similar decrease in hoop rupture strain with an increase in diameter inner void was also observed for H-CFFT specimens. Indeed, as can be seen from Table 5, H-CFFTs with the larger circular and square inner voids experienced very low hoop rupture strains ($\varepsilon_{h,rup}$). Similar observations were previously reported by Wong et al. [32] for NSC H-CFFTs with larger inner voids and this phenomenon can be attributed to the failure type of these specimens, which is controlled by local damage and the spalling of the concrete core near the inner edge instead of the rupture of the FRP tube [32].

A closer examination of the $(\varepsilon_{h,rup})_{span}$ and $(\varepsilon_{h,rup})_{corner}$ values reported in Table 5 also reveals that hoop rupture strains recorded by strain gauges that were placed on spans were consistently larger than those obtained from corner strain gauges. This observation is in agreement with that previously reported for square and rectangular CFFTs [25].

3.4.2. Axial stress-strain behavior

The axial stress of concrete inside the DSTCs was calculated by dividing the axial load resisted by the concrete (P_c) with the net cross-sectional area of the concrete section. The load applied to the concrete was determined by subtracting the axial load resisted by the steel tube (P_s) for a given axial strain from the total load resisted by the DSTC (P_T) at the same axial strain. The axial strains were obtained from the full-height

LVDTs. The load acting on the steel tube was calculated by assuming that the load-strain behavior of the steel tube inside a DSTC was the same as the load-strain behavior of the corresponding unconfined steel tube obtained from a hollow tube compression test. The ultimate axial stress (f'_{cu}) and strain (ε_{cu}) of the concrete inside the DSTCs reported in Table 5 were calculated using the approach summarized in this section.

Figures 6 to 8 illustrate the concrete stress-strain relationships for the specimens of the present study. It is evident from the stress-strain relationship of the DSTC and CFFT specimens, which exhibit no major strength decay and high ultimate axial strain, that concrete inside the DSTCs and CFFTs was effectively confined. H-CFFT specimens, on the other hand, exhibited major strength decay and low ultimate axial strain with increases in steel tube diameter. Furthermore, Figs. 6 to 8 indicate that the performance of the specimens with square inner steel tubes did not perform as good as the companion DSTCs with circular inner tubes. The inferior performance of these specimens is caused by inward buckling of inner steel tubes, which resulted in a lower lateral resistance to concrete and confinement efficiency, as previously discussed in Louk Fanggi and Ozbakkaloglu [37].

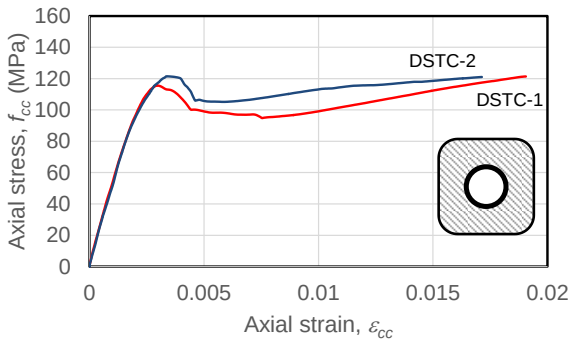

(a)

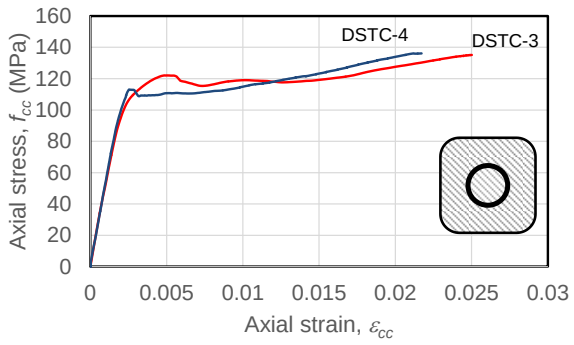

(b)

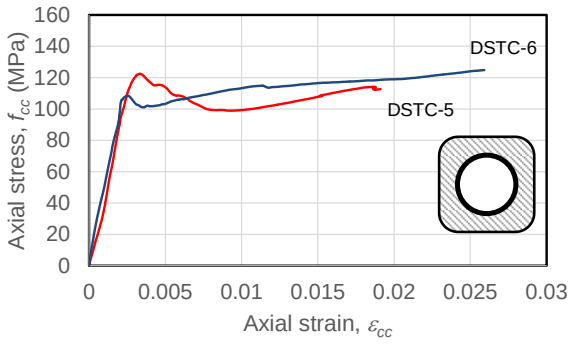
DSTC-6
DSTC-5
Axial stress, f_{cc} (MPa)
Axial strain, ε_{cc}

(c)

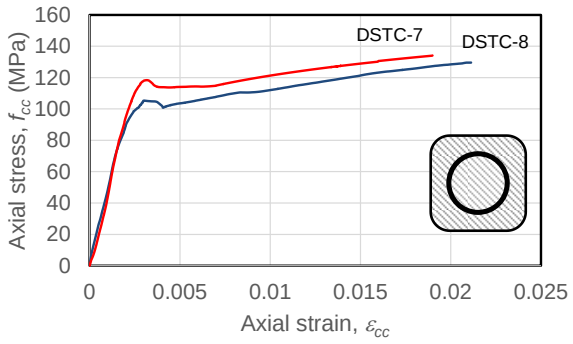
DSTC-7
DSTC-8
Axial stress, f_{cc} (MPa)
Axial strain, ε_{cc}

(d)

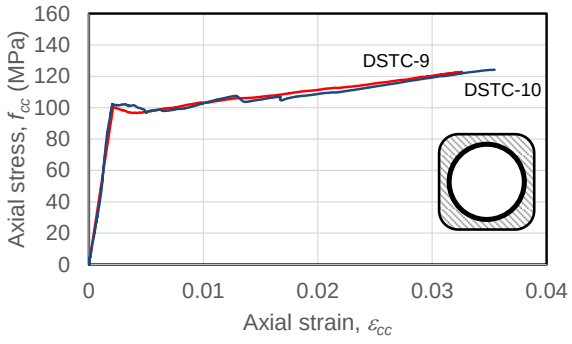
DSTC-9
DSTC-10
Axial stress, f_{cc} (MPa)
Axial strain, ε_{cc}

(e)

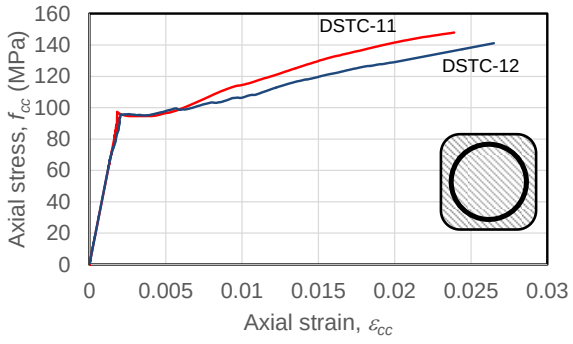
DSTC-11
DSTC-12
Axial stress, f_{cc} (MPa)
Axial strain, ε_{cc}

(f)

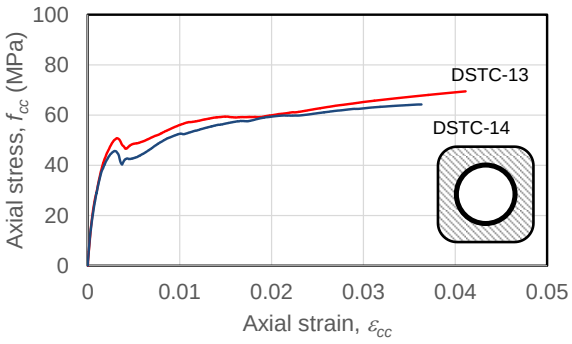
DSTC-13
DSTC-14
Axial stress, f_{cc} (MPa)
Axial strain, ε_{cc}

(g)

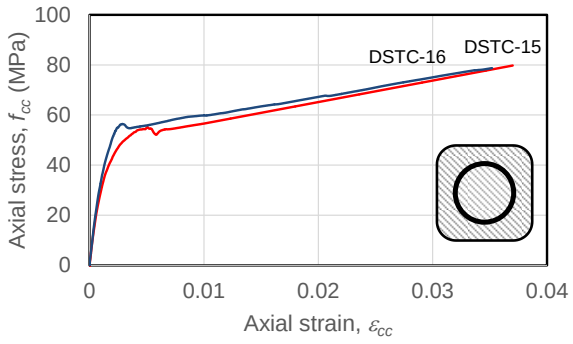
DSTC-16
DSTC-15
Axial stress, f_{cc} (MPa)
Axial strain, ε_{cc}

(h)

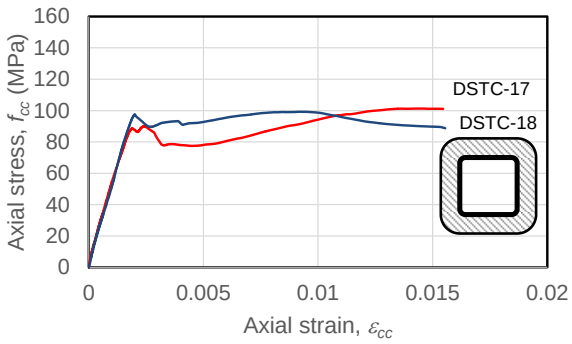
DSTC-17
DSTC-18
Axial stress, f_{cc} (MPa)
Axial strain, ε_{cc}

(i)

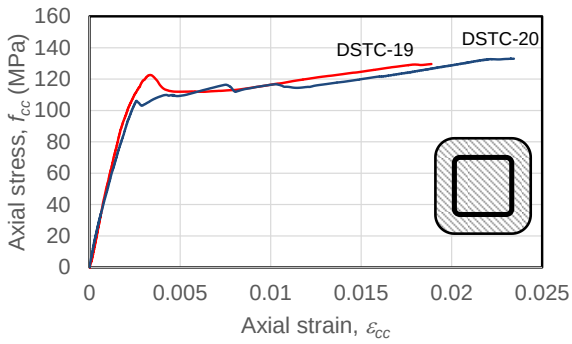
DSTC-19
DSTC-20
Axial stress, f_{cc} (MPa)
Axial strain, ε_{cc}

(j)

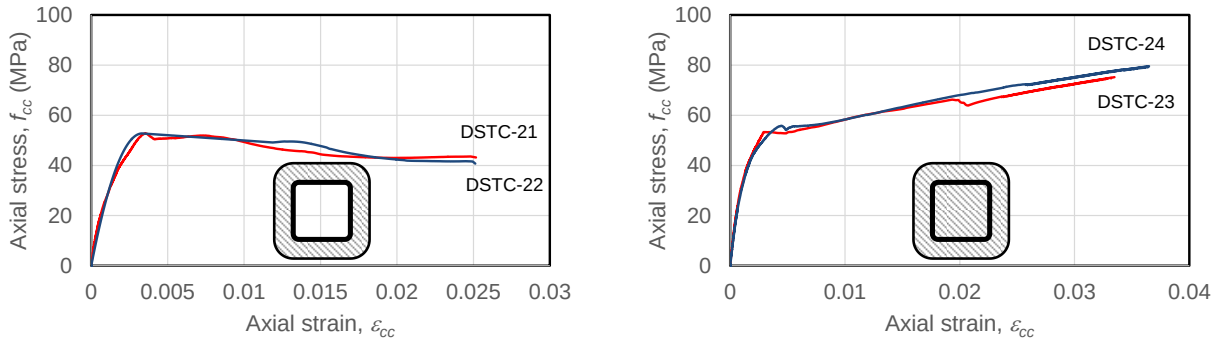

(k) (l)

Figure 6. Axial stress-strain behavior of concrete in DSTCs: (a) DSTC-1&2, (b) DSTC-3&4, (c) DSTC-5&6, (d) DSTC-7&8, (e) DSTC-9&10, (f) DSTC-11&12, (g) DSTC-13&14, (h) DSTC-15&16, (i) DSTC-17&18, (j) DSTC-19&20, (k) DSTC-21&22, (l) DSTC-23&24

As expected, the stress-strain behavior of the DSTC specimens along the second branch of the curve was influenced by the important parameters, including the presence (or absence) of a concrete-filling inside inner steel tube, concrete strength, and the shape and diameter of the inner steel tube. The influence of these parameters on the stress-strain behavior of DSTCs is discussed in the following sections, and followed by a discussion on the relative performance of DSTCs with respect to that of CFFTs and H-CFFTs.

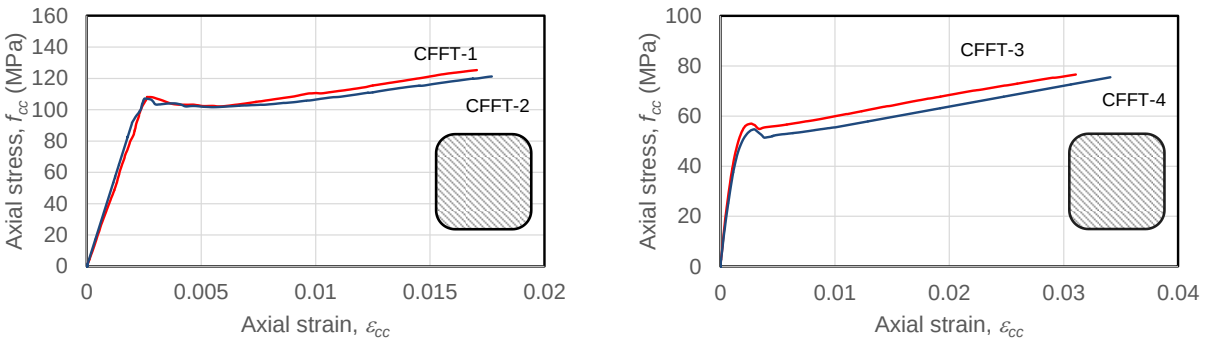

(a) (b)

Figure 7. Axial stress-strain behavior of concrete in CFFTs: (a) CFFT-1&2, (b) CFFT-3&4

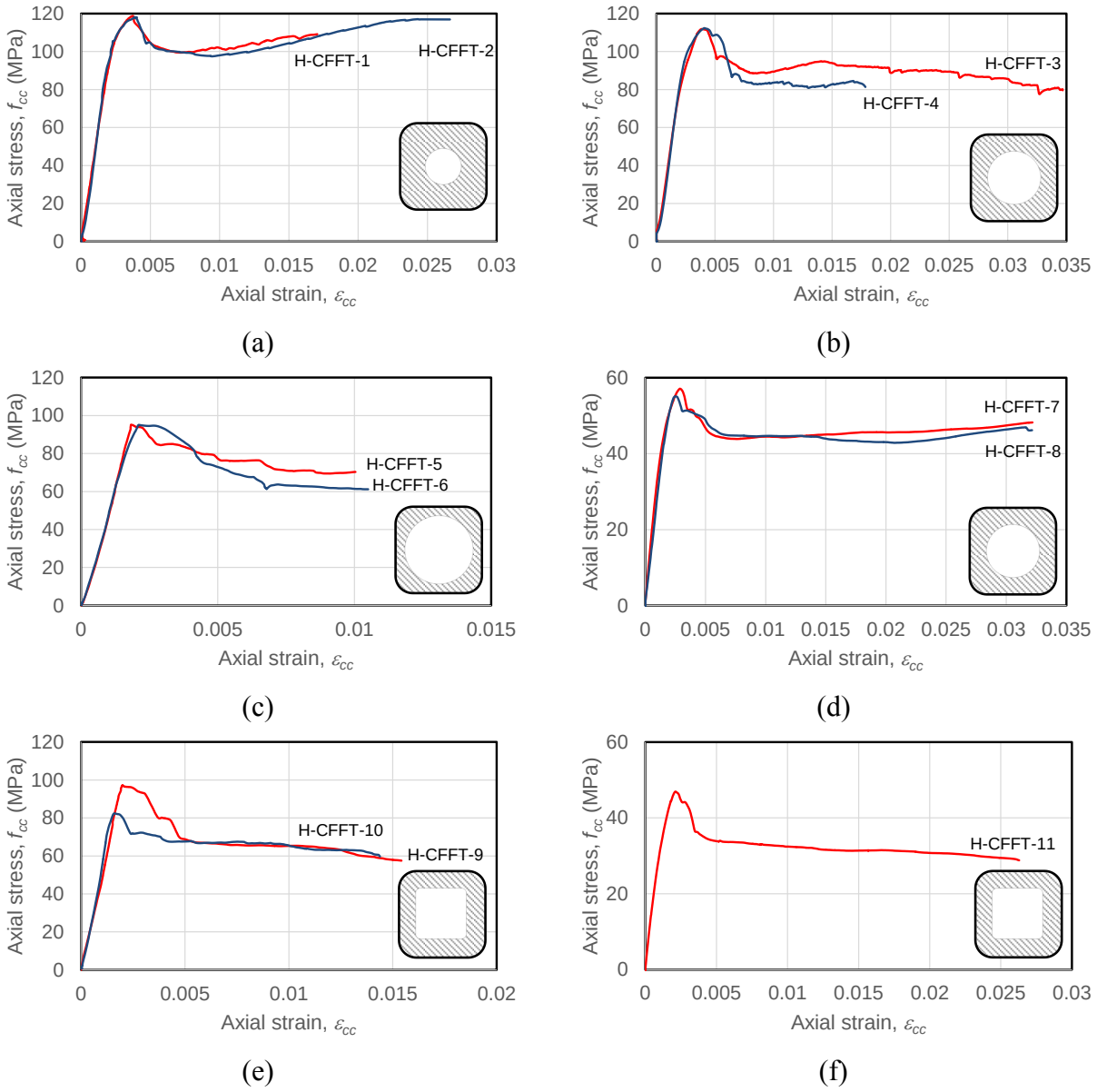

Figure 8. Axial stress-strain behavior of concrete in H-CFFTs: (a) H-CFFT-1&2, (b) H-CFFT-3&4, (c) H-CFFT-5&6, (d) H-CFFT-7&8, (e) H-CFFT-9&10, (f) H-CFFT-11

3.4.3. Effect of concrete-filling inner steel tube

Figure 9 illustrates the stress-strain relationships of the companion hollow and concrete-filled DSTCs. It can be seen from the figure that concrete-filled DSTCs with circular inner steel tubes developed higher ultimate axia l stresses (f'_{cu}) and, in most cases, lower strains (ε_{cu}) than the companion hollow DSTCs. This observation is in agreement

with those reported in Refs. 36 and 37 for DSTCs manufactured with circular outer tubes.

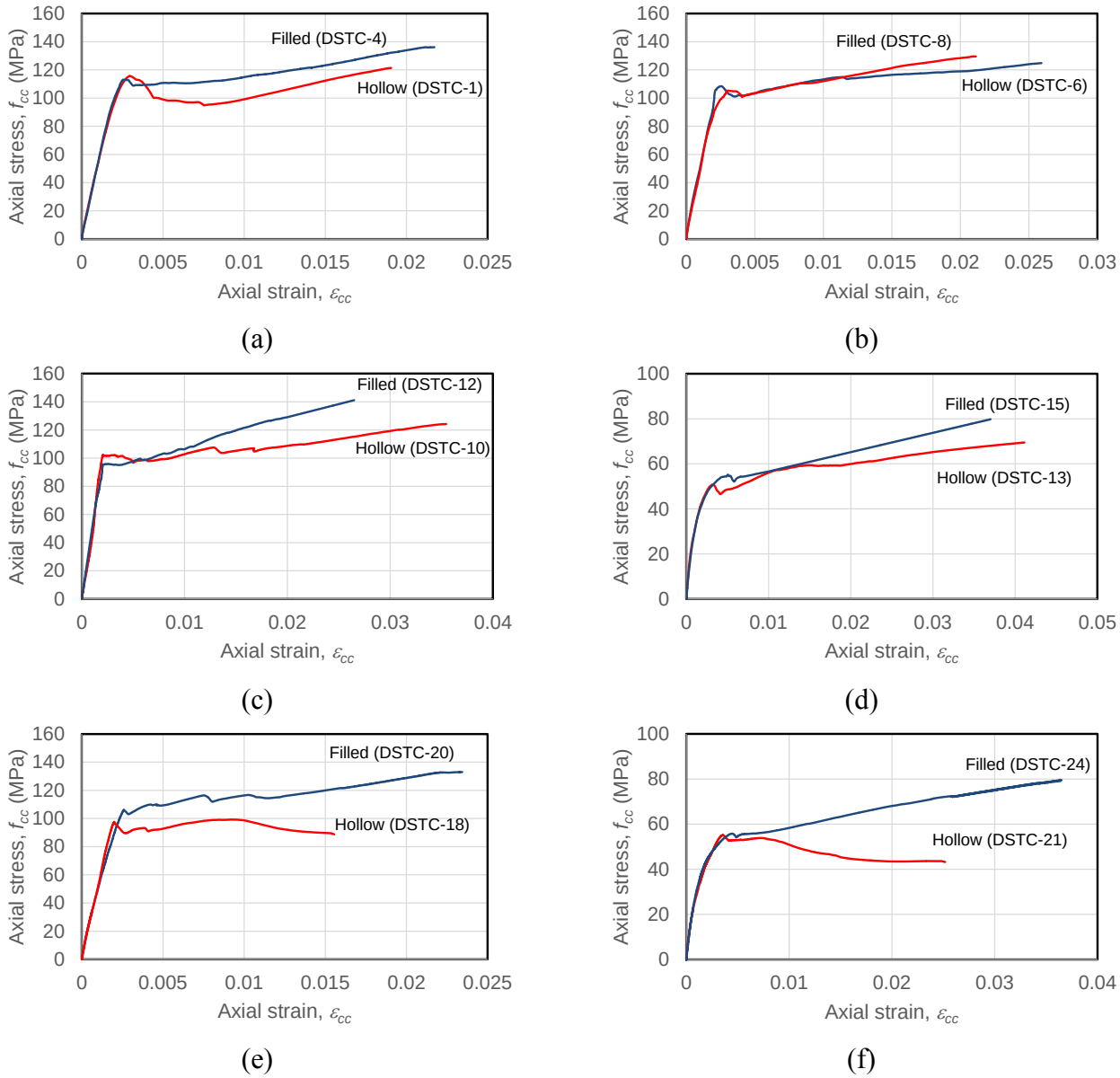

Figure 9. Influence of concrete filling inner steel tubes of DSTC: (a) HSC DSTCs with D_s=60.3 mm circular inner steel tube, (b) HSC DSTCs with D_s=88.9 mm circular inner steel tube, (c) HSC DSTCs with D_s=114.3 mm circular inner steel tube, (d) NSC DSTCs with D_s=88.9 mm circular inner steel tube, (e) HSC DSTCs with square inner steel tube, (f) NSC DSTCs with square inner steel tube

It can be seen from the Figs. 9e and 9f that hollow DSTCs with square inner tubes developed significantly lower ultimate axial stresses (f'_{cu}) and strains (ε_{cu}) than the companion concrete-filled DSTCs. The better performance of concrete-filled DSTCs

can be attributed to presence of the concrete core, which either prevents or delays the buckling of inner steel tube that causes the inferior performance of the hollow DSTCs.

3.4.4. Effect of concrete strength (f'c)

It was previously demonstrated for specimens with circular cross-sections that, for a given nominal confinement ratio confinement ratio (f_{lu}/f'_c), NSC exhibits a higher strength and strain enhancements than HSC in CFFTs [16, 31] and DSTCs [36, 37]. Based on these research findings, to achieve comparable performance levels, the HSC specimens of the present study were designed to have a slightly higher confinement ratio (f_{lu}/f'_c) than that of the NSC specimens, as illustrated in Table 5. Because the nominal confinement ratios were required only for establishing the relative confinement levels of the companion NSC and HSC specimens, the ratio was simply calculated by Eq.1 derived from statics by treating the section as a solid section and giving no consideration to nonuniform distribution of confining pressures in square FRP tubes.

$$\frac{f_{lu}}{f'_c} = \frac{2E_f t_f \varepsilon_f}{D_e f'_c} \tag{1}$$

where, f_{lu} is the ultimate confining pressure, E_f is the modulus of elasticity, t_f is the total nominal thickness and ε_f is the ultimate tensile strain of the fibers used in the FRP tube, and D_e is the cross-sectional dimension of the specimen, measured inside the FRP tube.

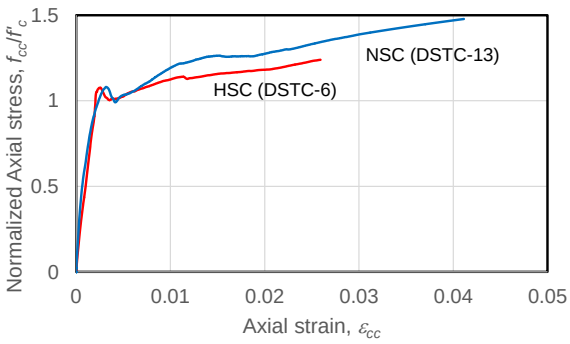

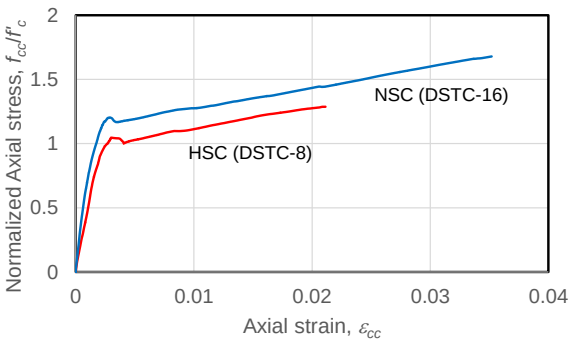

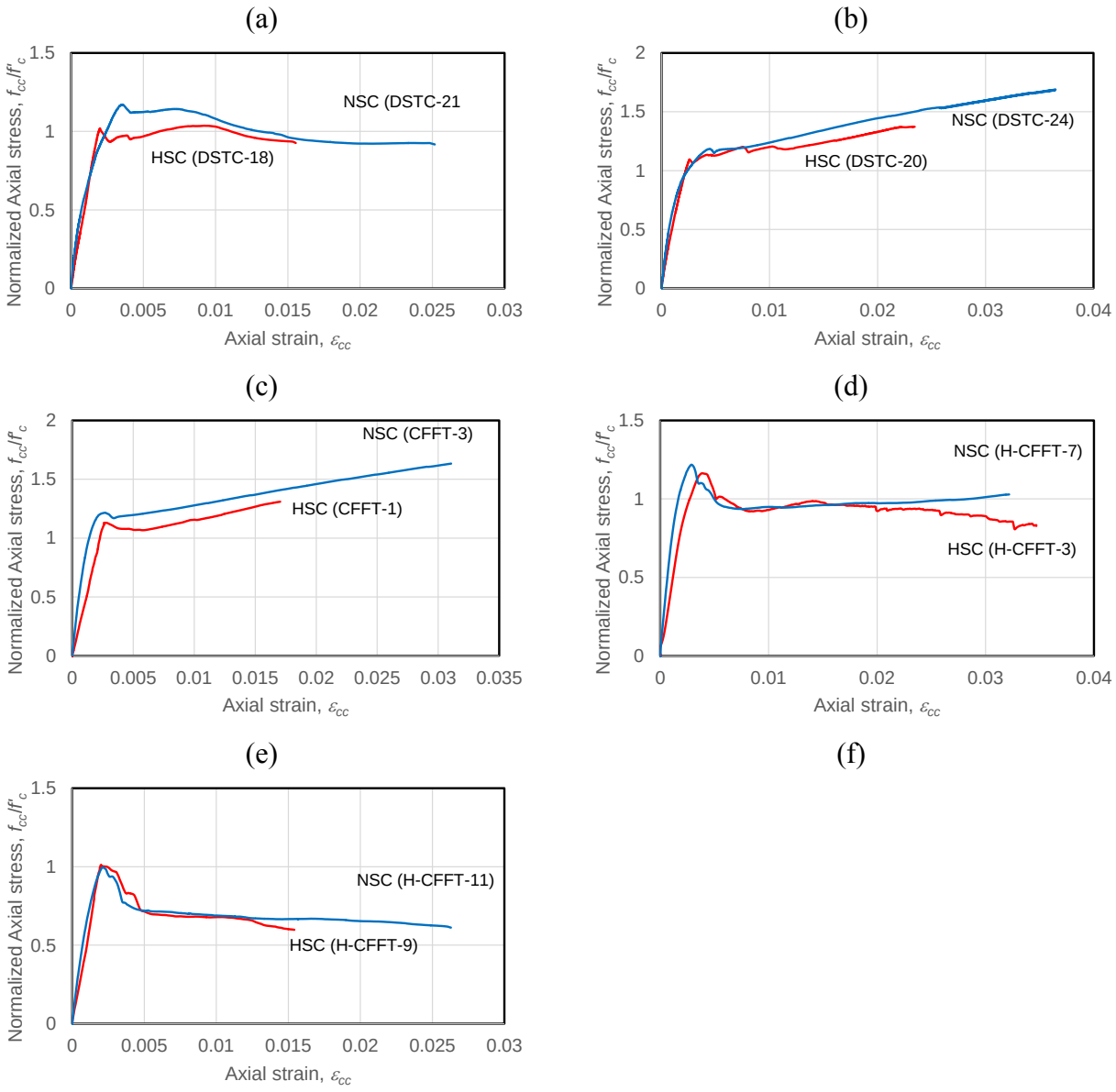

Figure 10. Influence of concrete strength: (a) Hollow DSTCs with D_s=88.9 mm circular inner steel tube, (b) Concrete-filled DSTCs with D_s=88.9 mm circular inner steel tube, (c) Hollow DSTCs with square inner steel tube, (d) Concrete-filled DSTCs with square inner steel tube, (e) CFFTs, (f) H-CFFTs with circular inner void=88.9 mm, (g) H-CFFTs with square inner void

To investigate the influence of concrete strength, the axial stresses (f_{cc}) of the specimens were normalized with their unconfined concrete strengths (f'_c) and were plotted against axial strains (ε_{cc}) as illustrated in Fig. 10. As can be seen from the figure, even with their lower f_{lu}/f'_c ratios, NSC specimens exhibited higher ultimate strain (ε_{cu}) and strength enhancement ratio (f'_{cu}/f'_c) than their companion HSC counterparts. As illustrated in the

figure, the performance difference was more pronounced for the DSTCs and CFFTs specimens than the H-CFFT specimens. These observations are also supported by the one derived from the comparison of the average values of the strength and strain enhancement ratios (f'_{cu}/f'_c) and $\varepsilon_{cu}/\varepsilon_{co}$) reported in Table 5 for all the companion specimens illustrated in Fig. 10. Similar findings on the better relative performance of NSC DSTCs over HSC DSTCs were previously reported by Ozbakkaloglu and Louk Fanggi [36] for DSTCs with circular inner and outer tubes.

3.4.5 Effect of diameter of inner steel tube/void (D_s)

Figure 11 illustrates the influence of diameter of inner steel tube/void on the stress-strain behavior of concrete in DSTCs and H-CFFTs. As can be seen in Fig 11a, hollow DSTCs with larger inner steel tube diameters developed similar ultimate axial stresses (f'_{cu}) to but significantly larger strains (ε_{cu}) than the companion DSTCs with smaller inner steel tubes. Likewise, comparison of the filled DSTCs with similar D_s/t_s ratios (i.e. DSTC-4 and 12) in Fig. 11b indicates that an increase in the steel tube specimens leads to an increase in both f'_{cu} and ε_{cu}. On the other hand, as evident from Fig. 11b, DSTC-8, with D_s = 88.9 mm but a higher D_s/t_s ratio than the companion specimen DSTC-4 with D_s = 60.3 mm, exhibited a slightly lower f'_{cu} and ε_{cu} than its companion. Both of these observations can be attributed to the variations in the level of confinement provided to the core concrete by the inner steel tube with variations in the diameter and diameter-to-thickness ratio of the tube.

Figure 11c illustrates that H-CFFTs experienced degradations in their ultimate axial stress (f'_{cu}) and strain (ε_{cu}) with in an increase in the void ratio. A similar observation was previously reported in Wong et al. [32] for NSC H-CFFTs with circular outer tubes, and this behavior is the result of the changing stress conditions of the concrete on the

inner face of the annular section with a change in void ratio, as the failure of these specimens are governed by the failure of concrete at these regions.

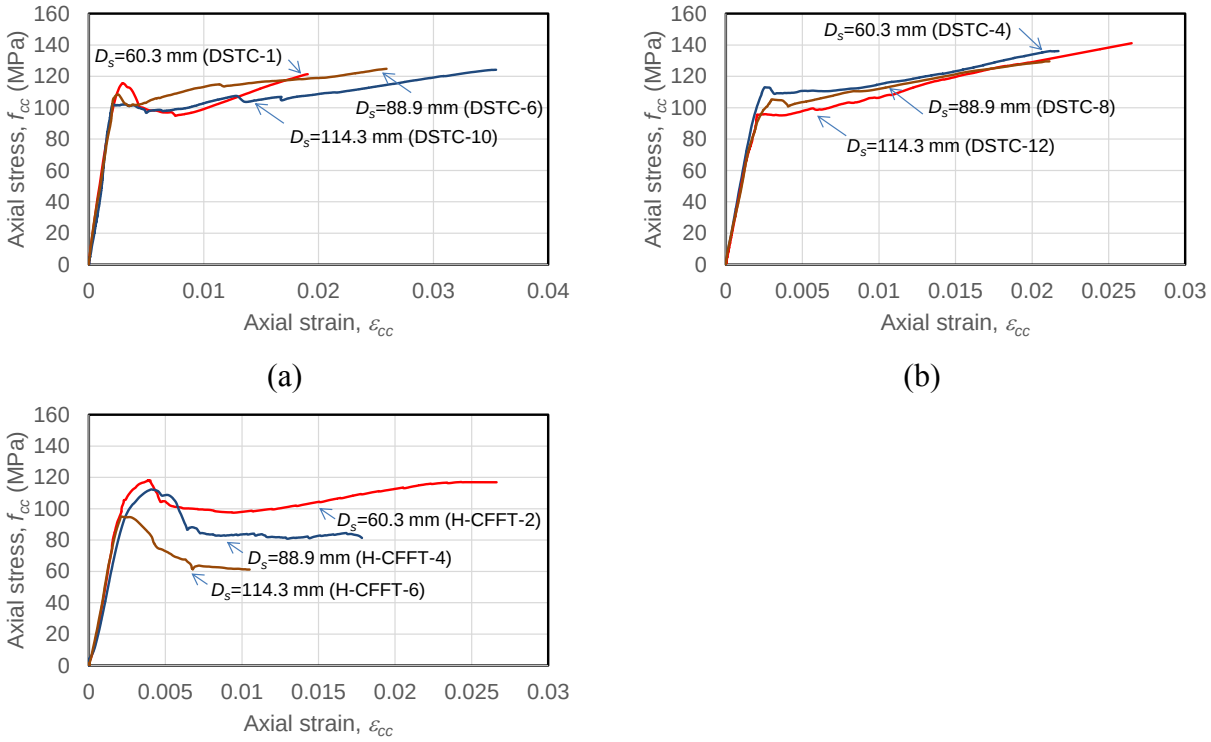

Figure 11. Influence of inner steel tube/ void diameter (D_s): (a) HSC hollow DSTCs, (b) HSC concrete-filled DSTCs, (c) HSC H-CFFTs

3.4.6 Effect of cross-sectional shape of inner steel tube/void

Figure 12 illustrates the influence of the inner steel tube/void cross-sectional shape on stress-strain relationships of hollow and concrete-filled DSTCs and H-CFFTs. It can be seen from Figs. 12a, 12c, 12e, and 12f that hollow DSTCs with circular inner steel tubes and H-CFFTs with circular inner voids developed larger ultimate axial stresses (f'_{cu}) and strains (ε_{cu}) than their companions with square steel tubes or inner voids. The difference in the compressive behavior was particularly pronounced for the DSTC specimens, which is caused by the negative influence of the inward buckling experienced by the hollow inner square steel tubes, as discussed previously. The inferior performance of the H-CFFTs with square voids, on the other hand, can be attributed to the stress

concentrations at the corners of the inner face of the concrete section, resulting of the progressive failure of the concrete inside H-CFFTs starting at these regions.

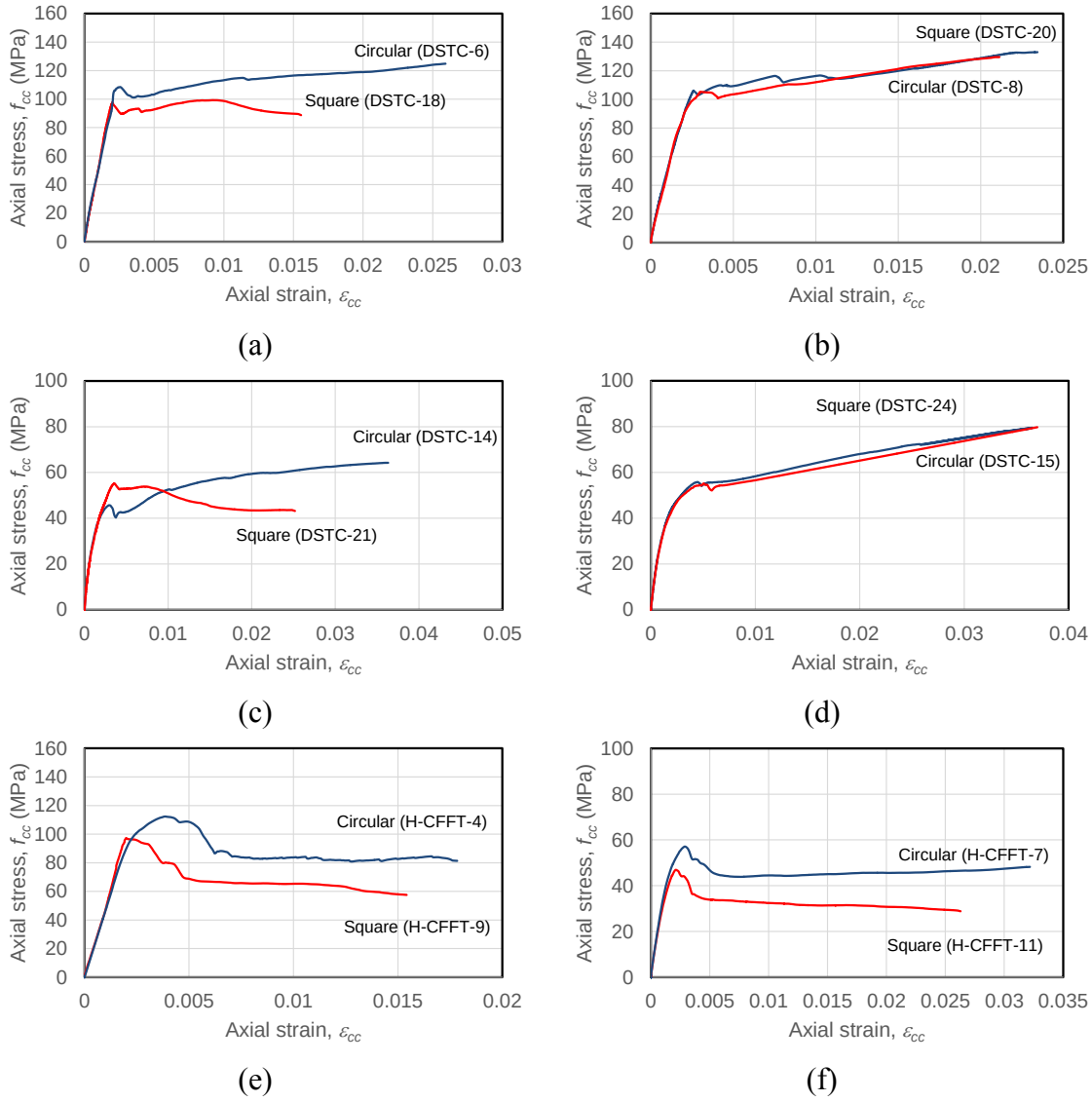

Figure 12. Influence of inner steel tube/ void cross-sectional shape: (a) HSC hollow DSTCs, (b) HSC concrete-filled DSTCs, (c) NSC hollow DSTCs, (d) NSC concrete-filled DSTCs, (e) HSC H-CFFTs, (f) NSC H-CFFTs

Figures 12b and 12d illustrate that the presence of a concrete-filling resulted in a significant improvement in the behavior of the DSTCs with square inner steel tubes. As can be seen from the figures, both NSC and HSC DSTCs with square inner steel tubes exhibited similar performance levels to the companion DSTCs with circular inner steel

tubes. This improvement can be can be attributed to the prevention of the inward buckling of the inner square tube due to the presence of a concrete-filling. These observations indicate that when the inward steel tube buckling is prevented through a concrete-filling, DSTC with square inner steel tubes can exhibit similar performance levels to those of their companions with circular inner steel tubes.

3.4.7. Comparison of DSTCs, CFFTs and H-CFFTs

Figure 13 presents the stress-strain curves of concretes in the companion DSTC, CFFT, and H-CFFT specimens. As can be seen from the figure, concrete in filled DSTCs exhibited higher ultimate axial stress (f'_{cu}) and strain (ε_{cu}) than that in CFFTs. This observation was true for DSTCs with both square and circular inner steel tubes. A Similar observation was recently reported in Ozbakkaloglu and Louk Fanggi [36] for DSTCs with circular external tubes. It can also be seen from the figure that hollow DSTCs with circular inner steel tubes developed similar f'_{cu} to the companion CFFTs but they exhibited a higher ε_{cu} than both CFFTs and concrete-filled DSTCs. Figure 13 further illustrates that H-CFFTs and hollow DSTCs with square inner steel tubes performed significantly worse than the companion CFFTs, filled DSTCs, and hollow DSTCs with circular inner steel tubes. The only exception to this observation was the H-CFFTs with a small diameter (i.e., D_s=60.3 mm) inner steel tubes, which displayed a similar behavior to the companion hollow DSTCs and CFFTs.

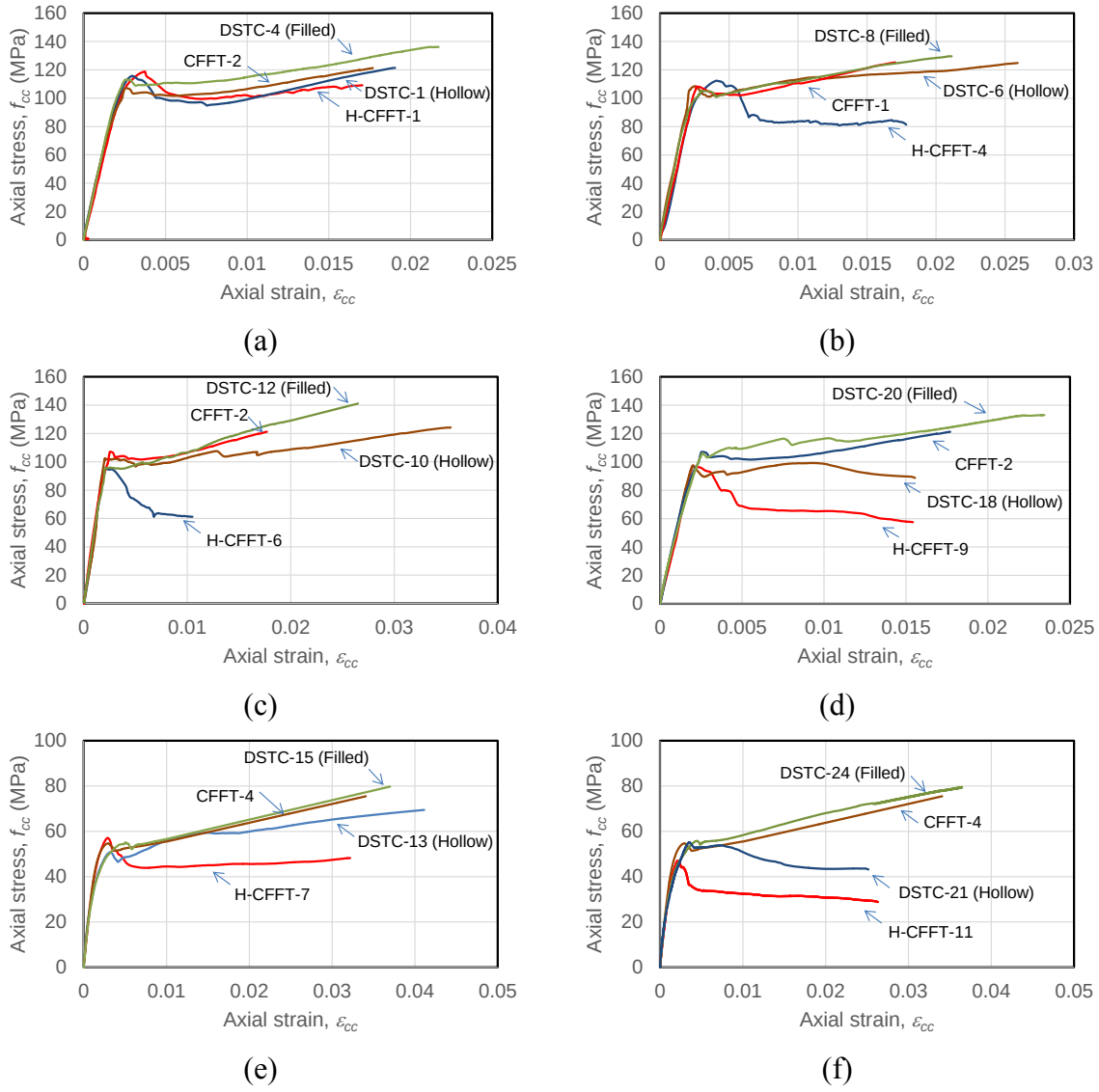

Figure 13. Comparison of different composite systems: (a) HSC specimens with D_s=60.3 mm circular inner steel tube/void, (b) HSC specimens with D_s=88.9 mm circular inner steel tube/void, (c) HSC specimens with D_s=114.3 mm circular inner steel tube/void, (d) HSC specimens with square inner steel tube/void, (e) NSC specimens with D_s=88.9 mm circular inner steel tube/void, (f) NSC specimens with square inner steel tube/void

4. CONCLUSIONS

This paper has presented the results of an experimental study on the compressive behavior of square FRP-concrete and concrete-steel composite columns. Twenty-four hollow and concrete-filled DSTCs, four CFFTs, and twelve H-CFFTs were designed,

manufactured, and tested to investigate the effect of key parameters on the compressive behavior of these composite systems. The results of the tests and analyses showed that:

1. Concrete-filled DSTCs develop larger hoop rupture strains ($\varepsilon_{h,rup}$) than companion hollow DSTCs. This has been found to be true for both NSC and HSC DSTCs with both circular and square inner steel tubes.
2. Hoop rupture strains ($\varepsilon_{h,rup}$) of H-CFFTs decrease with an increase in the size of inner void.
3. Concrete in hollow DSTCs with circular inner steel tubes develops larger ultimate axial strains (ε_{cu}) but lower stresses (f'_{cu}) than concrete in filled DSTCs. However, concrete in hollow DSTCs with square inner steel tubes develop significantly lower ultimate axial stresses (f'_{cu}) and strains (ε_{cu}) than concrete in the companion filled DSTCs. This phenomenon can be attributed to the tendency of the inner square tube to experience inward buckling, which results in the reduction of confinement effects in these specimens.
4. The NSC specimens exhibit higher strength enhancement ratios (f'_{cu}/f'_c) and ultimate strain (ε_{cu}) compared to companion HSC specimens. This observation has been shown to be true for DSTCs, CFFTs, and H-CFFTs.
5. Increasing the steel tube diameter results in an increase in ultimate axial strains (ε_{cu}) of concrete in hollow DSTCs. It was observed that steel tube diameter has no influence in the ultimate axial stresses (f'_{cu}) of hollow DSTCs.
6. In filled DSTCs with similar D_s/t_s ratios, increasing the steel tube diameter results in an increase in both axial stress (f'_{cu}) and strain (ε_{cu}) of concrete. However, if the increase in D_s results in a decrease D_s/t_s ratio, the performance benefits of larger diameter diminishes.

7. Concrete in hollow DSTCs with circular inner steel tubes and H-CFFTs with circular inner voids exhibits larger ultimate axial stresses (f'_{cu}) and strains (ε_{cu}) than those in their companions with square steel tubes or inner voids. On the other hand, the behavior of DSTCs with square inner steel tubes improves significantly through concrete-filling of their inner steel tubes. It is observed that filled DSTCs with square inner tubes exhibits similar performance levels to those of companion DSTCs with circular inner steel tubes.
8. Concrete in filled DSTCs develops higher ultimate axial stress (f'_{cu}) and strain (ε_{cu}) than concrete in companion CFFTs. This observation was true for DSTCs with both square and circular inner steel tubes.
9. Concrete in hollow DSTCs with circular inner steel tubes develops similar f'_{cu} to concrete in CFFTs but it exhibits higher ultimate ε_{cu} than concrete in both CFFTs and filled DSTCs. On the other hand, concrete in H-CFFTs and hollow DSTCs with square inner steel tubes performs significantly worse than concrete in both CFFTs and filled DSTCs.

REFFERENCES

1. Ozbakkaloglu, T., Lim, J. C., and Vincent, T. (2013). "FRP-confined concrete in circular sections: Review and assessment of the stress-strain models." *Engineering Structures*, 49: 1068-1088.
2. Pessiki, S., Harries, K. A., Kestner, J. T., Sause, R. and Ricles, J. M. (2001). "Axial behavior of reinforced concrete columns confined with FRP jackets." *Journal of Composites for Construction, ASCE*, 5(4), 237-245.
3. Lam, L., and Teng, J. G. (2004). "Ultimate condition of fiber reinforced polymer-confined concrete." *Journal of Composites for Construction, ASCE*, 8(6): 539-548.
4. Rousakis, T.C., Karabinis, A.I., & Kiousis, P.D. (2007). "FRP-confined concrete members: Axial compression experiments and plasticity modelling." *Engineering Structure*, 29: 1343-1353.

5. Colomb, F., Tobbi, H., Ferrier, E., and Hamelin, P. (2008) "Seismic retrofit of reinforced concrete short columns by CFRP materials." *Composite Structures*, 82 (4): 475-487.
6. Thermou, G. E., and Pantazopoulou, S. J. (2009) "Fiber-reinforced polymer retrofitting of predamaged substandard RC prismatic members." *Journal of Composites for Construction*, ASCE, 13 (6): 535-546.
7. Chastre, C., & Silva, M.A.G. (2010). "Monotonic axial behavior and modelling of RC circular columns confined with CFRP." *Engineering Structure*, 32: 2268-2267
8. Kusumawardaningsih, Y., and Hadi, M. N. S. (2010). "Comparative behavior of hollow columns confined with FRP composites." Composite Structures, 93(1): 198-205.
9. Wu, Y. F., and Wei, Y. Y. (2010). "Effect of cross-sectional aspect ratio on the strength of CFRP-confined rectangular concrete columns." *Engineering Structures*, 32: 32-45.
10. Zhang, D.J., Wang, Y.F., & Ma, Y.S. (2010). "Compressive behavior of FRP-confined square concrete columns after creep." *Engineering Structure*, 32: 1957-1963.
11. De Luca, A., Nardone, F., Matta, F., Nanni, A., Lignola, G.P., and Prota, A. (2011). "Structural evaluation of full-scale FRP-confined reinforced concrete columns." *Journal of Composites for Construction*, *ASCE,* 15 (1): 112-123.
12. Abdelrahman, K., and El-Hacha, R. (2012). "Behavior of large-scale concrete columns wrapped with CFRP and SFRP sheets." *Journal of Composites for Construction*, *ASCE,* 16 (4): 430-439.
13. Ozbakkaloglu, T., and Akin, E. (2012). "Behavior of FRP confined normal-and high-strength concrete under cyclic axial compression." *Journal of Composites for Construction, ASCE*, 16(4): 451-463.
14. Realfonzo, R., and Napoli, A. (2012). "Results from cyclic tests on high aspect ratio RC columns strengthened with FRP systems." *Construction and building materials*, 37: 606-620.
15. Vincent, T., and Ozbakkaloglu, T. (2013). "Influence of Concrete Strength and Confinement Method on Axial Compressive Behavior of FRP Confined High- and Ultra High-Strength Concrete." *Composites Part B-Engineering*, 50: 413-428.

16. Wang, Z. Y., Wang, D. Y., Smith, S. T., and Lu, D. G. (2012). "Experimental testing and analytical modeling of CFRP-confined large circular RC columns subjected to cyclic axial compression." *Engineering Structures,* 40: 64-74.
17. Seible, F., Burgueño, R., Abdallah, M. G., and Nuismer, R. (1996). "Development of advanced composite carbon shell systems for concrete columns in seismic zones." *Proc., 11th World Conf. Earthquake Engineering*, Pergamon, Elsevier Science, Oxford, Paper No. 1375.
18. Mirmiran, A., Shahawy, M., Samaan, M., El Echary, H., Mastrapa, J. C., and Pico, O. (1998). "Effect of Column Parameters on FRP-confined Concrete." *Journal of Composites for Construction, ASCE*, 2(4): 175-185.
19. Fam, A. Z., and Rizkalla, S. H. (2001). "Confinement model for axially loaded concrete confined by circular fiber-reinforced polymer tubes." *ACI Structural Journal*, 98(4): 451-461.
20. Fam, A. Z., Schnerch, D., and Rizkalla, S. (2005). "Rectangular Filament-Wound GFRP Tubes Filled with Concrete under Flexural and Axial Loading: Experimental Investigation." *Journal of Composites for Construction, ASCE*, 9(1): 25-33.
21. Zhu, Z., Ahmad, I., and Mirmiran, A. (2006). "Seismic performance of concrete-filled FRP tube columns for bridge substructure." *Journal of Bridge Engineering*, ASCE, 11(3): 359-370.
22. Ozbakkaloglu, T., and Saatcioglu, M. (2007). "Seismic Performance of Square High-Strength Concrete Columns in FRP Stay-in-Place Formwork." *Structural Engineering*, 133(1): 44-56.
23. Ozbakkaloglu, T., and Oehlers, D. J. (2008). "Manufacture and testing of a novel FRP tube confinement system." *Engineering Structures*, 30(9): 2448-2459.
24. Ozbakkaloglu, T. (2013). "Compressive behavior of concrete-filled FRP tube columns: Assessment of critical column parameters." *Engineering Structures*, 51: 151-161.
25. Ozbakkaloglu, T. (2013). "Behavior of square and rectangular ultra high-strength concrete-filled FRP tubes under axial compression." *Composites Part B: Engineering*, 54: 97-111.
26. Idris, Y., and Ozbakkaloglu, T. (2013). "Seismic Behavior of High-Strength Concrete-Filled FRP Tube Columns." *Journal of Composites for Construction, ASCE.* 17(6), 04013013.

27. Ozbakkaloglu, T. and Vincent, T. (2013). "Axial Compressive Behavior of Circular High-Strength Concrete-Filled FRP Tubes." *Journal of Composites for Construction, ASCE*, doi: 10.1061/(ASCE)CC.1943-5614.0000410.
28. Vincent, T., and Ozbakkaloglu, T. (2013). "Influence of fiber orientation and specimen end condition on axial compressive behavior of FRP-confined concrete." *Construction and Building Materials*, 47: 814–826.
29. Teng, J. G., Yu, T., and Wong, Y. L. (2004). "Behavior of hybrid FRP-concrete-steel double-skin tubular columns." *The 2nd International Conference on FRP Composites in Civil Engineering-CICE 2004,* Adelaide, Australia, 811-818.
30. Yu T, Wong YL, Teng JG, Dong SL, Lam SS. (2006). "Flexural behavior of hybrid FRP- concrete-steel double skin tubular members." *Journal of Composites for Construction, ASCE*, 10(5): 443–52.
31. Teng, J. G., Yu, T., Wong, Y. L., and Dong, S. L. (2007). "Hybrid FRP concrete steel tubular columns: concept and behavior." *Construction and Building Materials*, 21: 846-854.
32. Wong, Y. L., Yu, T., Teng, J. G., and Dong, S. L. (2008). "Behavior of FRP-confined concrete in annular section columns." *Composites Part B: Engineering*, 38: 451-466.
33. Yu, T., Wong, Y. L., and Teng, J. G. (2010). "Behavior of Hybrid FRP-Concrete-Steel Double-Skin Tubular Columns Subjected to Eccentric Compression." *Advances in Structural Engineering,* 13(5): 961-974.
34. Yu, T., Zhang, B., Cao, Y. B., and Teng, J. G. (2012). "Behavior of hybrid FRP-concrete-steel double-skin tubular columns subjected to cyclic axial compression." *Thin-Walled Structures*, 61: 196-203.
35. Yu, T. and Teng, J. G. (2013). "Behavior of hybrid FRP-Concrete-Steel double-skin tubular columns with a square outer tube and a circular inner tube subjected to axial compression." *Journal of Composites for Construction, ASCE*, 17(2): 271-279.
36. Ozbakkaloglu, T., and Louk Fanggi, B. A. (2013). "Axial compressive behavior of FRP-concrete-steel double-skin tubular columns made of normal- and high-strength concrete." *Journal of Composites for Construction, ASCE.* doi: 10.1061/(ASCE)CC.1943-5614.0000401.

37. Louk Fanggi, B.A., and Ozbakkaloglu, T. (2013). “Compressive behavior of aramid FRP-HSC-Steel double-skin tubular columns.” *Construction and Building Materials*, 48: 554-565.
38. Ozbakkaloglu, T., and Louk Fanggi, B. A. (2013). “FRP–HSC–steel composite columns: behavior under monotonic and cyclic axial compression.” *Materials and Structures.* doi: 10.1617/s11527-013-0216-0.
39. Ozbakkaloglu, T., and Idris, Y. (2014). "Seismic behavior of FRP-high-strength concrete-steel double skin tubular columns." *Journal of Structural Engineering, ASCE*, doi: 10.1061/(ASCE)ST.1943-541X.0000981, 04014019.
40. Albitar M., Ozbakkaloglu, T., and Louk Fanggi, B.A. (2014). “Behavior of FRP-HSC-Steel Double-Skin Tubular Columns under Cyclic Axial Compression.” *Journal of Composites for Construction, ASCE*, doi:10.1061/(ASCE)CC.1943-5614.0000510, 04014041.
41. Idris, Y., and Ozbakkaloglu, T. (2014). "Flexural behavior of FRP-HSC-steel composite beams." *Thin-walled Structures*, 80: 207-216.
42. Idris, Y., and Ozbakkaloglu, T. (2015). "Flexural Behavior of FRP-HSC-Steel Double Skin Tubular Beams under Reversed-Cyclic Loading." *Thin-walled Structures*, 87: 89-101.
43. Popovics, S. (1973). “A numerical approach to the complete stress-strain curves of concrete." *Cement and Concrete Research,* 3(5): 583-599.
44. Lim, J. C. and Ozbakkaloglu, T. (2013). “Confinement model for FRP-confined high-strength concrete.” *Journal of Composites for Construction, ASCE*, 17(2): 271-279. doi: 10.1061/(ASCE)CC.1943-5614.0000376.

Paper 7 Confinement Model for Concrete in Circular and Square FRP-Concrete-Steel Double-Skin Tubular Columns

Butje Alfonsius Louk Fanggi and Togay Ozbakkaloglu

School of Civil, Environmental, and Mining Engineering, University of Adelaide, 5000

(To be submitted)

Statement of Authorship

Title of Paper	Confinement model for concrete in circular and square FRP-concrete-steel double-skin tubular columns
Publication Status	○ Published ○ Accepted for publication ○ Submitted for publication ● Publication style
Publication Details	To be submitted

Author Contributions

By signing the Statement of Authorship, each author certifies that their stated contribution to the publication is accurate and that permission is granted for the publication to be included in the candidate's thesis.

Name of Principal Author (Candidate)	Butje Alfonsius Louk Fanggi		
Contribution to the Paper	Review of literature, analysis data, develop the model, and preparation of manuscript		
Signature		Date	28/07/2015

Name of Co-Author	Dr. Togay Ozbakkaloglu		
Contribution to the Paper	Research supervision and review of manuscript		
Signature		Date	28/07/2015

CONFINEMENT MODEL FOR CONCRETE IN CIRCULAR AND SQUARE FRP-CONCRETE-STEEL DOUBLE-SKIN TUBULAR COLUMNS

Butje Alfonsius LOUK FANGGI[1] , and Togay OZBAKKALOGLU[2]

ABSTRACT

This paper presents a new design-oriented model for predicting the ultimate conditions of concrete in FRP-concrete-steel double-skin tubular columns (DSTCs). An experimental test database consisting of 135 axial compression test results of DSTCs, which was assembled from the published literature is presented in this paper. The performance of the four existing models that were proposed to predict the ultimate condition of concrete in DSTCs was assessed using the database. A new concrete confinement model that which incorporates the failure mode of the inner steel tube was then proposed. Comparisons with experimental test results indicate that the predictions of the proposed model are in close agreement with the test results and that the proposed model shows improved accuracy compared to the existing models.

KEYWORDS: Fiber reinforced polymer (FRP); Concrete; High-strength concrete (HSC); Column; Confinement; DSTCs; Failure modes; Axial stress; Axial strain.

1. INTRODUCTION

As was demonstrated in a recent review by Ozbakkaloglu et al. [1], the use of fiber reinforced polymer (FRP) composites as a confinement material for concrete has received a great deal of attention over the past two decades. Initially research focused on the use of the material in retrofitting applications of concrete columns [e.g. (2-13)].

[1] PhD Candidate, School of Civil, Environmental and Mining Engineering University of Adelaide, Australia.
[2] (Corresponding author) Senior Lecturer, School of Civil, Environmental and Mining Engineering, University of Adelaide, SA 5005 Australia. Tel : + 618 8303 6477; Fax : +618 8303 4359; Email: togay.ozbakkaloglu@adelaide.edu.au

More recently, the focus has turned to the application of FRP composites for the development of new high-performance composite structural systems. As one of the most promising of these structural systems, concrete-filled FRP tubes (CFFTs) have been investigated extensively, with a large number of studies reporting on compressive [e.g. (14-19)], flexural [e.g. (20,21)] and seismic [e.g. (22-26)] behavior of CFFT beams and columns.

Following from the research on CFFTs, a new type of composites system, which consists of an inner steel tube, an outer FRP tube and a concrete-filling in-between the two tubes (and if preferred, inside the steel tube), has received significant recent research attention. These FRP-concrete-steel double-skin tubular (DST) beams and columns (the latter is referred to as DSTCs in this paper) benefit from the same FRP tube confinement mechanism that is present in CFFTs and they offer a long list of advantages, including: i) improved structural performance, ii) improved durability that prolongs the design life, thereby reducing the cost of structural maintenance and urban renewal, iii) significant improvements to the ease of construction that results in reduced construction costs, iv) significant reduction to carbon footprint through more efficient use of materials that reduces both the required amount of raw materials and generation of construction and demolition waste. A large number of experimental studies that were recently undertaken on composite members manufactured using FRP-concrete-steel DST system demonstrated the performance advantages offered by this system under various loading conditions, including monotonic [27-35] and cyclic [36,37] axial compression, flexure [38-40], and combined axial compression and lateral load reversals [41-43].

For a reliable design of DSTCs, the compressive behavior of concrete inside DSTCs needs to be clearly understood and accurately modeled. To this end, four models have been proposed in three different studies to predict the ultimate condition of concrete in DSTCs under axial compression [29, 31, 44]. These models were developed as an extension of selected models that were originally proposed for FRP-confined concrete columns based on the assumption that the stress-strain behavior of concrete in DSTCs is not influenced significantly by the behavior of the inner steel tube. However, it was recently shown in Louk Fanggi and Ozbakkaloglu [33] that the failure modes of inner steel tubes influence the compressive behavior of DSTCs and that the plastic deformation of the inner steel tube might lead to steel tube-induced failure of DSTCs, which results in lower load and displacement capacities. In addition, all of the existing models were proposed to predict the ultimate condition of concrete in DSTCs with a hollow inner steel tube. Therefore, there is currently no model that is applicable to DSTCs with concrete-filled inner steel tubes, which is a major limitation as concrete-filled DSTCs is an important application of this composite column system. Finally, the two existing models given for square DSTCs in Ref. [29] was based on a very small test database of eight specimens and hence their applicability to DSTCs with properties that fall outside the parametric space considered in the development of the models (e.g. DSTCs manufactured with high-strength concrete (HSC)) is questionable.

To address the research gaps outlined in the above summary, the authors have undertaken a series of carefully planned experimental studies followed by an analytical study that is presented in this paper and that resulted in the development of a new model to predict the ultimate condition of concrete in DSTCs. The proposed model consists of simple expressions and, as shown in this paper, it can be used to predict the ultimate

condition of concretes of up to 120 MPa compressive strength in both circular and square hollow and concrete-filled DSTCs.

2. TEST DATABASE

The test database used in the present study consists of 135 test results obtained from nine experimental studies published between 2008 and 2015. The summary of the database is presented in Table 1. As can be seen from Table 1, the majority of the specimens included in the database had a circular cross-section.

Tables 2 to 5 present the databases of test results for circular and square DSTCs, respectively. These databases were used in the present study for both model assessment and development after the application of a set of carefully chosen specimen selection criteria to ensure reliability and consistency of the process. As a result, only the specimens that failed as a result of FRP rupture were included in the model assessment and development. Specimens that failed prematurely due to other modes of failure, such as FRP shell debonding, or premature failure due to imperfections in the manufacture process were excluded and they are marked with the superscript 'a' in Tables 2 to 5. Furthermore, specimens that had a compressive strength (f'_{cu}) or ultimate axial strain (ε_{cu}) leading to a strength or strain enhancement ratio that deviated significantly (i.e. 25% for f'_{cu}/f'_{co} and 70% for $\varepsilon_{cu}/\varepsilon_{co}$) from the global trend of the relevant ratio were excluded and they are marked with the superscript 'b'. Specimens that exhibited descending second branch were also excluded in model assessment and development and they are marked with the superscript 'c'. In addition, a small number of specimens that were manufactured with a high-strength or square inner steel tube, special end condition, and dual-grade concrete were excluded in model assessment and development and they are marked with the superscripts 'd', 'e', 'f', and 'g', respectively. Assessment of the results

in the database based on these criteria resulted in a final database of 70 circular DSTCs and 23 square DSTCs. The database covers the results of DSTCs with and without a concrete-filling inside their inner steel tubes (concrete-filled and hollow DSTCs, respectively), with external tubes manufactured with different FRP materials (i.e. carbon FRP (CFRP), aramid FRP (AFRP), and glass FRP (GFRP) tubes) and different cross-sectional shapes (i.e. circular and square), and filled with concretes of compressive strengths varying from 29.3 to 118.3MPa.

3. INFLUENCE OF INNER STEEL TUBE FAILURE MODE ON ULTIMATE CONDITION OF DSTCs

It was reported in Refs. [30-34] that along the specimen height FRP tube rupture region of DSTCs often corresponds to the region of significant inelastic deformation of inner steel tube. Figure 1 illustrates the deformed shape of the inner steel tube and the failure mode of the FRP tube of a group of specimens tested by Louk Fanggi and Ozbakkaloglu [33]. Each specimen shown in Fig. 1 illustrates one of the four different deformation conditions the inner steel tube can exhibit at the time of specimen failure. The conditions shown in Figs. 1a and 1b relate to hollow DSTCs, where the inner steel tube either exhibits no buckling (as in Fig.1a) or local inward buckling near its top or bottom edge (as in Fig. 1b). The conditions of the inner steel tubes shown in Figs. 1c and 1d relate to concrete-filled DSTCs, where the either exhibits little to no bulging (as in Fig. 1c), or significant bulging near one of its top or bottom edge (as in Fig. 1d).

It is important to distinguish the plastic deformation condition of the inner steel tube, as the second and fourth conditions outlined above lead to a steel tube-induced failure of the DSTC (this type of failure is labeled in this paper with G2), whereas in the first and third modes the failure is caused by the overall dilation of the DSTC (referred to as

dilation-based failure and labeled with G1). This is because, in a steel tube-induced failure (G2), the FRP tube experiences a localized failure at a region along its height that corresponds to the local buckling region of the inner steel tube, which is caused by stress concentrations that result from the buckling of the inner tube as shown in Figs. 1b and 1d. In a dilation-based failure (G1), on the other hand, the FRP tube is free from localized stresses exerted by the inner steel tube and its failure is governed by the overall dilation behavior of the DSTC, with the failure occurring when the hoop rupture strain of the FRP tube is reached. Therefore, the steel tube-induced failure can be considered an early failure mode, in which the full capacity of the FRP tube could not be developed as a result of its early local failure under stress concentrations. These were experimentally demonstrated in Ref. [33].

After a careful investigation of the failure mode of all the DSTCs in the database, an expression is proposed in this study to separate the specimens into the aforementioned failure modes of G1 and G2. It was found that the diameter-to-thickness ratio of the steel tube (D_s/t_s) and the unconfined concrete strength (f'_{co}) were the two influential parameters that determined the failure mode of the specimen. This is illustrated in Fig. 2, which also shows the proposed expression (where f'_{co} is in MPa) to separate the failure modes G1 and G2. As can be seen in the figure, when f'_{co}-adjusted D_s/t_s ratio of a DSTC is higher than a certain value the specimen is expected to exhibit a steel tube-induced failure (i.e. G2). On the other hand, if this ratio is lower than this threshold value then a dilation-based failure (i.e. G1) is expected.

4. ASSESSMENT OF EXISTING ULTIMATE CONDITION MODELS FOR FRP-CONCRETE-STEEL DSTCs

Of the four models proposed to date for predicting the ultimate condition of concrete in FRP-concrete-steel DSTCs, the two models were proposed for circular DSTCs [31,44] and the others two for square DSTCs [29]. All of the existing models were intended for hollow DSTCs and they are not applicable to concrete-filled DSTCs.

Tables 6 and 7 present the performance of the existing models. 44 test results of circular hollow DSTCs presented in Tables 2 and 13 test results of square hollow DSTCs presented in Tables 4 were used in the assessment of the strength and strain enhancement ratios (f'_{cu}/f'_{co} and $\varepsilon_{cu}/\varepsilon_{co}$). It should be noted that there was a slight difference in the number of specimen used in the assessment of the strength and strain enhancement ratios (f'_{cu}/f'_{co} and $\varepsilon_{cu}/\varepsilon_{co}$) for circular hollow DSTCs (i.e. 40 and 44, respectively). This was due to the fact that f'_{cu} values of some of the specimens were not supplied in the original publications (i.e. Refs. [27] and [28]), which can be seen in Table 2 where the missing values were marked with a "-" to indicate their unavailability.

In the comparison of the model performances, three statistical indicators were used. Average absolute error (*AAE*) was used to establish the overall model accuracy and it was defined by Eq. 1, Standard Deviation (*SD*) was used to establish the magnitude of the associated scatter for each model and it was defined by Eq. 2, and Mean (*M*) was used to describe the associated average overestimation or underestimation of each model and it was defined by Eq. 3.

$$AAE = \frac{\sum_{i=1}^{n} \left| \frac{\mathrm{mod}_i - \exp_i}{\exp_i} \right|}{n} \tag{1}$$

$$M = \frac{\sum_{i=1}^{n}\left(\frac{\text{mod}_i}{\text{exp}_i}\right)}{n} \tag{2}$$

$$SD = \sqrt{\frac{\sum_{i=1}^{n}\left(\frac{\text{mod}_i}{\text{exp}_i} - \frac{\text{mod}_{avg}}{\text{exp}_{avg}}\right)^2}{n-1}} \tag{3}$$

In Eqs. 1-3, *mod* is the model prediction, *exp* is the experimental value, *n* is the total number of datasets and *avg* is the sample average.

Based on the results of the assessment presented in Tables 6 and 7, it can be seen that all of the models (i.e. Yu et. al [44], Louk Fanggi and Ozbakkaloglu [31], Yu and Teng 1 and 2 [29]) obtained an *AAE* of less than 15%, which indicates a reasonable accuracy, in the prediction of the strength enhancement ratio. However, only the model proposed by Louk Fanggi and Ozbakkaloglu [31] obtained an *AAE* of less than 15% in the prediction of the strain enhancement ratio. These observations indicate that further modelling improvements are possible for the prediction of the strain enhancement ratio ($\varepsilon_{cu}/\varepsilon_{co}$). In addition, as was pointed out previously, the existing models are limited to hollow DSTCs, and hence there is a need for a new model with improved modelling accuracy that is applicable to both hollow and concrete-filled circular and square DSTCs.

5. A NEW MODEL FOR FRP-CONCRETE-STEEL DSTCS

This section presents a new model that incorporates the plastic deformation modes of inner steel tubes to predict the ultimate condition of concrete in both circular and square hollow and concrete-filled DSTCs. This model is an extension of the model proposed by Louk Fanggi and Ozbakkaloglu [31] for circular hollow DSTCs with unconfined concrete strengths up to 120 MPa. The following expressions are proposed for the

prediction of the compressive strength (f'_{cu}) and ultimate axial strain (ε_{cu}) of concrete in DSTCs.

$$f'_{cu} = \left(c_1 f'_{co} + k_1\left(k_{s1} f_{lu,a} - f_{lo}\right)\right)\left(1 - \frac{D_s}{D_o}\right)^{-0.03}\left(1 + \emptyset_F\left(\frac{t_s}{D_s}\right)^{0.78}\right) \quad (4)$$

$$\varepsilon_{cu} = \left(c_2\varepsilon_{co} + k_2 k_{s2}\left(\frac{K_l}{f'_{co}}\right)^{0.9}{\varepsilon_{h,rup}}^{1.35}\right)\left(1.28\left(1 - \frac{D_s}{D_o}\right)^{-0.36}\right)(1 - 0.15\emptyset_F) \quad (5)$$

In Eqs. 4 and 5, c_1 and c_2 are the concrete strength and strain factors; f'_{co} and ε_{co} are the compressive strength and peak axial strain of unconfined concrete; k_1 and k_2 are the strength and strain enhancement coefficients; ks_1 and ks_2 are the strength and strain efficiency factors; D_s and D_o are the external diameter of inner steel tube and internal diameter of outer FRP tube, respectively; t_s is the thickness of inner steel tube; $\emptyset_F$ is the solidity factor of inner steel tube; K_l is the lateral confinement stiffness; $\varepsilon_{h,rup}$ is the hoop rupture strain of FRP tube; $f_{lu,a}$ is the actual lateral confining pressure at ultimate, and f_{lo} is the threshold confining pressure. In these equations $\emptyset_F$ is used to distinguish the application of the model to hollow and filled DSTCs, as such when $\emptyset_F$=0 the model becomes applicable to hollow DSTCs and when $\emptyset_F$=1 to concrete-filled DSTCs.

In Eq. 5, K_l is determined from Eq. 6 where E_f and t_f are the elastic modulus and total nominal thickness of fibers in the FRP tube, respectively. In the same equation, c_2 is calculated from Eq. 7 and ε_{co} is determined from Eq. 8, which was proposed by Tasdemir et al. [46] and given in Eq. 8. In Eqs. 7 and 8, f'_{co} is in MPa.

$$K_l = \frac{2E_f t_f}{D} \quad (6)$$

$$c_2 = 2 - \left(\frac{f'_{co}-20}{100}\right) \text{ and } c_2 \geq 1 \quad (7)$$

$$\varepsilon_{co} = \left(0.067{f'_{co}}^2 + 29.9f'_{co} + 1053\right) \times 10^{-6} \quad (8)$$

In the proposed model a confinement stiffness threshold (K_{lo}) is introduced to differentiate the specimens exhibiting stress-strain curves with ascending and descending second branches, which is the minimum stiffness of the FRP confining shell required by the confined concrete to exhibit a stress-strain curve with an ascending second branch. It was previously shown that the confinement stiffness threshold (K_{lo}) changes with the unconfined concrete strength (f'_{co}) and the relationship was defined as shown in Eq. 9 [47].

$$K_{lo} = {f'_{co}}^{1.65} \quad (9)$$

This boundary condition is used in the proposed model to distinguish the stress-strain curves of concrete in DSTCs. A value of K_l greater than K_{lo} represents a specimen having confinement stiffness above the minimum threshold, for which a full ascending second branch is expected. When the confinement stiffness (K_l) is lower than the threshold stiffness (K_{lo}), but the actual confining pressure ($f_{lu,a}$) at the ultimate condition is greater than the threshold confining pressure (f_{lo}), an ascending second branch with an initial loss of axial stress during the transition is expected. When the actual confining pressure ($f_{lu,a}$) is lower than the threshold confining pressure (f_{lo}), a full descending second branch is expected, and the proposed expression (Eq. 4) is not intended to predict the ultimate axial stress (f'_{cu}) of these specimens. The relationships between the threshold confining pressure (f_{lo}), initial peak stress (f'_{c1}), and the second transition stress (f'_{c2}), are discussed in detail in Lim and Ozbakkaloglu [47] and an illustration of

this is presented in Fig. 3. Based on the approach summarized in this section, the values of c_1 and f_{lo} in Eq. 4 are to be calculated using the expressions given in Eqs. 10-13.

$$\text{If } K_l \geq K_{lo},\ c_1 = \frac{f'_{c1}}{f'_{co}} = 1 + 0.0058\frac{K_l}{f'_{co}} \tag{10}$$

$$f_{lo} = f_{l1} = K_l\varepsilon_{l1}, \qquad \varepsilon_{l1} = \left(0.43 + 0.009\frac{K_l}{f'_{co}}\right)\varepsilon_{co} \tag{11}$$

$$\text{If } K_l < K_{lo},\ c_1 = \frac{f'_{c2}}{f'_{co}} = \left(\frac{K_l}{{f'_{co}}^{1.6}}\right)^{0.2} \tag{12}$$

$$f_{lo} = f_{l2} = K_l\varepsilon_{l2}, \qquad \varepsilon_{l2} = 24\left(\frac{f'_{co}}{{K_l}^{1.6}}\right)^{0.4}\varepsilon_{co} \text{ where } f_{lu,a} \geq f_{lo} \tag{13}$$

In the calculation of the actual confining pressure ($f_{lu,a}$), the hoop rupture strain $\varepsilon_{h,rup}$ is calculated through Eq. 15 as a product of the hoop strain reduction factor ($k_{\varepsilon,f}$) and the ultimate tensile strain of fibers (ε_f). The expression for $k_{\varepsilon,f}$ given in Eq. 16 was developed by Lim and Ozbakkaloglu [47] based on two large test databases of FRP-confined NSC and HSC presented in Ozbakkaloglu and Lim [48] and Lim and Ozbakkaloglu [47], respectively.

$$f_{lu,a} = \frac{2E_f t_f \varepsilon_{h,rup}}{D} \tag{14}$$

$$\varepsilon_{h,rup} = k_{\varepsilon f}\varepsilon_f \tag{15}$$

$$k_{\varepsilon f} = 0.9 - 2.3f'_{co} \times 10^{-3} - 0.75E_f \times 10^{-6} \tag{16}$$

In Eq. 16, f'_{co} and E_f are in MPa, and 100,000 MPa $\leq E_f \leq$640,000 MPa.

In Eqs. 4 and 5, k_{s1} and k_{s2} are defined by Eqs. 17 and 18, which were adopted for square specimens from Lim and Ozbakkaloglu's model [45] proposed for FRP-confined

concrete. In Eqs. 17 and 18, r is the corner radius of the FRP tube, which is equal to $0.5D_o$ in the case of circular tubes.

$$k_{s1} = \left(\frac{2r}{D_o}\right)^{0.67} \tag{17}$$

$$k_{s2} = \left(2 - \frac{2r}{D_o}\right)^{2} \left(\frac{2r}{D_o}\right) \tag{18}$$

Based on the experimental observations that the compressive strength (f'_{cu}) of concrete in DSTCs is influenced by the void ratio (D_s/D_o) in hollow DSTCs, and by both D_s/D_o and t_s/D_s in concrete-filled DSTCs, the equation given in Louk Fanggi and Ozbakkaloglu [31] is modified to include the functions of $(1\text{-}D_s/D_o)^{-0.03}$ and $(1+\emptyset_F(t_s/D_s)^{0.78}$, as shown in Eq. 4. Likewise, based on the observation that the ultimate axial strain (ε_{cu}) of concrete in concrete-filled DSTCs is consistently lower than that in hollow DSTCs, the equation given in Louk Fanggi and Ozbakkaloglu [31] is modified to include the function of $(1\text{-}0.15\emptyset_F)$ as shown in Eq. 5.

The strength and strain enhancement coefficients (k_1 and k_2) in Eqs. 4 and 5 were established based on the test database separately for the two different failure modes that were introduced earlier in the paper (i.e. G1 and G2). The average values of k_1 and k_2 are presented in Tables 8 and 9 for circular and square DSTCs, respectively. It can be seen from Table 8 that k_1 values of concrete-filled DSTCs were higher than those of hollow DSTCs, even in the presence of the factor of $(1+\emptyset_F(t_s/D_s)^{0.78}$ in Eq. 4. It can also be seen from Table 8 that hollow and concrete-filled DSTCs had similar k_2 values. It should be noted, however, that once the reduction in ε_{cu} of filled DSTCs through the factor $(1\text{-}0.15\emptyset_F)$ given in Eq. 5 is considered, this resulted in lower ε_{cu} predictions for these DSTCs, consistent with the experimental observations. It can be seen in Tables 8

and 9 that k_1 and k_2 of circular DSTCs were higher than those of square DSTCs. This indicates that the reductions seen in f'_{cu} and ε_{cu} of square DSTCs over those of the circular DSTCs were higher than those suggested by k_{s1} and k_{s2} calculated from Eqs. 17 and 18. In addition, as can be seen in Table 9, square NSC DSTCs developed significantly larger k_1 and k_2 compared to those of square HSC DSTCs. For that reason, in Table 9, k_1 and k_2 values of square specimens were reported separately for NSC and HSC DSTCs. It is worth noting that such a difference between NSC and HSC specimens was not seen in circular DSTCs. It should also be noted that due to the smaller size of the square DSTC database, the values of k_1 and k_2 presented in Table 9 for square DSTCs should be treated as best estimates, which are to be further improved once additional test results become available.

6. COMPARISONS WITH TEST RESULTS

Figure 4 shows the comparison of predictions of the proposed model with test results of circular hollow DSTCs. It can be seen from the figure that the prediction of proposed model is in close agreement with *AAE*s of 5.7% and 10.5% for the strength and strain enhancement ratios, respectively. It can also be seen from the comparison of the prediction statistics of the proposed model with those of the existing models by Yu et al. [44] and Louk Fanggi and Ozbakkaloglu [31] presented in Table 6 that the proposed model provides improved accuracy. Figure 5 shows the comparison of the model prediction of proposed model with test results of circular concrete-filled DSTCs. It can be seen from the figure that the proposed model provides accurate predictions of experimental test results, with *AAE*s of 5.1% and 12.4% for the strength and strain enhancement ratios, respectively.

Figure 6 shows the comparison of the model predictions with the experimental results of square hollow DSTCs. It can be seen from Figure 6 that the predictions of the proposed model are in good agreement with the experimental results, with *AAEs* of 4.7% and 14.3% for the strength and strain enhancement ratios, respectively. It can also be seen from the comparison of predictions of the proposed model with those of the two models proposed by Yu and Teng [29] shown in Table 7 that the proposed model provides improved accuracy. Figure 7 shows the comparison of the model predictions with the experimental results of square concrete-filled DSTCs. From Figure 7, it can be seen that the predictions of proposed model are in close agreement with the test results, with *AAEs* of 2.5% and 12.2% for the strength and strain enhancement ratios, respectively. It is worth noting however that as can be seen from Figs. 6 and 7 and Tables 4 and 5, the number of square specimens available for the assessment and development of the proposed model was limited, and hence refinement of the model coefficients k_1 and k_2 will be possible once additional test results become available for square DSTCs.

7. CONCLUSIONS

This paper has presented a new model for predicting the ultimate conditions of concrete in hollow and concrete-filled FRP-concrete-steel DSTCs with circular and square cross-sections. The model was developed based on a carefully assembled test database that consisted of all the results reported to date on concentrically loaded DSTCs. It is the first model that is applicable to concrete-filled DSTCs. Close examination of the test results have revealed that plastic deformations of the inner steel tube influences the compressive behavior of DSTCs. Based on these observation, inner steel tube failure modes were incorporated into the proposed model to represent the condition of the inner steel tube at specimen failure. The predictions of the proposed model are in close

agreement with the test results and the model shows improved performance compared to the existing models.

REFFERENCES

[1] Ozbakkaloglu, T., Lim, J. C., and Vincent, T. (2013). "FRP-confined concrete in circular sections: Review and assessment of the stress-strain models", *Engineering Structures*, Vol. 49, pp. 1068-1088.

[2] Lam, L., and Teng, J. G. (2004). "Ultimate condition of fiber reinforced polymer-confined concrete", *J. Compos. Constr., ASCE*, Vol. 8, No. 6, pp. 539-548.

[3] Lignola, G. P., Prota, A., Manfredi, G., and Cosenza E. (2007). "Experimental performance of RC hollow columns confined with CFRP", *Journal of Composites for Construction, ASCE*, Vol. 11, No. 1, pp. 42–49.

[4] Colomb, F., Tobbi, H., Ferrier, E., and Hamelin, P. (2008). "Seismic retrofit of reinforced concrete short columns by CFRP materials", *Composite Structures*, Vol. 82, No. 4, pp. 475-487.

[5] Ilki, A., Peker. O., Karamuk, E., Demir, C., and Kumbasar, N. (2008). "FRP retrofit of low and medium strength circular and rectangular reinforced concrete columns", *J. Mater. Civ. Eng*., Vol. 20, No. 2, pp. 169–188.

[6] Rousakis, T., and Karabinis, A. (2008). "Substandard reinforced concrete members subjected to compression: FRP confining effects", *Materials and Structures*, Vol. 41, No. 9, pp. 595 – 1611.

[7] Dai, J. G., and Teng, J. G. (2011) "Behavior and modeling of concrete confined with FRP composites of large deformability", *Journal of Composites for Construction, ASCE*, Vol. 13, No. 6, pp. 963-973.

[8] Wu, Y. F., and Wei, Y. Y. (2010). "Effect of cross-sectional aspect ratio on the strength of CFRP-confined rectangular concrete columns", *Engineering Structures*, Vol. 32, pp. 32-45.

[9] De Luca, A., Nardone, F., Matta, F., Nanni, A., Lignola, G.P., and Prota, A. (2011). "Structural evaluation of full-scale FRP-confined reinforced concrete columns", *Journal of Composites for Construction, ASCE*, Vol. 15, No. 1, pp. 112-123.

[10] Ozbakkaloglu, T., and Akin, E. (2012). "Behavior of FRP confined normal-and high-strength concrete under cyclic axial compression", *Journal of Composites for Construction, ASCE*, Vol. 16, No. 4, pp. 451-463.

[11] Realfonzo, R., and Napoli, A. (2012). "Results from cyclic tests on high aspect ratio RC columns strengthened with FRP systems", *Construction and Building Materials*, Vol. 37, pp. 606-620.

[12] Wang, Z. Y., Wang, D. Y., Smith, S. T., and Lu, D. G. (2012). "Experimental testing and analytical modeling of CFRP-confined large circular RC columns subjected to cyclic axial compression", *Engineering Structures*, Vol. 40, pp. 64-74.

[13] Vincent, T., and Ozbakkaloglu, T. (2013). "Influence of Concrete Strength and Confinement Method on Axial Compressive Behavior of FRP Confined High- and Ultra High-Strength Concrete", *Composites Part B-Engineering*, Vol. 50, pp. 413-428.

[14] Fam, A. Z., and Rizkalla, S. H. (2001). "Behavior of axially loaded concrete-filled circular fiber-reinforced polymer tubes", *ACI Structural Journal*, Vol. 98, No. 3, pp. 280-289.

[15] Mirmiran, A., Shahawy, M., & Beitleman, T. (2001). "Slenderness limit for hybrid FRP-concrete columns", *Journal of Composites for Construction."* Vol. 5, No. 1, pp. 26-34.

[16] Ozbakkaloglu, T. (2013). "Compressive behavior of concrete-filled FRP tube columns: Assessment of critical column parameters", *Engineering Structures*, Vol. 51, pp. 188-199.

[17] Lim, J. C., and Ozbakkaloglu, T. (2014). "Influence of silica fume on stress–strain behavior of FRP-confined HSC", *Construction and Building Materials*, Vol. 63, pp. 11-24.

[18] Vincent, T. and Ozbakkaloglu, T. (2015). "Influence of slenderness on stress-strain behavior of concrete-filled FRP tubes: experimental study", *Journal of Composites for Construction*, Vol. 19, No. 1, pp. 04014029.

[19] Xie, T. and Ozbakkaloglu, T. (2015),"Behavior of steel fiber-reinforced high-strength concrete-filled FRP tube columns under axial compression", *Engineering Structures*, Vol 90, pp. 158-171.

[20] Davol, A., Burgueno, R., and Seible, F. (2001), "Flexural Behavior of Circular Concrete Filled FRP Shells", *Journal of Structural Engineering*, Vol. 127, No. 7, pp. 810-817.

[21] Cole, B., and Fam, A. (2006), "Flexural load testing concrete filled FRP tubes with longitudinal steel and FRP rebar", *Journal of Composites for Construction, ASCE*, Vol. 10, No. 2, pp. 161-171.

[22] Ozbakkaloglu, T. and Saatcioglu, M. (2006),"Seismic Behavior of High Strength Concrete Columns Confined by Fiber-Reinforced Polymer Tubes", *Journal of Composites Construction, ASCE*, Vol.10, No. 6, pp. 538-549.

[23] Ozbakkaloglu, T. and Saatcioglu, M. (2007), "Seismic Performance of Square High Strength Concrete Columns in FRP stay in place formwork", *Journal of Structural Engineering, ASCE*, Vol. 133, No. 1, pp. 44-56.

[24] ElGawady, M.A., Booker, A.J, and Dawood, H.M. (2010). "Seismic behavior of posttensioned concrete-filled fiber tubes", *Journal of Composites for Construction, ASCE*, Vol. 14, No. 5, pp. 616-628.

[25] Zohrevand, P., and Mirmiran A. (2012). "Cyclic behaviour of hybrid columns made of ultra-high performance concrete and fiber reinforced polymers", *Journal of Composites for Construction, ASCE*, Vol. 16, No. 1, pp. 91-99.

[26] Idris, Y., and Ozbakkaloglu, T. (2013). "Seismic behavior of square high-strength concrete-filled FRP tube columns", *Journal of Composites for Construction, ASCE*, Vol. 17, No. 6, pp. 04013013.

[27] Wong, Y. L., Yu, T., Teng, J. G., and Dong, S. L. (2008). "Behavior of FRP-confined concrete in annular section columns", *Composites part B: Engineering*, Vol. 38, pp. 451-466.

[28] Xie, P., Yu, T., Wong, Y. L., and Teng, J. G. (2011). "Compressive behavior of large scale hybrid FRP-concrete-steel double-skin tubular columns", *Adv. Mater. Res.*, Vols. 243-249, pp.1138-1144.

[29] Yu, T., and Teng, J. G. (2013). "Behavior of hybrid FRP-concrete-steel double-skin tubular columns with a square outer tube and a circular inner tube subjected to axial compression", *Journal of Composites for Construction, ASCE*, Vol. 17, No. 2, pp. 271-279.

[30] Ozbakkaloglu, T., and Louk Fanggi, B. A. (2013). "Axial compressive behavior of FRP-concrete-steel double-skin tubular columns made of normal- and high-strength concrete", *Journal of Composites for Construction, ASCE*. doi: 10.1061/(ASCE)CC.1943-5614.0000401.

[31] Louk Fanggi, B.A., and Ozbakkaloglu, T. (2013). "Compressive behavior of aramid FRP-HSC-Steel double-skin tubular columns", *Construction and Building Materials*, Vol. 48, pp. 554-565.

[32] Ozbakkaloglu, T., and Louk Fanggi, B. A. (2015). "FRP-HSC-Steel double-skin tubular columns: behavior under monotonic and cyclic axial compression", *Materials and Structures*, Vol. 48, pp. 1075-1093.

[33] Louk Fanggi, B.A., and Ozbakkaloglu, T. (2015). "Behavior of hollow and concrete-filled FRP-HSC and FRP-HSC-Steel composites columns subjected to concentric compression", *Advances in Structural Engineering*, Vol. 18, No. 5, pp. 715-738.

[34] Louk Fanggi, B.A., and Ozbakkaloglu, T. (2015). "Square FRP-HSC-Steel Composite Columns: Behavior under Axial Compression", *Engineering Structures*, Vol. 92, pp. 156-171.

[35] Linpeng, C., Fang, H., Junzhu, W., and Yuxiang, W. (2013). "Confinement effectiveness of concrete-filled tube and hybrid double-skin tubular column systems", *Honour's Thesis*, The School of Civil, Environmental, and Mining Engineering, The University of Adelaide.

[36] Yu, T., Zhang, B., Cao, Y. B., and Teng, J. G. (2012). "Behavior of hybrid FRP-concrete-steel double-skin tubular columns subjected to cyclic axial compression", *Thin-Walled Structures*, Vol. 61, pp. 196-203.

[37] Albitar M., Ozbakkaloglu, T., and Louk Fanggi, B.A. (2015). "Behavior of FRP-HSC-Steel Double-Skin Tubular Columns under Cyclic Axial Compression", *Journal of Composites for Construction, ASCE*, Vol. 19, No. 2, pp. 04014041.

[38] Yu, T., Wong, Y., Teng, J., Dong, S., and Lam, E. (2006). "Flexural Behavior of Hybrid FRP-Concrete-Steel Double-Skin Tubular Members", *Journal of Composites for Construction, ASCE*, Vol. 10, No. 5, pp. 443-452.

[39] Idris, Y., and Ozbakkaloglu, T. (2014). "Flexural behavior of FRP-HSC-steel composite beams", *Thin-Walled Structures*, Vol. 80, pp. 207-216.

[40] Idris, Y., and Ozbakkaloglu, T. (2015). "Flexural behavior of FRP-HSC-steel tubular beams under reversed cyclic loading", *Thin-Walled Structures*, Vol. 87, pp. 89-101.

[41] Han, L. H., Tao, Z., Liao, F. Y., and Xu, Y. (2010). "Tests on cyclic performance of FRP-concrete-steel double-skin tubular columns", *Thin-Walled Structures*, Vol. 48, No. 6, pp. 430-439.

[42] Ozbakkaloglu, T., and Idris, Y. (2014), "Seismic behavior of FRP-high-strength concrete-steel double skin tubular columns", *Journal of Structural Engineering, ASCE*, Vol. 140, No. 6, pp. 04014019.

[43] Zhang, B., Teng, J. G., and Yu, T. (2015). "Experimental behavior of hybrid FRP-concrete-steel double-skin tubular columns under combined axial compression and cyclic lateral loading", *Engineering Structures*, Vol. 99, pp. 214-231.

[44] Yu, T., Teng, J. G., and Wong, Y. L. (2010). "Stress-strain behavior of concrete in hybrid FRP-Concrete-Steel double skin tubular columns", *Journal of Structural Engineering*, Vol. 136, No. 4, pp. 379-389.

[45] Lim, J.C., and Ozbakkaloglu, T. (2014). "Design model for FRP-confined normal- and high-strength concrete square and rectangular columns", *Magazine of Concrete Research*, doi:10.1680/macr.14.00059.

[46] Tasdemir, M. A., Tasdemir, C., Jefferson, A. D., Lydon, F. D., Barr, B. I. G. (1998). "Evaluation of strain at peak stresses in concrete: a three-phase composite model approach", *Cem. Concr. Res*. Vol. 20, pp. 301-318.

[47] Lim, J.C., and Ozbakkaloglu, T. (2014). “Confinement model for FRP-confined high-strength concrete”, *Journal of Composites for Construction, ASCE*, Vol. 18, No. 4, pp. 04013058.

[48] Ozbakkaloglu, T., and Lim, J. C. (2013). "Axial Compressive Behavior of FRP-Confined Concrete: Experimental Test Database and a New Design-Oriented Model", *Composites Part B: Engineering*, Vol. 55, pp. 607-634.

LIST OF TABLES

Table 1. Summary of test database

Type of DSTC	Outer FRP tube cross-section	Inner steel tube condition	Number of specimens
Circular hollow	Circular	Hollow	67
Circular concrete-filled	Circular	Filled	32
Square hollow	Square	Hollow	22
Square concrete-filled	Square	Filled	14

Table. 2 Test database of circular hollow DSTCs

Paper	Specimen label	Specimen dimensions		FRP tube properties				Steel tube dimensions		Concrete properties		Measured ultimate condition			Failure mode
		D (mm)	H (mm)	FRP type	t_f (mm)	E_f (GPa)	ε_f (%)	D_s (mm)	t_s (mm)	f'_{co} (MPa)	ε_{co} (%)	f'_{cu} (MPa)	ε_{cu} (%)	$\varepsilon_{h.rup}$ (%)	
Ref. [27]	D37-A2-I	152.5	305	GFRP	0.34	80.1*	2.28	42.0	2.3	36.7	0.21	54.6	1.92	-	G1
	D37-A2-II	152.5	305	GFRP	0.34	80.1*	2.28	42.0	2.3	36.7	0.21	49.6	1.57	-	G1
	D40-B1-I[c]	152.5	305	GFRP	0.17	80.1*	2.28	76.0	3.3	39.6	0.21	41.5	1.48	-	-
	D40-B1-II[c]	152.5	305	GFRP	0.17	80.1*	2.28	76.0	3.3	39.6	0.21	40.1	1.41	-	-
	D40-B2-I	152.5	305	GFRP	0.34	80.1*	2.28	76.0	3.3	39.6	0.21	56.3	2.20	-	G1
	D40-B2-II	152.5	305	GFRP	0.34	80.1*	2.28	76.0	3.3	39.6	0.21	55.0	1.83	-	G1
	D40-B3-I	152.5	305	GFRP	0.51	80.1*	2.28	76.0	3.3	39.6	0.21	68.7	2.34	-	G1
	D40-B3-II	152.5	305	GFRP	0.51	80.1*	2.28	76.0	3.3	39.6	0.21	67.8	2.37	-	G1
	D47-B2-I	152.5	305	GFRP	0.34	80.1*	2.28	76.0	3.5	46.7	0.23	60.0	2.23	-	G1
	D47-B2-II	152.5	305	GFRP	0.34	80.1*	2.28	76.0	3.5	46.7	0.23	55.7	1.45	-	G1
	D37-C1-I[b]	152.5	305	GFRP	0.17	80.1*	2.28	88.0	2.1	36.9	0.21	42.9	1.66	-	-
	D37-C1-II[b]	152.5	305	GFRP	0.17	80.1*	2.28	88.0	2.1	36.9	0.21	41.4	1.33	-	-
	D37-C2-I	152.5	305	GFRP	0.34	80.1*	2.28	88.0	2.1	36.9	0.21	55.9	2.35	-	G1
	D37-C2-II	152.5	305	GFRP	0.34	80.1*	2.28	88.0	2.1	36.9	0.21	52.9	1.88	-	G1
	D37-C3-I	152.5	305	GFRP	0.51	80.1*	2.28	88.0	2.1	36.9	0.21	69.4	2.41	-	G1
	D37-C3-II	152.5	305	GFRP	0.51	80.1*	2.28	88.0	2.1	36.9	0.21	69.2	2.77	-	G1
	D40-D2-I	152.5	305	GFRP	0.34	80.1*	2.28	115.0	5.2	40.1	0.21	-	2.96	-	G1
	D40-D2-II	152.5	305	GFRP	0.34	80.1*	2.28	115.0	5.2	40.1	0.21	-	2.52	-	G1
Ref. [28]	CC245-W6	400.0	800	GFRP	1.02	80.1*	2.28	245.8	8.0	29.3	0.19	-	2.87	-	G1
	CC325-W6	400.0	800	GFRP	1.02	80.1*	2.28	323.6	9.3	37.3	0.21	-	2.55	-	G1
	CC325-W4[a]	400.0	800	GFRP	0.68	80.1*	2.28	323.6	9.3	40.1	0.21	-	1.05	-	-
Ref. [30]	DSTC-1	152.5	305	CFRP	0.23	240.0	1.55	101.6	3.2	37.0	0.21	58.3	2.77	1.07	G1
	DSTC-2	152.5	305	CFRP	0.23	240.0	1.55	101.6	3.2	37.0	0.21	62.5	2.49	1.16	G1
	DSTC-5[b]	152.5	305	CFRP	0.23	240.0	1.55	76.1	3.2	37.0	0.21	46.8	1.86	0.82	-
	DSTC-6[b]	152.5	305	CFRP	0.23	240.0	1.55	76.1	3.2	37.0	0.21	47.7	1.87	0.98	-

	DSTC-9[b]	152.5	305	CFRP	0.70	240.0	1.55	101.6	3.2	37.0	0.21	114.0	5.40	0.95	-
	DSTC-10[b]	152.5	305	CFRP	0.70	240.0	1.55	101.6	3.2	37.0	0.21	119.2	4.78	0.90	-
	DSTC-11[a]	152.5	305	CFRP	0.70	240.0	1.55	101.6	3.2	106.0	0.35	120.9	1.63	0.54	-
	DSTC-12[a]	152.5	305	CFRP	0.70	240.0	1.55	101.6	3.2	106.0	0.35	105.2	0.96	0.11	-
	DSTC-15	152.5	305	CFRP	0.70	240.0	1.55	76.1	3.2	106.0	0.35	135.5	1.74	0.86	G2
	DSTC-16	152.5	305	CFRP	0.70	240.0	1.55	76.1	3.2	106.0	0.35	122.1	1.53	0.86	G2
	DSTC-19	152.5	305	CFRP	0.70	240.0	1.55	38.1	3.2	107.0	0.35	121.7	1.50	1.00	G1
	DSTC-20	152.5	305	CFRP	0.70	240.0	1.55	38.1	3.2	107.0	0.35	113.5	1.54	0.72	G1
	DSTC-21	152.5	305	CFRP	0.70	240.0	1.55	38.1	1.6	106.0	0.35	133.7	1.66	0.58	G2
	DSTC-22	152.5	305	CFRP	0.70	240.0	1.55	38.1	1.6	106.0	0.35	139.1	1.67	0.92	G2
	DSTC-23[d]	152.5	305	CFRP	0.70	240.0	1.55	38.1	1.6	108.0	0.35	114.5	1.53	0.79	-
	DSTC-24[d]	152.5	305	CFRP	0.70	240.0	1.55	38.1	1.6	108.0	0.35	136.3	1.66	1.10	-
Ref. [31]	DSTC-1[a]	152.5	305	CFRP	0.70	240.0	1.55	88.9	3.2	113.8	0.36	109.3	0.86	0.10	-
	DSTC-2[a]	152.5	305	CFRP	0.70	240.0	1.55	88.9	3.2	113.8	0.36	109.8	0.88	0.10	-
	DSTC-3	152.5	305	AFRP	0.80	116.0	2.50	88.9	3.2	113.8	0.36	130.6	2.89	1.39	G2
	DSTC-4	152.5	305	AFRP	0.80	116.0	2.50	88.9	3.2	113.8	0.36	134.3	2.92	1.35	G2
	DSTC-5	152.5	305	AFRP	1.20	116.0	2.50	88.9	3.2	113.8	0.36	157.7	2.94	1.77	G2
	DSTC-6	152.5	305	AFRP	1.20	116.0	2.50	88.9	3.2	113.8	0.36	158.3	3.10	1.32	G2
	DSTC-7	152.5	305	AFRP	0.60	116.0	2.50	88.9	3.2	49.8	0.24	109.4	4.22	1.84	G1
	DSTC-8	152.5	305	AFRP	0.60	116.0	2.50	88.9	3.2	49.8	0.24	101.3	3.80	1.63	G1
	DSTC-9	152.5	305	AFRP	1.20	116.0	2.50	60.3	3.6	113.8	0.36	156.4	2.41	1.30	G1
	DSTC-10	152.5	305	AFRP	1.20	116.0	2.50	60.3	3.6	113.8	0.36	159.0	2.13	1.15	G1
	DSTC-11	152.5	305	AFRP	1.20	116.0	2.50	88.9	5.5	113.8	0.36	176.8	3.21	1.26	G1
	DSTC-12	152.5	305	AFRP	1.20	116.0	2.50	88.9	5.5	113.8	0.36	177.2	2.96	1.27	G1
	DSTC-13	152.5	305	AFRP	1.20	116.0	2.50	114.3	6.0	113.8	0.36	184.0	3.33	1.44	G1
	DSTC-14	152.5	305	AFRP	1.20	116.0	2.50	114.3	6.0	113.8	0.36	171.2	3.11	1.18	G1
	DSTC-15[e]	152.5	305	AFRP	1.20	116.0	2.50	89.0	3.5	113.8	0.36	91.1	1.96	-	-
	DSTC-16[e]	152.5	305	AFRP	1.20	116.0	2.50	89.0	3.5	113.8	0.36	78.0	1.89	0.08	-
Ref. [32]	DSTC-15	152.5	305	AFRP	1.20	116.0	2.50	101.6	3.2	104.6	0.34	161.4	3.46	1.03	G2
	DSTC-16	152.5	305	AFRP	1.20	116.0	2.50	101.6	3.2	104.6	0.34	161.3	3.49	1.00	G2
	DSTC-17[f]	152.5	305	AFRP	1.20	116.0	2.50	101.6	3.2	104.6	0.34	160.3	3.20	1.02	-

	DSTC-18[f]	152.5	305	AFRP	1.20	116.0	2.50	101.6	3.2	104.6	0.34	171.9	3.02	0.61	-
Ref. [33]	DSTC-1	152.5	305	GFRP	1.20	86.9	3.50	60.3	3.6	96.2	0.33	175.3	3.51	1.94	G1
	DSTC-2	152.5	305	GFRP	1.20	86.9	3.50	60.3	3.6	96.2	0.33	154.2	2.78	1.77	G1
	DSTC-3	152.5	305	GFRP	1.20	86.9	3.50	76.1	3.2	96.2	0.33	176.1	3.94	1.65	G1
	DSTC-4	152.5	305	GFRP	1.20	86.9	3.50	76.1	3.2	96.2	0.33	170.8	3.60	1.86	G1
	DSTC-5	152.5	305	GFRP	1.20	86.9	3.50	88.9	3.2	96.2	0.33	154.6	2.99	1.03	G2
	DSTC-6	152.5	305	GFRP	1.20	86.9	3.50	88.9	3.2	96.2	0.33	166.2	3.52	0.75	G2
	DSTC-7[a]	152.5	305	GFRP	1.20	86.9	3.50	101.6	3.2	96.2	0.33	139.3	2.50	1.09	-
	DSTC-8[a]	152.5	305	GFRP	1.20	86.9	3.50	101.6	3.2	96.2	0.33	144.5	3.03	0.80	-
	DSTC-9[a]	152.5	305	GFRP	1.20	86.9	3.50	114.3	6.0	96.2	0.33	161.6	3.18	1.02	-
	DSTC-10[a]	152.5	305	GFRP	1.20	86.9	3.50	114.3	6.0	96.2	0.33	143.0	2.77	0.88	-

G1= No buckling or mild buckling at mid-height of inner steel tube
G2= Buckling at top or bottom edge of inner steel tube
-= Not available
a= Specimen experienced premature failure
b= Specimen showed significant deviation from relevant global trends of strength and strain enhancement ratios
c= Specimen exhibited a stress-strain curve with a descending or almost flat second branch
d= Specimen manufactured with a high-strength steel (HSS)
e= Specimen manufactured with a square inner steel tube
f= Specimen had a special end condition
*Obtained from coupon tests based on nominal fibre thickness of coupons

Table. 3 Test database of circular concrete-filled DSTCs

Paper	Specimen label	Specimen dimensions		FRP tube properties				Steel tube dimensions		Concrete properties		Measured Ultimate condition			Failure mode
		D (mm)	H (mm)	FRP type	t_f (mm)	E_f (GPa)	ε_f (%)	D_s (mm)	t_s (mm)	f'_{co} (MPa)	ε_{co} (%)	f'_{cu} (MPa)	ε_{cu} (%)	$\varepsilon_{h.rup}$ (%)	
Ref. [30]	DSTC-3[a]	152.5	305	CFRP	0.23	240.0	1.55	101.6	3.2	36.7	0.21	47.5	2.13	0.84	-
	DSTC-4	152.5	305	CFRP	0.23	240.0	1.55	101.6	3.2	36.7	0.21	57.9	2.63	1.37	G1
	DSTC-7[a]	152.5	305	CFRP	0.23	240.0	1.55	76.1	3.2	36.4	0.21	41.8	1.58	0.92	-
	DSTC-8[a]	152.5	305	CFRP	0.23	240.0	1.55	76.1	3.2	36.4	0.21	44.0	1.58	0.85	-
	DSTC-13[a]	152.5	305	CFRP	0.70	240.0	1.55	101.6	3.2	106.0	0.35	133.4	0.90	0.52	-
	DSTC-14	152.5	305	CFRP	0.70	240.0	1.55	101.6	3.2	106.0	0.35	169.5	2.06	1.20	G2
	DSTC-17	152.5	305	CFRP	0.70	240.0	1.55	76.1	3.2	107.0	0.35	137.2	1.58	0.95	G2
	DSTC-18	152.5	305	CFRP	0.70	240.0	1.55	76.1	3.2	107.0	0.35	130.7	1.50	0.85	G2
Ref. [32]	DSTC-1	152.5	305	AFRP	0.60	116.0	2.50	88.9	3.2	47.3	0.23	109.9	3.71	1.93	G1
	DSTC-2	152.5	305	AFRP	0.60	116.0	2.50	88.9	3.2	47.3	0.23	107.4	3.41	1.85	G1
	DSTC-3[g]	152.5	305	AFRP	1.20	116.0	2.50	88.9	3.2	64.9	0.27	200.9	4.98	1.65	-
	DSTC-4[g]	152.5	305	AFRP	1.20	116.0	2.50	88.9	3.2	64.9	0.27	197.7	5.15	1.90	-
	DSTC-5	152.5	305	AFRP	1.20	116.0	2.50	88.9	3.2	104.6	0.34	183.1	2.80	1.57	G2
	DSTC-6	152.5	305	AFRP	1.20	116.0	2.50	88.9	3.2	104.6	0.34	172.9	2.23	1.24	G2
	DSTC-7	152.5	305	AFRP	1.20	116.0	2.50	88.9	5.5	104.6	0.34	179.0	2.73	1.37	G1
	DSTC-8	152.5	305	AFRP	1.20	116.0	2.50	88.9	5.5	104.6	0.34	202.1	3.37	1.76	G1
	DSTC-9	152.5	305	AFRP	1.20	116.0	2.50	60.3	3.6	104.6	0.34	185.2	2.79	1.68	G1
	DSTC-10	152.5	305	AFRP	1.20	116.0	2.50	60.3	3.6	104.6	0.34	175.2	2.31	1.43	G1
	DSTC-11	152.5	305	AFRP	1.20	116.0	2.50	101.6	3.2	104.6	0.34	198.7	3.09	1.68	G2
	DSTC-12	152.5	305	AFRP	1.20	116.0	2.50	101.6	3.2	104.6	0.34	190.8	2.90	1.43	G2
	DSTC-13	152.5	305	AFRP	1.20	116.0	2.50	114.3	6.0	104.6	0.34	198.9	2.64	1.68	G1
	DSTC-14	152.5	305	AFRP	1.20	116.0	2.50	114.3	6.0	104.6	0.34	179.2	2.28	1.62	G1
Ref. [33]	DSTC-11	152.5	305	GFRP	1.20	86.9	3.50	60.3	3.6	96.2	0.33	189.5	3.64	1.97	G1
	DSTC-12	152.5	305	GFRP	1.20	86.9	3.50	60.3	3.6	96.2	0.33	174.6	3.19	1.92	G1
	DSTC-13	152.5	305	GFRP	1.20	86.9	3.50	76.1	3.2	96.2	0.33	175.8	3.09	1.75	G1

	DSTC-14	152.5	305	GFRP	1.20	86.9	3.50	76.1	3.2	96.2	0.33	187.0	3.76	1.94	G1
	DSTC-15	152.5	305	GFRP	1.20	86.9	3.50	88.9	3.2	96.2	0.33	179.2	2.88	1.72	G2
	DSTC-16	152.5	305	GFRP	1.20	86.9	3.50	88.9	3.2	96.2	0.33	191.6	3.50	1.76	G2
	DSTC-17	152.5	305	GFRP	1.20	86.9	3.50	101.6	3.2	96.2	0.33	184.3	3.24	1.54	G2
	DSTC-18	152.5	305	GFRP	1.20	86.9	3.50	101.6	3.2	96.2	0.33	190.5	3.32	1.72	G2
	DSTC-19	152.5	305	GFRP	1.20	86.9	3.50	114.3	3.2	96.2	0.33	194.0	3.37	1.74	G2
	DSTC-20	152.5	305	GFRP	1.20	86.9	3.50	114.3	3.2	96.2	0.33	183.9	3.03	1.57	G2

G1= No bulging or mild bulging at mid-height of inner steel tube
G2= Bulging at top or bottom edge of inner steel tube
-= Not available
a= Specimen experienced premature failure
g= Specimen manufactured using two different grades of concrete

Table. 4 Test database of square hollow DSTCs

Paper	Specimen label	Specimen dimensions			FRP tube properties				Steel tube dimensions		Concrete properties		Measured ultimate conditions			Failure mode
		B (mm)	H (mm)	r (mm)	FRP type	t_f (mm)	E_f (GPa)	ε_f (%)	D_s (mm)	t_s (mm)	f'_{co} (MPa)	ε_{co} (%)	f'_{cu} (MPa)	ε_{cu} (%)	$\varepsilon_{h.rup}$ (%)	
Ref. [29]	D37-A2-1[c]	150	300	25	GFRP	0.34	80.1*	2.28	76.3	3.3	37.5	0.21	37.8	1.47	-	-
	D37-A2-II[c]	150	300	25	GFRP	0.34	80.1*	2.28	76.3	3.3	37.5	0.21	34.1	1.03	-	-
	D37-A3-I	150	300	25	GFRP	0.51	80.1*	2.28	76.3	3.3	37.5	0.21	46.7	2.26	-	G1
	D37-A3-II	150	300	25	GFRP	0.51	80.1*	2.28	76.3	3.3	37.5	0.21	47.5	2.18	-	G1
	D37-B2-I	150	300	25	GFRP	0.34	80.1*	2.28	114.5	5.2	37.5	0.21	39.8	2.19	-	G1
	D37-B2-II	150	300	25	GFRP	0.34	80.1*	2.28	114.5	5.2	37.5	0.21	36.7	2.38	-	G1
	D37-B3-I[c]	150	300	25	GFRP	0.51	80.1*	2.28	114.5	5.2	37.5	0.21	48.9	-	-	-
	D37-B3-II[c]	150	300	25	GFRP	0.51	80.1*	2.28	114.5	5.2	37.5	0.21	45.0	2.72	-	-
Ref. [34]	DSTC-1	150	300	30	AFRP	1.60	118.2	2.20	60.3	3.6	98.2	0.33	121.4	1.91	0.89	G1
	DSTC-2	150	300	30	AFRP	1.60	118.2	2.20	60.3	3.6	98.2	0.33	121.0	1.71	1.03	G1
	DSTC-5[c]	150	300	30	AFRP	1.60	118.2	2.20	88.9	3.2	98.2	0.33	112.7	1.92	0.67	-
	DSTC-6	150	300	30	AFRP	1.60	118.2	2.20	88.9	3.2	98.2	0.33	124.8	2.59	0.81	G2
	DSTC-9	150	300	30	AFRP	1.60	118.2	2.20	114.3	6.0	98.2	0.33	122.9	3.26	0.47	G1
	DSTC-10	150	300	30	AFRP	1.60	118.2	2.20	114.3	6.0	98.2	0.33	124.2	3.55	0.65	G1
	DSTC-13	150	300	30	AFRP	0.60	118.2	2.20	88.9	3.2	47.0	0.23	69.3	4.11	0.68	G1
	DSTC-14	150	300	30	AFRP	0.60	118.2	2.20	88.9	3.2	47.0	0.23	64.0	3.63	0.88	G1
	DSTC-17[e]	150	300	30	AFRP	1.60	118.2	2.20	89.0	3.5	98.2	0.33	101.1	1.55	0.13	-
	DSTC-18[e]	150	300	30	AFRP	1.60	118.2	2.20	89.0	3.5	98.2	0.33	88.7	1.56	0.14	-
	DSTC-21[e]	150	300	30	AFRP	0.60	118.2	2.20	89.0	3.5	47.0	0.23	43.2	2.52	0.39	-
	DSTC-22[e]	150	300	30	AFRP	0.60	118.2	2.20	89.0	3.5	47.0	0.23	40.7	2.51	0.34	-
Ref. [35]	S-0.6-N-114.3-6.02-E	150	300	30	AFRP	0.60	118.2	2.20	114.3	6.0	50.7	0.24	75.6	3.41	-	G1
	S-0.6-N-114.3-6.02-E-D	150	300	30	AFRP	0.60	118.2	2.20	114.3	6.0	50.7	0.24	76.3	3.45	-	G1

G1= No buckling or mild buckling at mid-height of inner steel tube
G2= Buckling at top or bottom edge of inner steel tube
-= Not available
c= Specimen exhibited a stress-strain curve with a descending or almost flat second branch
e= Specimen manufactured with a square inner steel tube
*Obtained from coupon tests based on nominal fibre thickness of coupons

Table. 5 Test database of square concrete-filled DSTCs

Paper	Specimen label	Specimen dimensions			FRP tube properties				Steel tube dimensions		Concrete properties		Measured ultimate conditions			Failure mode
		B (mm)	H (mm)	r (mm)	FRP type	t_f (mm)	E_f (GPa)	ε_f (%)	D_s (mm)	t_s (mm)	f'_{co} (MPa)	ε_{co} (%)	f'_{cu} (MPa)	ε_{cu} (%)	$\varepsilon_{h.rup}$ (%)	
Ref. [34]	DSTC-3	150	300	30	AFRP	1.60	118.2	2.20	60.3	3.6	98.2	0.33	135.1	2.50	0.96	G1
	DSTC-4	150	300	30	AFRP	1.60	118.2	2.20	60.3	3.6	98.2	0.33	136.1	2.17	1.07	G1
	DSTC-7	150	300	30	AFRP	1.60	118.2	2.20	88.9	3.2	98.2	0.33	134.1	1.90	0.80	G2
	DSTC-8	150	300	30	AFRP	1.60	118.2	2.20	88.9	3.2	98.2	0.33	129.6	2.11	0.72	G2
	DSTC-11	150	300	30	AFRP	1.60	118.2	2.20	114.3	6.0	98.2	0.33	148.0	2.39	0.88	G1
	DSTC-12	150	300	30	AFRP	1.60	118.2	2.20	114.3	6.0	98.2	0.33	141.1	2.65	0.83	G1
	DSTC-15	150	300	30	AFRP	0.60	118.2	2.20	88.9	3.2	47.0	0.23	79.8	3.70	0.88	G1
	DSTC-16	150	300	30	AFRP	0.60	118.2	2.20	88.9	3.2	47.0	0.23	78.7	3.52	0.74	G1
	DSTC-19[e]	150	300	30	AFRP	1.60	118.2	2.20	89.0	3.5	98.2	0.33	129.6	1.89	1.04	-
	DSTC-20[e]	150	300	30	AFRP	1.60	118.2	2.20	89.0	3.5	98.2	0.33	133.0	2.34	1.10	-
	DSTC-23[e]	150	300	30	AFRP	0.60	118.2	2.20	89.0	3.5	47.0	0.23	75.2	3.35	1.07	-
	DSTC-24[e]	150	300	30	AFRP	0.60	118.2	2.20	89.0	3.5	47.0	0.23	79.6	3.65	1.05	-
Ref. [35]	S-0.6-N-114.3-6.02-N	150	300	30	AFRP	0.60	118.2	2.20	114.3	6.0	50.7	0.24	80.3	2.90	-	G1
	S-0.6-N-114.3-6.02-N-D	150	300	30	AFRP	0.60	118.2	2.20	114.3	6.0	50.7	0.24	82.1	3.35	-	G1

G1= No or less bulging at mid-height of inner steel tube
G2= Bulging at top or bottom edge of inner steel tube
-= Not available
e= Specimen manufactured with a square inner steel tube

Table 6. Statistics on performance of existing models for hollow circular DSTCs

Model	Prediction of f'_{cu}/f'_{co}			Prediction of $\varepsilon_{cu}/\varepsilon_{co}$			No. of test results used in assessment
	Average absolute error (%)	Mean (%)	Standard deviation (%)	Average absolute error (%)	Mean (%)	Standard deviation (%)	
Yu et al. [44]	12.2	96.6	14.1	27.3	73.8	16.9	44*
Louk Fanggi and Ozbakkaloglu [31]	6.6	103.3	9.3	11.0	100.5	13.8	44*

*40 specimens were used in assessment of f'_{cu}/f'_{co} as f'_{cu} values were missing for some of the specimens, as shown in Table 2

Table 7. Statistics on performance of existing models for hollow square DSTCs

Model	Prediction of f'_{cu}/f'_{co}			Prediction of $\varepsilon_{cu}/\varepsilon_{co}$			No. of test results used in assessment
	Average absolute error (%)	Mean (%)	Standard deviation (%)	Average absolute error (%)	Mean (%)	Standard deviation (%)	
Yu and Teng 1 [29]	14.1	111.8	14.5	43.2	86.5	50.0	13
Yu and Teng 2 [29]	9.3	102.0	11.7	52.4	47.6	20.2	13

Table 8. Strength and strain enhancement coefficients (k_1 and k_2) of circular DSTCs

Enhancement coefficients	Hollow DSTCs		Concrete-filled DSTCs		Concrete strength range
	G1	G2	G1	G2	
k1	3.02	2.50	3.14	3.02	NSC & HSC
k2	0.30	0.26	0.31	0.24	NSC &HSC

Table 9. Strength and strain enhancement coefficients (k_1 and k_2) of square DSTCs

Enhancement coefficients	Hollow DSTC		Concrete-filled DSTC		Concrete strength range
	G1	G2	G1	G2	
k1	2.00	-	2.40	-	NSC
	0.65	0.45	0.76	0.49	HSC
k2	0.23	-	0.29	-	NSC
	0.17	0.15	0.20	0.16	HSC

-= Not available

LIST OF FIGURES

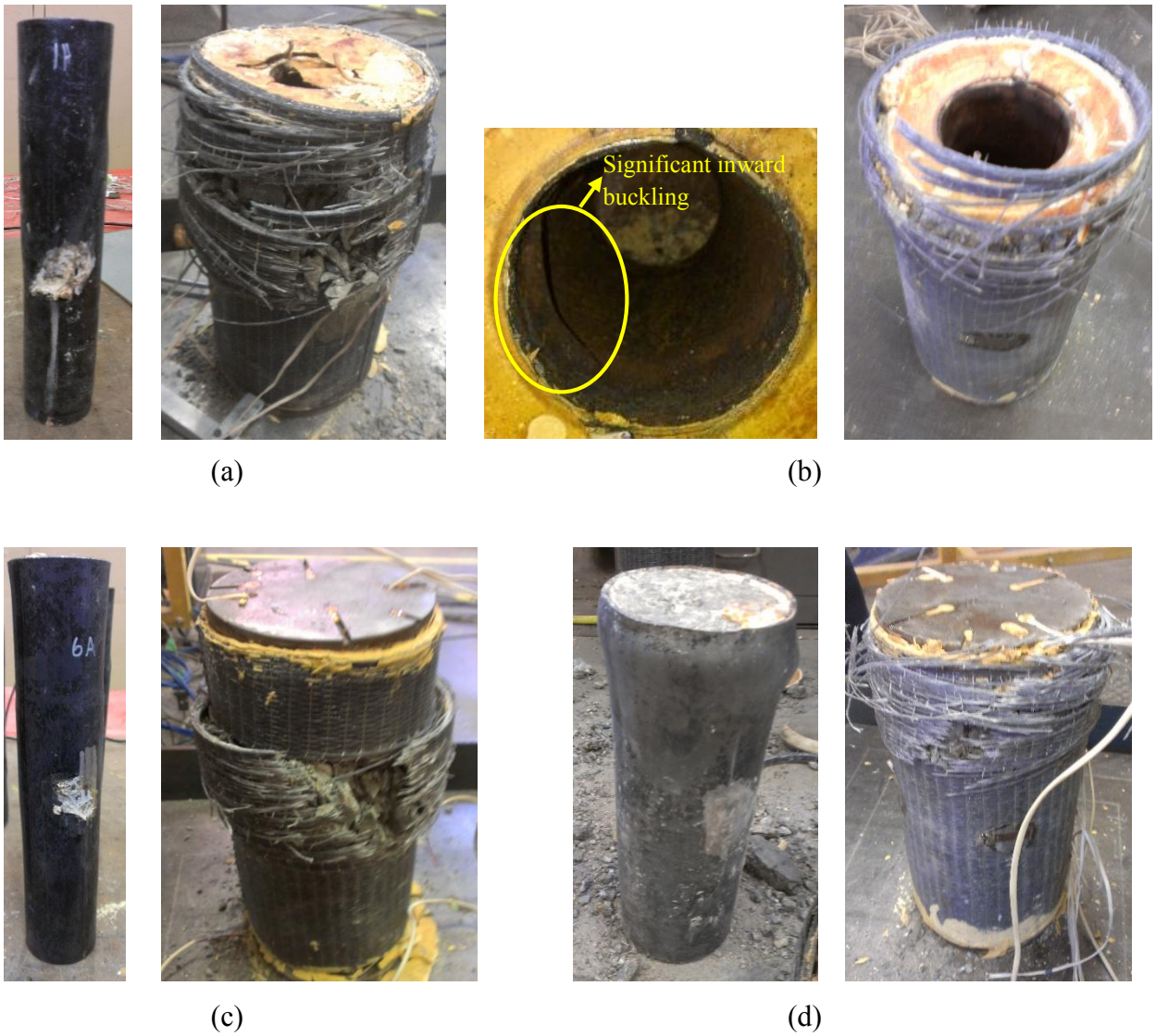

Figure 1. Failure modes of inner steel tubes and external FRP tubes as observed in Ref. [33]: (a) No buckling (Hollow DSTC with D_s = 60.3 mm, DSTC-1), (b) Local inward buckling (Hollow DSTC with D_s = 88.9 mm, DSTC-5), (c) No bulging (Concrete-filled DSTC with D_s = 60.3 mm, DSTC-11), (d) Bulging at top (Concrete-filled DSTC with D_s = 101.6 mm, DSTC-17)

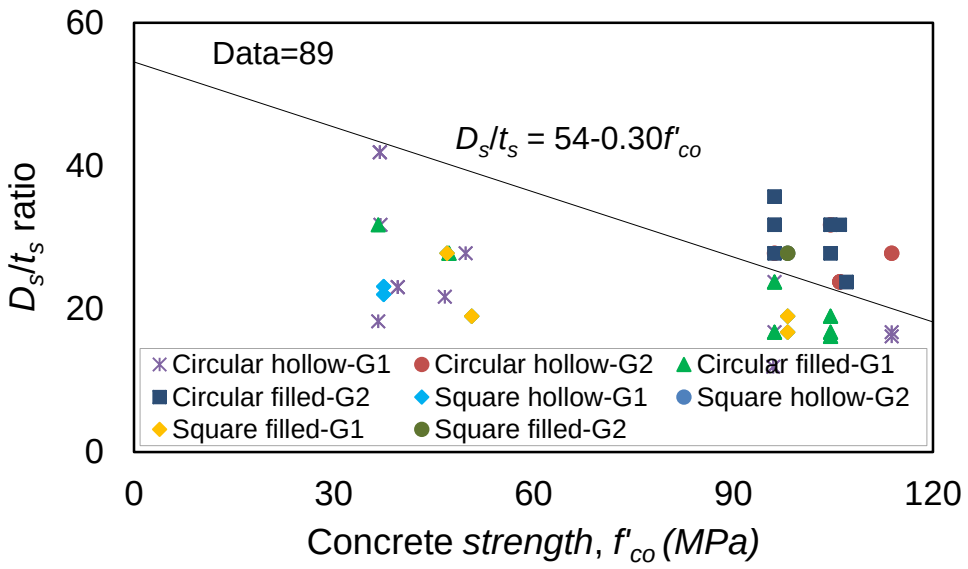

Figure 2. Identification of inner steel tube failure mode based on D_s/t_s and f'_{co} relationship

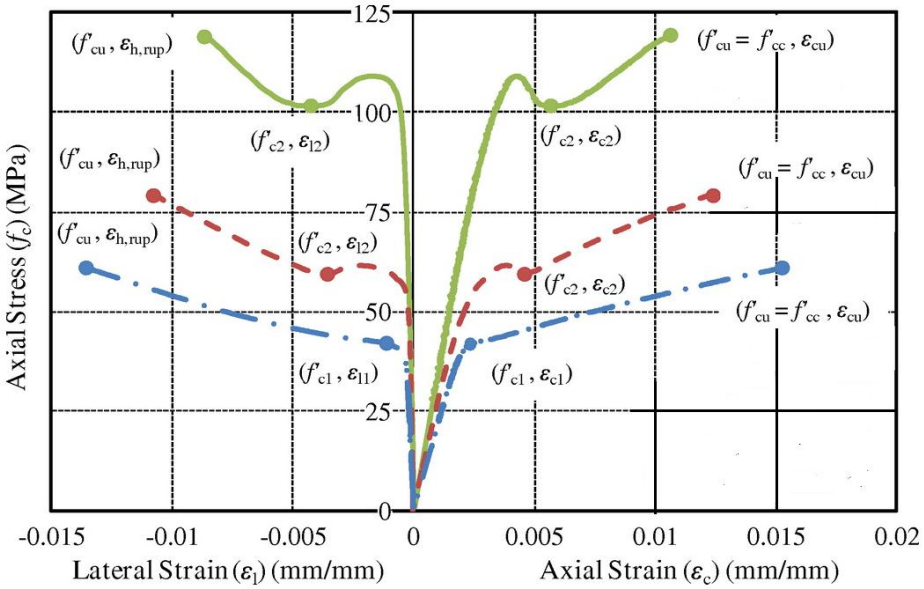

Figure 3. Critical coordinates on stress-strain relationship of FRP-confined concrete (Ref. [45])

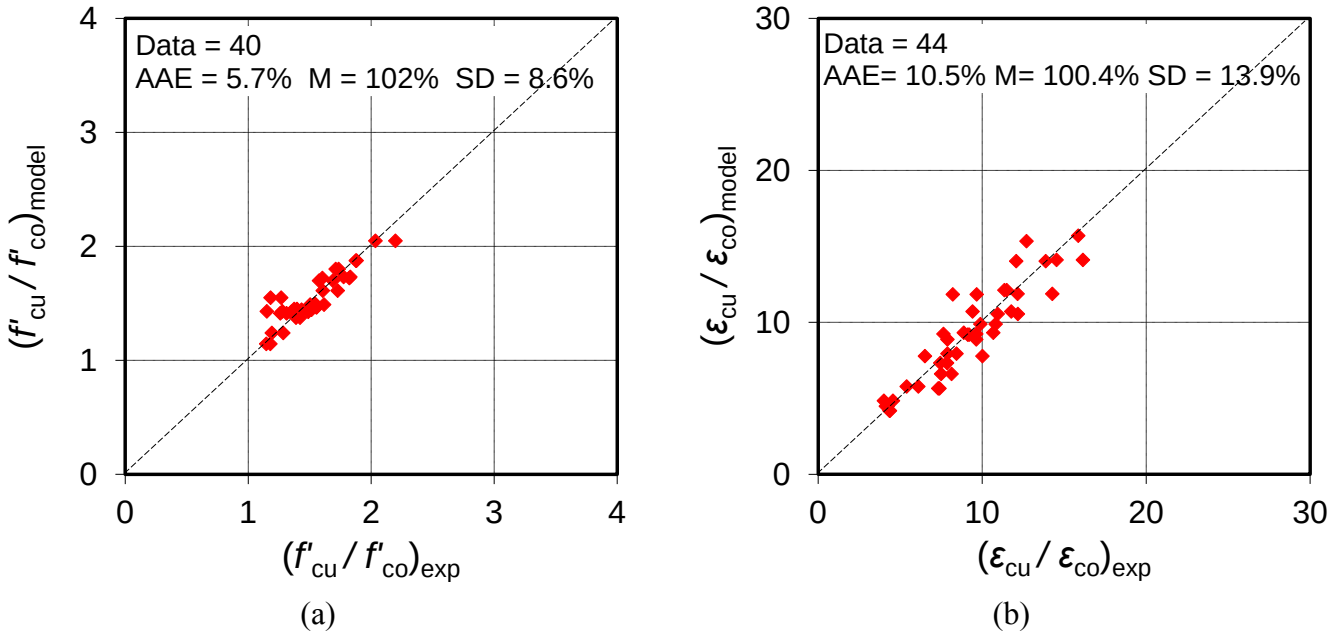

Figure 4. Comparison of predictions of proposed model with experimental data for circular hollow DSTCs: (a) Strength enhancement ratio (f'_{cu}/f'_{co}), (b) Strain enhancement ratio ($\varepsilon_{cu}/\varepsilon_{co}$)

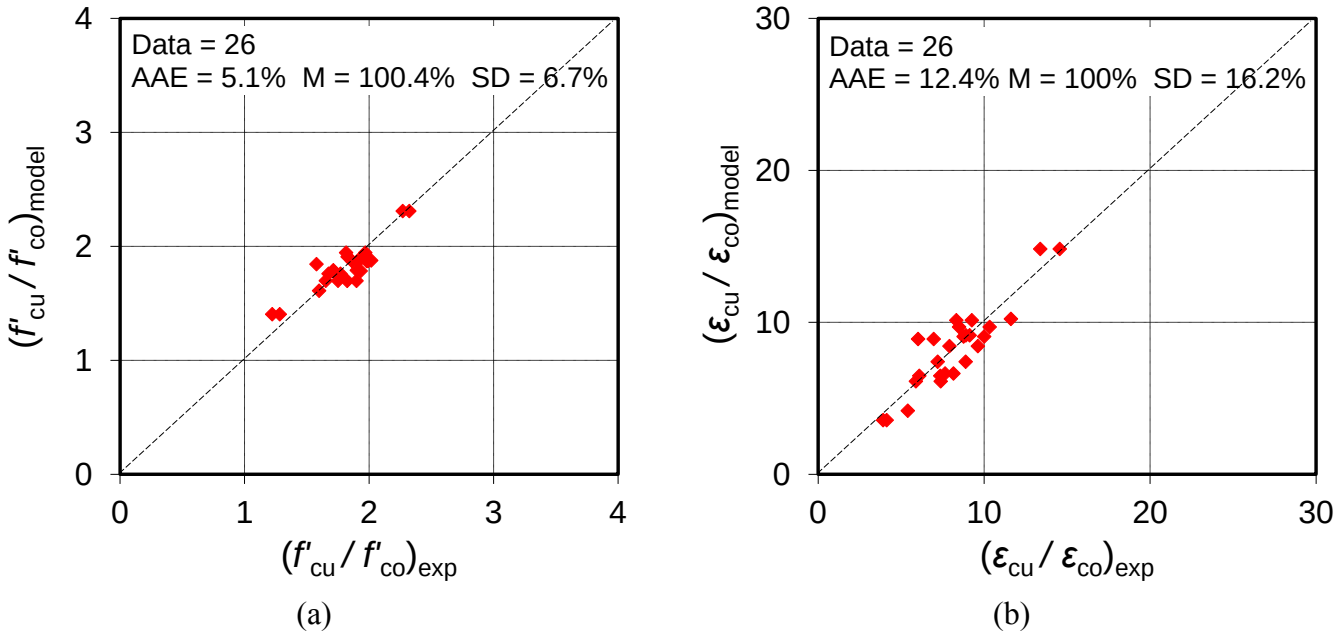

Figure 5. Comparison of model predictions of proposed model with experimental data of circular concrete-filled DSTCs: (a) Strength enhancement ratio (f'_{cu}/f'_{co}), (b) Strain enhancement ratio ($\varepsilon_{cu}/\varepsilon_{co}$)

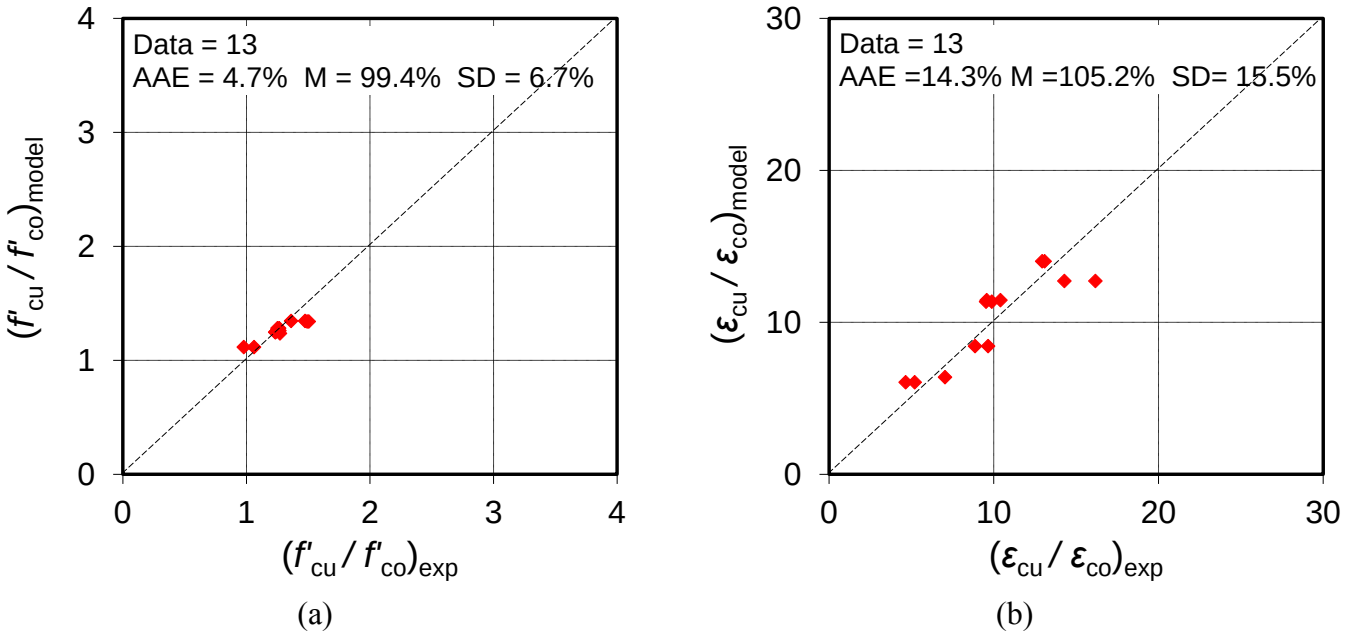

Figure 6. Comparison of model predictions of proposed model with experimental data of square hollow DSTCs: (a) Strength enhancement ratio (f'_{cu}/f'_{co}), (b) Strain enhancement ratio ($\varepsilon_{cu}/\varepsilon_{co}$)

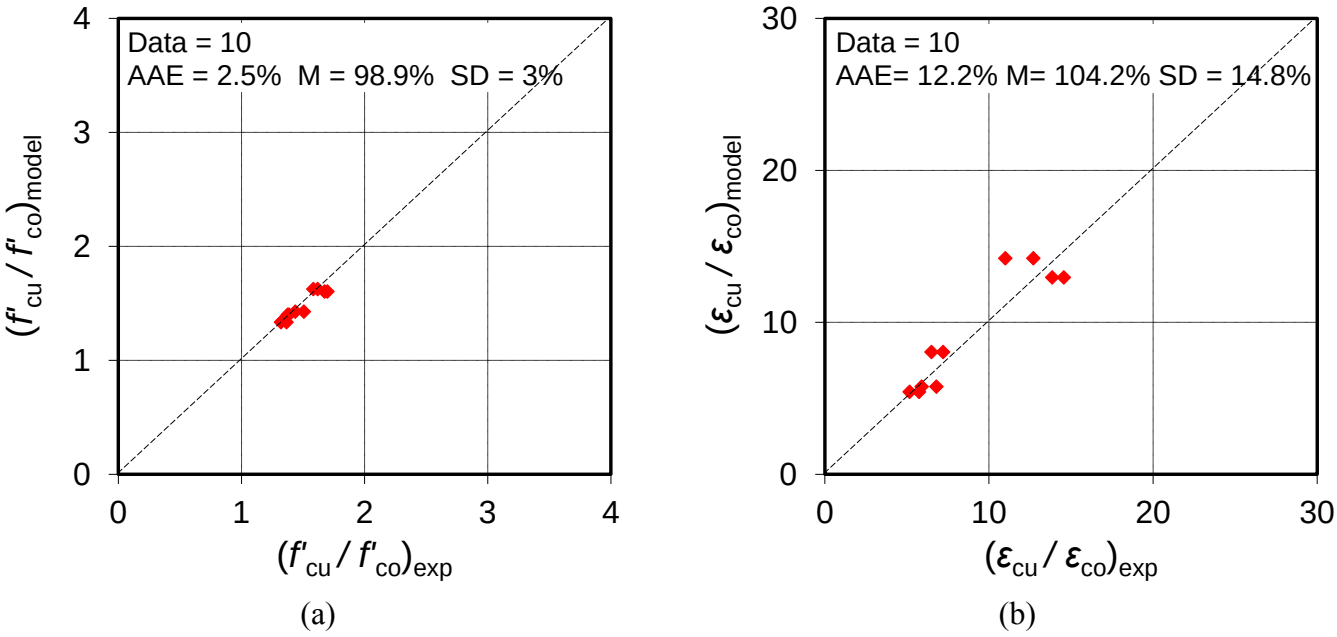

Figure 7. Comparison of model predictions of proposed model with experimental data of square concrete-filled DSTCs: (a) Strength enhancement ratio (f'_{cu}/f'_{co}), (b) Strain enhancement ratio ($\varepsilon_{cu}/\varepsilon_{co}$)

CONCLUSIONS

A new type of composite system was recently proposed in the form of FRP-concrete-steel double-skin tubular columns (DSTCs). This composite system consists of a steel tube inside, an FRP tube outside with concrete in between, and it offers a long list of advantages, including: i) improved structural performance, ii) improved durability that prolongs the design life, thereby reducing the cost of structural maintenance and urban renewal, iii) significant improvements to the ease of construction that results in reduced construction costs, iv) significant reduction to carbon footprint per year through more efficient use of materials that reduces both the required amount of raw materials and generation of construction and demolition waste.

To this end, six experimental studies were undertaken at the University of Adelaide. In each of these studies, the key parameters that influence the axial compressive behavior of DSTCs were identified and investigated. The results of these experimental studies indicate that concrete in a DSTC system is confined effectively by FRP and steel tubes. Both the normal-and high-strength concrete DSTCs exhibited a highly ductile compressive behavior under monotonic and cyclic axial compression. However, it is found that, for a given nominal confinement ratio, an increase in the concrete strength results in a decrease in the ultimate axial strain of DSTCs. The results also indicate that increasing the inner steel tube diameter leads to an increase in the ultimate axial stress and strain of concrete in DSTCs. It is observed that the concrete-filling of the inner steel tubes of DSTCs results in an increase in the compressive strength and a slight decrease in the ultimate axial strain of concrete in DSTCs, compared to the values observed in companion specimens with hollow inner steel tubes. It is also observed that cyclically loaded normal-strength concrete (NSC) DSTCs developed similar strength and strain

enhancement ratios to those of monotonically loaded NSC DSTCs. Furthermore, it is found that the residual plastic strain of concrete in cyclically loaded DSTCs is linearly related to the envelope unloading strain, and this relationship is not influenced by concrete strength, FRP type, diameter of the inner steel tube, and presence/absence of a concrete filling inside the steel tube. The results also show that concrete in hollow DSTCs manufactured with square inner steel tubes develops significantly lower ultimate axial stresses and strains than those of concrete in companion hollow DSTCs with circular inner steel tubes. It is found, however, that the performance of these specimens improves dramatically when the square inner steel tube is filled with concrete.

Apart from these experimental studies, this thesis also presents analytical models that were developed to predict the compressive strength and ultimate axial strain of concrete in DSTCs. The first of these models was developed to predict the compressive strength and ultimate axial strain of concrete in hollow circular DSTCs. After undertaking additional studies to expand the test database of square and concrete-filled DSTCs a second model that is applicable to both circular and square and hollow and concrete-filled DSTCs was proposed. Comparison with experimental test results show that of the proposed models are in close agreement with the test results, and the models provide improved accuracy compared to the existing models. Although the proposed models can also be applied to predict the capacities of DSTCs that are under combined axial compression and bending through sectional analysis, it is recommended that additional experimental studies be undertaken on eccentrically loaded DSTCs to validate the accuracy of the models for members under such loading conditions.

Research contributions

This study contribute to improve the understanding of the axial compressive behavior and develop an accurate design-oriented models for the prediction the the compressive behavior of DSTCs. The contributions of each of the publication reported in this study [1-7] are summarized in Table 1.

In addition to the journal publications, the other publications related to this study have been shared with other researchers in the field through a number of refereed conference papers [8-13].

Tabel 1. Summary of publications and research contributions

Publication	Contributions
Ozbakkaloglu and Louk Fanggi [1]	This paper has presented the results of an experimental study on circular DSTCs made of carbon FRP tube. The influence of concrete strength, thickness of FRP tube, diameter, strength, and thickness of inner steel tube, and also presence (absence) of concrete filling inner steel tube on the axial compressive behavior of DSTCs have been reported in this paper.
Louk Fanggi and Ozbakkaloglu [2]	This paper has presented the results of an experimental study on circular DSTCs made of aramid FRP. The column parameters investigated in this test included concrete strength, thickness of FRP tube, diameter, shape, and thickness of inner steel tube. A new stress-strain model that provides improved predictions compared to the existing stress-strain model also proposed in this paper.
Ozbakkaloglu and Louk Fanggi [3]	This paper has presented the results of an experimental study on circular DSTCs made of aramid FRP and subjected to monotonic and cyclic axial compression. The parameters investigated in this study included loading patterns, concrete strength, diameter, thickness, end condition of inner steel tube, and the presence (absence) of concrete filling inside inner steel tube. The relative performance levels of DSTCs compared to CFFTs and I-CFFTs was also reported in this paper.
Louk Fanggi and Ozbakkaloglu [4]	This paper has presented the results of an experimental study on circular DSTCs made of S-glass FRP tubes. Inner steel tube diameter, presence (absence) of concrete filling inside inner steel tube, and loading patterns were investigated and reported in this paper. The influence of the type of inner steel tube buckling was also discussed in this paper. In addition, the relative performance levels of DSTCs compared to CFFTs and I-CFFTs was reported in this paper.
Albitar et al. [5]	This paper has presented the results of an experimental study on circular DSTCs made of aramid and S-glass FRP tubes subjected to cyclic axial compression. The effect of FRP type and thickness, concrete

	strength, inner steel tube diameter, and presence (absence) of concrete filling inside inner steel tube have been presented in this paper.
Louk Fanggi and Ozbakkaloglu [6]	This paper has presented the results of an experimental study on square DSTCs made of aramid FRP tube subjected to axial compression. The key parameters examined in this test included concrete strength, cross-sectional shape, dimension of inner steel tube, and the presence (absence) of concrete filling inside inner steel tube. The relative performance levels of DSTCs compared to CFFTs and I-CFFTs were also discussed in this paper.
Louk Fanggi and Ozbakkaloglu [7]	This paper has presented the development of a design-oriented model for predicting the ultimate condition of concrete DSTCs by modifying the first proposed model and incorporating a new parameter which is the plastic deformation of inner steel tube in the proposed model. The proposed model can be used for predicting circular and square hollow and concrete-filled DSTCs through one simple equation. The model provides good and improved predictions to test results and compared with the existing models.

LIST OF PUBLICATIONS

[1] Ozbakkaloglu, T., and Louk Fanggi, B.A. (2013). "Axial compressive behavior of FRP-concrete-steel double-skin tubular columns made of normal- and high-strength concrete." *Journal of Composites for Construction*, 18(1): 04013027-1-040113027-13.

[2] Louk Fanggi, B.A., and Ozbakkaloglu, T. (2013). "Compressive behavior of aramid FRP-HSC-steel double-skin tubular columns." *Construction and Building Materials*. 48: 554-565.

[3] Ozbakkaloglu, T., and Louk Fanggi, B.A. (2015). "Behavior of FRP-HSC-steel composite tubular columns under monotonic and cyclic axial compression." *Materials and Structures*. 48: 1075-1093.

[4] Louk Fanggi, B.A., and Ozbakkaloglu, T. (2015). "Behavior of Hollow and Concrete-Filled FRP-HSC and FRP-HSC-Steel Composite Columns Subjected to Concentric Compression." *Advanced in Structural Engineering*. 18(5): 715-738.

[5] Albitar, M., Ozbakkaloglu, T., and Louk Fanggi, B.A. (2015). "Behavior of FRP-HSC-Steel double-skin tubular columns under cyclic axial compression." *Journal of Composites for Construction*. 19(2): 04014041.

[6] Louk Fanggi, B.A., and Ozbakkaloglu, T. (2015). "Square FRP-HSC-steel composite columns: Behavior under Axial Compression." *Engineering Structures*. 92: 156-171.

[7] Louk Fanggi, B.A., and Ozbakkaloglu, T. (2015). "Confinement model for concrete in circular and square FRP-concrete-steel double-skin tubular columns." (To be submitted).

[8] Ozbakkaloglu, T. and Louk Fanggi, B.A. (2013). "An Experimental Study on Behavior of FRP-HSC-Steel Double-Skin Tubular Columns under Concentric Compression." *3rd International Conference on Civil Engineering, Architecture and Building Materials (CEABM 2013)*, Jinan, China, May 25-26.

[9] Louk Fanggi, B.A, and Ozbakkaloglu, T. (2013). “Influence of Inner Steel Tube Properties on Compressive Behavior of FRP-HSC-Steel Double-Skin Tubular Columns." *2nd International conference of civil engineering, architecture and sustainable infrastructure (ICCEASI 2013)*, Zhengzhou, China, July 13-15.

[10] Louk Fanggi, B.A, and Ozbakkaloglu, T. (2013). “Influence of Concrete-Filling Inner Steel Tube on Compressive Behavior of Double-Skin Tubular Columns.” *2nd Global Conference on Civil, Structural and Environmental Engineering (GCCSEE 2013)*, Shenzhen, China, September 28-29.

[11] Louk Fanggi, B.A. and Ozbakkaloglu, T. (2013). "Relative Performance of FRP-Concrete-Steel Double Skin Tubular Columns versus Solid and Hollow Concrete-filled FRP Tubes." *3rd International Conference on Civil Engineering and Transportation (ICCET 2013)*, Kunming, China, December 14-15.

[12] Louk Fanggi, B.A., and Ozbakkaloglu, T. (2014). "Effect of Loading Pattern on Performance of FRP-HSC-Steel Double Skin Tubular Columns." *4th International Conference on Structures and Building Materials (ICSBM 2014)*, Guangzhou, China, March 15-16.

[13] Louk Fanggi, B.A., and Ozbakkaloglu, T. (2014). "Effect of steel tube cross-sectional shape on compressive behavior of square FRP-Concrete-Steel double-Skin tubular columns." *Advanced Materials, Structures and Mechanical Engineering Conference*, Je-Ju Island, South Korea, August 9-10.